INSTITUT FÜR
KRAFTFAHRWESEN
AACHEN

Univ.-Prof. Dr.-Ing. Henning Wallentowitz

Henning Wallentowitz

Automotive Engineering II

Lateral Vehicle Dynamics

Steering ●
Axle Design ●

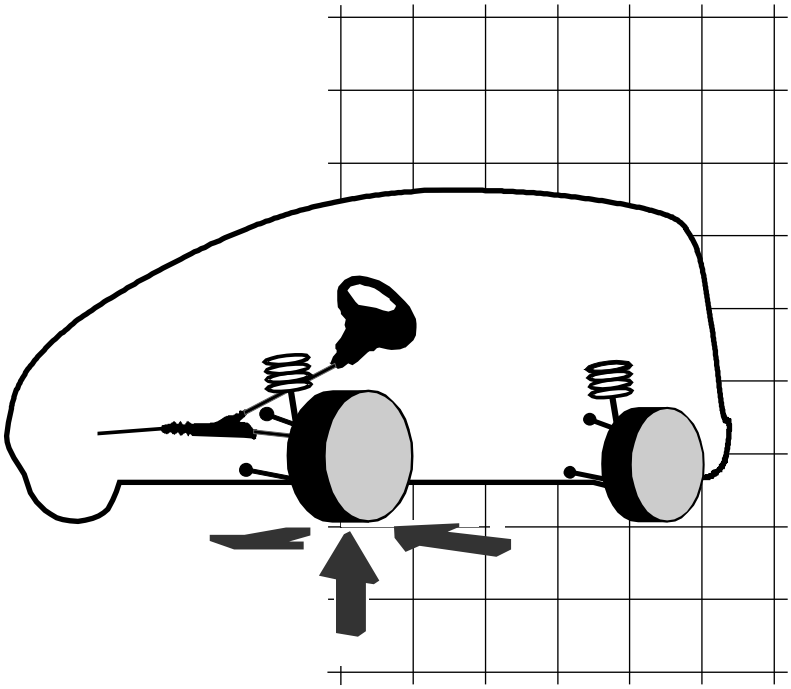

Editor
Prof. Dr.-Ing. Henning Wallentowitz
Institut Für Kraftfahrwesen Aachen (ika) RWTH Aachen
Steinbachstraße 7, D-52074 Aachen - Germany
Telephone (0241) 80-25 600 **Fax** (0241) 80 22-147
e-mail office@ika.rwth-aachen.de
internet htto://www.ika.rwth-aachen.de

Editorial Staff
Dipl.-Ing. Florian Fuhr
Telephone (0241) 80-25 646,
Dipl.-Ing. Ingo Albers
80-25 612

4th Edition, Aachen, February 2004

Printed by
Vervielfältigungsstelle der Hochschule

Contents

2 Lateral Dynamics (Driving Stability)

2.1 Demands on Vehicle Behavior

Like at all vehicles which are not track-bound, the driver of the motor vehicle has to manage not only the control respectively the regulation of driving speed, but also driving direction.

Determination of driving direction by the control activity of the driver contains three cybernetic tasks, Fig. 2.1- 1:

1. From all provided routes, a particular route based on criteria such as time need or distance has to be selected.

2. Within the selected route the desired course has to be defined, whereby information continuously monitored during driving (traffic in the same direction as well as oncoming traffic, signalling systems, routing of the road) are evaluated.

3. The vehicle has to be navigated on the previously defined desired course by its control elements.

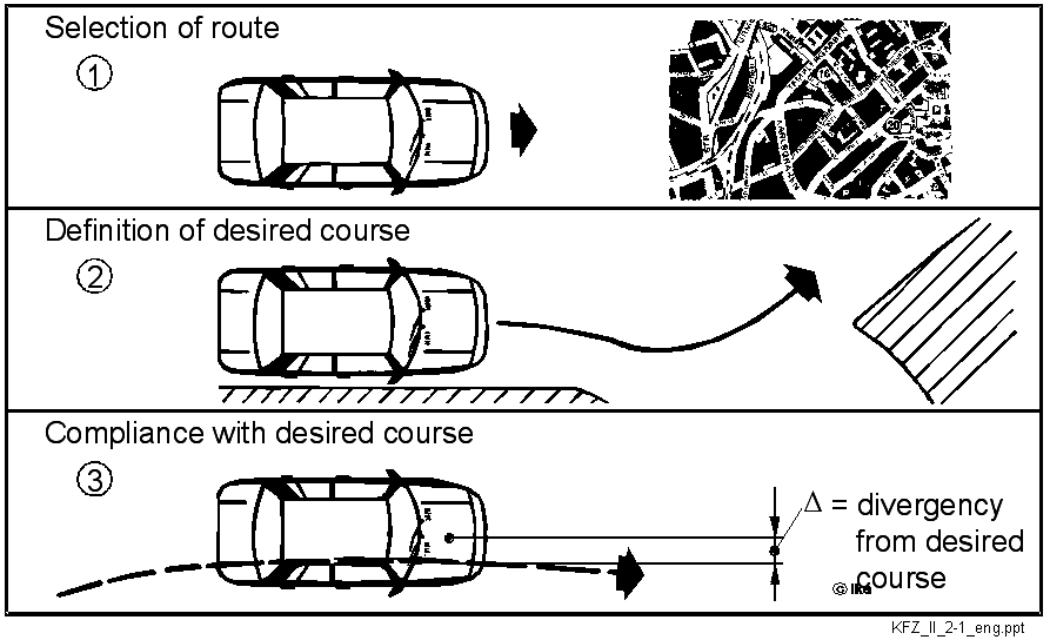

Fig. 2.1- 1: Cybernetic tasks of the driver in the guidance of a motor vehicle

Man undertakes function of a control device in terms of driving stability by the last of this three functions. The vehicle represents the control travel. So interactions between driver action and vehicle response can be understood as operations in a closed control loop, Fig. 2.1- 2.

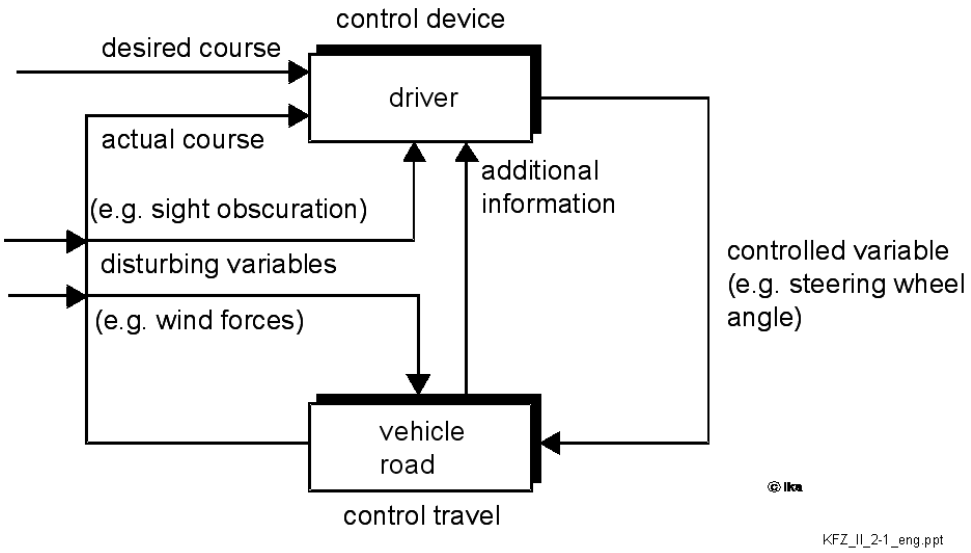

Fig. 2.1- 2 : Control loop driver - vehicle

In this control loop disturbance variables act on the driver (e.g. relative motion driver - vehicle, sight obscuration) and on the vehicle (e.g. crosswind, road irregularity). The controlled variable with respect to the vehicles transverse dynamics particularly is the steering-wheel angle. System deviation is noticed as difference between the desired course and the actual course by the driver.

The closed control loop is a dynamically operating system. Because of limited adaptation possibilities of the control device "driver", it substantially depends on legality of vehicle behavior, if the overall system driver - vehicle acts stable when large course deviations have to be compensated quickly and under the influence of disturbance variables regarding tracking.

Characteristics of the control travel "vehicle" have to be suited to abilities of the control device "driver". Quality of this adjustment is characterized by the term of "handling". With regard to achieve "non-problematic handling" the following demands are made on vehicle characteristics:

- A reasonable and clear relationship between the steer angle change and change of course has to exist for the driver (transmission behavior of the control travel "vehicle", driving stability)
- The driver must receive reasonable information about the vehicles condition of movement (e.g. modification of characteristics of the steering-wheel torque, increasing sideslip angle and tire noise before reaching the physical limits of driving stability).
- external disturbances acting on the vehicle (e.g. wind forces) should cause no or little course deviation (inherent stability of the control travel vehicle).

- Achievable cornering speed and lateral acceleration of the vehicle should be high in view of driving safety and driving performance (stability margin of the control travel vehicle).

Legal regulations in relation to vehicle handling are not available at present.

In view of these demands the following chapter of lateral dynamics describes the legalities and mechanics of the vehicles transverse dynamics by investigating the control travel "vehicle" after separating it from the control device "driver".

As basis of the study of vehicle dynamics tire characteristics are considered at first. A presentation of the basic physical relationship of vehicle movement in plane follows on the basis of a simplified vehicle model with linearized characteristics (Single-track vehicle model).

The most important aspects of driving stability during stationary and transient vehicle movement can already be pointed out here. Afterwards the effect of nonlinear tire characteristics on the vehicles lateral dynamic response in connection with design features of the vehicle (wheel control, suspension) can be discussed by means of simulation results, which are based on calculations from a three-dimensional nonlinear vehicle model, and on the basis of measurement results from driving tests.

How design features and hence certain vehicle characteristics regarding transverse dynamics can be implemented concretely will be explained in the sections "steering" and "wheel suspension“.

2.2 Tires

2.2.1 Demands on Tires

The tire being the essential constructional element transfers and influences the forces between vehicle and road.

Type and field of duty of the vehicle (road vehicle, off-road vehicle, passenger car, truck, tractor, earthmoving machine) are the determining coefficients according to which the appropriate tire must be selected.

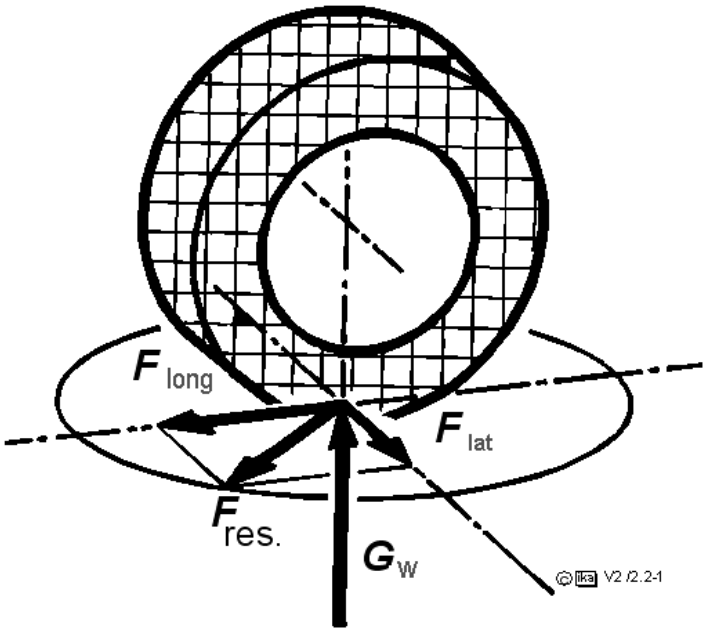

Fig 2.2-1: Forces in the tire contact patch

The following demands are made on a tire for road vehicles:

1. Security

- high friction coefficients for all operating conditions
- adequate (permanent-) top speed
- little wheel-load variation
- collapse saftey
- flat-running properties

2. Comfort

- slight roll off hardness, well matched suspension characteristics
- smoothness

3. Economy

- high durability
- low rolling resistance
- low dynamic wheel loads (road load)
- low construction volume (space requirements of wheel houses, spare-wheel recess)
- high load rating

These demands are to be fulfilled individually during selection of suitable tire construction parameter. Ideally, a tire should meet as many of the demands as possible. As constructional possibilities of implementation are partly contradictory, however a compromise must be found, which is appropriate to the tire specification in the vehicles field of duty.

2.2.2 Tire Design

Todays vehilce tires are differentiated to following constructional elements (fig.2.2-2):

-tire bead

-carcass

-sidewall

-tread

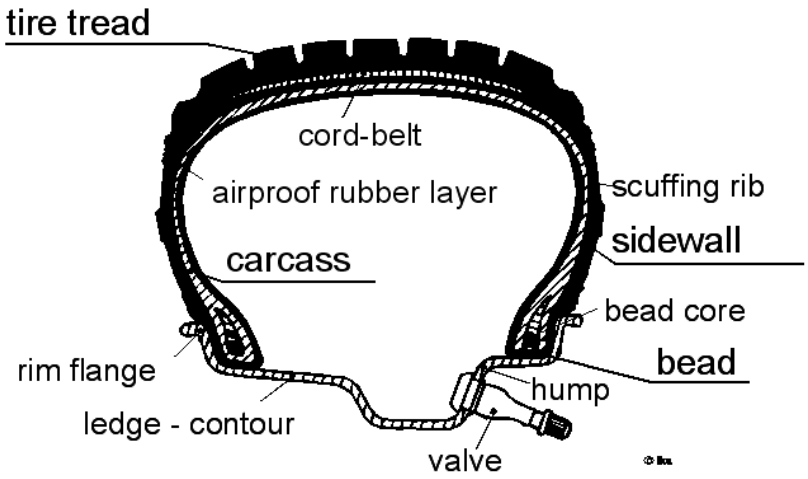

Fig 2.2-2: Section of a tubeless car belted tire

tire bead

The tire beads function is to guarantee fastening of the tire on the rim. In order to preclude a linear expansion of the tire at the rim contour, one or more bead wires are included in the tire bead. In the case of tubeless tires, the tire bead also seals off the locked in air volume towards the environment.

sidewall

The sidewall with it`s scuffing rib is implemented as rubber covering of the carcass reaching from the tire bead to the tread. It serves to protect the layers of the carcass against destruction by external influences.

tread

The tread surrounds the carcass at its outer circumference and maintains the adherent respectively the positive-engaged contact between road and tire. Based on the scope of duties of the tire, rubber mixture and profile of it`s tread are carried out. For example there are rubber mixtures and profiles for summer tire, winter tire and all-season tire differentiated.

carcass

The carcass, which is tightened by the internal pressure, forms the supporting structure of a tire. It consists of several fabric layers which are embedded in rubber without mutual contact. The fabric materials used in the past were cotton, followed by rayon and predominantly Nylon and Polyester today. The casing strength is determined by number and material of the fabric layers. It is indicated by the PR-number (ply rating), which is not necessarily corresponding to the actual number of plies.

The cord angle γ, also designated as the crown angle, is defined as angle between the threads of the fabric plies and the centerline of the tires circumference, Fig 2.2-3.

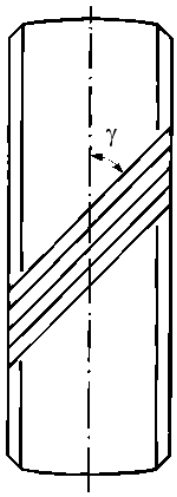

Fig 2.2-3: Definition of cord angle

The cord angles modulus influences the rigidity of the carcass substantially. Furthermore it affects the tire characteristics regarding rolling resistance, suspension characteristics, suitability for high-speed and tire slip rigidity (chap. 2.2.4). The cord angles influence on stiffness of the carcass in principle is shown in Fig. 2.2-4.

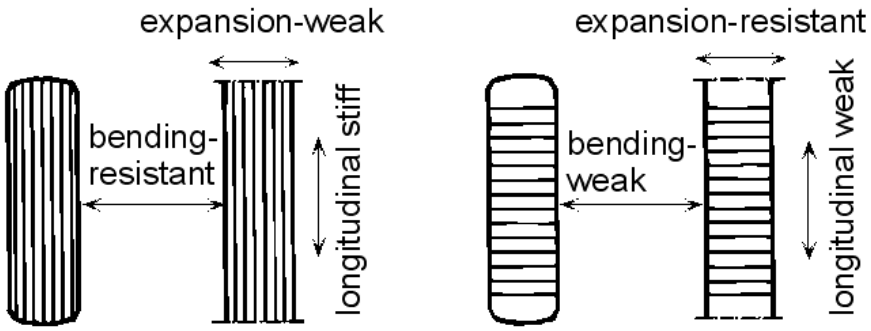

Fig 2.2-4: Influence of the carcasses cord angle /9/

According to /9/ the tire (description on the left) can be wind off for explanation of the cord angles influence and can be contemplated as a simple tube (description on the right).

At a cord angles amount of zero all threads run parallel to the wheels circumference, or in longitudinal direction in case of the tube. Tube length or the tires circumference are given by the threads length. So the tire is rigid in circumferential direction and relatively rigid to transversal forces, while on the other hand an inflation in radial direction is possible.

When taking a look at a cord angle of 90°, the threads are running perpendicular to the wheels circmference. The tube appears to be wound. Blowing up of the tire e.g. due to centrifugal force at high peripheral speeds is prevented, on the other hand expansion in

cirumferential direction of the tire as well as bending from the effect of a transversal force is possible.

In summary the following can be fixed:

Small cord angles:

- rigid tire tread (horizontal)
- soft sidewall (radial)

Large cord angles:

- soft tire tread (horizontal)
- rigid sidewall (radial)

This classification applies approximatley to the comparison of different bias ply tires (s. chapter 2.2.2.1). In case of radial-ply tires this classification cannot be employed (s. chapter 2.2.2.2). Their carcass contains fewer fabric layers, but additional bracing plies, which strongly influence the tire characteristics.

2.2.2.1 Bias Ply Tires

Bias ply tires show diagonally crossed fabric layers in their substructure; resulting from this, the denomination of this tire design is dissipated. At normal tires of this type the cords main direction of the carcass fabric layers intersect the tires circumfernce line at a cord angle of 35° - 38°. In high-speed tire and racing tire the cord angle approximately amounts 26°.

Fig. 2.2-5 shows a bias ply tire with intersecting cords und four layers in it`s substructure. Depending upon the demands on strength, textile fibers or steel cords are used as material for the fabric layers.

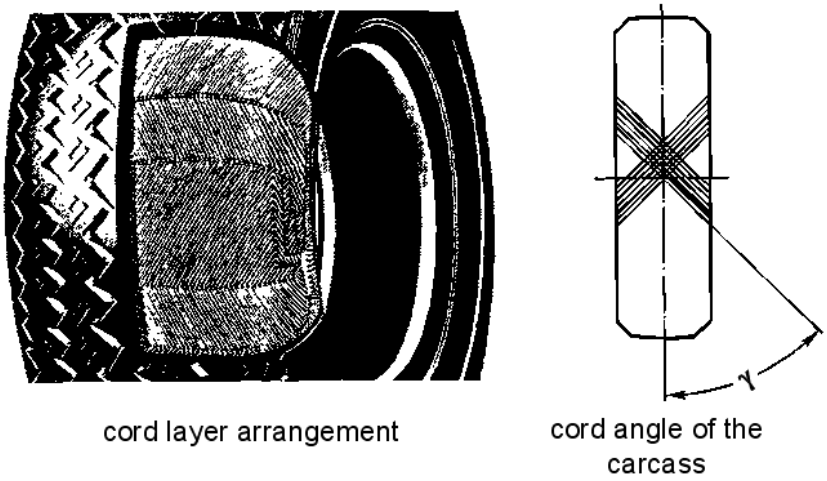

Fig. 2.2-5: Bias ply tire

2.2.2.2 Radial Tires

Radial tires feature a substantially blunt cord angle in the substructure of the carcass, which ammounts between 85° and 90°.

According to this the cords main direction runs radially to the tire, whereon the denomination of this tire design is due to.

Above the layers of the carcasses substructure there are bracing plies in the circumferential direction. Depending on manufacturer and demand materials such as polyester cords, steel cords or other materials such as glass fibre and similar materials are used.

The individual bracing plies show a cord angle from 6° to 20° to the tires circumferential line, fig.2.2–6.

The rotating, only slightly flexible belt,which distorts the substructure, hardens the tread and also is responsible for the flat shape of the tire. This also justifies the fact, that car tires in radial design do not exceed an aspect ratio of 0.82 in general.

Lower weight of the radial-ply tire due to the smaler aspect ratio in comparison to the bias ply tire has a positive effect on riding comfort and driving safety.

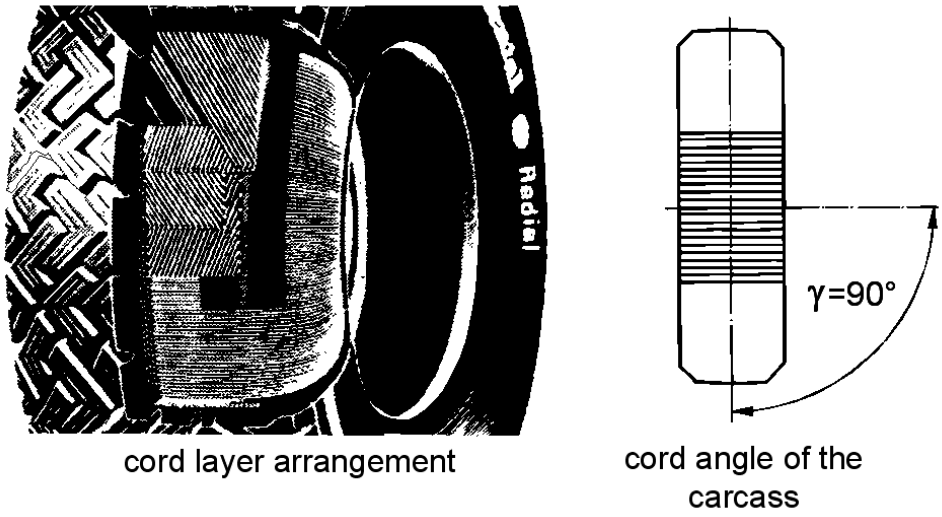

Fig. 2.2-6: Radial-ply tire (belted tire)

The structure of the carcass consiting of substructure and bracing ply allows to optimise the tire characteristics within certain limits independendly from each other.

Radial-ply tires feature fewer fabric layers in their substructure, so there is fewer quantity of rubber in the sidewall as compared to bias ply tires, by what the radial rigidity of the carcass is reduced. Rigidity of the tread obviously increases by using bracing plies. Due to the uniform distribution of pressure at the center of tire contact, fig.2.2-7, the usable friction coefficient is higher, i.e. larger peripheral forces and lateral forces can be transmitted between tire and lane.

Less rigid sidewalls implicate a smaller conversion of deformation energy into heat during the radial tire deflection while rolling. Higher rigidity of the tread causes flexing energy in the area of the tread to be lower also. Conditional on lower rolling-resistance power operating temperatures of the radial-ply tire are lower than operating temperatures of the bias ply tire under similar conditions. Thus high-speed stability is better and reachable performance is higher.

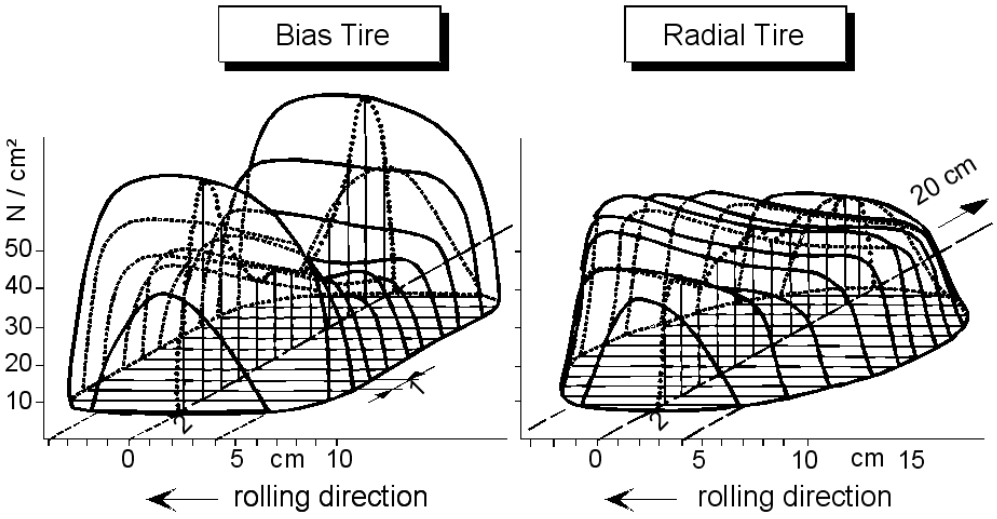

Fig. 2.2-7: Pressure distribution in the contact area of straight ahead rolling tires of different designs / 15 /

2.2.3 Force Transmission in circumferential Direction

Contact surface of the tire with the road is called tire contact area. Here the physical and chemical processes, which enable force transmission take place. Power transmission can result from adhesion and positive engagement.

- Adhesion: Adhesion in the contact surface between road and tire.

- Positive Engagement: toothing between tire and road surface by intrusion of irregularity (e.g. granulation of road surface) into tire rubber or by intrusion of a plastic track (terrain) into tread pattern.

According to the classical law of friction (Coulomb) the maximum force transferred in the tire contact area is commensurate with the wheel load. The factor of proportanality between frictional force F_R and wheel load G_R is called frictional coefficient μ:

$$F_R = \mu \cdot G_R \qquad (2.2-1)$$

This relationship only applies to the combination of available material (e.g. concrete-rubber), if the traction coefficient μ is assumed as addicted variable to a set of influencing factors.

Due to the elastic characteristics of rubber material in the tread circumferential forces can be transferred only in combination with rotational slip, i.e. a speed differential between the wheel circumferential speed v_R and driving speed v.

Usually the following definitions of rotational slip are used for acceleration and braking, which result in positive values for $1 \geq \lambda \geq 0$.

$$\lambda_A = \frac{r_{dyn} \cdot \omega_w - v}{r_{dyn} \cdot \omega_w} \qquad (v \geq 0,\ \omega_w \geq 0,\ r_{dyn} \cdot \omega_W \geq v) \qquad (2.2\text{–}2)$$

$$\lambda_B = \frac{v - r_{dyn} \cdot \omega_w}{v} \qquad (v \geq 0,\ \omega_W \geq 0,\ r_{dyn} \cdot \omega_W \leq v) \qquad (2.2\text{–}3)$$

Fig.2.2-8 shows the relationship between rotational slip and utilized adhesion for the transfer of circumferential force on different roadway surfaces / 33 /.

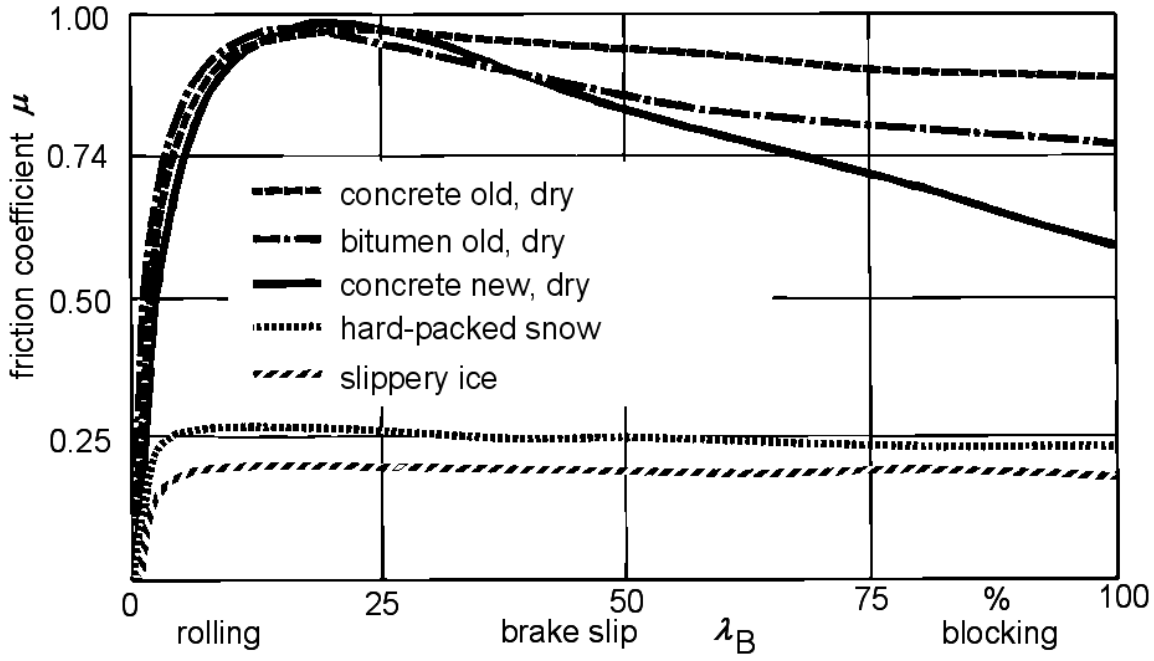

Fig.2.2-8: Relationship between rotational slip and friction coefficient for circumferential forces acting on a pneumatic tire

On antiskid roadways the utilized friction coefficient initially rises with increasing slip up to a maximum value and then declines to the sliding coefficient at a slip of 100%. On slippery roadways the maximum friction coefficient and the sliding coefficient only differ marginally from each other.

The relationship between rotational slip and frictional coefficient for circumferential direction depends not only on condition of the roadway surface, but also on condition of the tire.

In addition to tire design (see above) the tread layout is significant too. Task of the tire tread is to maintain contact between road and tire in case of contamination or wetness. In the following the influence of tread pattern on friction coefficient μ with dry or wet lane is going to be discussed.

Influence of tread on the friction coefficient μ on dry roadways:

Experiments show that transferable forces rise with decreasing tread depth and driving speed on clean, dry roadways, fig.2.2-9.

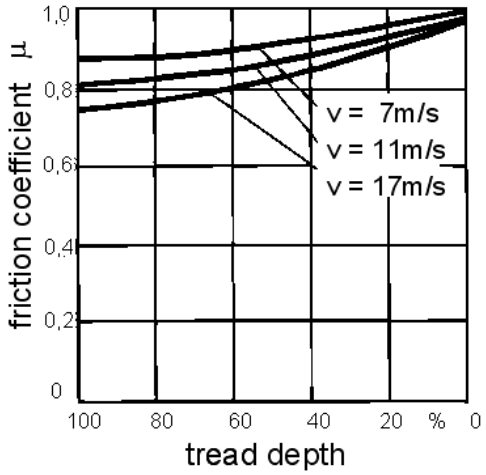

Fig.2.2-9: Friction coefficient as a function of driving speed and tread depth on dry roadways

A possible explanation can be seen in the fact that decreasing tread depth causes the surface pressure to be spread equably on the surface of the individual tire profile elements. So the total amount of sheer stress on the entire tire-contact length results in a higher grip. A smaller driving speed has a similar effect because centrifugal forces which cause a upwards warpage of the tread become smaller. So the road-contact area of the tire becomes marginally larger at the same total load. In the case of radial tires upwards warpage of the contact surface is widely prevented by the bracing ply.

Influence of tread on the friction coefficient μ on wet roadways:

The tire tread enables road contact on wet roadways by displacing liquid. The tread pattern of the tire has to take up a part of water or displace it from the area of road contact. The water volume displaced is commensurate to the velocity v and the film thickness of the water z_F.

$$\dot{Q} \sim v \cdot z_F \qquad (2.2\text{-}4)$$

Increasing driving speed reduces the time used to produce road contact. A wedge of water is formed between tire and road , which invades the tire contact at increasing velocity and reduces the contact surface between tire and road, fig.2.2-10.

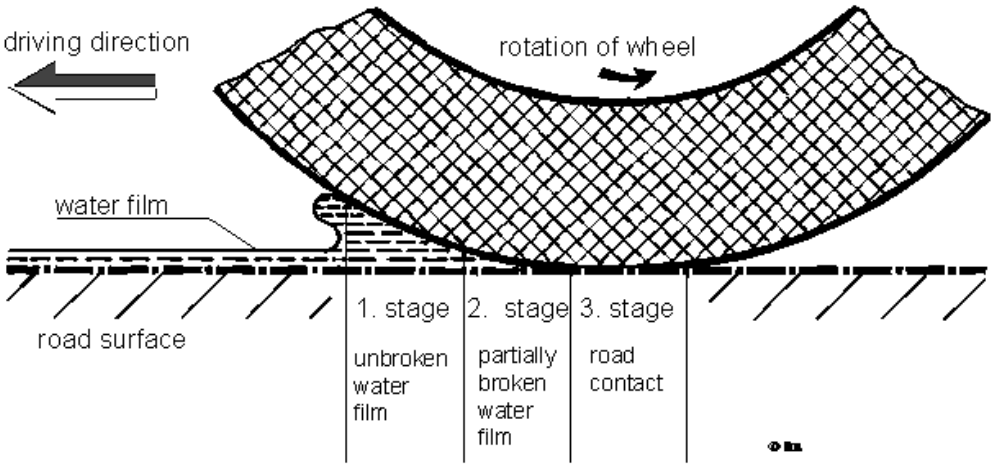

Fig.2.2-10: Displacement of a water film from the contact area between tires and roadway

The transferable horizontal forces in the tire contact area fall, since a part of the wheel load is transferred in vertical direction, similar to a hydrodynamic bearing. Only the remaining part in conjunktion with the locally usable friction coeficient contributes to the transfer in horizontal direction. The phenomenon of total buoying upwards on the water wedge is called „aquaplaning“.

In Fig 2.2–11 the dependence of the maximal friction coefficient for braking from driving speed and level of the water film by the example of a steel-belted tire (measurement on inner drum test bench) is shown. Fig.2.2 –12 shows the influence of tread depth.

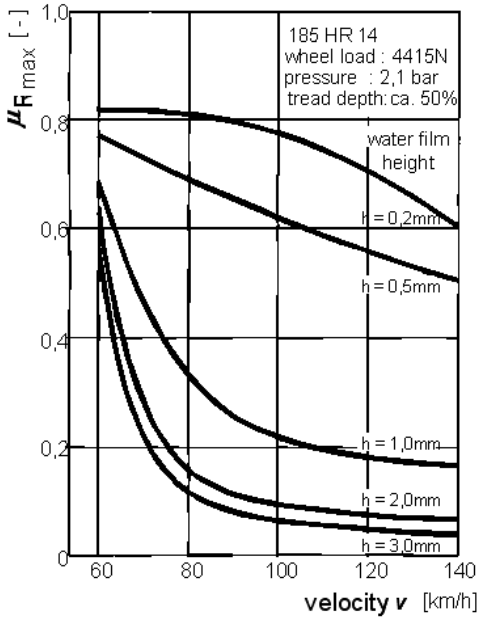

Fig.2.2-11: Friction coefficient for braking force as a funciton of driving speed and water film height on the roadway / 16 /

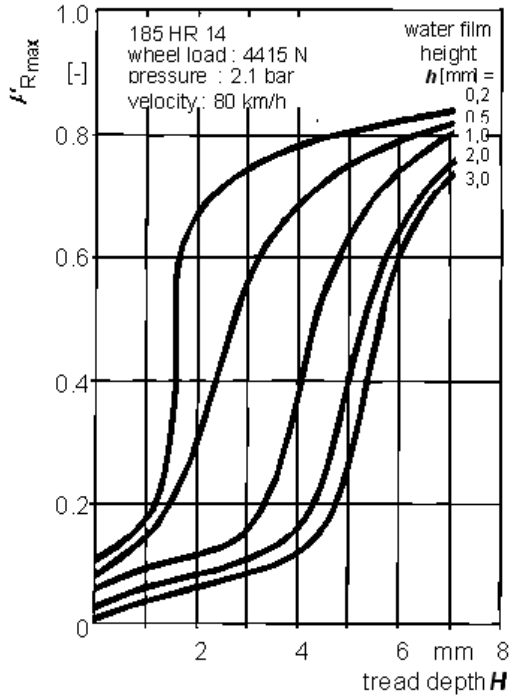

Fig 2.2-12: Friction coefficient for braking force as a funciton of tread depth and water film height on the roadway / 16 /

In progression of the development of motor vehicle, the demand on load-carrying capacity and power transmission characteristics of the tires constantly rose. The development of tires with larger width and reduced aspect ratio (Fig 2.2-13) allows a reduction of tire diameter at a matchable load-carrying capacity.

$$x = \frac{h_{tire}}{w_{tire}} \cdot 100\%$$

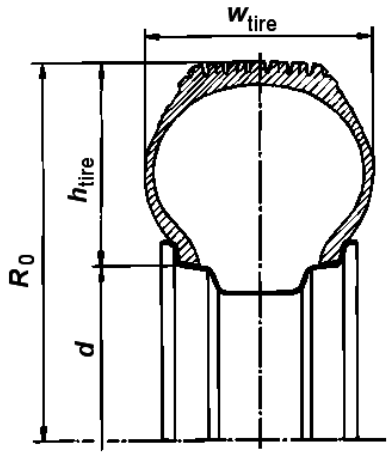

(aspect ratio)

Fig.2.2-13: Aspect ratio

Even after introduction of radial-ply tires at the beginning of the 60`s the trend towards a reduced aspect ratio has remained. However not in connection with smaller outside diameters today, but larger rim diameters, which facilitates the accommodation of high-performance wheel brakes.

Smaller aspect ratios offer the advantage of uniform and smaller surface pressure in the tire contact area by the larger footprint. With it they enable a better power transmission between tread and roadway.

Furthermore the vehicles appearance resulting of small ground clearance of the body corresponds to a modern sense of styling.

Disadvantages of wider tires are the increased danger of aquaplaning on wet roads as well as reduced damping properties and suspension properties. As better power transmission in the tire contact area improves the driving performances of a vehicle substantially, the disadvantages of these tires are either accepted (e.g. renunciation on comfort in favor of better driving performance at sports cars) or by additional measures as far as possible reduced (e.g. specific design of the tire tread for reduction of the danger of aquaplaning).

2.2.4 Force Transmission in Lateral Direction

2.2.4.1 Lateral Forces and aligning Torque by Tire Slip

A rolling wheel exclusively moves under the influence of circumferential forces towards the intersecting straight line of wheel plane and roadway plane. If a lateral force is acting on the wheel, a angle is formed between the direction of movement of the wheel and this intersecting straight line. This angle is called the slip angle α, fig.2.2-14.

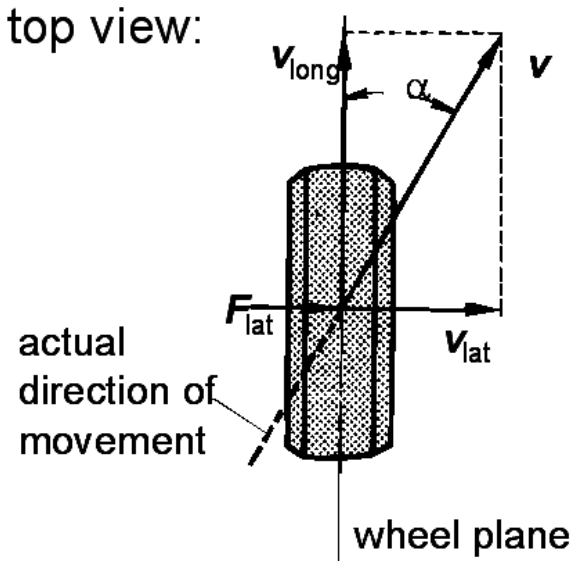

Fig.2.2-14: Definition „slip angle“

The reason for tire slip is a continuous lateral deflection of the rolling tire in the range of the tire contact area under the effect of the lateral force transferred between tire and roadway.

Only by this deflection of the elastic tire material shear stresses, which are necessary for transferring the lateral force, can be established in the tire contact area. In analogy to rotational slip the tire slip is also called transversal slip. A detailed illustration of tire deformation when transferring side forces is possible on the basis of fig.2.2-15.

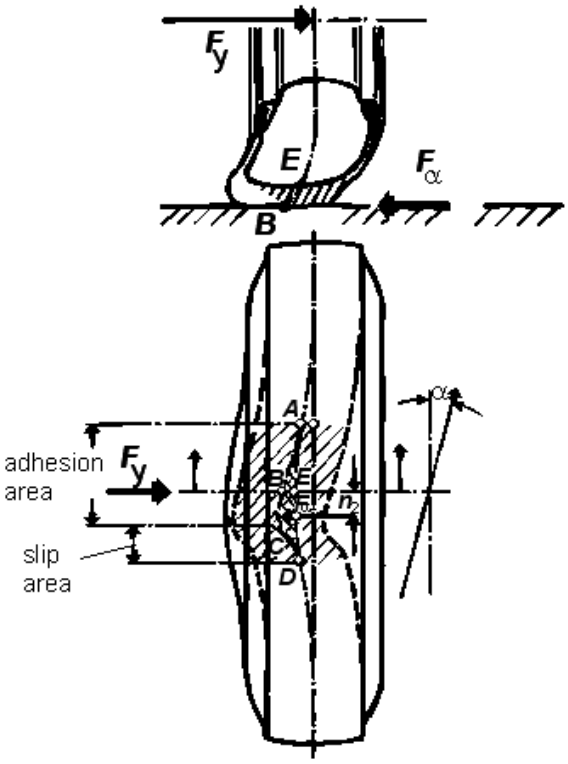

Fig.2.2-15: Deflection of the rolling tire by a lateral force F_y

The non–deflected part of a rotating tire is deformed gradually while contact between tire surface and road is set, as represented in fig.2.2-15 (upper picture).

In the tire contact area the equator of the tire body is moved from the wheel plane into the position AED (fig.2.2-15, lower picture). The circumference of the tread in the tire contact area comes into contact with the ground along the line ABCD and is increasingly deformed in the course from A to C. Here the friction coefficient between rubber and road is sufficiently large, in order to prevent a resilience of the rubber. Next to C the deflection by shear stress is that large that grip on the road is exceeded and slipping back to D takes place.

The line AC runs at an angle to the wheel plane. It shows the direction of movement of the wheel, since the surface of the tire adheres to the road within the area of this line. The angle between wheel plane and the line AC is identical to the slip angle α.

The surface included between the lines AED and ABCD is a measure for shear deformation of the crown rubber compared to the tire body and for the local distribution of shear forces in the tire contact area. The total ammount of shear forces result in the cornering force F_α.

As this force acts in the center of gravity of the surface, about caster n_2 behind the wheel center, a aligning torque M_α results:

$$M_\alpha = F_\alpha \cdot n_2 \qquad (2.2\text{-}5)$$

The relationship between slip angle α and cornering force F_α depends on a multiplicity of parameters. In particular the wheel load G_W has a large influence on size of the cornering force at constant slip. Fig.2.2-16 indicates a corresponding tire performance map for a PC tire. It was determined on a test bench.

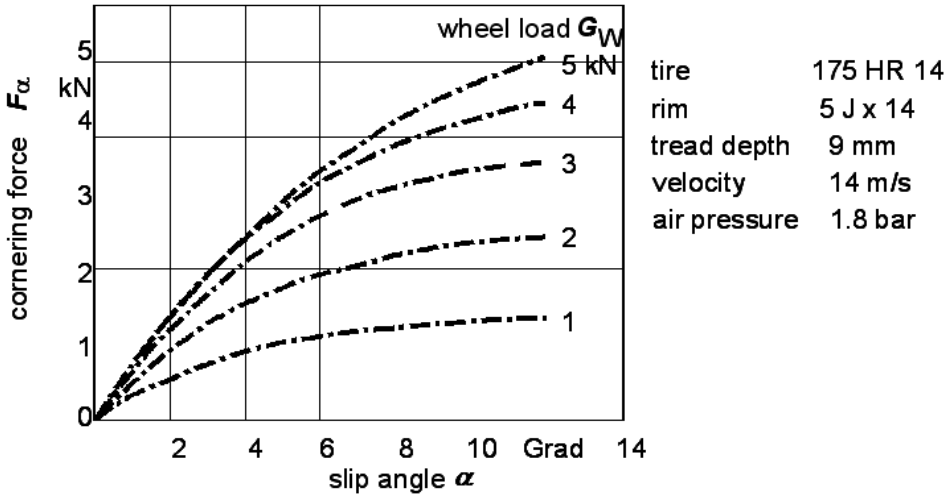

Fig.2.2-16: Cornering force subject to the slip angle (wheel load as a parameter)

With another illustration of this diagram, fig.2.2-17, it becomes clear that not only the relationship between F_α and α at a constant G_W shows a degressive distribution, but also the dependence between F_α and G_W at α=const. features a degressive trend.

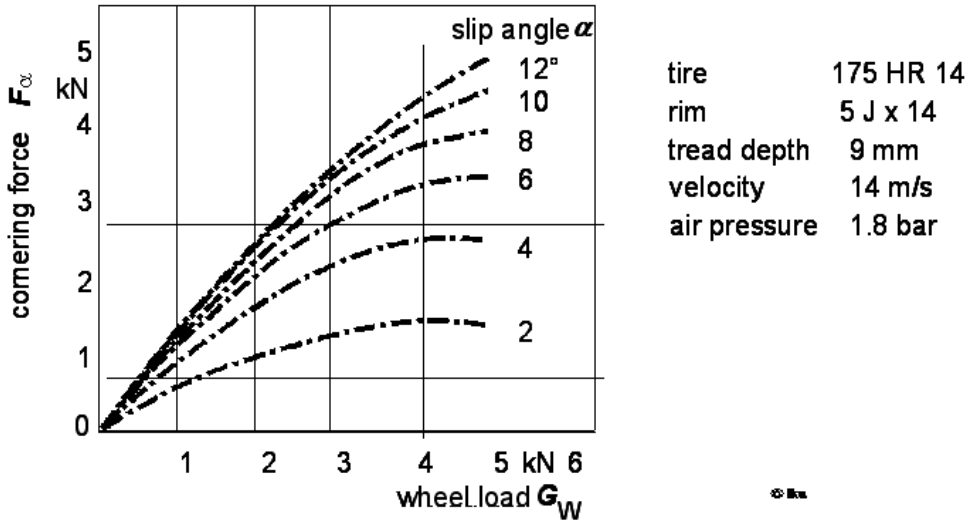

Fig.2.2-17: Cornering force subject to the wheel load (slip angle as a parameter)

Influence of the tire inflation pressure on the transmission behavior of lateral forces of the exemplary tire is shown in Fig2.2-18. The measured values of the cornering force indicate maximum values for a certain air pressure, for which the tire design is optimized.

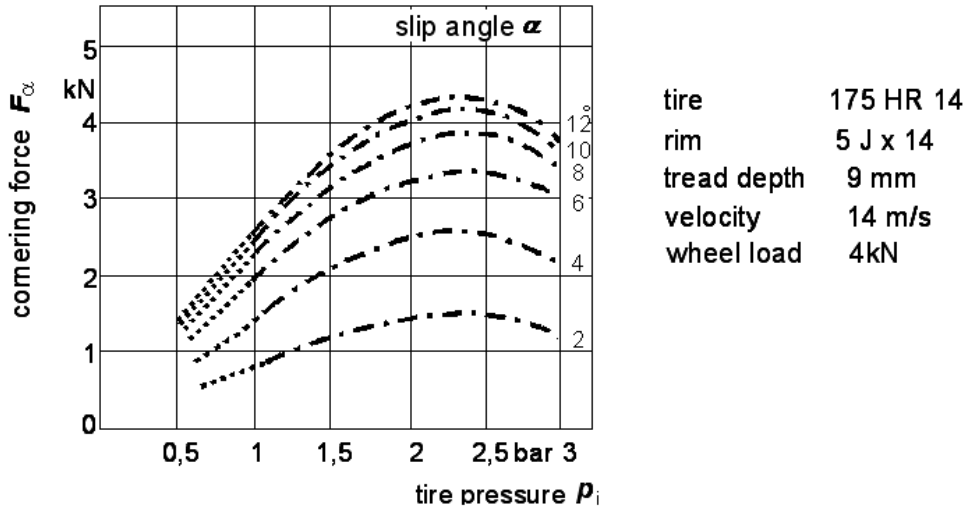

Fig.2.2-18: Cornering force subject to the tire inflation pressure (slip angle as a parameter)

Fig.2.2-19 shows the tire performance map for aligning torques. The size of aligning torques depend on the particular magnitude respective specification of adhesion and sliding in the tire contact area (s.fig. 2.2-15).

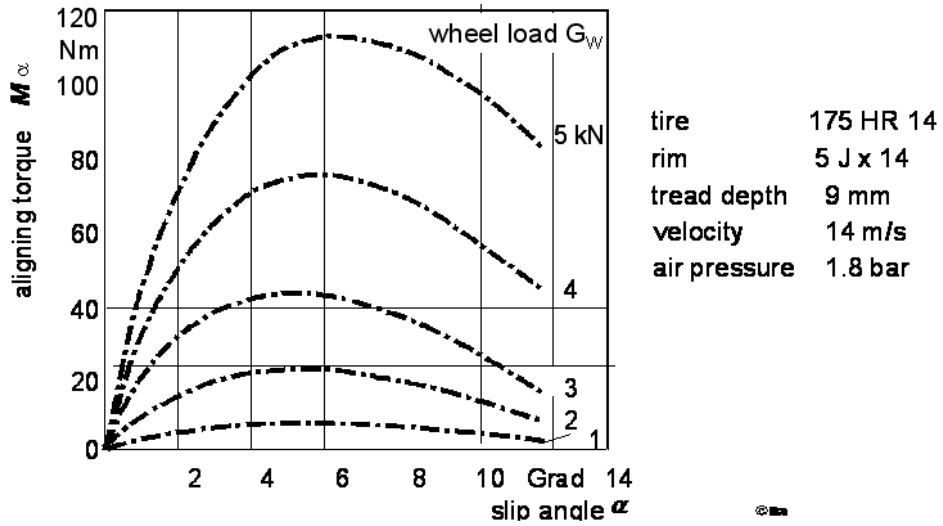

Fig.2.2-19: Aligning torques M_α subject to the slip angle (wheel load as a parameter)

A recapitulatory representation of side force characteristics and aligning torque characteristics of a tire displays the so called GOUGH diagram, fig.2.2-20. In a characteristic operating point of the tire specified by the current wheel load G_w and the current slip angle α the resulting lateral force as well as the aligning torque and the tire caster n_2 can be read off here (cp.fig.2.2-15).

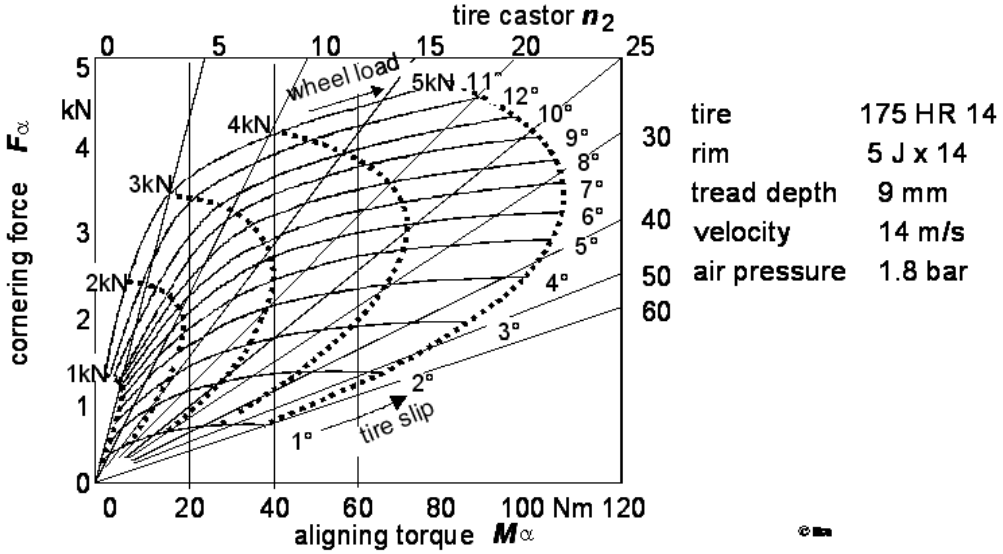

Fig.2.2-20: Tire performance map by GOUGH /19

2.2.4.2 Lateral Forces and aligning Torques generated by Wheel Camber

The camber angle γ is defined as the angle between the wheel plane and the normal of the roadway in the transversal plane of the automobile. One differentiates between positive and negative camber, fig.2.2-21.

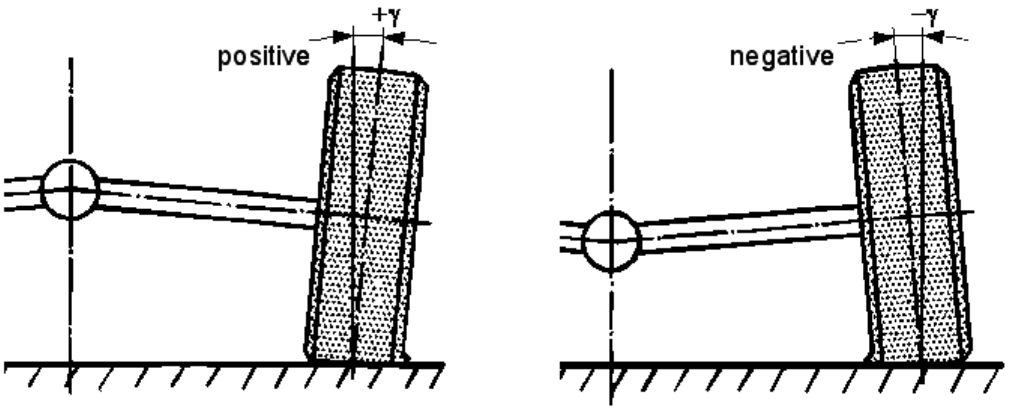

Fig.2.2-21 : Definition wheel camber

A freely rolling wheel running under camber would be moving on a circular path around the center of the trajectory 0. Because of the wheel suspension the wheel is forced to straight-ahead driving. Thereby the camber force F_γ and a camber torque M_γ is developed, fig.2.2-22.

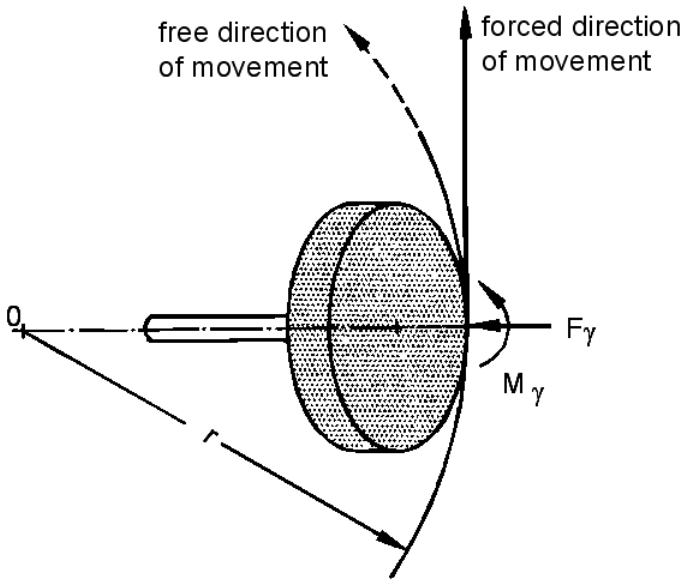

Fig.2.2-22 : camber force F_γ and camber torque M_γ

The value of the camber force F_γ increases approximately linear with the camber angle up to a camber angle of γ=10° at a constant wheel load. At a constant camber angle the camber force changes commensurate with the wheel load. As to gather from fig.2.2-23, the forces and torques resulting from wheel camber are very small compared to those, which are caused by tire slip.

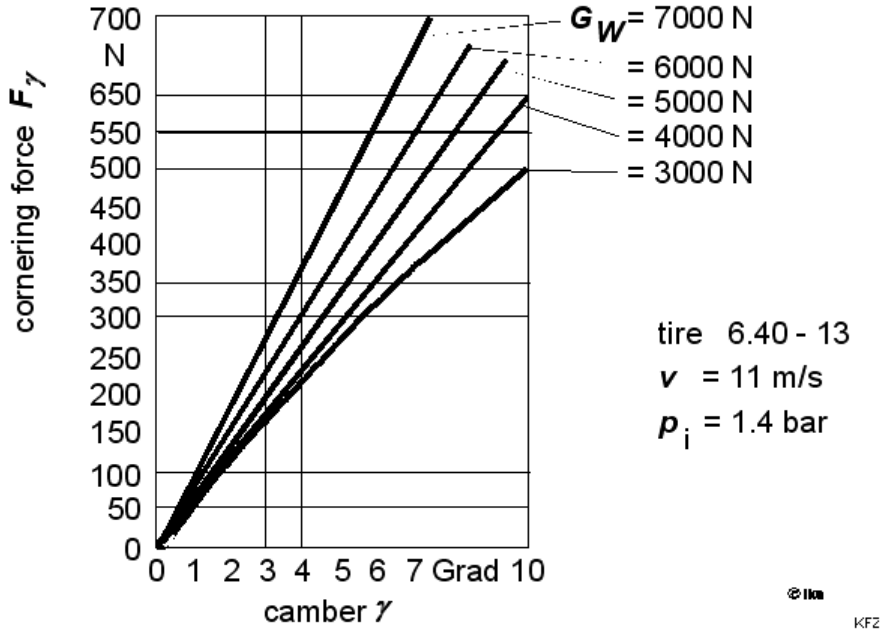

Fig.2.2-23: Cornering force F_γ subject to the camber angle for different wheel loads

2.2.5 Superposition of lateral Forces and circumferential Forces

In service circumferential forces and lateral forces are usually transferred simultaneously from the tire to the roadway.

In fig. 2.2-24 the resulting lateral force F_α subject to the simultaneous driving power and braking power forced upon the wheel is represented for different slip angles α. The characteristic map was recorded on a tire test bench.

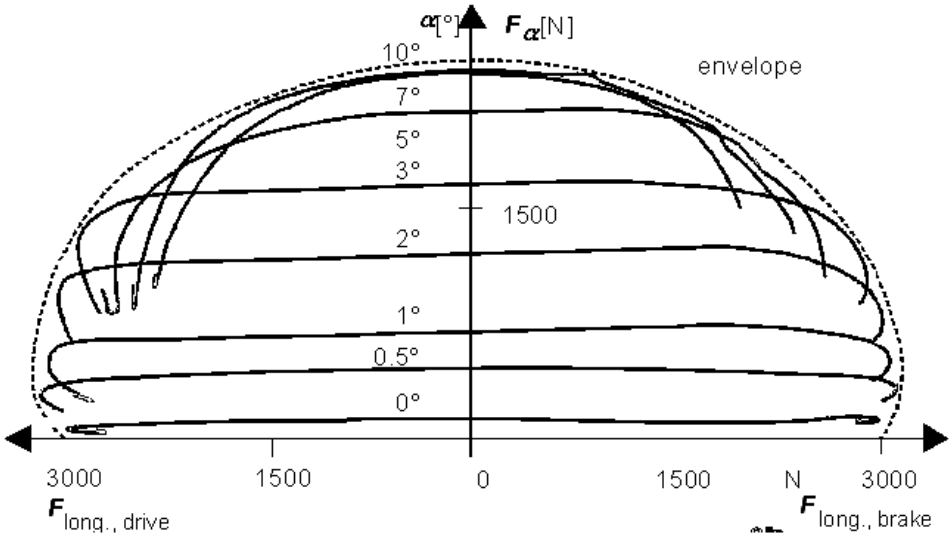

Fig.2.2-24: Characteristic map for lateral force, traction (Krempel graph) / 26 /, tire 165 SR 15, tread 60 %, Rim 4 x 15, G_W = 3000 N, p_i = 1.8 bar, v = 14 m/s

By means of the envelope it should be made clear, that the maximal transmittable lateral force F_α gets smaller, all the more larger the circumferential force F_c is respectively the maximal admissible circumferential force F_c must become smaller, the larger the lateral Force F_α required for tracking is.

The curves of constant tire slip α indicate particularly for the larger tire slip angles a decrease of the cornering force at increasing circumferential force F_u, i.e. with increasing rotational slip λ.

The functional relationship of the Krempel-chart is described in the following:

With the rotational slip λ as a parameter the tire performance map as shown in fig 2.2-25 top right is received. Its characteristic line at $\lambda = 0$ corresponds with the illustration in fig.2.2-16, but continues in the range of larger tire slip angles.

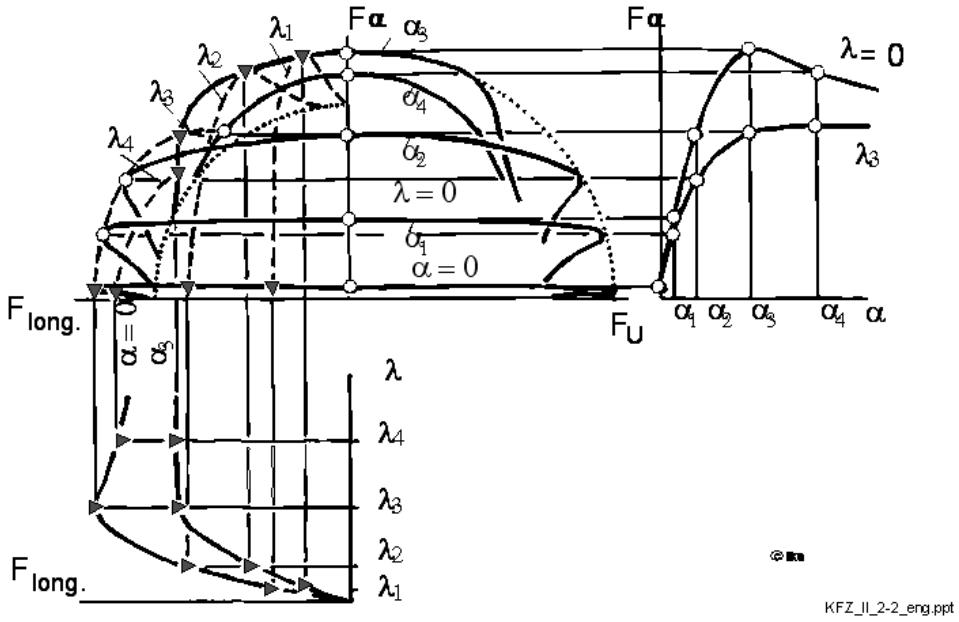

Fig.2.2-25: Superposition of tire forces, lateral forces and peripheral forces / 41 /

At the beginning of paragraph 2.2.4.1 it was already mentioned that tire slip in analogy to rotational slip can also be understood as transversal slip. Therewith for the relationship between rotational slip λ and peripheral force F_U with the tire slip α as a parameter a corresponding representation to the field top right in the field at the lower left is received, fig.2.2-25.

If both fields are transferred into one diagram, which represents the lateral force as a function of the peripheral force in turn, it becomes clear where the shape of the curves of constant tire slip with their undercuts in fig.2.2-24 results from. The curves initially tangent to the envelope with increasing rotational slip and huddle against the inner ellipse of sliding friction with further increase of slip. In fig. 2.2-25 curves of constant slip λ are alluded in analogy. They

hint at the formal equivalence of rotational slip and tire slip respectively transversal slip and the regularities of the superposition once more. Another representation of the relationship between lateral forces and peripheral forces is shown in fig. 2.2-26. Here a characteristic map of lateral force and traction is indicated as a function of the rotational slip λ_B. It is interesting e.g. with regard to the design of brake-power regulators (ABS).

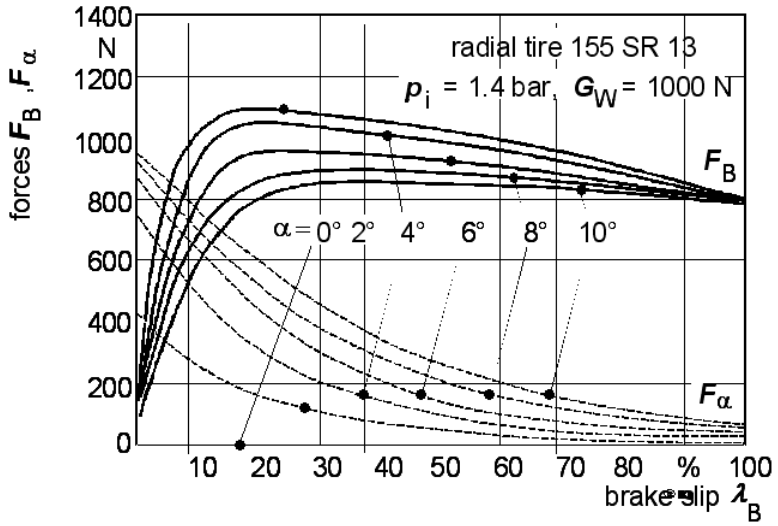

Fig.2.2-26: Lateral force – traction map subject to the brake slip λ_B

2.2.6 Transient Tire Behavior

Tire characteristics described in the preceding paragraph strictly speaking only obtain to stationary conditions respectively very slow temporal modifications of the contemplated influencing variables.

As a result of the nonlinearity of the tire characteristics and the breaking-in process in the tire contact area at changes of the operating parameters the tire characteristics vary from the relationships described by the characteristic map at normal (transient) driving.

Fig.2.2-27 displays the influence of nonlinearity in temporally varied operating point parameters by example of a harmonic wheel load fluctuation.

Fig.2.2-27: Determination of the quasi-static loss of lateral force and changes of the aligning torque as a result of harmonic wheel load fluctuations on the basis of static characteristic lines (PC-tires 185/70 R 14, p_i = 2 bar, v = 20 km/h) / 27 // 43 /

Due to the degressive F_y-F_z-trend the mean lateral forces are smaller with wheel load fluctuations than the static values are. In case of the aligning torque M_z a magnification compared to the static amounts is incidental because of the usually progressive M_z-F_z-lines.

The influence of the breaking-in processes in the tire contact area by the example of a harmonic modification in the slip angle is shown in Fig.2.2-28. With increasing steering frequency a hysteresis loop is formed at first, which results from a phase shift between tire slip angle (steering angle) and lateral force. With further increasing steering frequency the maximum of the slip angle passes through so quickly, that the lateral force achieves only a part of the maximum value at low steering frequency.

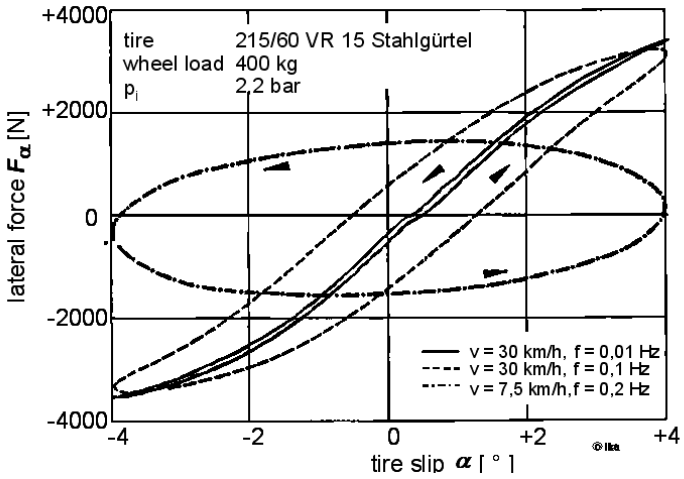

Fig.2.2-28: Lateral forces as a function of slip at sinusoidal excitation for slip behalf different velocities and frequencies

The breaking-in processes in the tire contact area take place faster with cumulative wheel speed. According to this the phase shift between slip angle and lateral force as well as the weakening of amplitude of the lateral force at a constant steering frequency becomes smaller with increasing driving speed, fig.2.2-29 respectively fig.2.2-30.

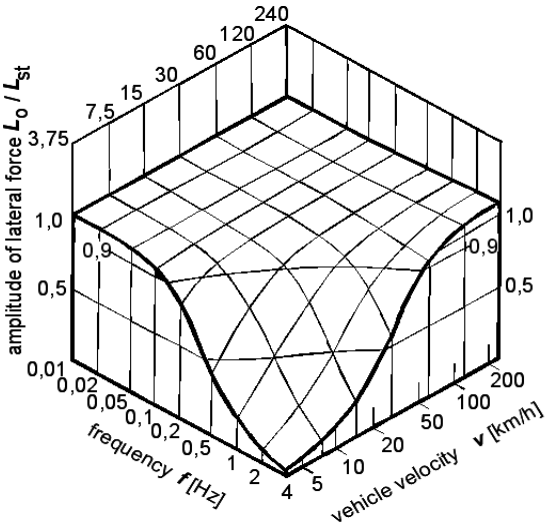

Fig. 2.2-29: Amplitude, frequency and velocity (215/60 VR 15, amplitude of slip 1°, F_R = 400 kg , p_i = 2.2 bar)

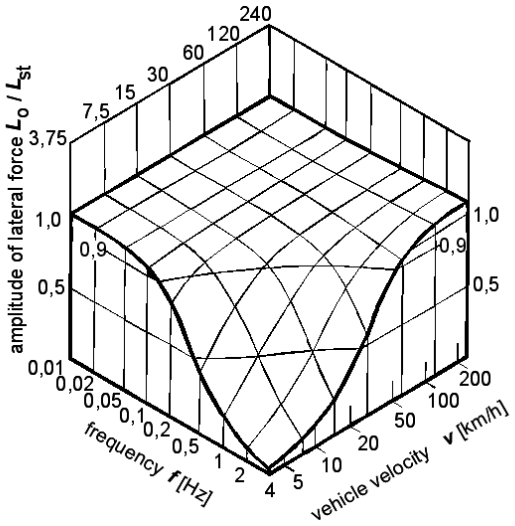

Fig. 2.2-30: Phase angle, frequency and velocity in spatial representation (tire data like fig. 2,2-29) / 42 /

For theoretical investigations on driving dynamics of motor vehicles with the aid of mathematical simulation models, the tire characteristics are often represented in the form of characteristic maps for stationary operating states. The temporal behavior is simulated by dint of delay elements. Exemplary, the approach developed by Böhm is presented / 45 /:

$$F_\alpha + \frac{c_\alpha}{v \cdot c_{Ly}} \cdot \frac{dF_\alpha}{dt} = c_\alpha \cdot \alpha \qquad (2.2-6)$$

With: F_α = cornering force

c_α = stiffness of tire slip

α = slip angle

v = driving speed

c_{Ly} = transversal stiffness of the tire contact area in relation to the rim

Beyond the linear formulation the model considers a transversal displacement of the tire contact area on the rim. Thus different slip angles for rim and tire contact area on the roadway result in the non-stationary instance. In the stationary case they correspond with each other again ($dF_\alpha/dt = 0$).

Another transient tire model is the Schlippe/Dietrich modell. It tolerates not only a transversal motion as a dynamic degree of freedom, but also the rotation of the tire contact area in relation to the rim / to 45 /:

$$F_\alpha + \frac{c_\alpha}{v \cdot c_{Ly}} \cdot \frac{dF_\alpha}{dt} = c_\alpha \cdot \alpha \; - \; \frac{c_\alpha \cdot r_{Lx}}{v} \cdot \frac{d\alpha}{dt} \qquad (2.2\text{-}7)$$

With: r_{Lx} = half tire-contact length of the tire

With the aid of the software tool MATLAB simulated frequency progression functions for the formulations according to Böhm and Schlippe/Dietrich are shown in fig. 2.2-31.

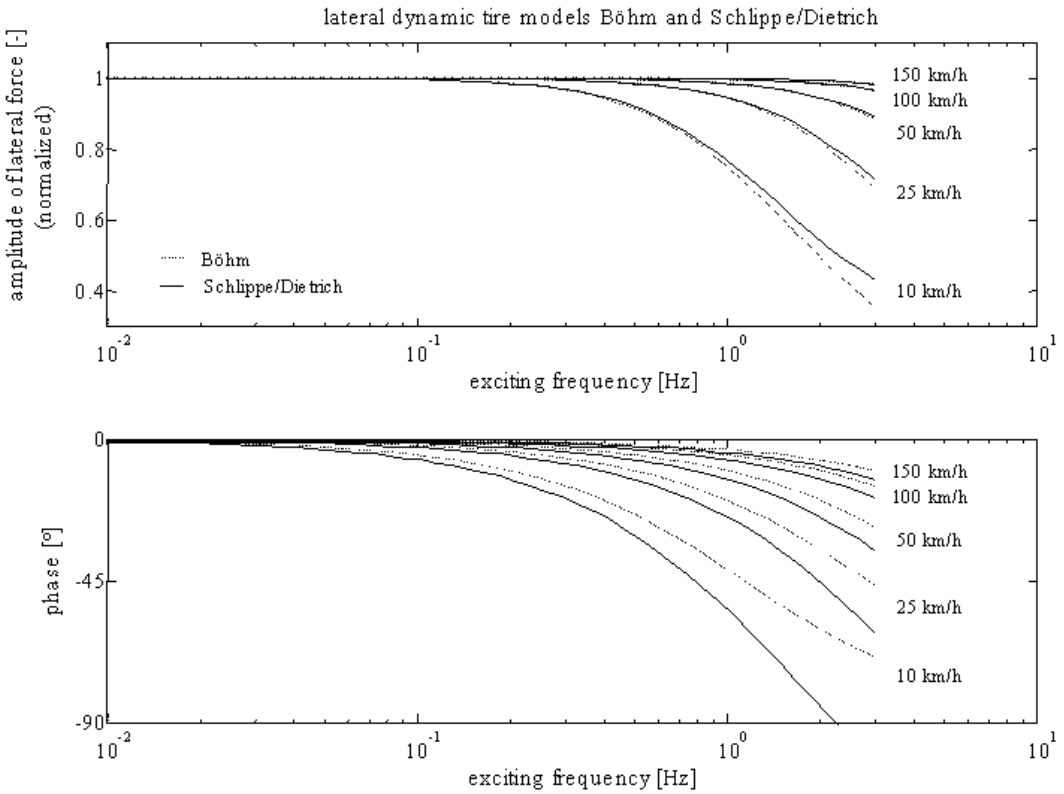

Fig.2.2-31: Tire behavior of transient tire models for the variation of driving speed

Differences in the ideas of the models can obviously be located in the phase responses. As a result of the rate action element ($Tv = c_\alpha \, r_{Lx}/v$, s.eq. 2.2-7) precise larger phase lags at decreasing driving speed are indicated in the model formulation according to Schlippe/Dietrich than in the Böhm model. The amplitude responses show an almost identical characteristic.

Consecutively the influence of the parameters tire-contact length (r_{Lx}) and the transversal stiffness between the tire contact area and the rim (c_{Ly}) for the more realistic formulation of the Schlippe/Dietrich model are presented in fig.2.2-32.

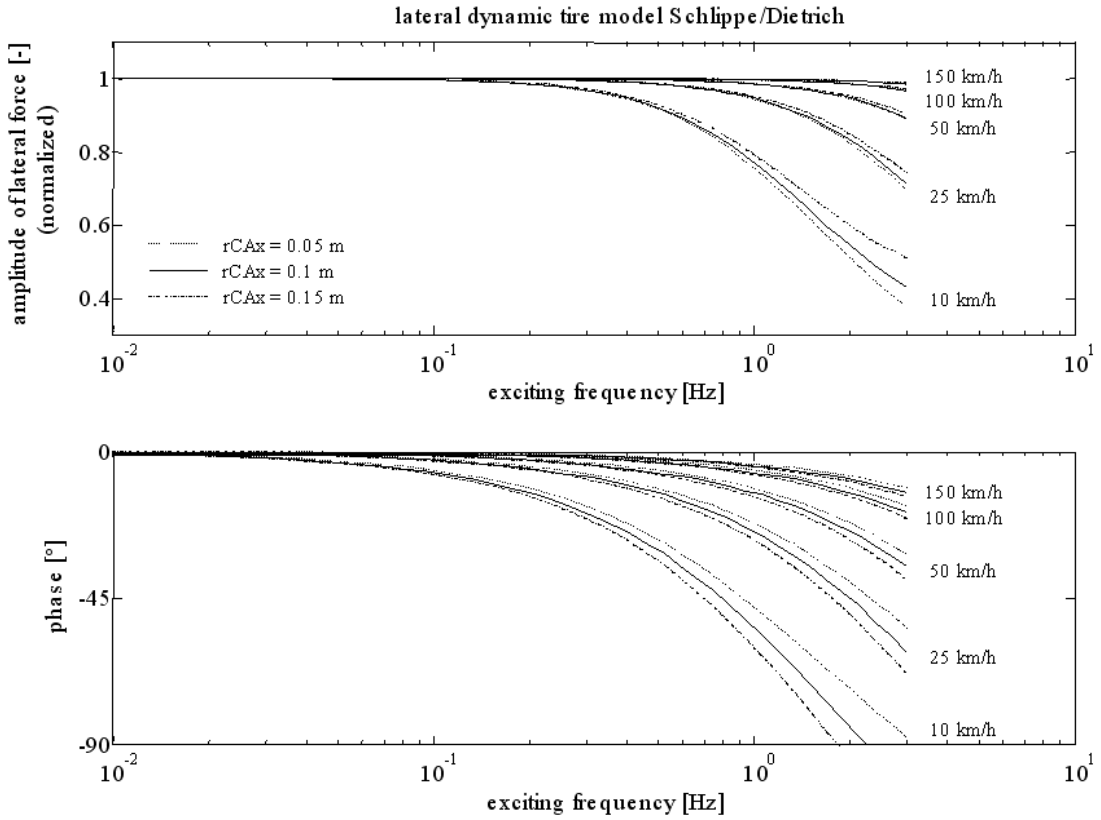

Fig.2.2-32: Transient tire behavior

2.3 Single Track Vehicle Model

To understand the driving dynamics of motor vehicles, theoretical knowledge of the mechanics of the vehicle movement is a prerequisite.

Theoretical investigations of driving dynamics are usually executed today by simulation programs, for which a very complex mechanical back-up model is the basis for further discussion.

However, for the representation of the basic connections of the driving dynamics, simplified vehicle models are better suitable, since the number of degrees of freedom which can be considered remain easy to survey.

A simplified description of the vehicle lateral dynamics is possible with the help of the single track vehicle model as shown in Fig 2.3-1 .

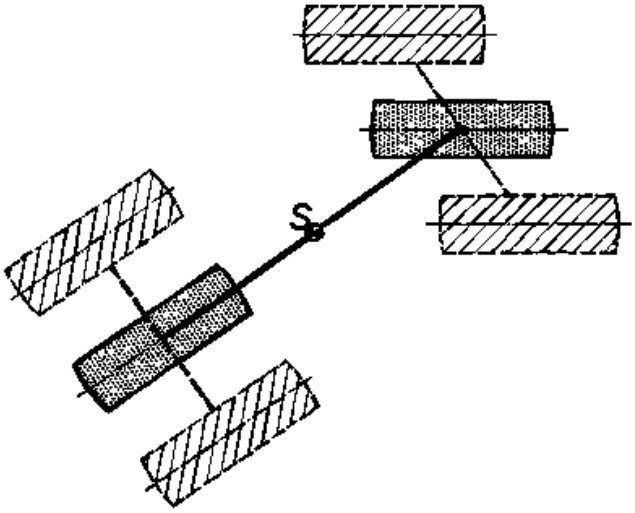

Fig 2.3-1: Single Track vehicle model

The tire contact points, where the tire is hold in position by the lateral forces is summarized axle-wise. Longitudinal forces in the tire contact point as well as wheel load fluctuations, are not considered. The height of the center of gravity is zero..

For analytical considerations the motion equations for the single track model are linearized, i.e. only small angles with sin α~ α and cosα~1 are considered and a linear tire behavior is assumed.

The linearization of the tire characteristics results via declaration of a tire slip stiffness C_α which characterizes the connection between the tire lateral force and the tire side slip angle α with at constant wheel load:

$$c_\alpha = \frac{F_\alpha}{\alpha} \qquad (2.3\text{-}1)$$

This linearization can be regarded as suffice exact with car tire side slip angles up to 3°, because thereafter the errors become excessive due to the degressive characteristic line. The side slip rigidity not only depends on the wheel load and the inflation pressure, but to a large extent also on the type of tire, Fig 2.3-2.

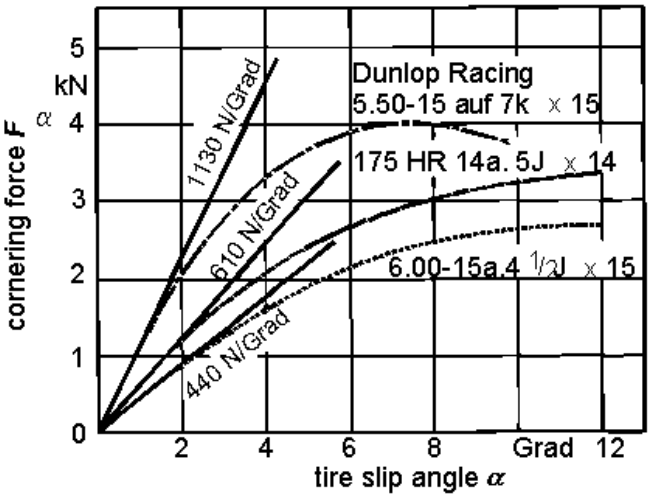

Fig 2.3-2: Linearized Side Slip rigidity Cα for different tires

Despite of simplification, the Single Track vehicle model is suitable not only for obtaining a view of fundamental relations of the driving dynamics but also provides useful results regarding trend estimations for the influence of individual vehicle parameters such as wheel base, weight distribution and tire characteristics.

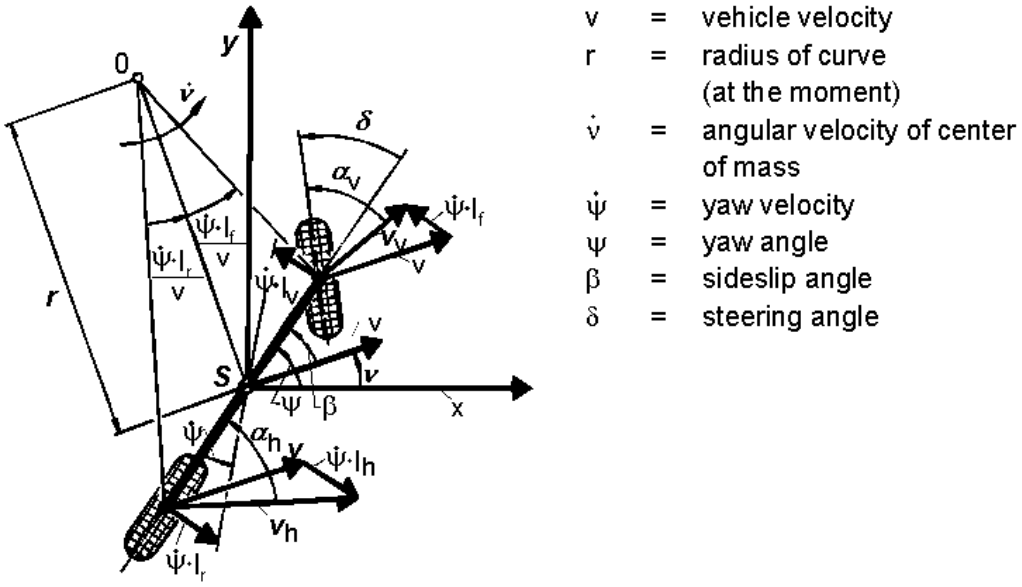

Fig 2.3-3: Single Track vehicle model

1.Newton' equation of motion for the vehicle lateral direction:

$$m \cdot a_y = F_{sf} + F_{sr} \qquad (2.3\text{-}2)$$

2. Gyroscopic effect about the z-axis at the vehicle´s center of gravity

$$\theta \cdot \ddot{\psi} = F_{sf} \cdot l_f - F_{sr} \cdot l_r \qquad (2.3\text{-}3)$$

The force of inertia acting in the vehicle center of gravity $m \cdot a_y$ corresponds to the centrifugal force resulting from the momentary road curvature:

$$m \cdot a_y = m \cdot \frac{v^2}{r} = m \cdot \frac{v}{r} \cdot \dot{\nu} \cdot r = m \cdot v \cdot (\dot{\psi} - \dot{\beta}) \qquad (2.3\text{-}4)$$

with: v = driving speed

r = course radius (momentary)

$\dot{\nu}$ = course angular speed of the movement of the vehicle´s center of gravity

$\dot{\psi}$ = yaw velocity (angular speed of the vehicle around the Z-axis)

$\dot{\beta}$ =side slip angle speed (angular change between speed vector in the vehicle center of gravity and vehicle longitudinal axis)

For the tire side forces valid:

$$F_{sf} = c_{sf} \cdot \alpha_f \qquad (2.3\text{-}5)$$

$$F_{sr} = c_{sr} \cdot \alpha_r \qquad (2.3\text{-}6)$$

Note: Instead of tire slip rigidity c_α, a tire slip rigidity c_s is applied, in which the elasticities of the wheel controls are considered, which influences the vehicle reactions substantially.

Side Slip angles ß, for small angles, can be formulated considering the geometrical relations as follows (viz. Fig 2.3-3 below).

$$\alpha_f = \delta + \beta - \frac{l_f \cdot \dot{\Psi}}{v} \qquad (2.3\text{-}7)$$

$$\alpha_r = \beta + \frac{l_r \cdot \dot{\Psi}}{v} \qquad (2.3\text{-}8)$$

with: ψ = yaw angle (angle between vehicle longitudinal axis and x axis)

ß = Side Slip angle (angle between vehicle longitudinal axis and velocity vector in the center of gravity)

α = Tire Slip angles at wheel (angle between wheel circumferential direction and velocity vector at tire contact point)

δ = Steering angles at the wheel (angles between wheel circumferential direction and vehicle longitudinal axis)

2.3.1 Steady State circular Course Driving

The steady state stationary circular course driving of a road vehicle is characterized by the fact that apart from the driving speed v, the yaw velocity $\dot{\psi}$ and the side slip angle ß are also constant, i.e, $\ddot{\psi} = 0$, $\dot{\beta} = 0$.

In place of the gyroscopic effect (eqn. 2.3-3), in this case, a torque equilibrium can be formulated around the front and rear tire contact point.

$$F_{sf} \cdot l = m \cdot a_y \cdot l_r \tag{2.3-9}$$

$$F_{sr} \cdot l = m \cdot a_y \cdot l_f \tag{2.3-10}$$

with 2.3-5 and. 2.3-6 one receives

$$c_{sf} \cdot \left(\delta + \beta - \frac{l_f \cdot \dot{\Psi}}{v} \right) = \frac{l_r}{l} \cdot m \cdot a_y \tag{2.3-11}$$

$$c_{sr} \cdot \left(\beta + \frac{l_r \cdot \dot{\psi}}{v} \right) = \frac{l_f}{l} \cdot m \cdot a_y \tag{2.3-12}$$

Because at the steady state circular course travel $\dot{\beta} = 0$, follows from (eqn. 2.3-4):

$$\dot{\Psi} = \frac{v}{r}$$

After resolving the equations 2.3-11 and 2.3-12 for ß and equating follows after transformation:

$$\delta = \frac{l}{r} + \frac{m}{l} \cdot \left(\frac{l_r}{c_{sf}} - \frac{l_f}{c_{sr}} \right) \cdot a_y \tag{2.3-13}$$

A substantial statement about the behavior of a vehicle while driving along curves can be derived from this equation.

The necessary steering angle during driving along a curve composes itself out of a part, which depends only on geometrical data (l/r) (Ackermann angle) and a second part which characterizes the influence of lateral acceleration. Driving at higher speeds additional to low speeds ($a_y \sim 0$) necessary steering angle one has to add the steering angles at higher speeds($a_y > 0$) which can increase or reduce the steering angle.

To amplify $\left(\frac{l_r}{c_{sf}} > \frac{l_f}{c_{sr}}\right)$

To diminish $\left(\frac{l_r}{c_{sf}} < \frac{l_f}{c_{sr}}\right)$

For the exceptional case $\left(\frac{l_r}{c_{sf}} = \frac{l_f}{c_{sr}}\right)$ no modification of steering angle, as a function of a_y, is existing.

This regularity is of special importance for the interactions between actions of the driver and vehicle handling in the control loop consisting of the driver and vehicle. While driving along curves, the driver has to set a steering angles, which depends not only on the curve radius, but additionally on the present lateral acceleration.

A reason for the dependency of the steering angles on the lateral acceleration is that at the vehicle wheels, under the effect of a lateral force, slip angle result, which amounts normally diverge on front and rear wheel.

The side slip angles difference at the Single Track model is as follows:

$$\alpha_{fv} = \delta + \beta - \frac{l_f \cdot \dot{\psi}}{v} \qquad (2.3\text{-}14)$$

$$\alpha_r = \beta + \frac{l_r \cdot \dot{\psi}}{v} \qquad (2.3\text{-}15)$$

$$\Delta\alpha = \alpha_f - \alpha_r = \delta - \frac{l \cdot \dot{\psi}}{v} \qquad (2.3\text{-}16)$$

with $v = \psi \cdot r$:

$$\Delta\alpha = \delta - \frac{l}{r}$$

with (eqn. 2.3-13): $$\Delta\alpha = \frac{m}{l} \cdot \left(\frac{l_h}{c_{sv}} - \frac{l_v}{c_{sh}}\right) \cdot a_y \qquad (2.3\text{-}17)$$

Equation 2.3-13 can also be interpreted in such a way that the steering angle which has to be set by the driver must contain a part apart from the geometrical part l/r, which results out of the necessary side slip angle difference $\Delta\alpha$ (eqn. 2.3-16). The dependence of the necessary in the side slip angle difference on lateral acceleration determined by vehicle and

tire parameters. The dependence of the steering characteristics of a vehicle, on these parameters is called "Self-steering response ".

Concerning the in a special way influencing parameters (that means the parameters of eqn. 2.3-17 for the linearized single track vehicle model) it is the matter of a quantities, whose possibilities of dimension are relatively limited because of the determined vehicle concept. Therefore, the effect of the self-steering response must be considered at a very early phase of the vehicle development.

Since the driver has to compensate the side slip angle difference with steering wheel angle δ it can be regarded as a quantifiable measured variable for the assessment of the steering characteristics. It forms the basis for the classical definition of the over steer and under steer given by OLLEY (1940) / 31 /.

over steer	$\Delta\alpha = \alpha_f - \alpha_r < 0$
neutral	$\Delta\alpha = \alpha_f - \alpha_r = 0$
under steer	$\Delta\alpha = \alpha_f - \alpha_r > 0$

According to this definition, for driving on a circular track, with an over steering vehicle smaller steering angles and with a under steering vehicle larger steering angles would be necessary compared to neutral handling, Fig 2.3-4 is.

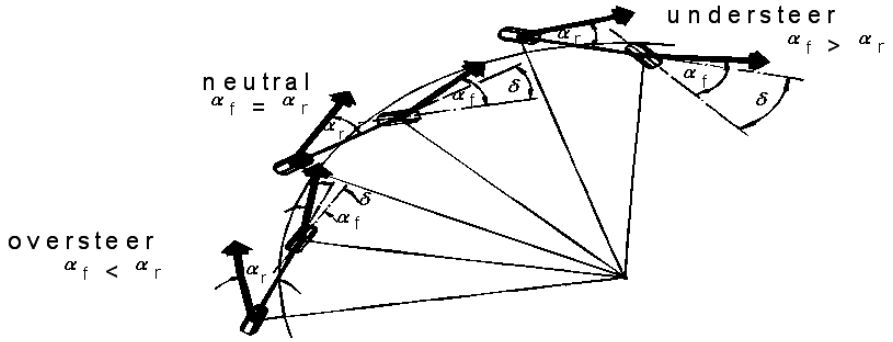

oversteer	$\Delta\alpha = \alpha_f - \alpha_r < 0$
neutral	$\Delta\alpha = \alpha_f - \alpha_r = 0$
understeer	$\Delta\alpha = \alpha_f - \alpha_r > 0$

Fig 2.3-4: Characteristic driving behavior according the definition of Olley

If one lays the equation 2.3-13 in the form of a diagram, then the basic effects of the front and the back slip rigidity and the axle load distribution can be discussed. Fig 2.3- 5 and Fig 2.3- 6:

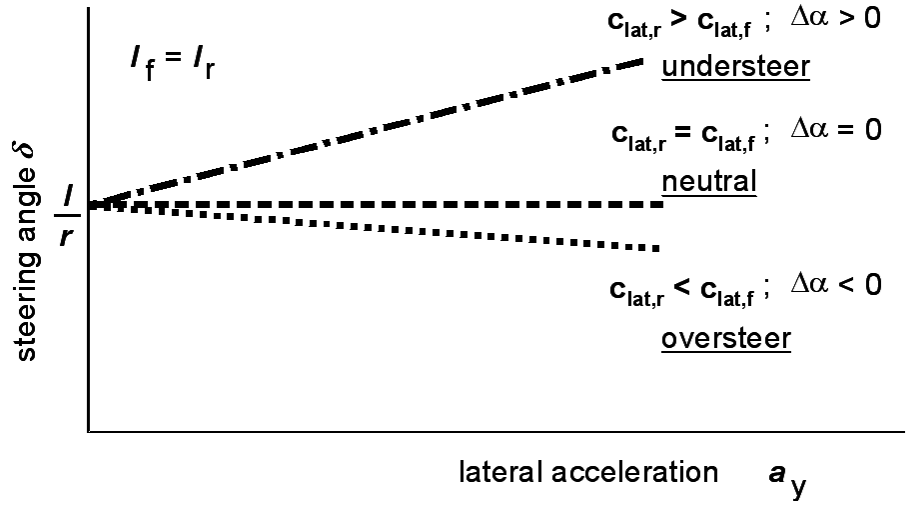

Fig 2.3- 5: Steering angle characteristic of the Single Track model with variation of the side slip rigidity. (curve radius r = const.)

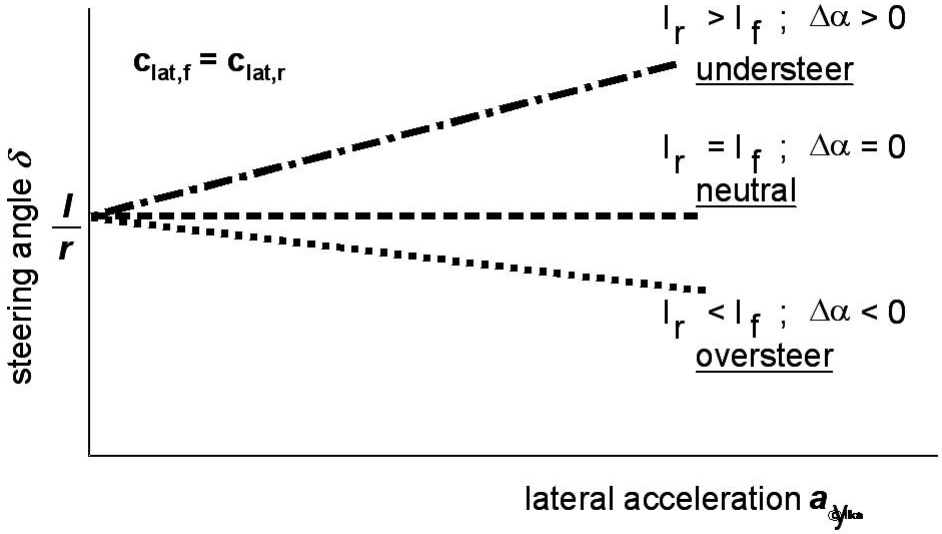

Fig 2.3- 6: Steering angle characteristic of the Single Track model with variation of the axle load distribution (curve radius r = const.)

For the evaluation of the self steering response the instantaneous value of the gradient $d\delta / da_y$ is more important than the absolute values of slip angle difference or rather steering angle.

The definition of the self-steering behavior, according to Olley, is useful therefore only in region of small lateral accelerations, in which the vehicle and tire characteristics can be linearized with sufficient accuracy.

During higher lateral accelerations, the effective slip rigidity changes in the respective operating points of the tires (viz. Fig 2.3-1). Thus the linear relation between the side slip angle difference and the lateral acceleration or rather the necessary steering angle and the lateral acceleration is lost. The sign of the gradient $d\delta / da_y$ does not correspond necessarily to the sign of the side slip angles difference.

Fig 2.3- 7 shows an appropriate curve of the steering angle over lateral acceleration. Instead of the classification of the self-steering response into the areas under steer, neutral and over steer according to the definition of Olley, a classification became generally accepted , which is oriented at the sign of the gradient $d\delta / da_y$.

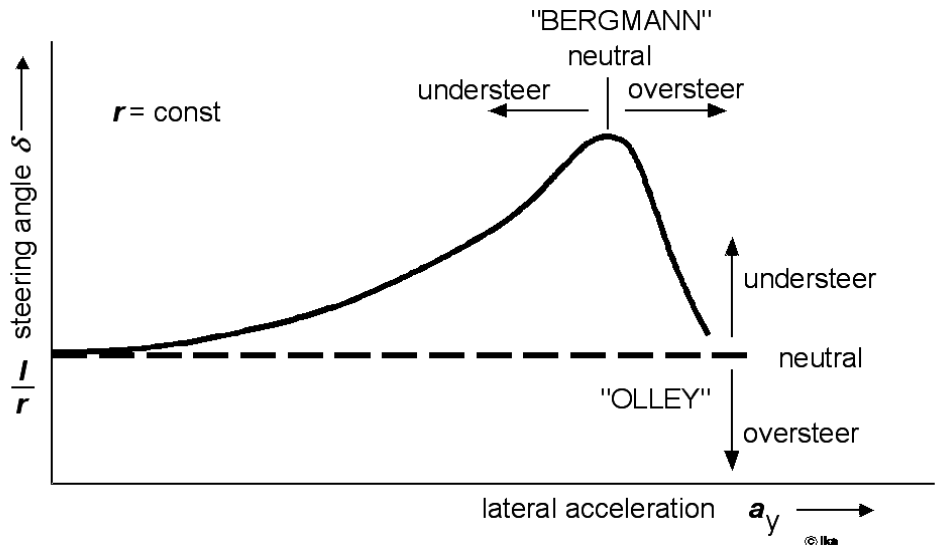

Fig 2.3- 7: Different definitions of the steering behavior

Definition of the steering behavior after Bergmann from the year 1965: / 3 /

$d\delta / da_y > 0$ $\Rightarrow$ Understeering

$d\delta / da_y = 0$ $\Rightarrow$ Neutral

$d\delta / da_y < 0$ $\Rightarrow$ Over steering

Within the linear area the results of both definitions match.

As described by eq. 2,3-13, the important relation between steering behavior and vehicle /tire parameters, is also applied in differential form under non-linear tire characteristics.

With $$F_{sf} = \int_0^{\alpha_v} c_{sf}(\alpha)\, d\alpha \qquad (2.3\text{-}18)$$

$$F_{sr} = \int_0^{\alpha_h} c_{sr}(\alpha)\, d\alpha \qquad (2.3\text{-}19)$$

one also receives here:

$$\frac{d\delta}{da_y} = \frac{m}{l} \cdot \left(\frac{l_r}{c_{sf}(\alpha_f)} - \frac{l_f}{c_{sr}(\alpha_r)} \right) \qquad (2.3\text{-}20)$$

In dependence of the actual operating points of the tires, or the resulting tire slip rigidity at front and rear axle, the following relations apply:

$c_{sr}(\alpha_r) \cdot l_r > c_{sf}(\alpha_f) \cdot l_f$ Understeering

$c_{sr}(\alpha_r) \cdot l_r = c_{sf}(\alpha_f) \cdot l_f$ neutral steering behavior

$c_{sr}(\alpha_r) \cdot l_r < c_{sf}(\alpha_f) \cdot l_f$ Oversteering

On reaching the max. lateral acceleration a_y, the adhesion limit is exceeded, first at the front axle in an under-steering vehicle and first at the rear axle in an over steering vehicle i.e. the slip angle rises uncontrolled at the axle concerned.

With the under-steering vehicle, at the rear axle, an acceptance of the side slip angle ß and therefore a relative decline of the tire slip angle α_h results. The associated decrease of lateral force at the rear axle causes the vehicle to stabilize at a bigger curve radius with less lateral acceleration.

With the over steering vehicle, a fast increase of the slip angle at the rear axle causes an increase of the side slip angles ß and thus a relative enlargement of the slip angle α_f on the front axle. The appropriate lateral force increase causes an increase of the swerve tendency of the vehicle. A stabilization on a larger curve radius is possible by quick reduction of the steering angles by the driver, whose correct dosing is difficult to bring about by a normal driver. Therefore, during the layout of the self-steering response, an under steering a behavior is aimed.

2.3.2 Transient Behavior

In order to reach statements about the transient behavior of road vehicles, the motion equations introduced in paragraph 2,3 for the linearized single track vehicle model are substituted in one another. Out of eqn. 2.3-2 and eqn. 2.3-3 results with eqn. 2.3-4, eqn. 2.3-5, eqn 2.3-6 at first:

$$m \cdot v \cdot (\dot{\psi} - \dot{\beta}) = c_{sf} \cdot \left(\delta + \beta - \frac{l_f}{v} \cdot \dot{\psi} \right) + c_{sr} \cdot \left(\beta + \frac{l_r}{v} \cdot \dot{\psi} \right) \qquad (2.3\text{-}21)$$

$$\Theta_Z \cdot \ddot{\psi} = c_{sf} \cdot \left(\delta + \beta - \frac{l_f}{v} \cdot \dot{\psi} \right) \cdot l_f - c_{sr} \cdot \left(\beta + \frac{l_r}{v} \cdot \dot{\psi} \right) \cdot l_r \qquad (2.3\text{-}22)$$

eqn . 2,3-21 can be resolved for yaw velocity: $\dot{\psi}$

$$\dot{\psi} = \frac{m \cdot v \cdot \dot{\beta} + c_{sf} \cdot (\delta + \beta) + c_{sr} \cdot \beta}{m \cdot v - c_{sr} \cdot \frac{l_h}{v} + c_{sf} \cdot \frac{l_v}{v}} \qquad (2.3\text{-}23)$$

Under the prerequisite, v = const, one receives by derivation:

$$\ddot{\psi} = \frac{m \cdot v \cdot \ddot{\beta} + c_{sf} \cdot (\dot{\delta} + \dot{\beta}) + c_{sr} \cdot \dot{\beta}}{m \cdot v - c_{sr} \cdot \frac{l_r}{v} + c_{sf} \cdot \frac{l_f}{v}} \qquad (2.3\text{-}24)$$

With it $\dot{\psi}$ yaw velocity and $\ddot{\psi}$ yaw acceleration can be replaced in Eqn. 2.3-22:

$$\ddot{\beta} + \left(\frac{c_{sf} + c_{sr}}{m \cdot v} + \frac{c_{sf} \cdot l_f^{\,2} + c_{sr} \cdot l_r^{\,2}}{v \cdot \Theta_Z} \right) \cdot \dot{\beta}$$

$$+ \left(\frac{c_{sr} \cdot l_r - c_{sf} \cdot l_f}{\Theta_Z} + \frac{c_{sf} \cdot c_{sr} \cdot l^2}{\Theta_Z \cdot m \cdot v^2} \right) \cdot \beta$$

$$= \left(\frac{c_{sf} \cdot l_f}{\Theta_Z} - \frac{c_{sf} \cdot c_{sr} \cdot (\quad l_f \cdot l_r + l_r^{\,2})}{\Theta_Z \cdot m \cdot v^2} \right) \cdot \delta - \frac{c_{sf}}{m \cdot v} \cdot \dot{\delta} \qquad (2.3\text{-}25)$$

Therefore, one receives an inhomogeneous linear differential equation of the 2nd order for the side slip angle ß. The steering angles δ and the steering angular velocity $\dot{\delta}$ in the inhomogeneous part of this equation appear as disturbance variables. (with real vehicles additional disturbances are effected bumps and wind forces). The homogeneous part of the differential equation has the form of the motion equation of a simple oscillator with damping.

$$\ddot{\beta} + A \cdot \dot{\beta} + B \cdot \beta = 0$$

$$\underbrace{2 \cdot D \cdot \omega_e} \quad \underbrace{\omega_e^{\,2}}$$

Thus, a road vehicle can execute movements in the form of damped oscillations about the vertical axis. By a comparison of the coefficients in the differential equation for ß, one receives the undamped natural frequency ω_e and the damping rate D:

$$\omega_e = \sqrt{\frac{c_{sr} \cdot l_r - c_{sf} \cdot l_f}{\Theta_Z} + \frac{c_{sf} \cdot c_{sr} \cdot l^2}{\Theta_Z \cdot m \cdot v^2}} \qquad (2.3.26)$$

$$D = \frac{\frac{c_{sf} + c_{sr}}{m \cdot v} + \frac{c_{sf} \cdot l_f^{\,2} + c_{sr} \cdot l_r^{\,2}}{\Theta_Z \cdot v}}{2 \cdot \omega_e} \qquad (2.3\text{-}27)$$

$$\omega_{e\ m.D.} = \sqrt{1 - D^2} \cdot \omega_e \qquad (2.3\text{-}28)$$

Although above parameters are obtained from a differential equation for the side slip angles β, they are designated as yaw natural frequency and yaw damping rate. This purely formal step is enabled by the fact that both the side slip angle and the yaw angle describe a movement of the vehicle around the vertical axis. Therefore, an oscillation about this axis possess only one frequency and one damping rate for both angles.

Fig 2.3- 8 shows the typical pattern of yaw natural frequency and yaw damping. The diagrams are based on the following vehicle specifications:

(The mathematical acknowledgement of above predicate follows from a view of the curve angles ν, which consists of the difference of yaw angles y and side slip angles β (see Fig 2.3-3):

$$\nu = \psi - \beta$$

Accordingly the derivatives of the angles are as follows:

$$\dot{\nu} = \dot{\psi} - \dot{\beta}$$

$$\ddot{\nu} = \ddot{\psi} - \ddot{\beta} \qquad \text{eg.} \qquad \ddot{\psi} = \ddot{\beta}$$

if the curve angular acceleration is neglected ($\ddot{\nu} = 0$). With the help of these relations the side slip angles β can be replaced by the yaw angles ψ in Eqn. 2.3-25. One then receives again an inhomogeneous linear differential equation of the2. Order:

$$\ddot{\psi} + A \cdot \dot{\psi} + B \cdot \psi = X_1 \cdot \delta + X_2 \cdot \dot{\delta} + Y_1 \cdot \nu + Y_2 \cdot \dot{\nu}$$

In the inhomogeneous part of this equation, apart from the motion quantities of the steering angles δ the curve angles also appear as disturbance variables. The natural frequency and the damping rate of the homogeneous proportion remain however unchanged.)

L = 2,5 m m = 1300 kg

l_f = 1,3 m Θ_z = 1960 kgm^2

l_r = 1,2 m c_{sf} = 30000 N/rad

The side slip stiffnes of the rear wheels c_{sr} is varied, so that altogether three vehicles with different steering behavior result:

c_{sr} = 30000 N/rad: $c_{sr} . l_r < c_{sf} . l_f$ = over steer

c_{sr} = 35000 N/rad: $c_{sr} . l_r > c_{sf} . l_f$ = under steer

c_{sr} = 40000 N/rad: $c_{sr} . l_r > c_{sf} . l_f$ = under steer

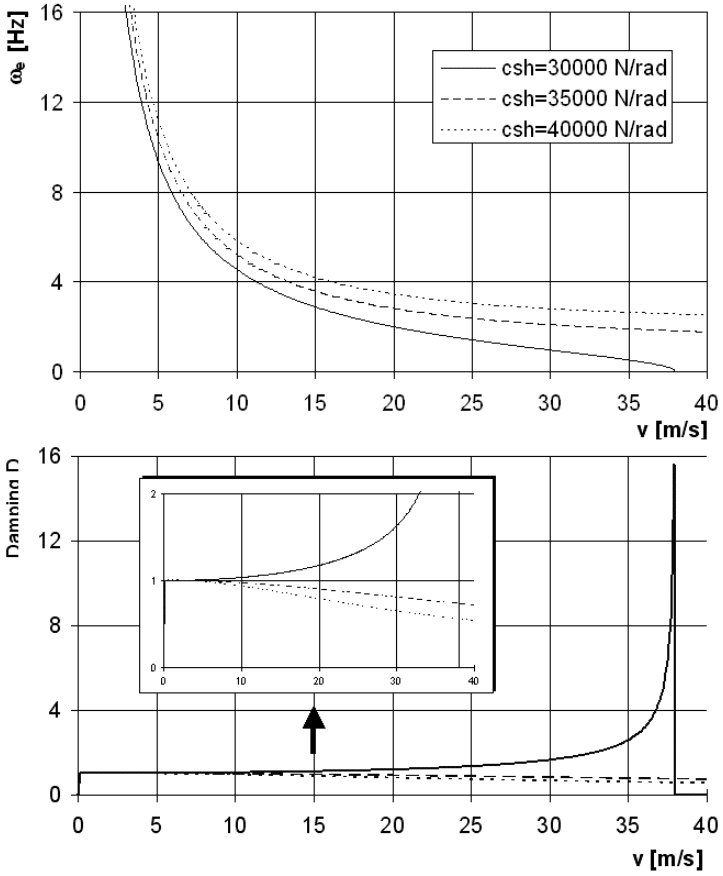

Fig 2.3- 8: Yaw natural frequency and yaw damping as function of the driving speed

For under-steering vehicles ($c_{sr} . l_r > c_{sf} . l_f$) the yaw damping decreases with the driving speed.

With over steering vehicles ($c_{sr} . l_r < c_{sf} . l_f$) a critical driving speed exists v_{crit}, with which the undamped yaw natural frequency becomes zero or the yaw damping D becomes negative (viz. Eqn. 2,3-26 or Eqn. 2,3-27). The yaw motion does not fade away after exceeding this critical driving speed. The vehicle loses it's cornering stability and begins to swerve.

By appropriate vehicle interpretation one achieves that the critical driving speed is so large that it cannot be reached or it does not exist at all.(under steering vehicle).

However, in extreme driving conditions, the operating points of the tires can change (high grip demand by the combination of lateral and longitudenal forces, unfavorable wheel load changes), in which the momentary slip rigidity takes values which leads to " dynamic over steering " / /.With corresponding high driving speed, the limit of cornering stability can be exceeded.

The aim in the vehicle construction regarding the steering behavior can be generally indicated by the demand of fast response to steering angles, whereby no overshooting should occur. Fig 2.3- 9 shows the connection between the vehicle interpretation and the system parameters yaw natural frequency and yaw damping.

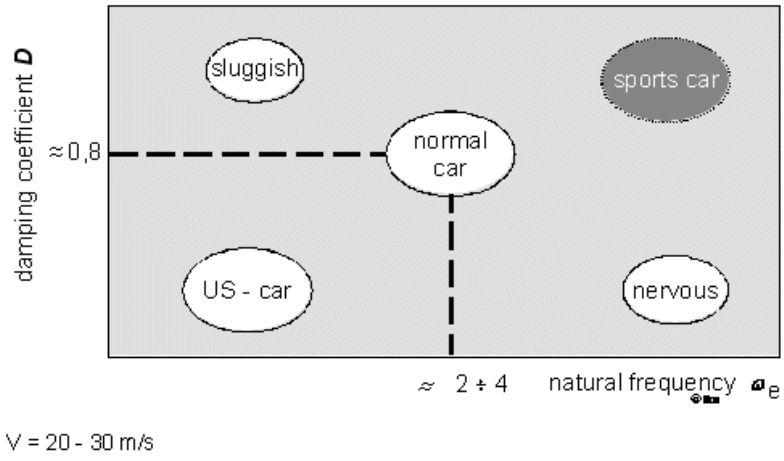

Fig 2.3- 9: Vehicle characteristic as a function of the yaw damping and the yaw natural frequency (v = 20 - 30 m/s)

Because the influencing vehicle parameters are also determined through specifications of other vehicle characteristics (suspension characteristics, additional load possibilities, engine arrangement), an optimum design is not possible with each vehicle concept.

The reaction of the vehicle to steering movements is regarded more detailed in the following paragraph.

2.3.3 Vehicle as a Control Loop Element

At the beginning of chapter 2 was described that the relations between driver actions and vehicle reactions can be understood as a closed control loop process.

Therefore the steering behavior of the linearized single track vehicle model is to be examined now as a reaction of the control travel vehicle to the control variable or input steering angles δ. As an output variable to the control travel vehicle, the yaw velocity $\dot{\psi}$ and lateral acceleration a_y are regarded.

2.3.3.1 Static Behavior of the controlled Travel Vehicle

For the description of the static behavior of the controlled travel vehicle, one uses the relationship between steering angles δ and lateral acceleration a_y for steady state cornering of the linearized single track model., deduced in paragraph eqn.2.3-13.

As in control engineering common, the output variable $\dot{\psi}$ is referred to the input variable δ. With $1/r = \dot{\psi} / v$ and $a_y = v \cdot \dot{\psi}$ follows from Eqn. 2,3-13 after transforming:

$$\left(\frac{\dot{\psi}}{\delta}\right)_{stat.} = \frac{v}{l + \frac{m}{l} \cdot \left(\frac{l_r}{c_{sf}} - \frac{l_f}{c_{sr}}\right) \cdot v^2} \qquad (2.3\text{-}29)$$

$$\left(\frac{\dot{\psi}}{\delta}\right)_{stat.} = \frac{v}{l + \frac{d\delta}{da_y} \cdot v^2} \qquad (2.3\text{-}30)$$

The relation $\dot{\psi}/\delta$ is designated as stationary yaw amplification factor. Fig 2.3- 10 shows the dependency of the yaw amplification factor on the driving speed v for vehicles with different self-steering response (eqn 2.3-20).

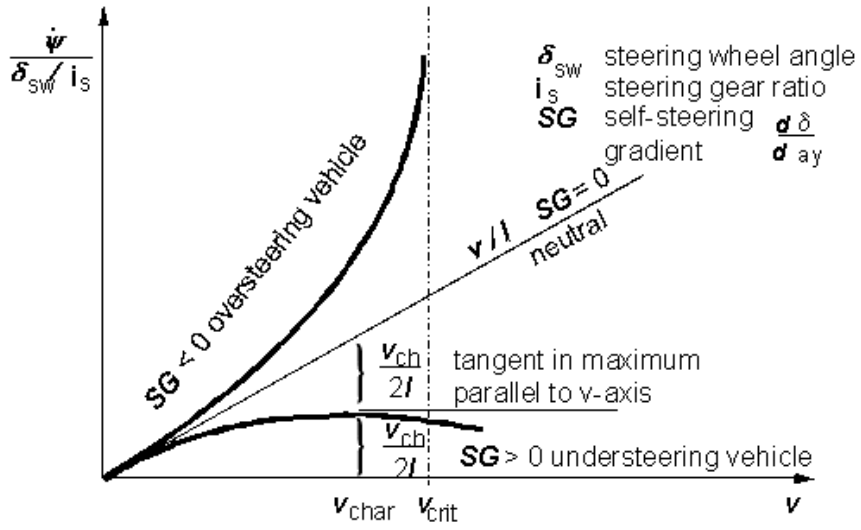

Fig 2.3- 10: Yaw amplification factor as function of the driving speed / 45 /

The meaning of the critical velocity v_{crit} was already described in the preceding paragraph. On reaching the critical velocity, the steering sensitivity of the over steering vehicle tends to infinity and therefore the vehicle cannot be stabilized.

The curve for the steering sensitivity of the under-steering vehicle indicates a maximum value. The appropriate driving speed is called characteristic velocity V_{char}. With V_{char} eqn . 2,3-30 can be written in another form for the stationary yaw amplification factor :

$$\left(\frac{\psi}{\delta}\right)_{stat.} = \frac{v}{l \cdot \left(1 + \frac{v^2}{v_{char}^{\ 2}}\right)} \qquad (2.3\text{-}31)$$

Today's passenger cars are designed in such a way that max. steering sensitivity is at a driving speed between v_{char} = 65 km/h and 100 km/h. The necessary under steer tendency can be estimate with Eqn 2.3_30

2.3.3.2 Dynamic Behavior of the Control Travel Vehicle

For an analysis of the dynamic behavior of the control travel vehicle, one refers to the differential equations for the movements of the linearized single track vehicle model in the paragraph 2,3,2, Eqn. 2,3-21 and Eqn. 2.3-22.

After a Laplace transform / 32 / the motion equations can be related to one another and we receive after certain transformations, the transmission function of yaw velocity / 45 /:

$$\frac{\psi}{\delta} = F(s) = \left(\frac{\psi}{\delta}\right)_{stat.} \cdot \frac{1 + T_z \cdot s}{1 + \frac{2 \cdot D}{\omega_e} \cdot s + \frac{1}{\omega_e^2} \cdot s^2} \qquad (2.3\text{-}32)$$

with: s: Laplace transform

$(\psi / \delta)_{stat}$: stationary yaw amplification factor

T_z: Counter time constant

ω_e: undamped yaw natural frequency

D: yaw damping

Yaw natural frequency ω_e and yaw damping rate D were already introduced in paragraph2,3-2.

One finds the counter time constant T_z similar to ω_e and D by a coefficient comparison:

$$T_z = \frac{m \cdot v \cdot l_f}{c_{sr} \cdot l} \qquad (2.3\text{-}33)$$

From a control engineering view the linearized single track vehicle model reacts to a steering angles input thus with a yawing movement like a control travel with a series connection of PT2-Elements and an PD item.

The Laplace transformation of the motion equations can be resolved in such a way that the transfer function of lateral acceleration can be determined / 45 /:

$$\frac{a_y}{\delta} = F'(s) = \left(\frac{a_y}{\delta}\right)_{stat.} \cdot \frac{1 + T_1 \cdot s + T_2 \cdot s^2}{1 + \frac{2 \cdot D}{\omega_e} \cdot s + \frac{1}{\omega_e^2} \cdot s^2} \qquad (2.3\text{-}34)$$

with: $(a_y/\delta)_{stat}$ stationary amplification factor of lateral acceleration:

$T_1 = \frac{l_h}{v}$ Time constant:

$T_2 = \frac{\Theta}{c_{sh} \cdot l}$ Time constant

In paragraph 2.3-2, the connection between yaw natural frequency, yaw damping and transient steering behavior of a vehicle was represented in an allude way.(Fig 2.3- 10) Since the specification of these two system parameters describes the intermittent steering behavior

only partly and the parameters are not directly measurable, for an objective evaluation the methodology well-known from control engineering is generally accepted to judge the behavior of an control loop system on the basis of the reactions to special input signals

With the linearized single track vehicle model, the vehicle reactions can be determined analytically, by using the Laplace transformation of the time-function for the input signal in Eqn. 2,3-31and later executing an inverse transform into the time interval, which supplies the appropriate time-function of the output signal. With real vehicles the vehicle reactions are experimentally determined.

The most important test procedures are thereby the driving maneuvers " Step steer " (sudden input signal function) and " Sinus steering "(frequency response determination). Fig 2.3- 11 shows the course of yaw velocity and lateral acceleration during a step steer.

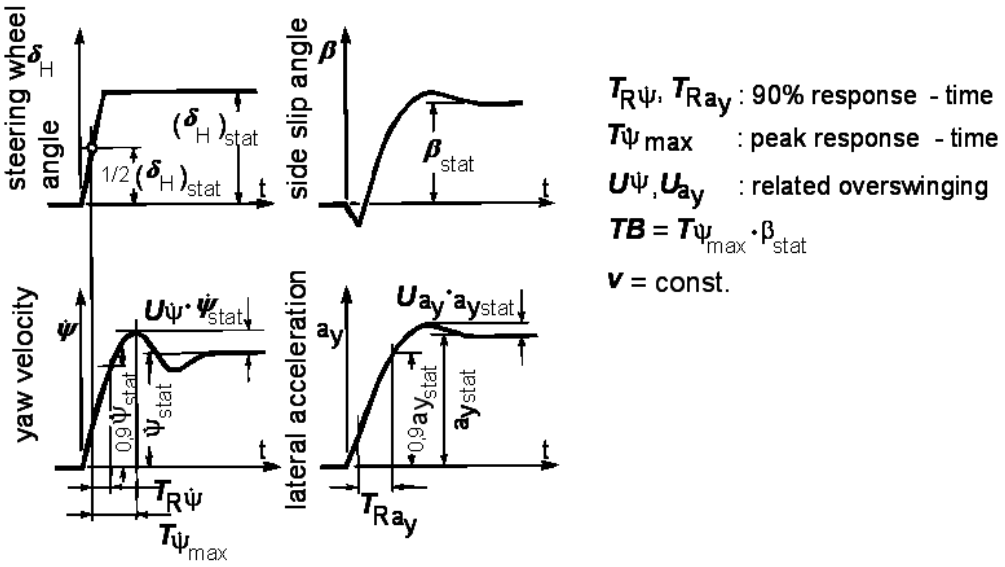

Fig 2.3- 11: Time function of the vehicle motion quantities at step steer 5 /

During the vehicle dimension a compromise between a fast response on steering movements and the demand of small overshooting of the motion quantities has to be found. Today's passenger cars value of the response time as represented in Fig 2.3- 12 is between 200 ms and 400 ms / 45 /.

For a sinusoidal steering angle process, the transfer function of the yaw velocity ψ for the linearized single track vehicle model (Eqn. 2,3-32) takes the following form:

$$F(i\cdot\omega) = \left(\frac{\psi}{\delta}\right)_{stat.} \cdot \frac{1 + T_z \cdot i\cdot\omega}{1 + \frac{2\cdot D}{\omega_e}\cdot i\cdot\omega - \frac{\omega^2}{\omega_e{}^2}} \qquad (2.3\text{-}35)$$

The amplitude ratio $\hat{\psi}/\hat{\delta}$ = |F (iω) | is thus frequency dependent. The same applies to the frequency response of lateral acceleration, which one receives from Eqn. 2.3-34:

$$F'(i\cdot\omega) = \left(\frac{a_y}{\delta}\right)_{stat.} \cdot \frac{1 + T_1\cdot i\cdot\omega - T_2\cdot\omega^2}{1 + \frac{2\cdot D}{\omega_e}\cdot i\cdot\omega - \frac{\omega^2}{\omega_e{}^2}} \qquad (2.3\text{-}36)$$

Additionally in each case a frequency dependent phase shift φ occurs between the sinusoidal output signal and the sinusoidal input signal.

$$\varphi(i\cdot\omega) = \arctan\frac{Im\left(F(i\cdot\omega)\right)}{Re\left(F(i\cdot\omega)\right)} \qquad (2.3\text{-}37)$$

Regarding the frequency responses, a vehicle dimension is aimed, with which on the one hand the drop of the lateral acceleration amplitude response does not apply to low frequencies (important for steering reaction during fast steering movement), and on the other hand, the peak of the yaw velocity amplitude response is not too high,. / 2 /.

Besides, if possible, small phase shifts are to occur in both phase responses up to high frequencies (there would be an increased need of the abilities of the driver as an automatic controller). The coupling between the transfer functions of yaw velocity and lateral acceleration permits however only a compromise between these needs./ 37 /.

Simulated gained frequency response functions by MATLAB, are to be seen in the following pictures. Here, a variation of the driving speed v, the yaw inertia moment □ and the slip rigidity of the rear axle c_{sh} was done

- **Variation of the Driving Speed V:**

In Fig 2.3- 12 the frequency response functions (amplitude response or amplification and phase response) under variation of the driving speed are represented. For frequencies of ω = 0 stationary conditions are present. The amplitude increasement then reads:

$$\left(\frac{\psi}{\delta}\right)_{stat.} = \frac{v}{l + \frac{d\delta}{da_y}\cdot v^2} \qquad (2.3\text{-}30)$$

$$\left(\frac{a_y}{\delta}\right)_{stat.} = \frac{v^2}{l + \frac{d\delta}{da_y}\cdot v^2} \qquad (2.3\text{-}38)$$

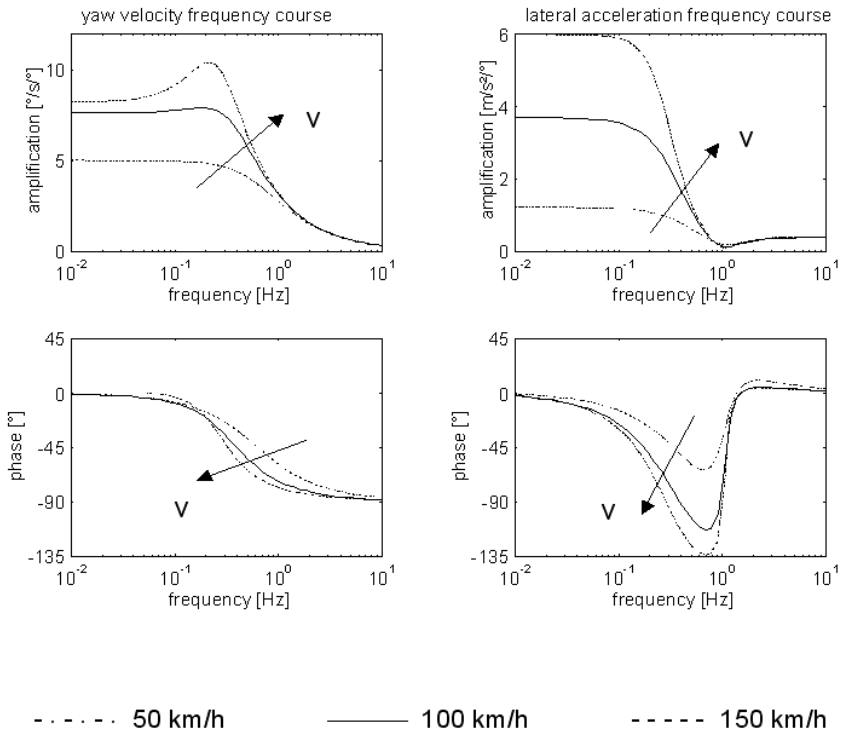

Fig 2.3- 12: Frequency response functions under variation of the driving speed V

As shown in Fig 2.3- 12, there is higher stationary amplification with increasing driving speed. From the respective base values, the amplitude curves drop strongly and tend for high frequencies asymptotic to a limit value.

The phase responses show that the phase lag and thus the vehicle reactions on steering angle inputs becomes larger with increasing driving speed.

Variation of the Yaw Moment of Inertia θ

Fig 2.3- 13 shows the results of the frequency response analysis under variation of the yaw moment of inertia θ

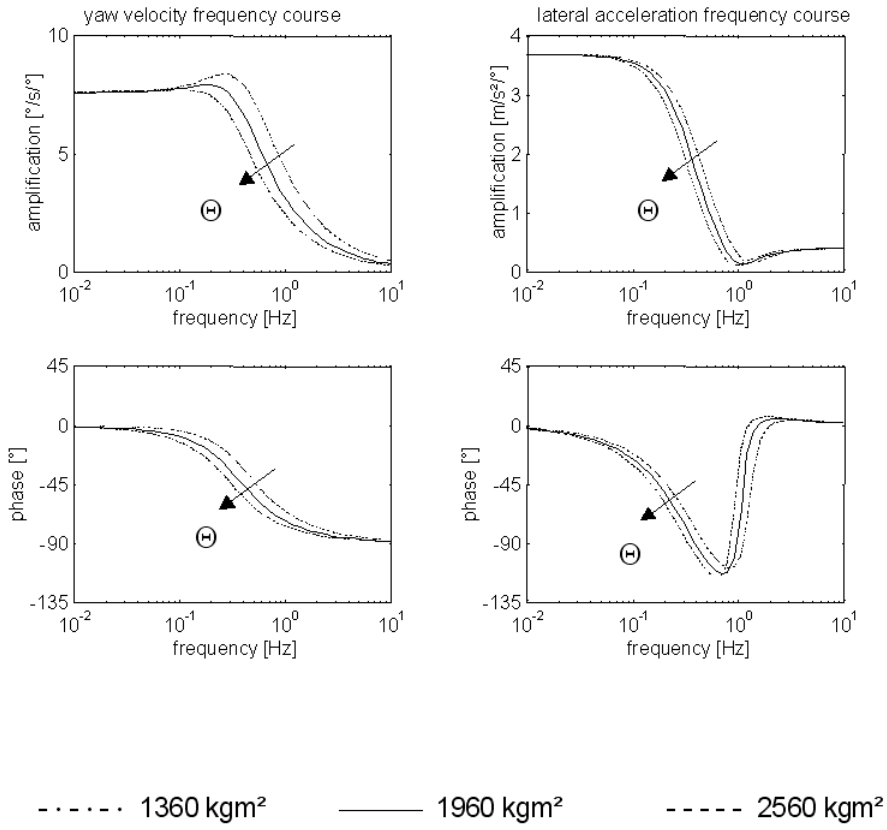

Fig 2.3- 13: Frequency response functions under variation of the yaw moment of inertia

According to the eqn. 2.3-30 and 2.3-38, the yaw moment of inertia does not have an influence on the stationary amplification ($\omega = 0$). For higher excitation frequencies, with increase of the yaw moment of inertia, the amplitude maximums move to lower frequencies, i.e. the amplitude responses drop for higher yaw moments of inertia at lower frequencies and move again asymptotic to a limit value.

Also the phase responses permit a unique influencing of the yaw moment of inertia on phase angles. With increasing yaw moment of inertia the vehicle reactions become more inert what leads to a higher lag.

- **Variation of the Tire Side Slip Stiffness of the Rear Axle c_{sr}:**

The following figure explains to what extent the under steer tendency of the test vehicle affects the frequency response functions, Fig 2.3- 14.

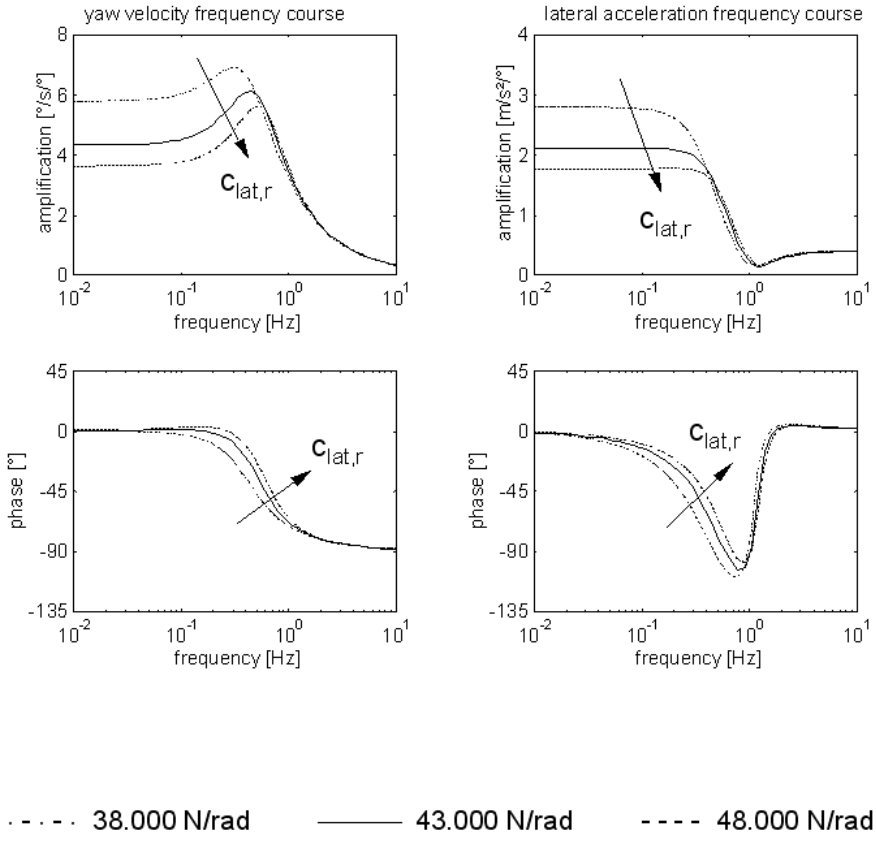

Fig 2.3- 14: Frequency response functions under variation of the tire side slip stiffness of the rear axle c_{sr}

With increasing under steer tendency (c_{sr} ↑) smaller stationary amplitude reinforcement and smaller phase lags are readable. Regarding the at the beginning formulated demand that the drop of the lateral acceleration amplitude response should not begin with to low frequencies, it shows that the most violently under-steering vehicle has the best handling. However, the most pronounced resonance peak shows up in the amplitude response of the yaw velocity for this vehicle.

During the evaluation of the simulation results it must be however noted that the analytic solutions for the linearized single track vehicle model can correspond not exact with frequency responses of real vehicles, since the movements of real vehicles are influenced by a large number by nonlinearities.

In particular the non-linear tire characteristics, which indicate a frequency response, influence the transient steering behavior substantially, as it is described in paragraph 2.2.6

2.4 Four-Wheel Vehicle Model

In addition to basic investigations about the stability behavior of the control system vehicle, the single-track vehicle model dealt with so far already permitted a qualitative study of the influences of some vehicle parameters, e.g., the effect of the location of the center of gravity or of different front or rear cornering stiffness (side slip stiffness) on understeer and oversteer.

The driving stability of real motor vehicles is determined by a multitude of further parameters, with center-of-gravity height, anti-roll suspension rates and wheel suspension kinematics constituting major factors of influence. When the stability limit regarding driving dynamics is approached, lateral dynamic response of a vehicle will be increasingly influenced by the drive concept.

Investigations about the dependence of steering behavior and driving stability on these parameters require replacement of the linearized single-track vehicle model by a three-dimensional four-wheel vehicle model, which above all also includes a more precise representation of the nonlinear tire characteristics.

2.4.1 Model Formulation

Section 2.3. contains linearized motion equations for the single-track vehicle model and an analysis of the influence of the vehicle parameters on steering behavior and tracking stability on the basis of these equations. The system of equations describing the motions of a three-dimensional four-wheel vehicle model cannot be analyzed because of its complexity. Therefore, a calculating model of a complete vehicle is generated by the ADAMS simulation program for the following parametric study.

To produce a vehicle computer model, representation of the individual parts of the vehicle is required first. In the ADAMS data record, each part is characterized by its mass, the coordinates of its center of gravity and its moments of inertia around the three main inertia axes. Points are indicated on the parts, for the various parts to be linked by joints and forces to be allowed to act on them.

The various joint types are offered in a "library", with the number of the degrees of freedom being stated for each joint.

A similar procedure is used for forces. From a list of linear forces, for example, general spring-and-damper elements or compression-only forces can be selected for the modeling of limit stops or collision points.

By means of self-written FORTRAN subroutines, random nonlinearities can be included in the calculation in addition to the standard elements for forces and movements. Thus, for example, tire characteristics can be fully described by means of measured maps (cf. Section 2.2.4.1). Fig. 2.4-1 shows the ADAMS model of a complete vehicle.

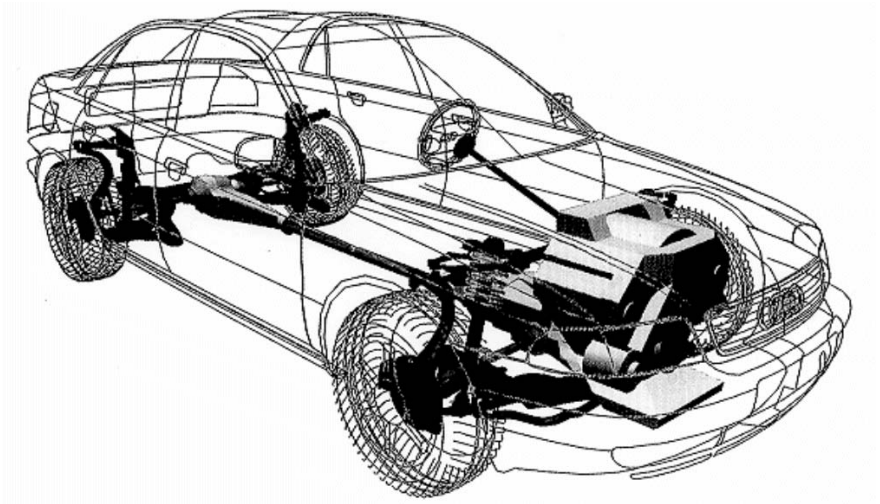

Fig. 2.4-1: ADAMS model of a complete vehicle for driving-dynamics simulations (Audi A8)

The vehicle on which the following simulation is based is clearly simpler than the very complex model shown in Fig. 2.4-1. Wheel-suspension elasticity, for example, is neglected for the number of influencing parameters to be reduced and interpretation of the calculating results to be facilitated.

The tire performance maps, on which the calculations are based, are shown in Fig. 2.4-2 and Fig. 2.4-3.

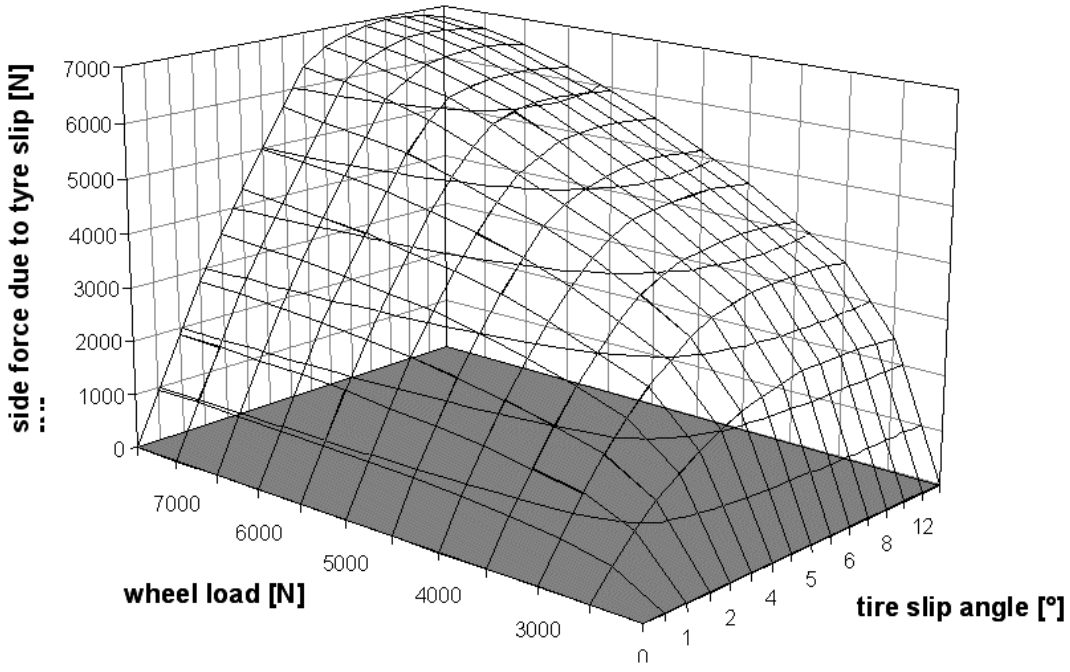

Fig. 2.4-2: Lateral force over slip angle (parameter wheel load) and over wheel load (parameter slip angle)

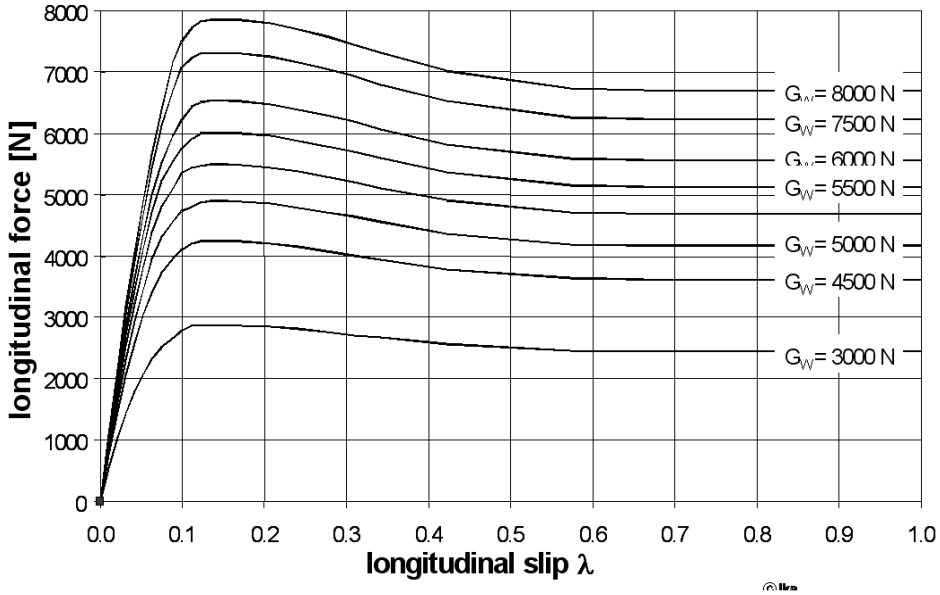

Fig. 2.4-3:Radial force over rotational slip, for wheel loads of G_R = 3000, 4500, 5000, 5500, 6000, 6500, 7500, 8000 N

Approximate consideration of transient tire behavior for fast tire slip angle variations is achieved by means of a response-delay formulation of the 1st order for the tire slip angles. The delay time is calculated in relation to a specified break-in period of the tire and the instantaneous wheel circumferential speed.

Wheel caster is considered by means of a specified map, from which the aligning torque around the roadway normal through the wheel center line in relation to the instantaneous wheel load and the slip angles is obtained through interpolation.

The steering movements needed for simulation calculation are specified as a time function or set via a PID controller in relation to a specified desired course. Traction forces are also specified as a time function, so that a desired speed pattern is obtained.

ADAMS permits calculation of vehicle movements during the most diverse driving maneuvers and offers the advantage over the driving test that vehicle parameters can without effort be varied within arbitrary limits.

2.4.2 Test Procedures and Assessment Criteria for Vehicle Handling

Use of the simulation method permits studies on the handling characteristics (operating behavior) of motor vehicles in the most diverse driving situations even on the basis of purely theoretical investigations.

Many test procedures have been developed for the assessment of handling characteristics, Fig. 2.4-4.

The bulk of the test procedures reflects idealized driving situations. Fig. 2.4-4 shows also test procedures originating rather from the investigation methods employed in control engineering (sudden steering-angle change, sinusoidal steering) and assigns them to the main driving situations.

Test procedures that are to provide information on the behavior of the "control system vehicle" within the driver-vehicle closed loop (cf. Section 2.3.3) are referred to as "closed-loop" driving maneuvers (e.g. lane-changing test). Assessment decisively depends on the adaptation of the "control system vehicle" to the abilities of the driver-controller.

Test procedures with controlled-variable changes specified in advance as time functions (e.g. sudden steering-angle change), i.e. the vehicle movements have no effect on the driver's actions, are referred to as open-loop driving maneuvers. These test procedures provide above all insights regarding the stability behavior of the control system vehicle and the system's susceptibility to external disturbances (e.g. crosswind).

main driving situation	driving manoeuvre	closed loop	open loop
cornering behaviour	steady state cornering (self-steering prop.)	-	+
	load-alteration effect	+	+
	non stat. cornering	+	+
	braking in curve	+	+
	aquaplaning	+	+
straight ahead driving behaviour	tracking stability	+	+
	lane keeping	+	+
	aquaplaning	+	+
	side wind	+	+
	load-alteration effect	+	+
	straight ahead braking	+	+
	drastic steer	-	+
	steering response	+	-
transient response	sudden steering input	-	+
	self alignment	-	+
	turning into curve	+	-
	exiting curve	+	-
	lane change	+	-
	ISO-lane change test	+	-
S bend behaviour	sinusoidal steering	-	+
	slalom	+	-
	wobble (drastic steer and accelerating)	-	+
	reaction- and obstacle avoiding test	+	-

Fig. 2.4-4: Test procedure for the handling of an automobile /35/

Every test procedure provides information on the handling characteristics of a vehicle in a certain discipline. A comprehensive assessment of operating behavior is therefore only possible if all individual results are considered.

Especially the "closed-loop" test procedures still lack universally accepted assessment criteria that would permit a quantifiable assessment on the basis of measured numerical values. Car setup is therefore largely dependent on the subjective assessments of experienced test drivers. Moreover, "closed-loop" test procedures are not really suitable for computer simulation, since mathematical description of the control behavior of humans driving a vehicle is still rudimentary. Investigations involving the use of a driving simulator are exceptions, since the driver is included in the computer simulation as a real element.

2.4.3 Parametric Study on Steering Behavior (Automobile)

Relying on the findings obtained in Section 2.3 on the basis of a linearized single-track vehicle model, this section deals with a parametric study with the aid of the above-described ADAMS kinematics four-wheel model, which permits categorizing individual design measures and their effects on steering behavior.

The test procedures employed are the "open-loop" driving maneuvers "steady-state cornering" for the description of steady-state steering behavior and the "sudden steering-angle change" for the description of non-stationary steering behavior (responsiveness) and stability behavior (attenuation of yawing motion):

• "steady-state cornering "

skidpad radius	R = 40m = const.
driving speed	v = 0-20 m/s

The driving speed v is increased slowly enough for the kinetic condition to be able to be considered stationary at any point in time. The desired values for driving speed and skidpad radius are set with the aid of PID controllers via the traction forces and the steering-wheel angle δ_H.

• "sudden steering-angle change"

driving speed	v = 27.8 m/s = const.
steering wheel angular velocity	$\dot{\delta}_H$ = 300 °/s

The step function of the steering-wheel angle δ_H is approximated by a steep ramp function, Fig. 2.4-5.

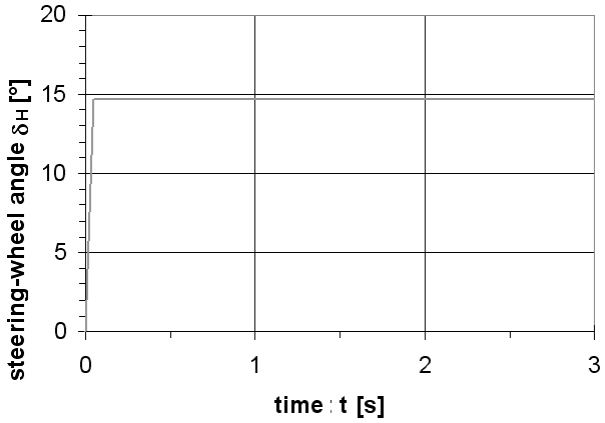

Fig. 2.4-5: Ramp function of the steering-wheel angle δ_H

The end deflection of the steering-wheel angle δ_H is set so that transversal acceleration during steady-state driving after the transient response amounts to a_y = 4.0 m/s^2, Fig. 2.4-6.

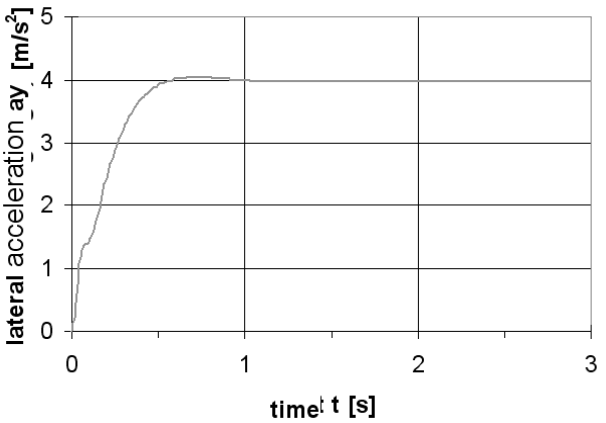

Fig. 2.4-6: Transversal acceleration after transient response

Yaw velocity, for example, can be used for simulation evaluation, Fig. 2.4-7.

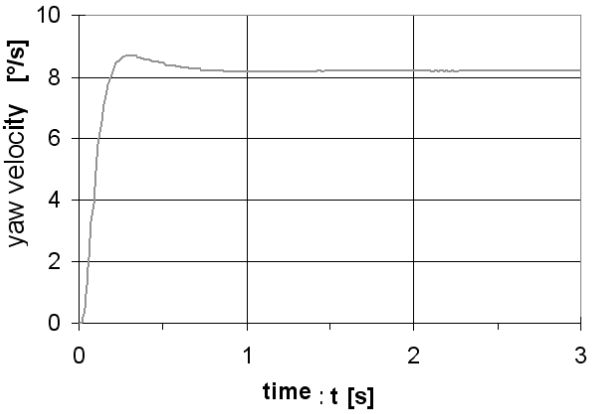

Fig. 2.4-7: Yaw velocity after transient response

• 0-version of the vehicle tested:

Fig. 2.4-8 shows the geometric terms and the position of the vehicle coordinate system.

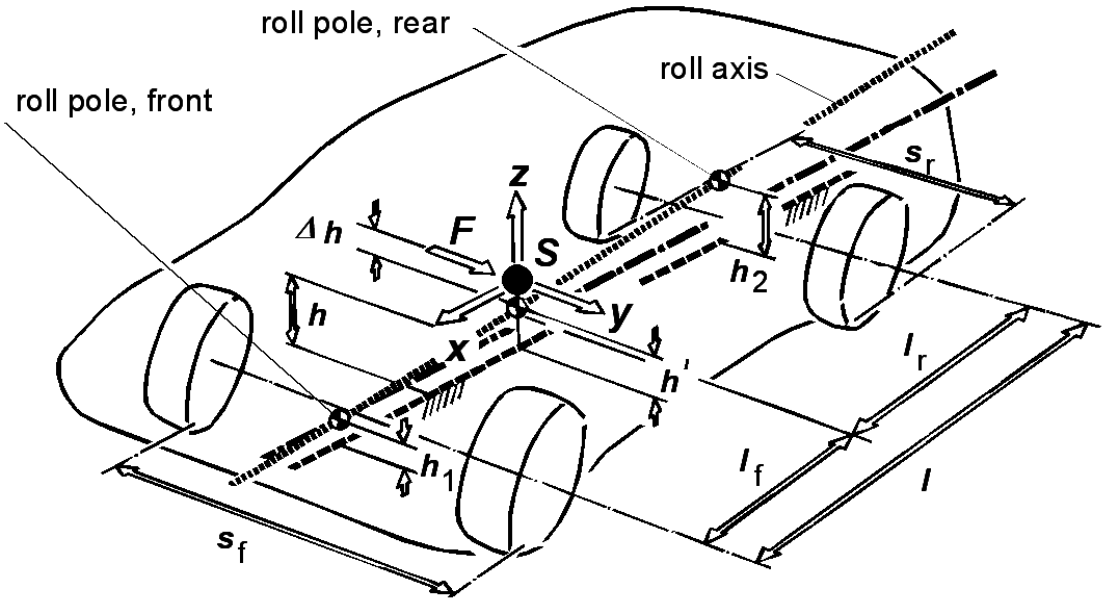

Fig. 2.4-8: Four-wheel vehicle model

Total vehicle mass:	m_{ges} = 1678 kg
Wheel mass:	m_{Rad} = 35 kg
Wheelbase:	l = 2680 mm
Front/rear track width:	$s_v = s_h$ =1520 mm
Center-of-gravity location (axle-load ratio):	l_v / l_h = 1080 mm / 1600 mm
Center-of-gravity height:	h = 520 mm
Roll-center heights:	$h_1 = h_2$ = 0 mm
Powered axle:	front axle
Tires (photos 2.4-2 - 2.4-4):	Michelin MXT 195/65 R15, 2 bar

Fig. 2.4-9 shows the simulation results for the zero version and steady-state cornering. The following parameters are considered for the description of steady-state steering quality:

Steering wheel angle: $\delta_H = f(a_y)$

Sideslip angle: $\beta = f(a_y)$

Roll angle: $\varphi = f(a_y)$

Yaw angle velocity: $\psi = f(a_y)$

The lateral forces and the vertical forces of all four wheels are plotted over the transversal acceleration.

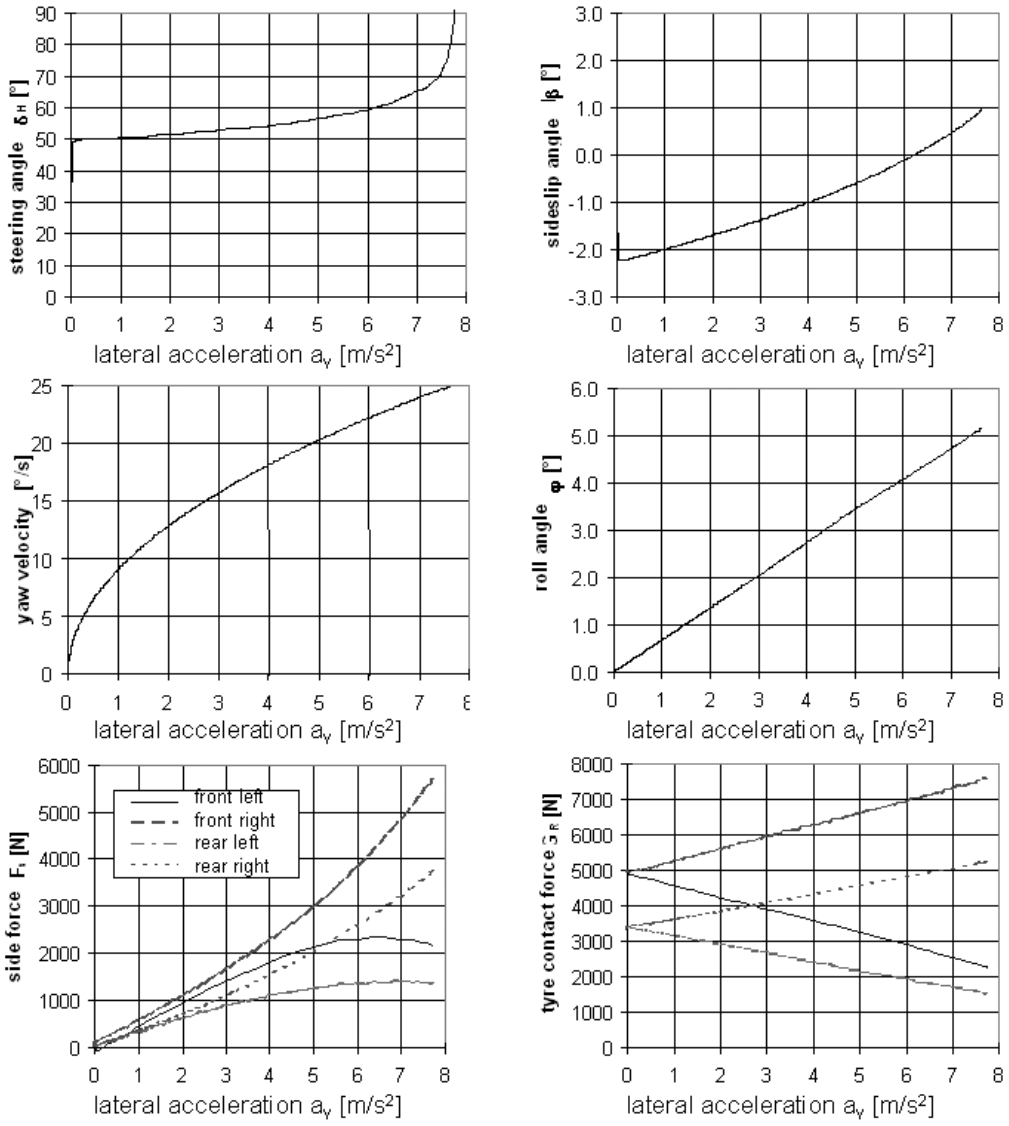

Fig. 2.4-9: Simulation results of steady-state cornering (left turn)

The main objective of steady-state cornering is to determine the steering-wheel angle δ_H as a function of transversal acceleration a_y. The initially linear and then progressively increasing steering-wheel angle together with increasing transversal acceleration is characteristic for the steering wheel angle function of the 0-version. That is, the zero version displays an increasingly understeering steady-state steering behavior as transversal acceleration increases.

According to equation 2.3-20, the linear part of the characteristic line can be described by the self-steering gradient EG:

The steering ratio i_S can be determined on the basis of the steering-wheel angle measured during transverse-force-free driving (δ_{HA} = 50°) and the Ackermann angle δ_A = l/R = 2.68m / 40m = 3.84°:

$$i_S = \frac{\delta_{HA}}{\delta_A} = 13$$

Since the Ackermann angle δ_A for the drive R = const. is a constant and therefore its derivation after transversal acceleration equals zero, the self-steering gradient can, in consideration of the steering ratio, be read off direct from the required steering-angle curve:

EG = 0,0017 rad/m/s²

The yaw-amplification factor is another significant parameter for the assessment of vehicle handling, cf. Fig. 2.3-10. In the linear range of driving dynamics there is the following relationship between yaw-amplification factor and self-steering gradient:

$$\frac{\dot{\psi}}{\delta_H / i_S} = \frac{v}{l + EG \cdot v^2}$$

If the parameters of the zero version are employed in this function, then the relation between yaw-amplification factor and driving speed as shown in Fig. 2.4-10 is obtained.

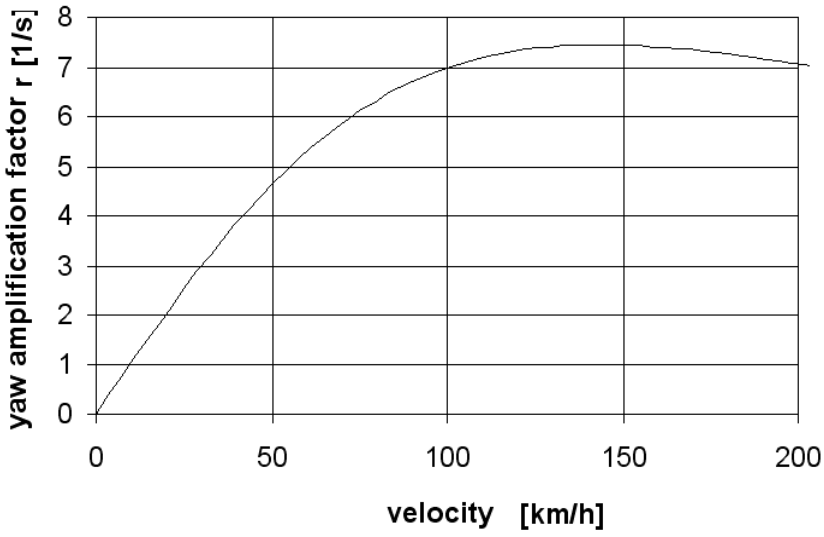

Fig. 2.4-10: Yaw-amplification factor as a function of driving speed

The characteristic line shown in Fig. 2.4-10 is typical for understeering vehicles, cf. Section 2.3.3.1.

Apart from the self-steering response, the steering behavior of a vehicle is significantly determined by the sideslip angle. The sideslip angle characteristic shown in Fig. 2.4-9 starts at a transversal acceleration of a_y = 0 m/s² with the negative value determined by the geometric conditions, which for a single-track model can be calculated as follows:

With increasing transversal acceleration, we will see a mildly progressive ascent of the characteristic line of the sideslip angle. On the present 40-m radius, zero transition, where vehicle longitudinal axis and skidpad tangent coincide, occurs at about 6 m/s². Thus a change in the sign of the sideslip angle only occurs at higher transversal acceleration values.

On the following pages, the vehicle versions listed in Fig. 2.4-11 will be compared with the zero version.

Version	varied parameter
1	center-of-gravity height h = 0 instead of h = 0.52m
2	center-of-gravity location l_f/l_r = 0.776 instead of 0.675
3	roll-center height front axle h_1 = 0.15 m instead of 0.0 m
4	stabilizer spring on front axle
5	negative static camber angle on front axle
6	kinematic bump toe-out on front axle ($\delta_f = c \cdot \Delta f$, Δf = compression)
7	rear-wheel drive instead of front-wheel drive
8	rear-axle auxiliary steering with homodirectional (parallel) steering angle ($\delta_r = 0{,}2 \cdot \delta_f$)

Fig. 2.4-11: Overview of parameter variations

2.4.3.1 Center-of-Gravity Height

To establish a connection to the single-track vehicle model dealt with before, the location of the vehicle center of gravity is lowered to the height of the roadway surface in contrast to the realistic location of the 0-version. Fig. 2.4-12 shows the simulation results for both vehicle versions.

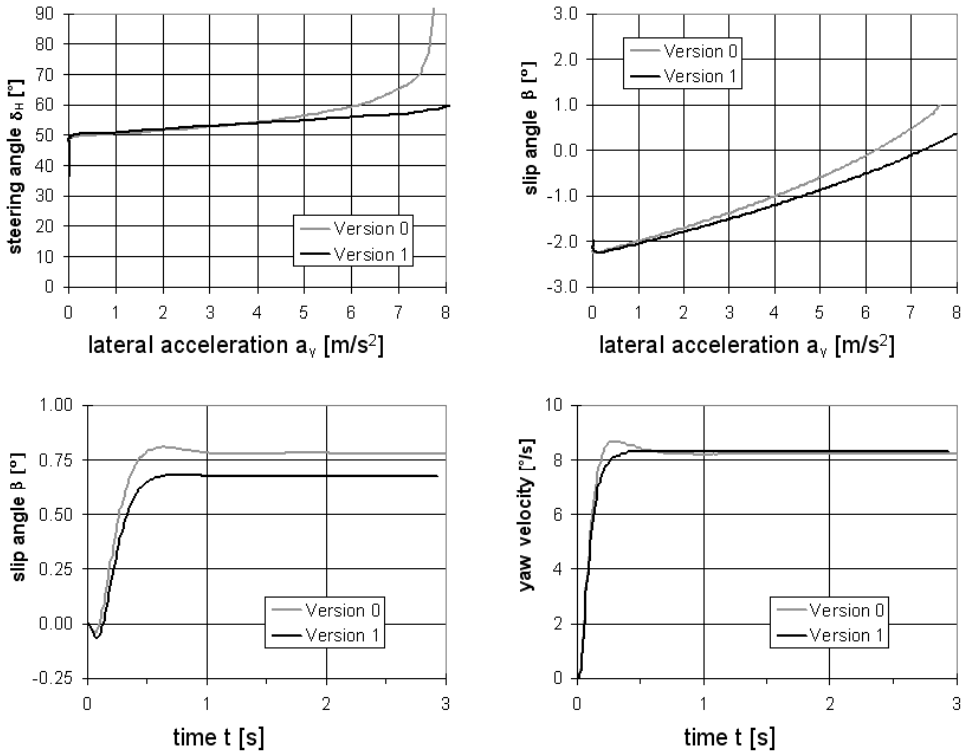

Fig. 2.4-12: Simulation results parameter variation no. 1 (center-of-gravity height h = 0)

While the 0-version shows an intensifying understeer tendency ($d\delta/da_y$) in steady-state steering behavior with increasing transversal acceleration, version 1 shows a virtually linear increase in the steering-wheel angle required until the limit is reached (maximum transversal acceleration). Steady-state steering behavior of version 1 thus roughly corresponds to that of a linearized single-track vehicle model. The mild understeer tendency of version 1 despite nearly identical center-of-gravity distances l_f, l_r and identical front and rear tires is due to a slight reduction of the effective slip stiffness c_{sf} on the front axle caused by the propulsive forces required to overcome the forces of rolling resistance and drag (cf. Section 2.3).

In the 0-version, the time function of yaw velocity shows a mild overshoot after the sudden steering-angle change. In version 1, the overshoot is insignificant, which suggests higher yaw damping. Both results are essentially due to the fact that with increasing center-of-gravity height the effective axle slip stiffness values c_{sf} and c_{sr} on front and rear axles will decrease (cf. equation 2.3-26 or equation 2.3-27).

The decrease in slip stiffness is caused by the fact that with increasing center-of-gravity height during cornering there will be greater wheel-load differences between the wheels of an axle, which in conjunction with the nonlinearity of the tire characteristics require greater slip angles for the same centrifugal force to be supported. These relations will be described in more detail because of their great significance for steering behavior:

The wheel-load differences between the wheels of an axle during cornering are obtained with the aid of a torque balance around a point on the roadway surface. For derivation of the relations, the two-track suspension model of Section 1.5.2 is used, Fig. 2.4-13.

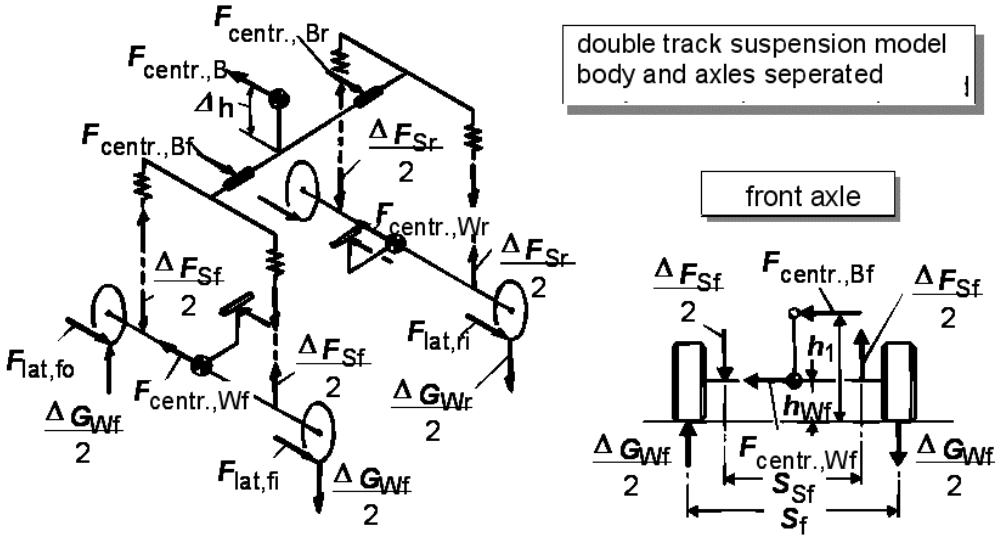

Fig. 2.4-13: Forces acting on the two-track suspension model during cornering

With this model, a simplified assumption is made according to which the position of the roll centers in the vehicle does not even change under suspension movement. Narrow angles and linear spring characteristics provided, it follows:

$$\sum M_{VA} = 0 \qquad (2.4\text{-}1)$$

$$F_{cf,\,Bf} \cdot h_1 + F_{cf,Wf} \cdot h_{Wf} + 2\,(\Delta F_{Sf} / 2) \cdot (s_{Sf} / 2) - 2\,(\Delta G_{Wf} / 2) \cdot (s_f / 2) = 0$$

with:

$F_{cf,\,Bf} = m_B \cdot a_y \cdot \frac{l_r}{l}$	:	Supported share of body centrifugal force, front axle
h_1	:	Front roll-center height
$F_{cf,\,Wf} = m_{Wf} \cdot a_y$	:	Centrifugal force of front-axle mass
h_{Wf}	:	Height of front-axle center of gravity above the roadway
ΔF_{Sf}	:	Front spring-force differential due to rolling motion
s_{Sf}	:	Front spring-track width
ΔG_{Wf}	:	Front wheel-load difference during cornering
s_f	:	Front track width

The spring-force differential depends on the dimension of the roll angle φ:

$$(\Delta F_{Sf} / 2) = c_{Bf} \cdot \Delta f + c_{stab,f} \cdot \Delta f_{stab,f}$$

$$= c_{Bf} \cdot \varphi \cdot (s_{Sf} / 2) + c_{stab,f} \cdot \varphi \cdot (s_{stab,f} / 2) \qquad (2.4\text{-}2)$$

The relation between roll angle φ and body centrifugal force $F_{cf;B}$ was already derived in Section 1.5.2:

$$\varphi = \frac{2 \cdot \Delta h}{c_{Bf} \cdot s_{Sr}^2 + c_{Br} \cdot s_{Sr}^2 + c_{stab,f} \cdot s_{stab,f}^2 + c_{stab,r} \cdot s_{stab,r}^2} \cdot F_{cf,B} \qquad (2.4\text{-}3)$$

With equation 2.4-1 and equation 2.4-2 after transformation we get for the wheel-load difference:

$$\Delta G_{Wf} = F_{cf,Wf} \cdot \frac{h_{Wf} \cdot 2}{s_f} + F_{cf,B} \cdot \left(\frac{l_r}{l}\right) \cdot \frac{h_1 \cdot 2}{s_f} + c_{Bf} \cdot \varphi \cdot \frac{s_{Sf}^2}{s_f} + c_{stab,f} \cdot \varphi \cdot \frac{s_{stab,f}}{s_f} \cdot s_{Sf} \qquad (2.4\text{-}4)$$

For the wheel-load difference on the rear axle:

$$\Delta G_{Wr} = F_{cf,Wr} \cdot \frac{h_{Wr} \cdot 2}{s_r} + F_{cf,B} \cdot \left(\frac{l_f}{l}\right) \cdot \frac{h_2 \cdot 2}{s_r} + c_{Br} \cdot \varphi \cdot \frac{s_{Sr}^2}{s_r} + c_{stab,r} \cdot \varphi \cdot \frac{s_{stab,r}}{s_r} \cdot s_{Sr} \qquad (2.4\text{-}5)$$

Thus the wheel load supported on each wheel during cornering can be calculated:

$$G_{Wfo} = \frac{1}{2} \cdot m_{tot} \cdot g \cdot \frac{l_r}{l} + \frac{1}{2} \cdot \Delta G_{Wf} \qquad (2.4\text{-}6)$$

$$G_{Wfi} = \frac{1}{2} \cdot m_{tot} \cdot g \cdot \frac{l_r}{l} - \frac{1}{2} \cdot \Delta G_{Wf} \qquad (2.4\text{-}7)$$

$$G_{Wro} = \frac{1}{2} \cdot m_{tot} \cdot g \cdot \frac{l_f}{l} + \frac{1}{2} \cdot \Delta G_{Wr} \qquad (2.4\text{-}8)$$

$$G_{Wri} = \frac{1}{2} \cdot m_{tot} \cdot g \cdot \frac{l_f}{l} - \frac{1}{2} \cdot \Delta G_{Wr} \qquad (2.4\text{-}9)$$

In the present case, the instantaneous-center heights (roll-center heights) h_1 and h_2 equal zero, front and rear body suspension stiffness including stabilizer stiffness are equal, and the spring-track widths correspond to the wheel-track widths (independent wheel suspension).

If the centrifugal-force shares of the wheel masses are neglected, the equations 2.4-4 and 2.4-5 are simplified and become:

$$\Delta G_{Wf} = \Delta G_{Wr} = (c_B + c_{stab}) \cdot \varphi \cdot s \qquad (2.4\text{-}10)$$

or with equation 2.4-3 and ?h = h ($h_1 = h_2 = 0$):

$$\Delta G_{Wf} = \Delta G_{Wr} = \frac{2 \cdot h}{s} \cdot F_{cf,B} \qquad (2.4\text{-}11)$$

The sum of tire lateral forces on one axle has to counteract the share of the total centrifugal force to be supported here:

$$F_{sfi} + F_{sfo} = F_{Lat,tot} \cdot \frac{l_r}{l} \qquad (2.4\text{-}12)$$

$$F_{sri} + F_{sro} = F_{Lat,tot} \cdot \frac{l_f}{l} \qquad (2.4\text{-}13)$$

If it is assumed that the tire slip angles on the wheels of an axle are the same, then the required "axle" slip angle will not only depend on the axle load G_A but also on the wheel-load difference ΔG_R on this axle, Fig. 2.4-14.

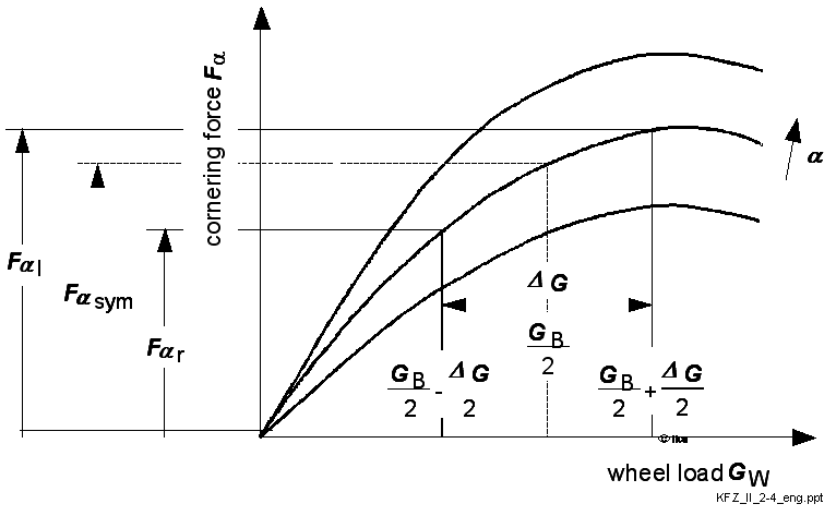

Fig. 2.4-14: Cornering force in relation to the wheel-load difference

If the axle load G_A was symmetrically distributed among both wheels ($G_W = G_A / 2$), each wheel would support half the transverse force share $F_{lat,f}$ or $F_{lat,r}$. If wheel-load differences occur on an axle, then the sum of the cornering forces will reach the amount required only in the presence of a wider slip angle (in contrast to $\Delta G_W = 0$) because of the degressive course of the tire characteristic curves $F_\alpha = f(G_W, \alpha = \text{const.})$.

The results of parametric variation 1 can thus be summarized as follows:

With increasing center-of-gravity height h, there will be greater wheel-load differences on front and rear axles during cornering (cf. equation 2.4-11). Wheel-load differences reduce axle cornering force with constant slip angle or increase slip angle requirement with specified

cornering force. This corresponds to a reduction of the effective slip stiffness c_s as a result of wheel-load differences (Fig. 2.4-14).

If slip stiffness decreases to the same extent on front and rear axles, as in the present case (version 1 → version 0), then an existing oversteer or understeer tendency will be intensified.

2.4.3.2 Center-of-Gravity Position

For the influence of axle-load distribution to be determined, a vehicle is compared with the 0-version, whose center of gravity is relocated rearward (l_f/l_r=0.776), Fig. 2.4-15.

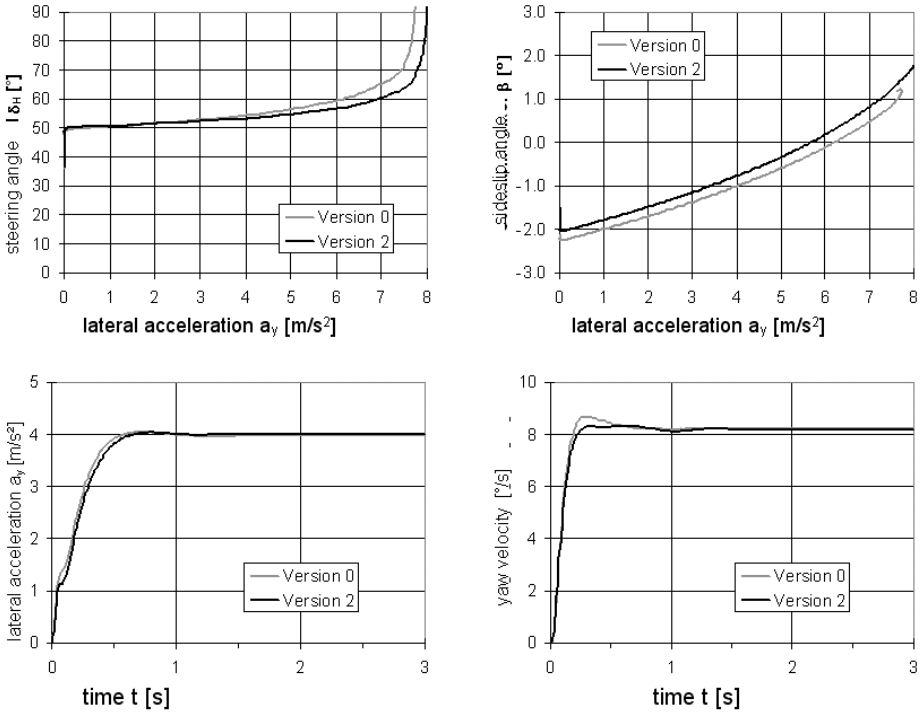

Fig. 2.4-15: Simulation result parametric variation no. 2 (center-of-gravity location l_f/l_r = 0.776)

The understeer tendency of the 0-version is reduced by rearward relocation of the vehicle center of gravity. The nonstationary behavior of version 2 points to a lower yaw natural frequency and a higher yaw damping compared to the 0-version.

Both results are in agreement with the relations (Section 2.3) derived with the help of the linearized single-track vehicle model. Due to the degressive nature of the tire characteristics $F_\alpha = f(G_W, \alpha = \text{const.})$, the decrease of the effective slip stiffness c_{sf} on the front axle is not of the same magnitude as the increase of the center-of-gravity distance l_f to the front axle.

2.4.3.3 Roll Axis

The instantaneous axis of rotation of the vehicle body in relation to the roadway, around which the vehicle body tilts during rolling motion (cf. Section 1.5.2), is referred to as "roll" or

"instantaneous axis". It constitutes the connecting line of the roll centers on front and rear axle, whose locations are determined by the kinematics of wheel suspension.

In the 0-version, the roll axis runs along the roadway surface. In version 3, the roll center on the front axle is 0.15 m above the roadway surface, and the roll axis descends towards the rear axle (cf. Fig. 2.4-8).

The lever arm Δh of the body centrifugal force around the roll axis is thus smaller in version 3 than in the 0-version:

With the same transversal acceleration we have a narrower roll angle and, as all other influencing parameters are unchanged, a lower wheel-load difference on the rear axle, equation 2.4-4.

In both vehicle versions, the sum of the wheel-load differences of front and rear axles has to compensate the same torque of the total centrifugal force around a track line.

The wheel-load difference on the front axle of version 3 is greater, equation 2.4-5.

As expected, the existing understeer tendency of the 0-version increases with elevation of the roll center on the front axle, because the effective slip stiffness values are influenced by the altered distribution of the wheel-load differences, Fig. 2.4-16.

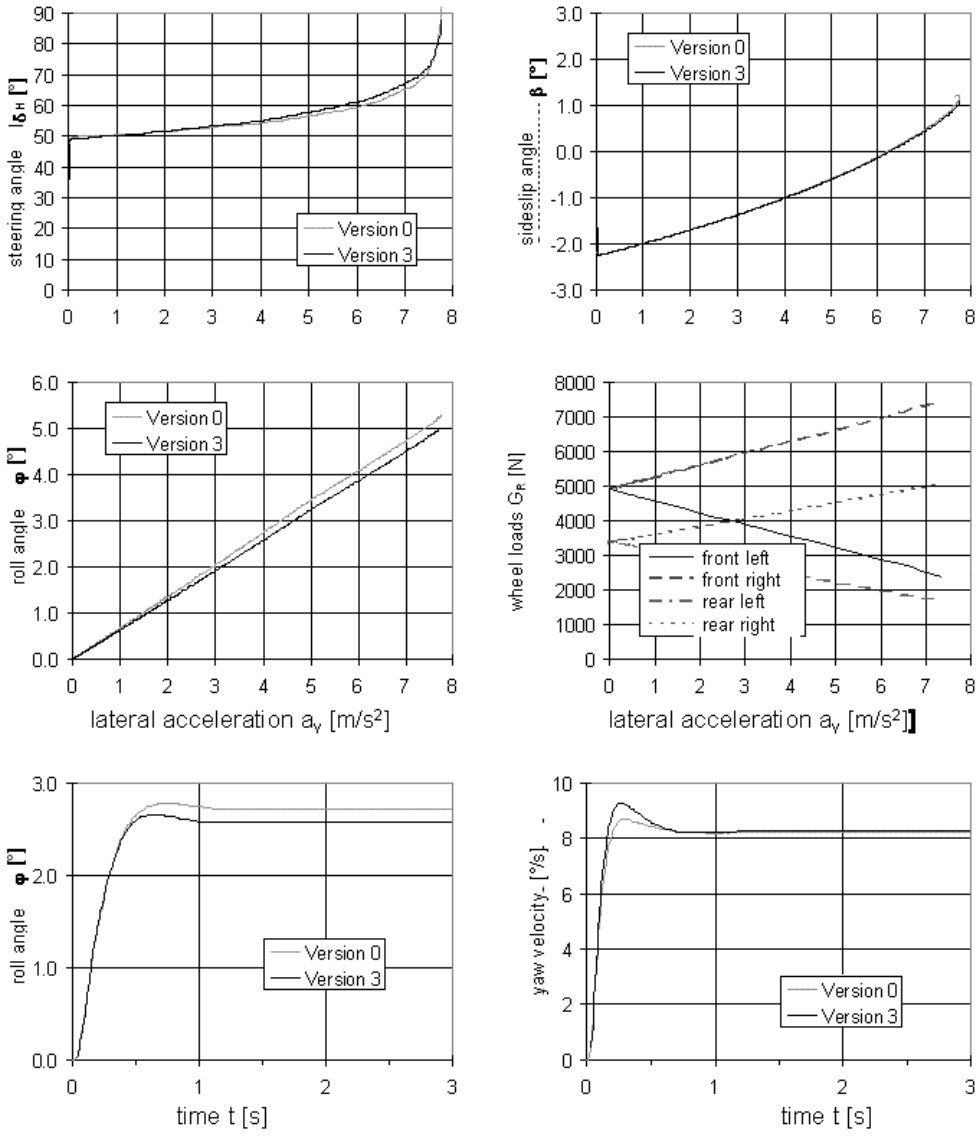

Fig. 2.4-16: Simulation result parametric variation no. 3 (front-axle roll-center height)

2.4.3.4 Anti-roll Suspension Distribution

So far only vehicle versions with symmetric distribution of anti-roll suspension stiffness have been studied, i.e. the torque of the body centrifugal force is supported at equal shares by the suspension on front and rear axles.

In version 4, stabilizer stiffness on the front axle was increased compared to the 0-version. With identical transversal acceleration, this results in a narrower roll angle φ, equation 2.4-3.

With the help of equation 2.4-4 and equation 2.4-5, the influence on the wheel-load differences and thus on steering behavior can be assessed:

The wheel-load difference ΔG_{Wr} on the rear axle decreases, since all influencing parameters in equation 2.4-5 are unchanged, except for the roll angle φ. Accordingly, the wheel-load difference ΔG_{Wf} on the front axle has to increase by the same amount, because – as already elucidated by the contemplation of the influence of the roll-center heights – the sum of the wheel-load differences on front and rear axles only depends on the dimension of the track widths and the height of the overall center of gravity above the roadway, but not on the layout of the suspension system.

Fig. 2.4-17 shows the influence of the stabilizer-stiffness-dependent share of the wheel-load difference on an axle during cornering on the sum of lateral forces.

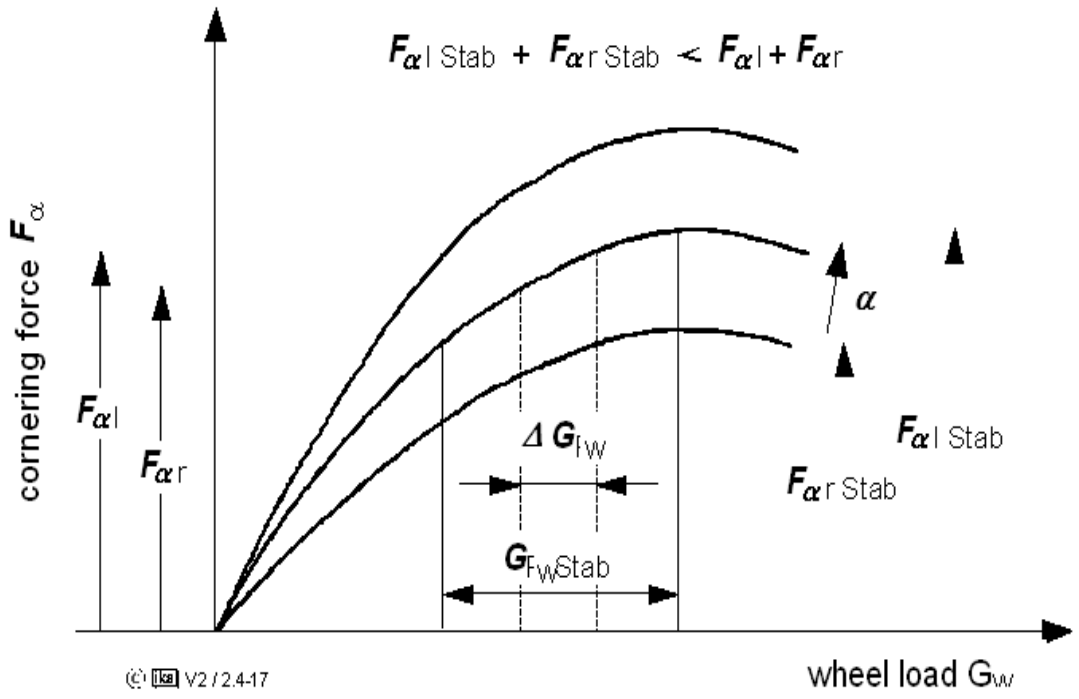

Fig. 2.4-17: Axle cornering forces with/without stabilizer spring

The axle slip angle required to support a certain total lateral force increases with growing stabilizer stiffness, i. e. the effective slip stiffness c_s decreases.

The theoretical considerations are verified by the simulation results. Version 4 shows an intensified understeer tendency compared to the 0-version, Fig. 2.4-18.

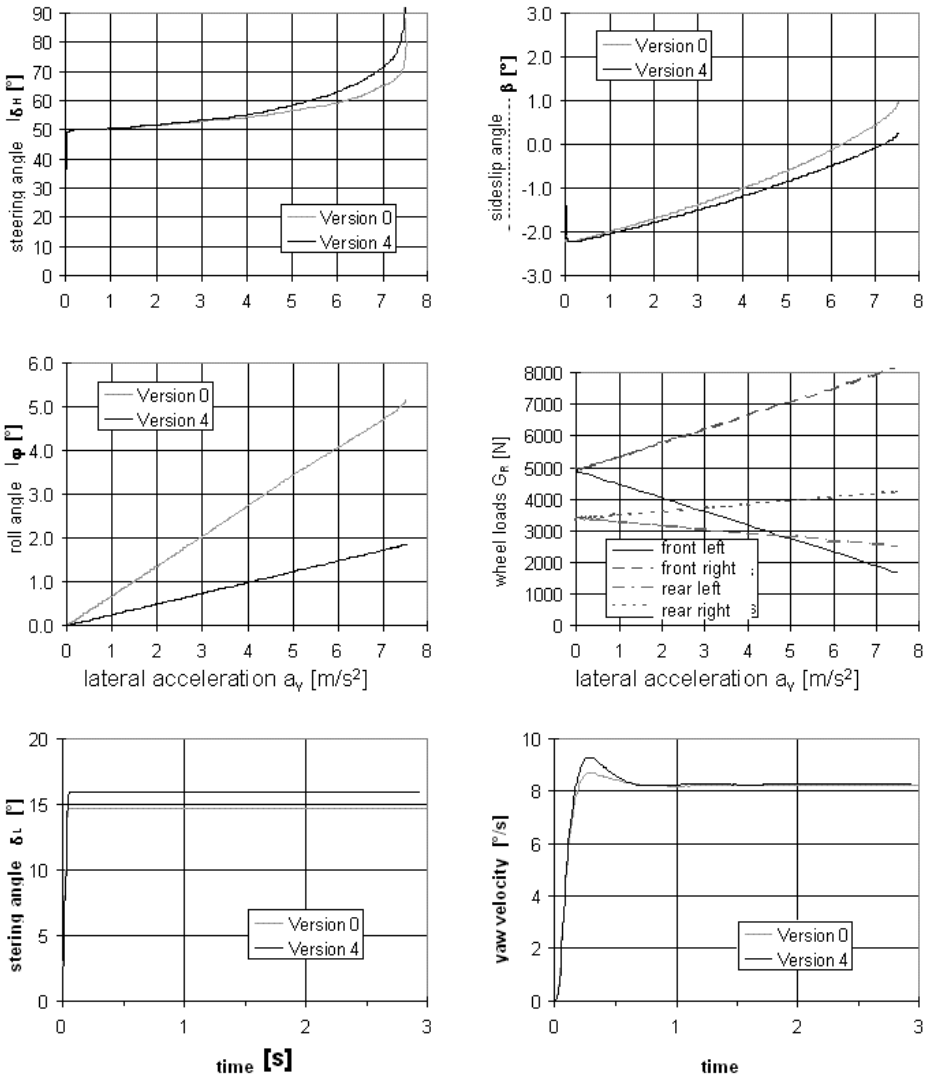

Fig. 2.4-18:Simulation result parametric variation no. 4 (stabilizer on front axle)

Increasing stabilizer stiffness on the rear axle would result in a decreasing understeer tendency. Distribution of total effective stabilizer stiffness among front and rear axles is an important instrument in the tuning of the steering behavior of an automobile.

2.4.3.5 Camber and Toe Angle

In all parametric variations considered so far, the influence exerted on the steering behavior was in the final analysis due to the nonlinearity of the tire characteristics.

Apart from the tire characteristics, the kinematic and elastic properties of wheel suspensions are of great significance for transverse dynamics.

As a rule, axle bodies - and wheel carriers in the case of independent wheel suspension – are guided by links (or joint rods) in relation to the body in a manner that essentially there is only one degree of freedom of compression left. As the links are of a finite length,

compression movements are associated with wheel position changes relative to the body, i.e. to changes of track width, wheelbase, wheel camber and steer angles (toe angle) determined by wheel suspension kinematics, Fig. 2.4-19.

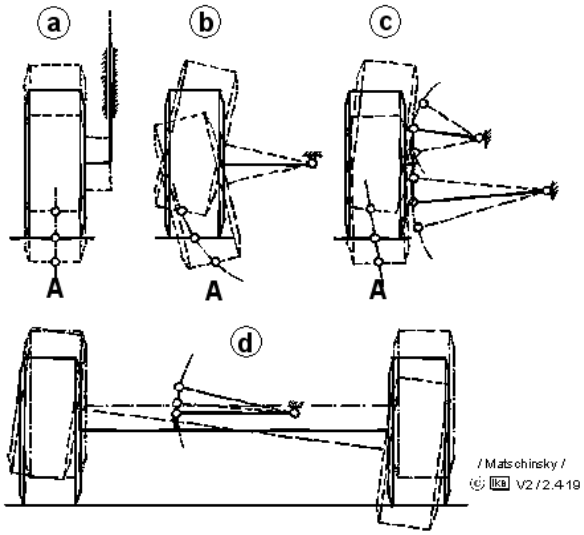

Fig. 2.4-19: Wheel position changes during suspension movement

For vibration isolation to be achieved between wheel suspension components and body, the body-mounted link mounts (pivots) are not designed as rigid bearing journals or ball joints but as rubber-metal elements. The angular flexibility required of the link mounts (pivots) is realized solely by the elasticity of the rubber elements, so that the mounts are without clearance and maintenance-free.

Due to the elasticity of the rubber mounts (silent bearings), wheel-position changes also occur as a result of the forces and torque acting in the tire-contact center of the vehicle.

By comparison with the kinematic wheel-position changes due to suspension movement, these wheel-position changes are referred to as elastokinematic changes, as they are dependent on wheel suspension kinematics and on wheel suspension elasticity.

The kinematic camber-angle variations and the kinematic and elastokinematic toe-angle variations are the most important wheel-position changes with regard to vehicle handling.

In section 2.2.4.2, the absolute camber angle γ of the wheel relative to the roadway surface was defined. The absolute camber angle γ is composed of the roll angle φ of the body and the relative camber γ_{rel} of the wheel relative to the body, Fig. 2.4-20.

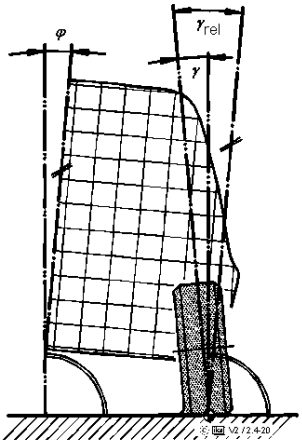

Fig. 2.4-20: Representation of absolute and relative camber angles

Arithmetically, the sign definitions of the camber angles of left and right vehicle sides are not uniform. The relative camber is negative if the upper edge of the wheel disk is inclined towards the vertical-longitudinal plane of symmetry of the body. The absolute camber is negative if the upper edge of the wheel disk is inclined towards a plane, which in vehicle longitudinal direction stands vertical relative to the roadway.

The camber forces (cf. Section 2.2.4.2) caused by the wheel camber and the slip lateral forces overlap and add up until the utilizable friction coefficient for lateral forces is attained.

During cornering, negative camber angles on the wheels of an axle increase the axle lateral force resulting from a certain axle slip, Fig. 2.4-21.

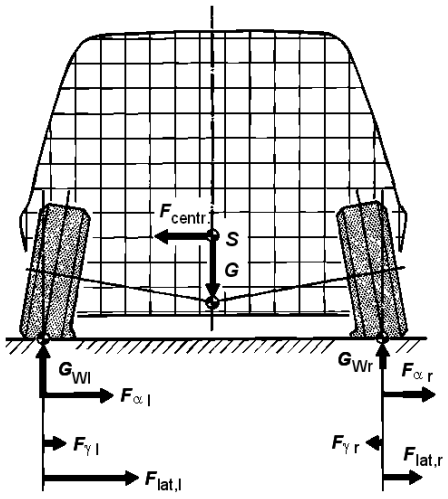

Fig. 2.4-21: Overlap of cornering forces due to slip and wheel camber

Vehicles with an oversteer tendency due to their rear-wheel drive concept usually feature negative camber angles on the wheels of the rear axle, which contribute to an understeer behavior that is more favorable regarding driving stability. Intensification of the understeer

tendency of RWD vehicles requires only slight kinematic camber changes if relatively large negative camber angles on the rear axle are provided for in the design attitude (ca. – 2.0°). Layout has to take into account the effect on tire wear.

Fig. 2.4-22 Shows the simulation results of version 5 "negative camber angles on front-axle wheels".

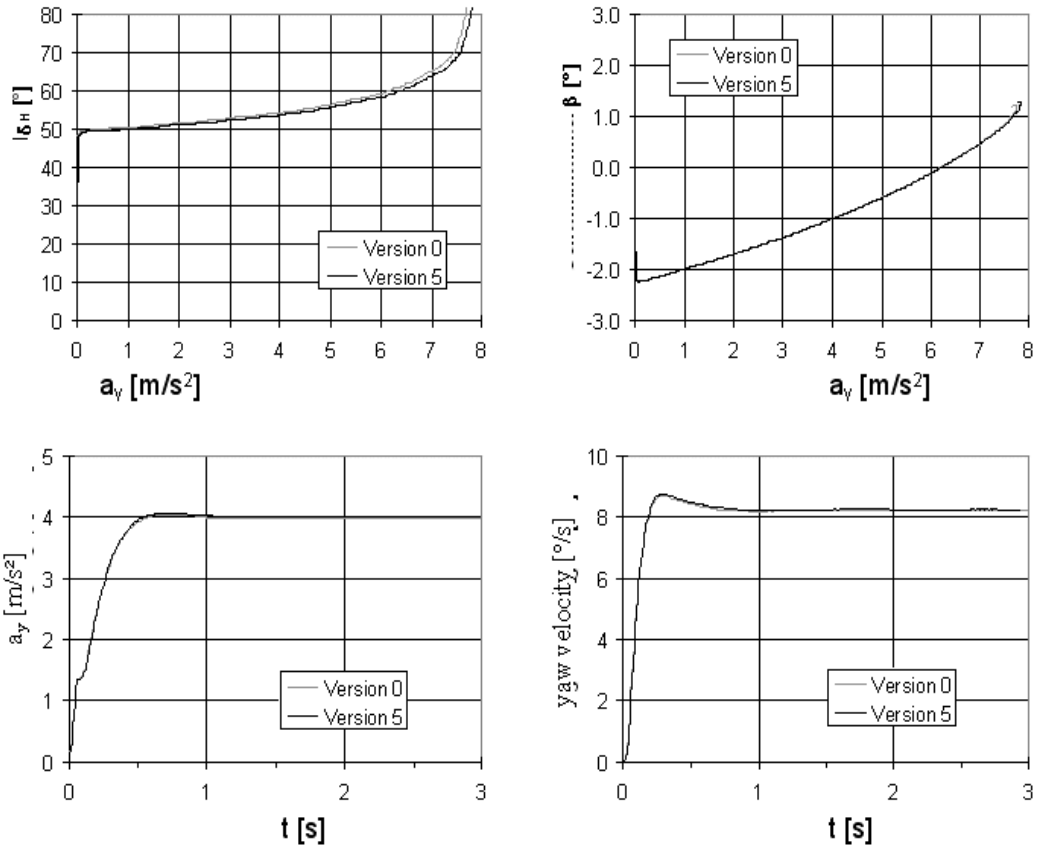

Fig. 2.4-22:Simulation results parametric variation no. 5 (negative camber angles on front-axle wheels)

Due to camber specification on the wheels of the front axle, higher lateral forces can be transmitted on this axle. The understeer tendency of the 0-version is thus reduced.

With increasing roll angle of the body during cornering, the amount of a negative camber angle on the outside wheel effective in the design attitude will, however, decrease, Fig. 2.4-20. By means of kinematic wheel-camber change during compression, this decrease in the absolute (negative) camber angle could be compensated.

However, layout of wheel suspension must take into consideration the fact that the significant kinematic camber changes required will result in the straight-running properties being affected, since they also become operative as a result of suspension movements caused by road irregularities and then produce undesired lateral force fluctuations.

Fig. 2.4-23 illustrates the sign definition for toe angles. Positive toe angles are referred to as toe-in, negative as toe-out. As a rule, a total toe-in angle δ_f is specified for the front axle because the wheel-related toe-in angles depend on the steering angle δ on the front axle.

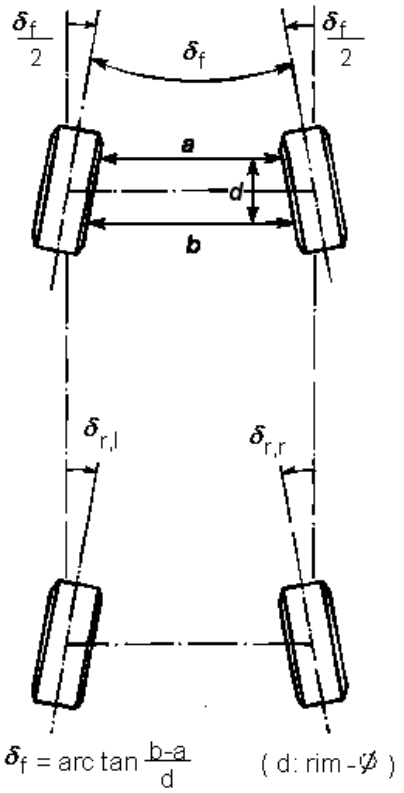

Fig. 2.4-23: definition toe angle

Toe-in angles on the outside wheel or toe-out angles on the inside wheel of an axle increase the tire slip angle operative at a certain axle slip angle and thus the resulting axle lateral force.

On account of a higher wheel load, the lateral-force increase due to the toe-in share of the outside wheel of an axle exceeds the lateral-force loss due to an identical toe-in share of the inside wheel.

A total toe-in angle on the front axle thus causes an increase in the axle lateral force resulting from a certain axle slip angle; a total toe-out angle causes a decrease.

During straight-ahead driving, toe-in angles cause unilateral wear of the tires on their outside shoulders. Static toe-in angles in the design attitude must therefore be small enough for them to be just about compensated by the bump toe-in caused by the rolling-resistance forces in conjunction with the elasticity of the wheel suspension.

Static toe-in angles are consequently not suited for the tuning of steering behavior. In many vehicles, kinematic bump toe-in during compression is used to specifically influence steering

behavior. For example, in vehicles with a concept-related oversteer tendency, the understeer tendency, which aids driving stability, can be intensified by a wheel suspension layout causing toe-out of the front wheels and toe-in of the rear wheels during compression. Such measures can be combined with camber changes, Fig. 2.4-24.

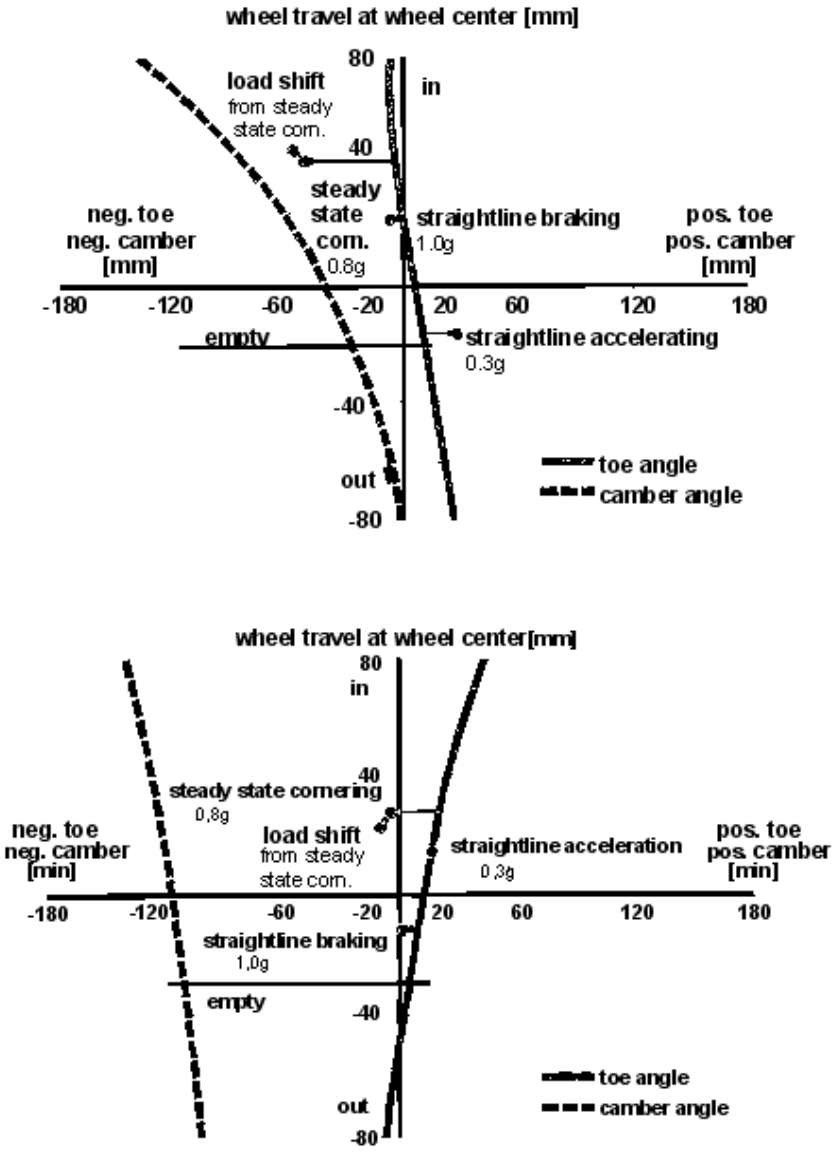

Fig. 2.4-24: Toe-in and camber characteristics (Audi A4, 1995)

The effect on steering behavior is referred to as "roll understeer", Fig. 2.4-25.

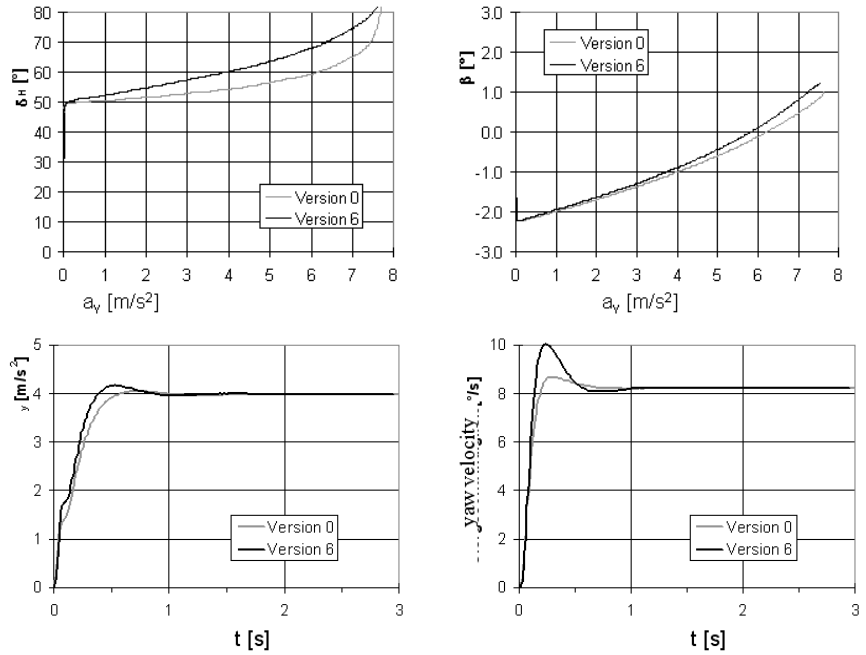

Fig. 2.4-25: Simulation results parametric variation no. 6 (toe-out on the front axle)

Layout must take into account the fact that kinematic bump toe-in, especially on the wheels of the rear axle, adversely affects straight-running properties, because suspension movements caused by roadway irregularity also result in bump toe-in and thus to undesired lateral-force fluctuation /45/.

As bump toe-in directly affects tire slip, only a few angular minutes suffice to bring about significant lateral-force variation. Vehicle handling is therefore not only affected by purely kinematic but also by elastokinematic bump toe-in.

Wheel suspension layout designed to fulfill certain elastokinematic properties as a rule requires very complex wheel control design. In many commonly used wheel suspension types, the elastokinematic properties caused by the rubber mounts needed for vibration isolation are therefore accepted, and the effect of the resulting wheel position changes (especially bump toe-in) is compensated by a specific kinematic layout, which is almost always easier to realize.

More recent designs, however, reflect the increasing efforts to realize a specific layout for elastokinematic properties.

The so-called "lateral-force oversteer", for example, can be avoided if rear-axle wheel suspension is designed in a manner that the lateral tire force during cornering does not cause toe-out of the outside wheel (which is more decisive for steering behavior because of a higher wheel load) /23/.

Elastokinematic bump toe-in not only occurs as a result of the effect of lateral tire forces but also due to the effect of longitudinal tire forces. Criteria for specific design are mentioned in Section 2.4.4.

2.4.3.6 Traction (Drive Concept)

Parametric variation regarding center-of-gravity height (version 0 - version 1) already included a reference to the fact that the traction forces required to overcome rolling-resistance forces and aerodynamic drag reduce instantaneous effective slip stiffness on the powered axle.

With narrow slip angles, the influence of the radial forces on the resulting lateral force is insignificant (cf. Section 2.2.4.2, Fig. 2.2-24, "Krempel Diagram").

With higher transversal acceleration, however, the slip angles required during cornering reach values at which simultaneously acting radial forces cause a reduction of the resulting lateral force, which has to be compensated by wider slip angles, which is tantamount to a reduction of the effective slip stiffness.

With increasing transversal acceleration during cornering on a constant track radius, not only the lateral forces will increase but also the radial forces on the powered wheels, since road resistance will increase with increasing driving speed.

As a result of this combined tire load, the axle slip angles required for the lateral forces to apply will increase progressively with increasing transversal acceleration. The effect is intensified by the wheel-load differences occurring during cornering.

Therefore, a front-driven vehicle features a steady-state steering behavior with an understeer tendency that increases until the stability limit is reached. A realistically responding vehicle with rear-wheel drive, i. e. a vehicle tuned for understeer by means of a specific layout of mass distribution, roll suspension rate, axle kinematics and tire inflation pressure, can show a trend reversal with regard to steady-state steering behavior, Fig. 2.4-26.

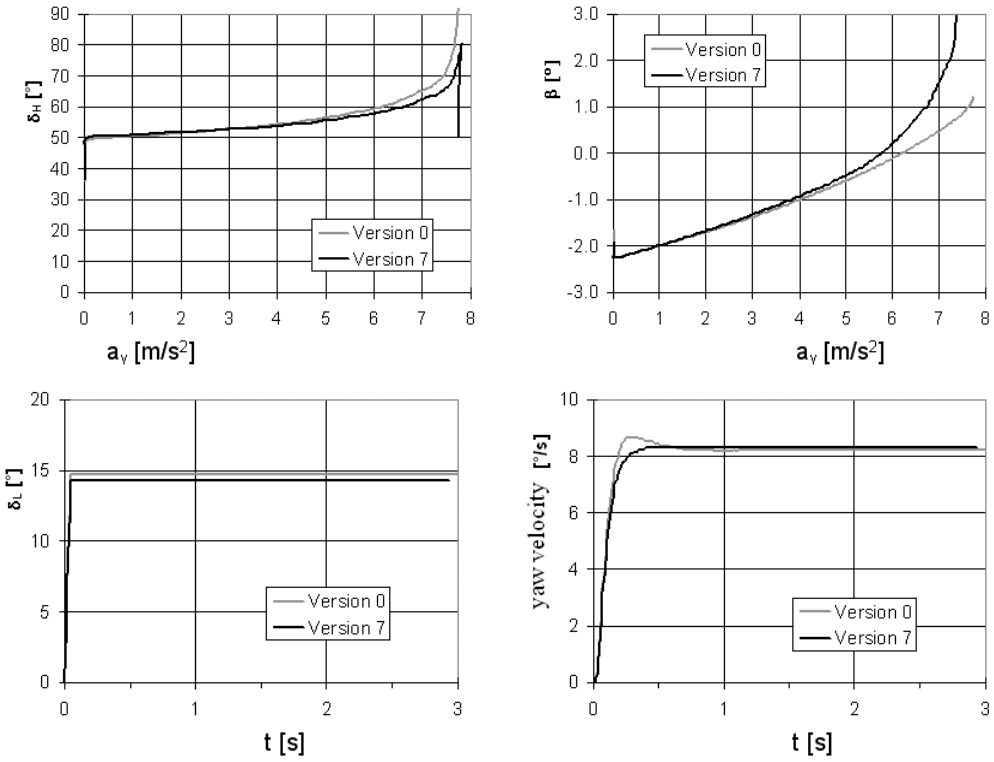

Fig. 2.4-26: Simulation results parametric variation no. 7 (RWD instead of FWD)

The trend reversal in steering behavior occurs when the decrease in slip stiffness on the powered axle due to the radial forces exceeds the decrease in slip stiffness on the front axle due to increasing wheel-load differences or other tuning measures.

The slip angles required on the rear axle thus bring about a very considerable sideslip angle. Front-axle slip angles corresponding to transversal acceleration require the steering angle to be reduced when the stability limit is approached (cf. equation 2.3-7, Section 2.3).

If driving speed is increased beyond the stability limit, the FWD vehicle with understeer tendency will drift with the front wheels to the outer edge of the curve. At the same time, the track radius driven is increased, transversal acceleration is reduced and the vehicle regains stability.

The RWD vehicle with trend reversal in steady-state steering behavior that is analyzed here, however, drifts with the vehicle tail to the outer edge of the curve when the stability limit is reached and thus turns into the curve. Consequently, transversal acceleration increases further, and without the driver promptly reducing the steering angle, the result will be a swerving motion of the vehicle around its vertical axis. Understeering on the stability limit is easier for the driver to control.

Of course, these statements only apply if the propulsive forces required to maintain the driving speed are constant. Vehicle behavior with load reversal or braking during cornering is dealt with in Section 2.4.4.

The behavior of AWD vehicles on the stability limit depends on propulsive-torque distribution among front and rear axles.

The design principle allows somewhat higher transversal acceleration than would be possible for a comparable vehicle with single-axle drive, since the tire load due to power transmission is more equally distributed among all wheels.

No matter what the drive concept is, in the tuning of steering behavior the fact has to be borne in mind that the transition from the stability limit to the range in which tracking is practically no longer possible will be more abrupt the closer the achievable limit transversal acceleration approaches the adherence-related, theoretically possible transversal acceleration and thus assessment of the approach of this transition cannot be handled by the driver.

2.4.3.7 Rear-axle auxiliary Steering

With the help of rear-axle auxiliary steering, the steering behavior of a vehicle can be influenced without narrow limitations.

In the parking range (low driving speed), the turning circle can be reduced by means of a heterodirectional steering angle of the rear wheels in relation to the steering angle of the front wheels, Fig. 2.4-27.

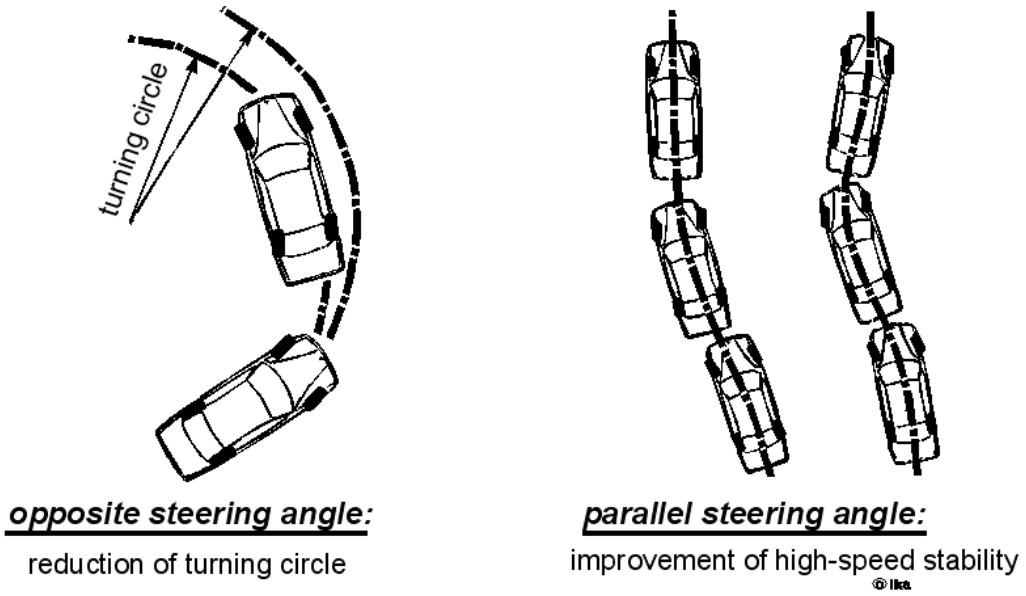

Fig. 2.4-27: Rear-axle auxiliary steering /40/

In a speed range that is interesting with regard to driving dynamics, a heterodirectional steering angle will, however, have a stability-reducing effect.

Nonstationary steering behavior can only be influenced positively by a homodirectional steering angle of the rear wheels. The effect is in a way similar to that of a rear axle whose elastokinematic design is such that the lateral force causes toe-in on the outside wheels.

Compared to such a passive rear-axle steering system, active rear-axle auxiliary steering, however, has the advantage that the build-up of lateral forces takes place immediately and not only after a change of the sideslip angle.

The effect of heterodirectional steering angles on the rear axle on driving dynamics can be assessed on the basis of the following consideration:

In a vehicle without rear-axle steering, lateral force will initially be built up only on the front axle as a result of a quick steering movement of the driver, Fig. 2.4-28.

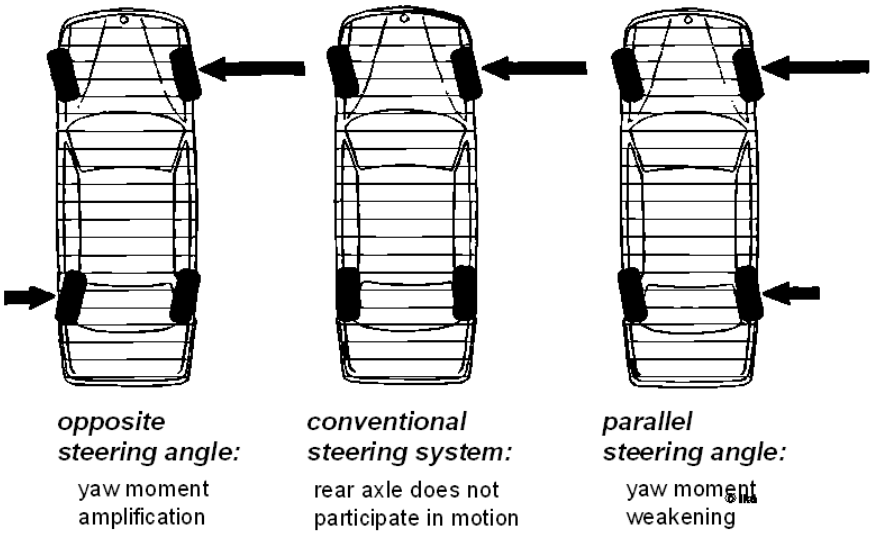

Fig. 2.4-28: Lateral-force buildup immediately after a sudden steering-angle change /40/

Not before the vehicle responds with transverse movement and yaw rotation to the excitation impulse caused, will there be a slip angle also on the rear axle; and a lateral force will be built up, which will result in a further increase in transversal acceleration and reduce yaw acceleration to zero (state of equilibrium of steady-state cornering).

In a vehicle with heterodirectional steering angle of the rear wheels, the lateral forces on front and rear axles are antagonistic immediately after a steering-angle change. The resulting transversal acceleration is thus at this point in time lower and yaw acceleration is higher than in a vehicle without rear-axle steering. Accordingly, a faster increase in yaw speed is to be expected, which will cause a distinct overshoot, while transversal acceleration will be slower in reaching its stationary final value.

The much more favorable steering response with regard to driving stability, fast increase in transversal acceleration in conjunction with a minor overshoot of yaw speed, can be achieved if lateral forces are built up on the front and on the rear axle immediately after the

steering-angle change, with these forces being directed towards the inside of the curve, that is with the help of a homodirectional steering angle on the rear axle. Fig. 2.4-29 shows the simulation results for steady state cornering.

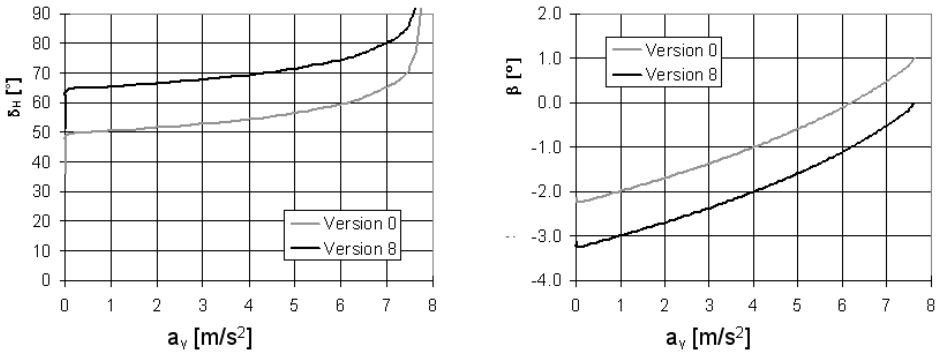

Fig. 2.4-29: Simulation results parametric variation no. 8
(rear-axle auxiliary steering $\delta_r = 0{,}2 \cdot \delta_f$)

With the aid of such elementary considerations it may be possible to answer the question of which would be the suitable direction of the steering angle on the rear axle, but they will not help determine a suitable functional relation between the steering angle on the front axle and the steering angle on the rear axle.

At least a theoretically meaningful control strategy for rear-axle steering can be achieved on the basis of the following consideration: Approach of the stability limit with regard to the driving dynamics of a motor vehicle is usually characterized by significant sideslip angles being reached very rapidly.

In such situations, the driver's reflex capacity is often overtaxed, because such vehicle movements and the steering movements required for stabilization are not within the range of stimulus-response mechanisms experienced by him in everyday traffic /11/.

Therefore, the obvious idea to fully compensate sideslip angles by means of rear-axle steering in the speed range that is interesting from the point of view of driving dynamics and thus to offer the driver a familiar steering behavior that remains virtually unchanged on the stability limit.

The basic makeup of the required functional relation between front and rear steering angles can be deduced with the aid of the linearized single-track vehicle model.

With a rear-axle steering angle being considered, the motion equations from Section 2.3 take the form:

$$m \cdot v \cdot \left(\dot{\psi} - \dot{\beta}\right) = c_{sf} \cdot \left(\delta_f + \beta - \frac{l_f}{v} \cdot \dot{\psi}\right) + c_{sr} \cdot \left(\delta_r + \beta + \frac{l_r}{v} \cdot \dot{\psi}\right) \qquad (2.4\text{-}16)$$

$$\Theta_z \cdot \ddot{\psi} = c_{sf} \cdot \left(\delta_f + \beta - \frac{l_f}{v} \cdot \dot{\psi} \right) \cdot l_f + c_{sr} \cdot \left(\delta_r + \beta + \frac{l_r}{v} \cdot \dot{\psi} \right) \cdot l_r \qquad (2.4\text{-}17)$$

Through insertion of the conditions for attitude-angle compensation? = 0, $\dot{\beta}$=0 in the two differential equations, the following transmission function between rear-axle and front-axle steering angles is obtained after a Laplace transformation /11/:

$$F_\delta(s) = \frac{\delta_r(s)}{\delta_f(s)} = P_r \cdot \frac{1 + T_D \cdot s}{1 + T_1 \cdot s} \qquad (2.4\text{-}18)$$

Attitude-angle compensation thus requires a transmission function equivalent to that of a PDT_1 element /32/.

- Amplification factor of the proportional component

$$P_h = -\frac{c_{sf} \cdot c_{sr} \cdot l_r \cdot l - c_{sf} \cdot l_f \cdot m \cdot v^2}{c_{sf} \cdot c_{sr} \cdot l_f \cdot l + c_{sr} \cdot l_r \cdot m \cdot v^2}$$

- Time constant of the D-proportion

$$T_D = \frac{\Theta_z \cdot v}{c_{sr} \cdot l_r \cdot l - l_f \cdot m \cdot v^2}$$

- Delay time constant

$$T_1 = \frac{\Theta_z \cdot v}{c_{sf} \cdot l_f \cdot l + l_r \cdot m \cdot v^2}$$

Attitude-angle compensation of stationary driving conditions consequently requires a speed-dependent steering ratio between front and rear axles.

Fig. 2.4-30 gives a qualitative representation of such a deduced "self-steering characteristic" for stationary driving conditions (only positive sideslip angles are compensated).

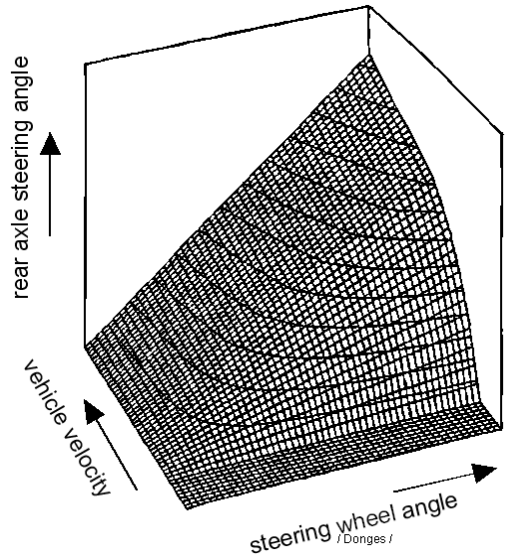

Fig. 2.4-30: Self-steering characteristic of rear-axle auxiliary steering for attitude-angle compensation (stationary) /11/

Attitude-compensation for nonstationary driving conditions also requires a certain time response of the control.

In real vehicles, the influence of the nonlinearity of the tire characteristics, the wheel-suspension kinematics etc. must be considered. A corresponding self-steering map would have to be experimentally determined instead of analytically.

Fig. 2.4-31 shows the effect of attitude-angle compensation on the nonstationary steering behavior of an automobile by means of simulation results of sinusoidal steering.

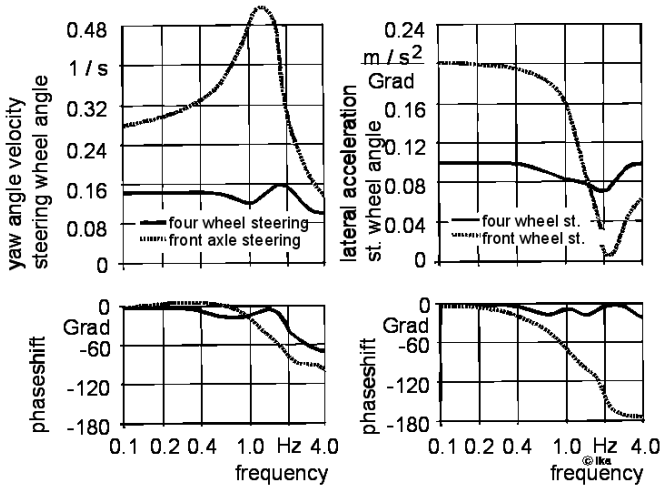

Fig. 2.4-31: Frequency curves of a vehicle with/without attitude-angle compensation by means of rear-axle auxiliary steering /4/

Driving speed is v = 150 km/h. The steering-angle amplitude was set for a transversal acceleration of $a_y = 4m/s^2$ to be reached for steady state cornering at v = 150 km/h.

In the vehicle with rear-axle auxiliary steering, a greater steering-angle amplitude is required, because a lower yaw-amplifying factor (cf. equation 2.3-30, Section 2.3.3.1) results from the homodirectional steering of the rear wheels simply because of the geometrical relations (cf. equation 2.3-7, equation 2.3-8). The yaw speed and transversal acceleration amplitudes relative to the steering-angle amplitude are therefore lower, which could be compensated by a more direct steering ratio on the front axle.

The vehicle without rear-axle steering shows a distinct resonance peak of the yaw speed amplitude in the range of the yaw natural frequency (ca. 1.1 Hz), which points to low yaw damping (due to the high driving speed; cf. Section 2.3.2). The low yaw damping results in after-vibration of the vehicle following steering movements of the driver, which affects driving stability.

In the same vehicle, but with rear-axle auxiliary steering, the yaw speed amplitude is almost independent of the excitation frequency of the steering motion. Yaw damping suffices to adequately dampen the yaw oscillation excited by the driver's steering movements. Yaw excitation is thus less intense in the vehicle with rear-axle auxiliary steering.

Moreover, the slight phase displacement between steering movement and transversal acceleration change, i.e. change of course of the vehicle, has a very positive effect on vehicle handling. With a steering frequency of about 1.1 Hz, a value associated with a fast lane-changing maneuver, for example, the change of course of the steering-angle change in the vehicle without rear-axle auxiliary steering is subject to a phase shift of about 90°. At the time the driver has already turned the steering wheel into the straight-ahead position, the vehicle will just about have reached maximum transversal acceleration or change of course. The vehicle will change its direction of motion although the driver is no longer steering. This effect is felt as a "shoving". In the vehicle with rear-axle auxiliary steering, the phase shift for this steering frequency amounts to only about 15°.

In addition to the control strategies of the nature described for rear-axle auxiliary steering systems, there are also control strategies conceivable that incorporate the rear-axle steering system in a closed loop for the control of desired values of driving dynamics. The yaw speed control system of the VW research vehicle IRVW4-Futura /34/ is an example for this. As such concepts are still of little practical relevance, they are not being dealt with in greater detail.

2.4.4 Influence of Processes of longitudinal Dynamics on transverse Dynamics

The primarily longitudinal-dynamical processes

- acceleration
- load reversal (releasing the accelerator, declutching)
- braking

during cornering usually also cause a transverse-dynamical vehicle response, which the driver has to compensate by means of steering correction.

On antiskid roadways, this vehicle response is mainly determined by the dynamic axle-load transfer between front and rear axles, which is caused during acceleration or deceleration by the force couple consisting of wheel radial forces and the inertia force acting in the center of gravity of the vehicle and the associated lateral tire force variations, Fig. 2.4-32.

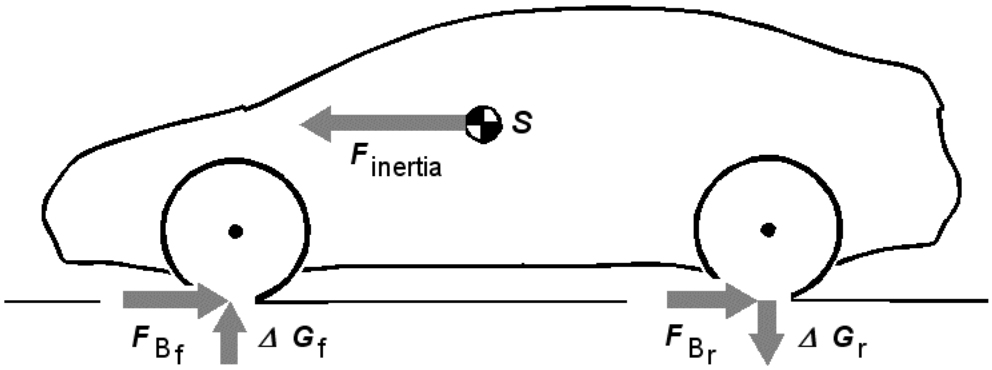

Fig. 2.4-32: Dynamic axle-load transfer during braking

On slippery roadways or in the case of very high longitudinal tire forces (high brake power), however, reduction of the transferable lateral tire forces with simultaneously forced longitudinal tire forces will have a stronger effect (cf. Section 2.2.5).

Especially during braking, a cross-dynamic vehicle response to be controlled by the driver will occur also during straight-ahead driving if there is a significant divergence of the friction coefficients of left and right lanes (μ-split).

2.4.4.1 Accelerating during Cornering

Accelerating results in the front axle being relieved and the rear axle being additionally loaded as a result of dynamic axle-load transfer. On an antiskid roadway and without steering correction, RWD vehicles as well as FWD vehicles will drift with their front axles towards the outer edge of the curve, because the resulting axle lateral force on the front axle decreases with the axle load, and the centrifugal force to be supported increases with the increase in driving speed.

FWD vehicles usually require more steering correction since the traction forces transmitted on the front axle reduce the simultaneously transmittable lateral forces, and this results in the dynamic understeer tendency being additionally intensified.

As a rating for the vehicle response to accelerating during cornering we may use the yaw speed difference at the point in time Δt, which results from the transition from steady state cornering at R = const. to accelerated skidpad drivíng, with the steering wheel being fixed. Fig. 2.4-33 shows the yaw speed differential after 1 sec in relation to longitudinal acceleration for various drive concepts.

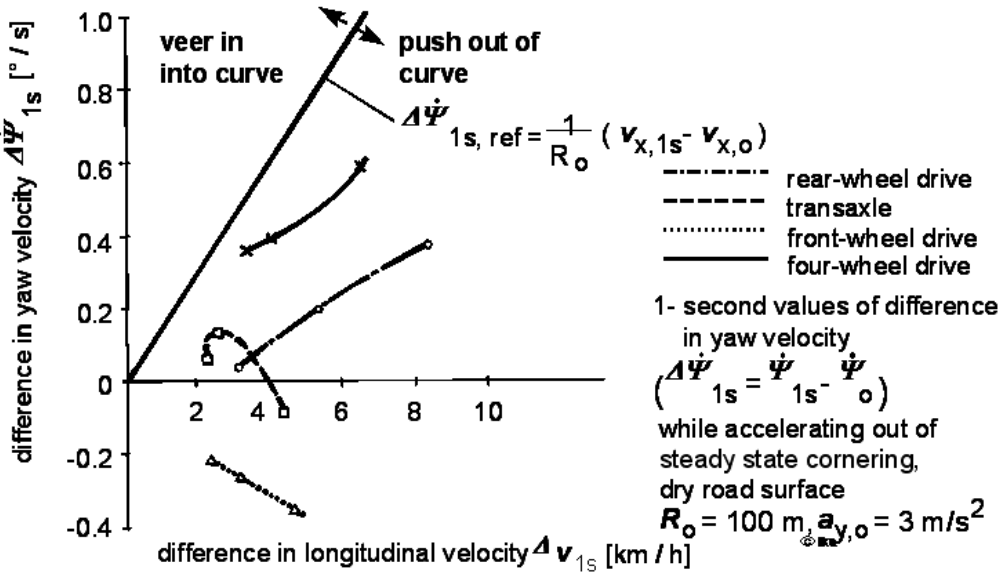

Fig. 2.4-33:Yaw speed variation for accelerating during cornering /37/ on an antiskid roadway

The reference straight marks the yaw speed increase that would result from the driving speed increase if acceleration was not associated with a deviation from the initial radius.

On slippery roadways, vehicle reactions are clearly more intense, Fig. 2.4-34. The dynamic oversteer of the tested RWD vehicles caused by overlapping lateral and longitudinal tire forces results in the vehicle veering into the initial radius.

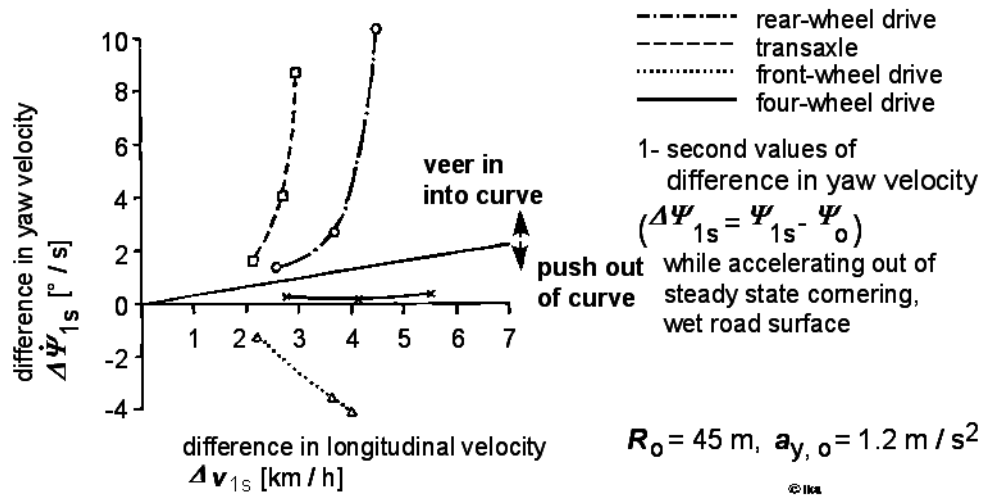

Fig. 2.4-34:Yaw speed variation for accelerating during cornering /37/ on a slippery roadway

The advantages of the distribution of the traction forces among four wheels in the case of AWD become obvious on a slippery roadway. On a dry roadway, however, the differences are rather due to the steady-state steering behavior (minor understeer tendency) than to the drive concept.

2.4.4.2 Load-Alteration during Cornering

Load-alteration is a sudden change in the traction forces caused by abrupt accelerator-position changes, during declutching or at the beginning of a gearshift of an automatic transmission.

During cornering, suddenly changing radial forces on the powered wheels cause a yaw response of the vehicle, which without steering correction by the driver will result in the vehicle veering into the curve. The most violent excitation is caused by the sudden release of the gas pedal, because the traction forces are not only reduced to zero but are converted into brake forces due to the engine-drag torque.

Since sudden release of the gas pedal is a natural reflex of a driver entering a curve to fast or faced with a narrowing curve, the load-alteration effect during cornering is of great importance for active driving safety. Moderate veering-in of the vehicle caused by load-alteration is considered favorable. It must not, however, be so vehement that the driver is unable to perform the steering corrections required to stabilize the vehicle. The load-alteration effect results from the superimposition of a number of individual factors, Fig. 2.4-35.

Causes of the load-alteration effect Transmission type	Tendency of change of self-steering response FWD	RWD	AWD
1. Traction influence			
- Change from drive to radial force = 0	↑	↓	-
- Change from radial force = 0 to decelerate	↓	↑	-
2. Influence of wheel-load transfer on cornering forces	↑	↑	↑
3. Reduction of understeer through reduction of speed	↑	↑	↑
4. Change of a traction-force component pulling into the radius	↓	-	↓
5. Kinematic wheel-position change due to pitching and rolling	Effect depending on wheel suspension		
6. Elastic wheel-position change due to changed wheel radial forces	Effect depending on wheel suspension		
7. Steering torque due to diffraction angles on drive joints	↑	-	↑
8. Twist due to yaw speed variation	↑	↑	↑
9. Change of lateral-force aligning torque with change of wheel radial forces	↑	↓	-
10. Influence of lateral displacement of the tire contact area	↑	↑	↑

(↑ = oversteer ; ↓= understeer); AWD with ideal force distribution

Fig. 2.4-35: Causes of the load-alteration effect /6/

The by far greatest influence on the load-alteration effect is exerted by the dynamic axle-load transfer, which results in the front axle being additionally loaded and the rear axle being relieved when the gas pedal is suddenly released. Fig. 2.4-36 illustrates the resulting lateral-force variations on front and rear axle.

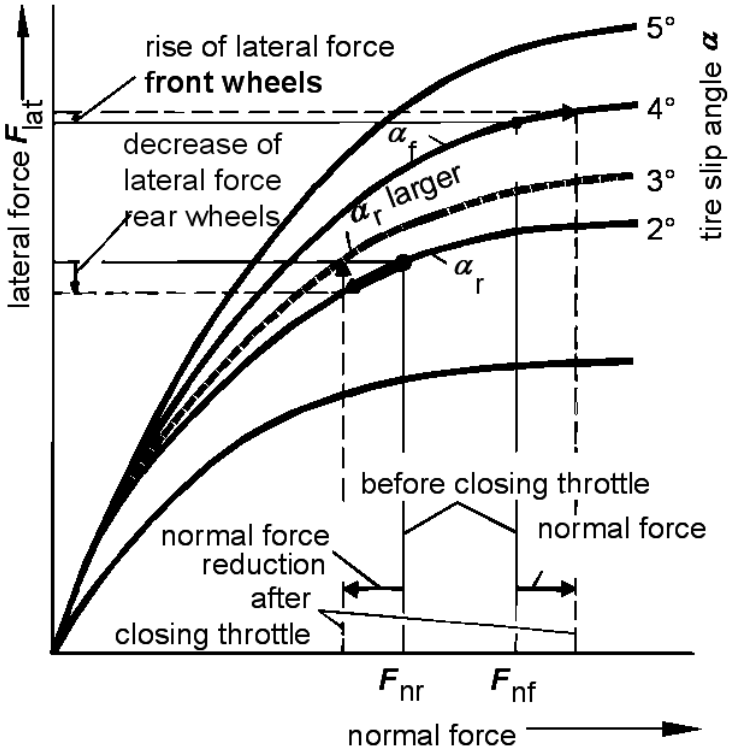

Fig. 2.4-36: Lateral-force variation associated with load reversal /6/

Lateral-force increase on the front axle and simultaneous lateral-force loss on the rear axle cause a veering-in yaw moment (dynamic oversteer) independent of the drive concept. As a result of the kinematic properties of the wheel suspension, veering-in is usually aided. Section 2.4.3.5 deals with the fact that toe-in angles and negative camber angles on the rear axle, which increase with the compression travel, will intensify the understeer tendency favorable for driving stability. Load reversal, however, is associated with a rebounding rear axle due to the dynamic axle-load transfer. The instantaneously effective lateral forces due to negative camber and toe-in are reduced in a vehicle with specifically designed rear-axle kinematics, and the lateral-force loss on the rear axle due to the axle-load transfer is intensified, and thus the load-alteration effect.

Mitigation of the load-alteration effect can be achieved by a specific design of the elastokinematic characteristics of the powered axle (cf. Section 2.6.3). If, for example, the traction forces of a RWD vehicle cause toe-out on the outside rear wheel while the brake forces cause toe-in, then this self-steering effect, which is controlled by the variation in longitudinal tire force, will immediately counteract the load-alteration effect.

Assessment of the load-alteration effect is based on the following criteria: Deviation of the center-of-gravity path from the initial radius following a load alteration during steady-state cornering and with fixed steering wheel, Fig. 2.4-37, as well as the associated deviations of the kinematic parameters from the initial values 1 s after load alteration (driver's response time).

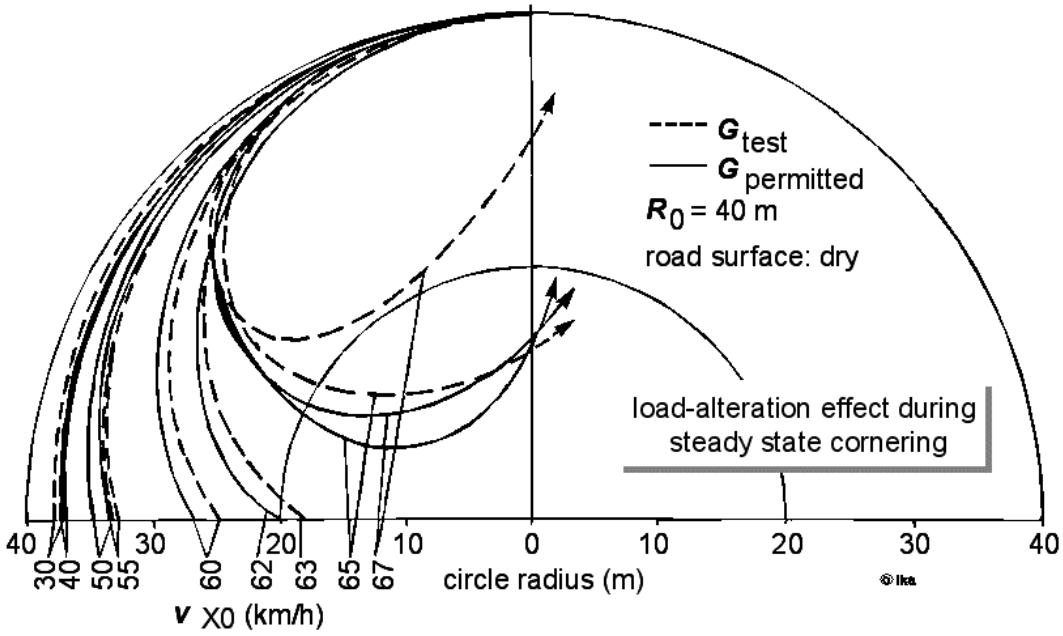

Fig. 2.4-37:Deviation of the center-of-gravity path associated with load alteration /37/

Initial radius and initial transversal acceleration are the parameters varied, Fig. 2.4-38.

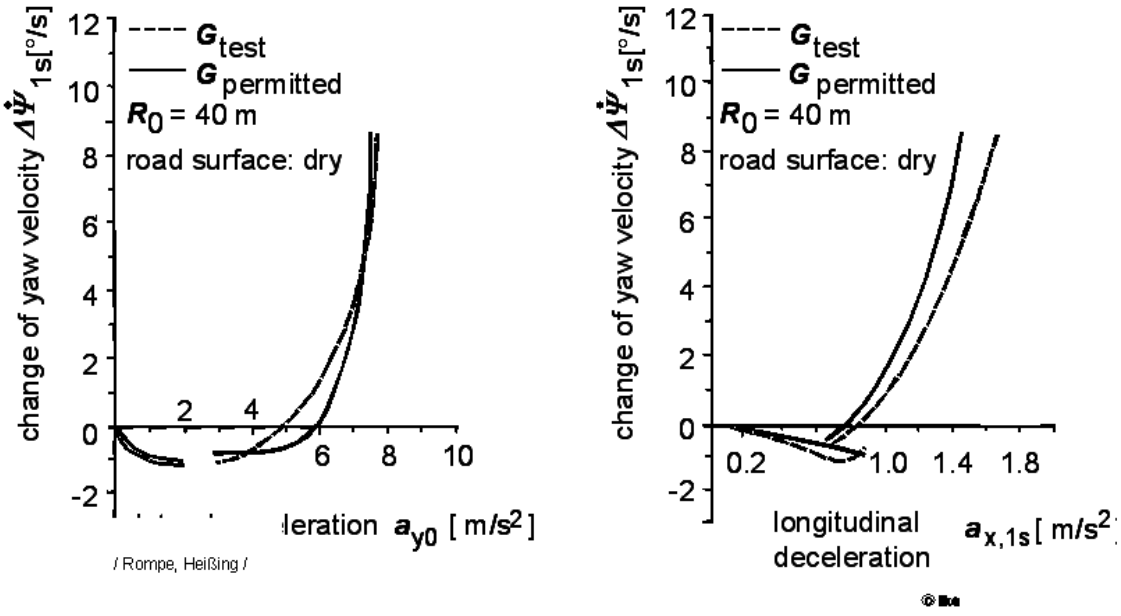

Fig. 2.4-38: Yaw speed deviation 1 s after load alteration (FWD vehicle) /37/

2.4.4.3 Braking during Cornering

Light, mean and hard deceleration must be differentiated when vehicle response to braking during cornering is examined. In the case of light to mean braking, the effect of the preceding load alteration will be intensified, i.e. there will be a stronger veering-in motion of the vehicle. As for load reversal, vehicle response is largely determined by the oversteer-generating yaw moment, which is caused by the dynamic axle-load transfer.

In the case of mean to hard braking, however, vehicle response will increasingly depend on the influence of the longitudinal tire forces on the simultaneously transmittable lateral tire forces.

Depending on brake-power distribution between front and rear axles, two borderline cases of vehicle response must be differentiated. If the rear axle is overbraked during cornering (i.e. the friction coefficient utilized on the rear axle exceeds that of the front axle), then the rear of the vehicle will break away when the adhesion limit is reached, and vehicle yaw stability will thus be lost. If, however, the front axle is overbraked, maneuverability will be lost when the adhesion limit is reached, but the vehicle will retain its yaw stability and be controllable again after release of the brake.

Safe yaw stability thus requires a brake power distribution providing an adequate safety distance between the curve of the installed brake power distribution and the parabola of the ideal brake power distribution for straightline braking, or the use of a brake-power controller for controlled brake-power distribution in relation to deceleration. With the help of an antilock system, steerability can also be retained in case of a hard stop.

Criteria of assessment used are the values of the kinetic parameters 1 s after the start of braking (driver's response time) for steady state cornering with fixed steering wheel, Fig. 2.4-39.

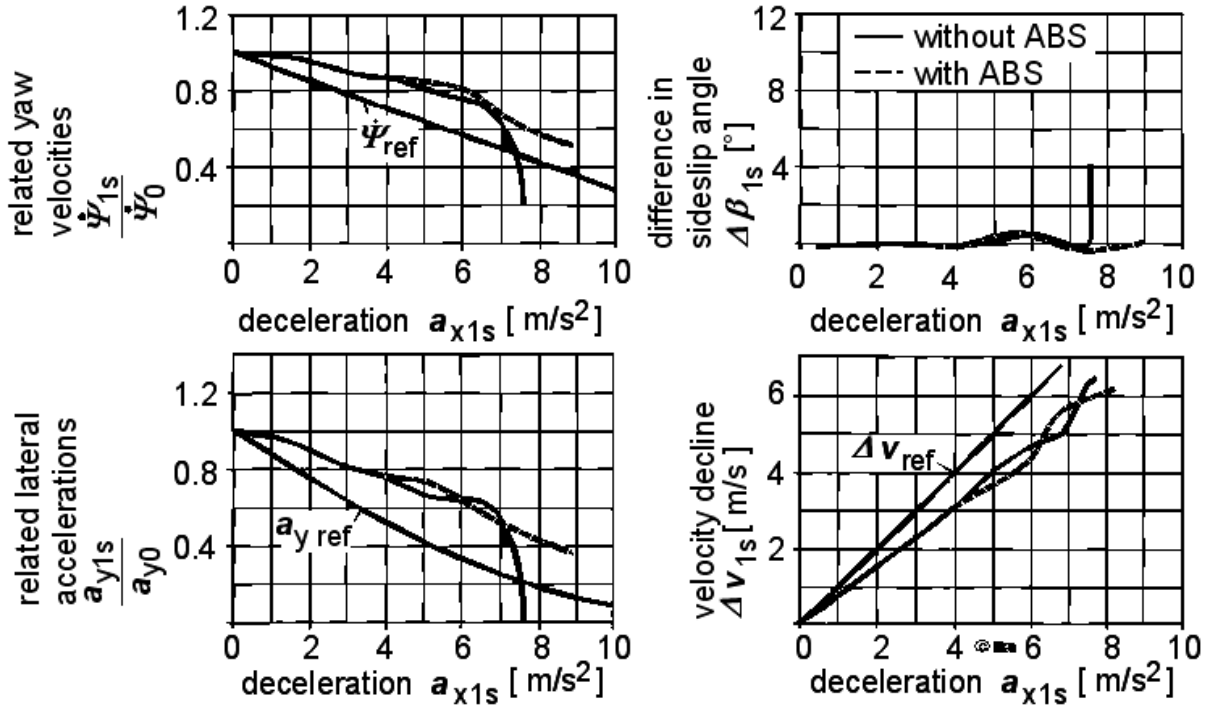

Fig. 2.4-39: Parameters for the description of vehicle response to braking during cornering /37/

Initial radius, initial transversal acceleration and longitudinal deceleration are the parameters varied. If these values are above the reference lines for braking deceleration with exact adherence to the initial radius, this will point to veering-in of the vehicle into the radius during braking. The limit of maneuverability is characterized by the fact that transversal acceleration after the start of braking drops to zero. Yaw velocity drops below the reference line in this case, because the vehicle drifts with its front axle towards the outer edge of the curve.

2.4.4.4 Braking on Roadways with Lanes of Different Friction Properties (μ-split)

Braking on a roadway with lanes of different Friction properties (e.g. roadway with icy curb lane) will cause a brake-power difference between right and left vehicle sides resulting in a yaw moment, which will make the vehicle turn into the lane with the higher friction properties. For this yaw moment to be compensated, a force couple composed of a lateral force acting on the front axle and an antagonistic lateral force acting on the rear axle must be realized, Fig. 2.4-40.

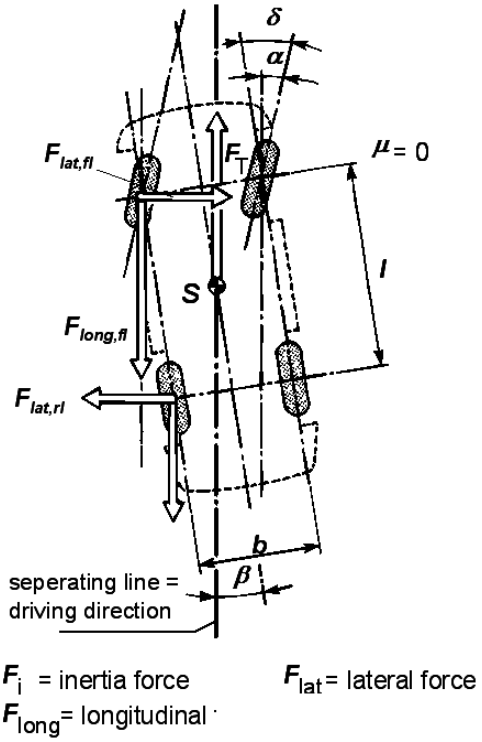

Fig. 2.4-40: Yaw moment balance for braking under μ-split conditions /8/

The slip angle required on the rear axle can only be realized if the vehicle-sideslip angle β during braking deceleration is oriented towards the direction of travel. On the front axle, a steering angle oriented towards the lane with inferior friction properties is required. Braking stability is improved if the elastokinematics of the wheel suspension is such that the brake power causes toe-in on the front wheel running on the antiskid surface, Fig. 2.4-41.

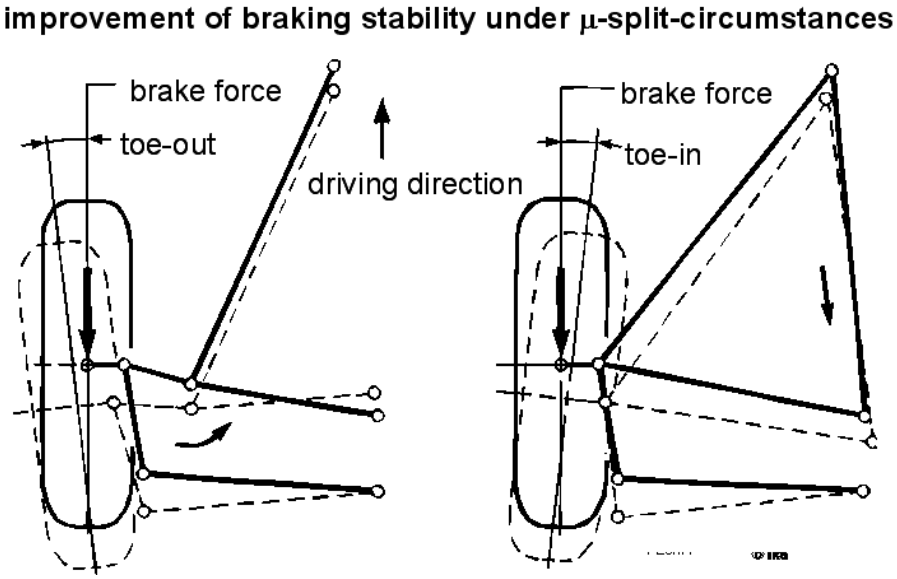

Fig. 2.4-41: Elastokinematic layout of front-wheel suspension for the improvement of braking stability under μ-split-conditions /28/ (right)

Immediately at the start of braking, before the driver's reflex time has lapsed and countersteering is initiated, a yaw moment is already built up which counteracts the yaw rotation caused by the brake-power differential. However, when tuning is carried out, the fact must be borne in mind that such a layout will aid veering-in of the vehicle into the curve.

Another way of making vehicle handling during braking on μ-split easier to control by the driver is offered by vehicles equipped with an antilock system (ABS). If the ABS-controlled wheel running on a high-friction surface is initially underbraked, then buildup of the yaw moment caused by the brake-power difference is delayed and timely countersteering by the driver is facilitated. The driving condition is determined through analysis of the rotational wheel acceleration during braking deceleration. An additional transversal acceleration sensor prevents response to cornering at high transversal acceleration.

Similar to braking during cornering, the deviations of the kinetic parameters at a certain point in time after the start of braking ($\Delta t = 0.5s$ or $\Delta t = 1.0s$) are used as assessment criteria for braking deceleration on μ-split, with the parameters initial driving speed and braking deceleration being used.

2.5 Steering

In the control loop consisting of the driver and the vehicle, the steering wheel angle forms a control variable, which has to be given by the driver in such a way that a deviation from the desired course remains small. However, there does not exist any distinct functional relation between the steering wheel turn executed by the driver and the change of direction necessary for a correction of course. The reasons for this are, for example, the elasticities in the steering system components and the occuring lateral accelerations. The relation between steering actuation and change of driving direction is represented in Fig. 2.5-1.

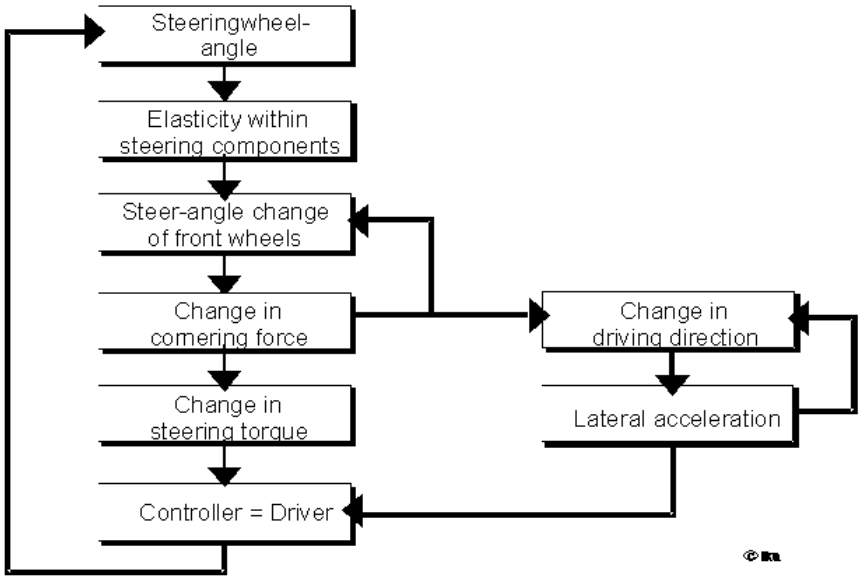

Fig. 2.5-1: Relation between steering actuation and change of driving direction

In order to drive a vehicle, the driver must constantly analyze the relation between steering wheel turn and change of driving direction. Apart from the optical information (deviation from the desired course), he receives a lot of further information, including for example lateral acceleration transmitted by the seat and steering torque passed on by the steering wheel.

The function of the steering system is not only to transfer the steering wheel angle by a distinct allocation into a wheel steering angle but also to transmit information about the status of the vehicle movement to the driver.

In the previous paragraphs (chapter 2.2 – 2.4), the part of the control system between wheel angle modification and change of driving direction was dealt with. Now, the requested features of the structural component which defines the relation between steering wheel angle and the steering angle of the wheels are treated.

2.5.1 Specifications of Steering Systems

Since humans are integrated into the overall system driver – vehicle by the steering, the demands on this component are defined by the characteristics of humans and those of the vehicle shown in Fig. 2.5- 2.

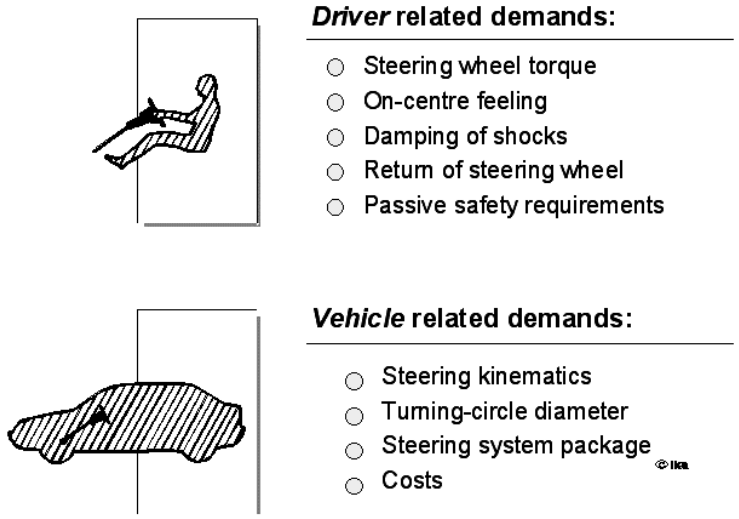

Fig. 2.5- 2: Demands on the steering system

2.5.1.1 Driver related Demands

- Hand force

The steering moment necessary for the movement of the turned-in wheels significantly depends on the driving velocity, Fig. 2.5-3.

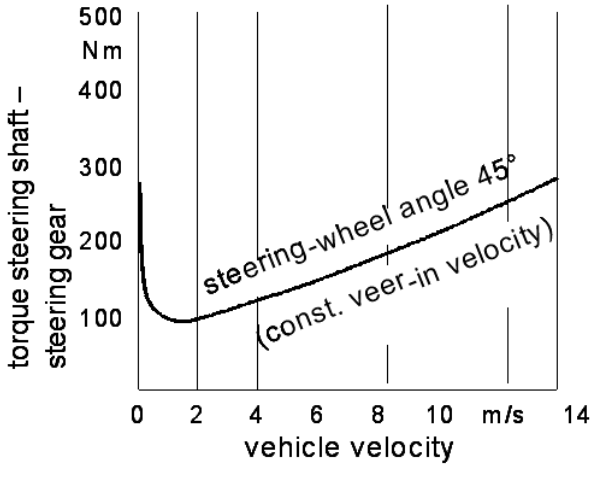

Fig. 2.5-3: Steering resistance as a function of the driving speed (passenger car) /13/

It must be ensured that the necessary steering forces can be applied by the driver in all conditions. The torque necessary for the steering movement is reduced to values which can be applied by the driver by a transmission ratio between the steering wheel movement and the rotation of the front wheels, Fig. 2.5-4. However, a large steering ratio increases not only the steering wheel way, but also the physical strain of the driver.

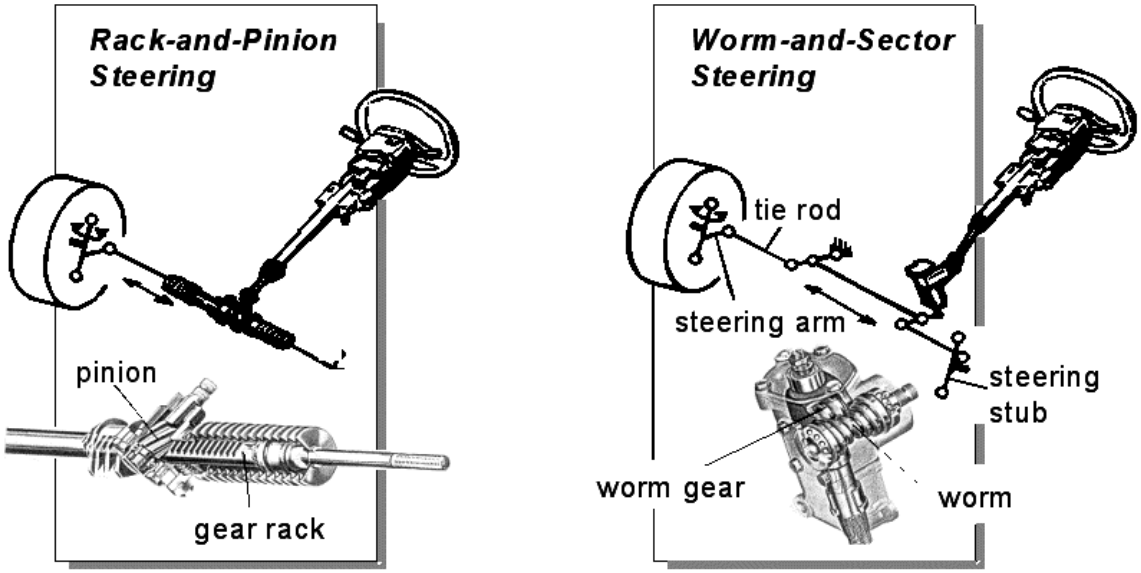

Fig. 2.5-4: Rack and pinion steering, worm and sector steering

- Sensitivity

The term ‘sensitivity’ defines the demand for the direct and distinct conversion of the steering wheel turn into a steering movement of the wheels and the feedback of the forces acting on the wheels. These demands prohibit any play in the steering system in extreme cases and cause small elasticities between steering wheel turn and steering movement of the wheels, as well as small frictional forces in the joints of the steering system.

- Damping of shocks

If an impact affecting the wheels is transmitted to the steering wheel undamped, a steering movement occurs before the driver is able to counterbalance the occurring forces. That means, that in the interest of a satisfying steering performance (comfort and safety), high frequency disturbances in the steering system should be damped or even compensated.

- Return of the steering wheel

The steering system should remain in the straight-ahead position without the driver’s intervention and turn back into the neutral position after a deflection automatically.

- Passive safety requirements

In the case of an accident it must be ensured that steering system components do not penetrate into the passenger compartment and that the steering wheel can sustain an impact of the driver (secondary collision), for example by an impact plate, a deformation element or a slewing device.

2.5.1.2 Vehicle-related Demands

- Steering kinetics

The steering linkage is placed between the steering gearbox and the steered wheels. Its layout fixes the connection between steering wheel turn and wheel deflection (fig. 2.5-4). Important boundary conditions for the definition of the linkage kinetics are:

- No steering reaction with spring movements of the wheels (condition for high straight-running stability) and spring processes

- Slip-free rolling of the tires while cornering with large steering angles (favorable for maneuverability of the vehicle within the parking area)

- Small toe-in variations with small steering angles (favorable for the build-up of the tire lateral forces while cornering normally)

Width requirement of the vehicle

The width requirement is described by the width of a circular ring, which is needed by a vehicle for driving along a curve. Regulations concerning the width requirement of vehicles are issued by the legislative assembly (StVZO § 32).

- Space requirement of the steering element

The arrangement of engine-gearbox unit, wheel suspension and steering system is determined on the one hand by the demand for a good economy of space in the front section of the body, and on the other hand there has to be considered the demand for high impact safety of the vehicle (crash performance) when integrating these components into the deformation zone. One criterion for the selection of a certain steering system design is therefore the space requirement in the vehicle and the integration possibility into the fixed package structures.

- Construction expenditure

In the objective of economy, the structure of a steering element should be as simple as possible.

2.5.2 Characteristic Values of the Front Wheel Adjustment

With steering movements, the wheels swivel around one wheel-fixed axis of rotation, which is called the ‘steering axis’ in the following. The position of the steering axis relative to the vehicle body or the roadway surface is described by the following characteristic values, Fig. 2.5-5:

- Wheel castor angle: Angle between steering axis and road normal in the vehicle longitudinal plane

- Wheel castor offset: Distance between the meeting point of the steering axle and the road surface and the idealistic center of tire contact in the vehicle longitudinal plane

- Spreading angle: Angle between steering axle and road normal in the vehicle lateral plane

- Kingpin offset: Distance between the meeting point of the steering axle and the road surface and the idealistic center of tire contact in the vehicle lateral plane

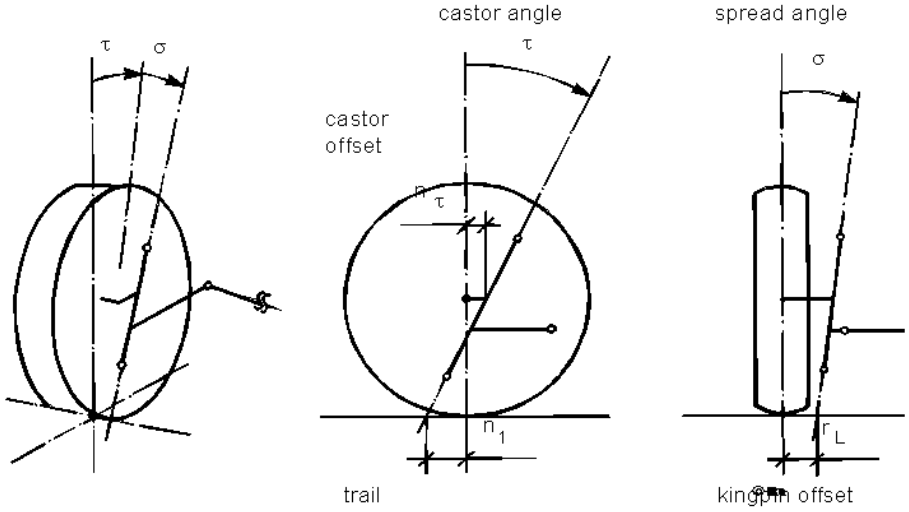

Fig. 2.5-5: Characteristic values for the position of the steering axis

As further characteristic values of the front wheel adjustment, for the characterization of the wheel position of the vehicle, the toe-in angle (paragraph 2.4.3.5) and the camber angle (paragraph 2.4.3.5) are indicated. The position of the steering axis and the wheel adjustment in the design position, have a large influence on the characteristics of a steering system. In particular, in order to achieve the driver-specific demands presented in the previous paragraphs, there is a special configuration necessary.

The steering axle is represented by a kingpin only in the case of a rigid truck front axle, Fig. 2.5-6.

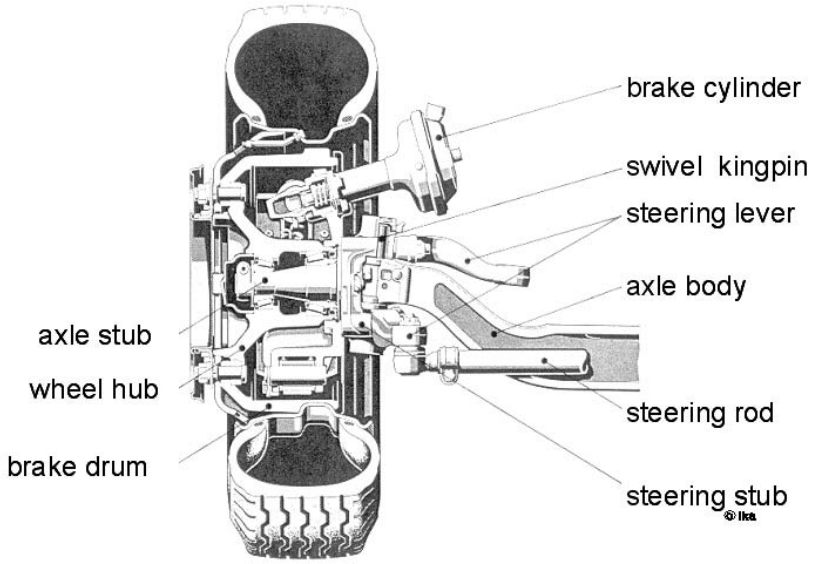

Fig. 2.5-6: Truck front axle (steering stub axle), Mercedes Benz

With modern double wishbone or suspension / shock-absorber strut front axles (McPherson axle) the steering axle either hits the ball-and-socket joints, which connect the wheel carrier to the wishbones, or it hits the upper body-facing journal bearing of the suspension / shock-absorber strut, Fig. 2.5-7 (right).

The complete resolution of a space-fixed axis of rotation is shown in Fig. 2.5-7 (left). With this four-link wheel suspension, the connecting line of the instantaneous centers of the upper and lower double joints represents the instantaneous axis while steering. This virtual steering axle can be fixed by very near to the wheel center by an appropriate arrangement of the ball-and-socket joints. By this fact, this design permits to shorten the so-called disturbing force lever arm significantly. The disturbing force lever arm represents the preponderant value for disturbing influences on the steering element by longitudinal forces.

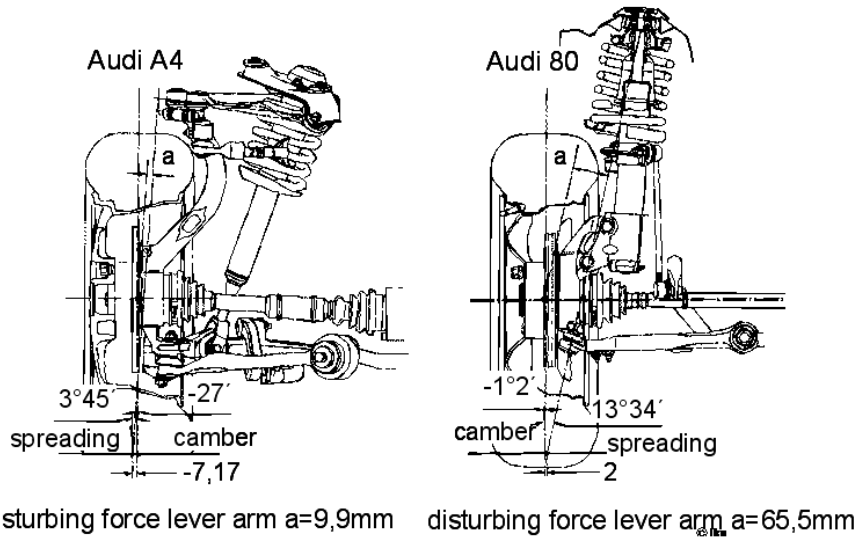

Fig. 2.5-7: Position of the steering axle of four-link wheel suspension and McPherson front axle

Fig. 2.5-8 gives a spatial impression of the displacement of the axis of rotation while steering. By the coupled movement of the two double joints, the motion of the virtual steering axis generates a surface curved to the center of the vehicle.

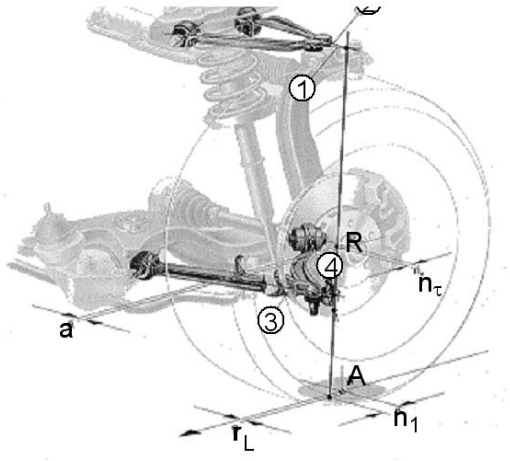

①-④ direction of suspension arms
R wheel centre
A tyre contact patch

Fig. 2.5-8: Movement of the virtual steering axis while steering, Audi A4

- Wheel castor angle and wheel castor offset

The wheel castor angle and castor trail in the wheel center together determine the resulting castor offset, Fig. 2.5-9.

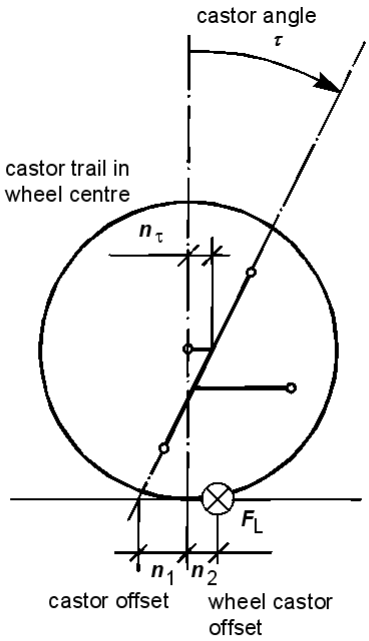

centrifugal castor: $M = F_L \cdot (n_1 + n_2) \cdot \cos \tau$

Fig. 2.5-9: Wheel castor angle, castor trail in the wheel center, constructional castor offset, tire castor and lateral force.

This constructional offset n_1 is added to the tire castor n_2 (paragraph 2.2.4.1). Lateral forces in the point of wheel contact produce an aligning torque around the steering axis in combination with the castor. The castor moment

$$M = F_s \cdot (n_1 + n_2) \cdot \cos \tau \qquad (2.5\text{-}1)$$

stabilizes the straight-running stability, since it is always acting against a deflection of the wheel from the straight-ahead position. While cornering, the centrifugal castor results in a partial value of the aligning torque, which causes the steering system to return into the straight-ahead position after releasing the steering wheel automatically.

Since the centrifugal castor depends on the forces transferred between tires and roadway, the driver receives information about the grip conditions between tire and roadway from the steering torque perceived at the steering wheel, which results from the centrifugal castor.

For the determination of the castor offset, a combination of castor angle and castor trail in wheel center is selected. As a consequence, one has the possibility of arranging the ball-and-socket joints or the support bearing (shock-absorber strut) of the kingpin mounting in such a way, that on the one hand a certain castor offset results, and that on the other hand the clamping friction in the suspension system is small. Additionally, there has to be considered, that a positive castor angle causes wheel camber variations, which reduce the understeering tendency of a vehicle during steering procedures.

Castor angle and castor offset are represented as a function of the steering angle in Fig. 2.5-10 for the two exemplary axles shown in Fig. 2.5-7.

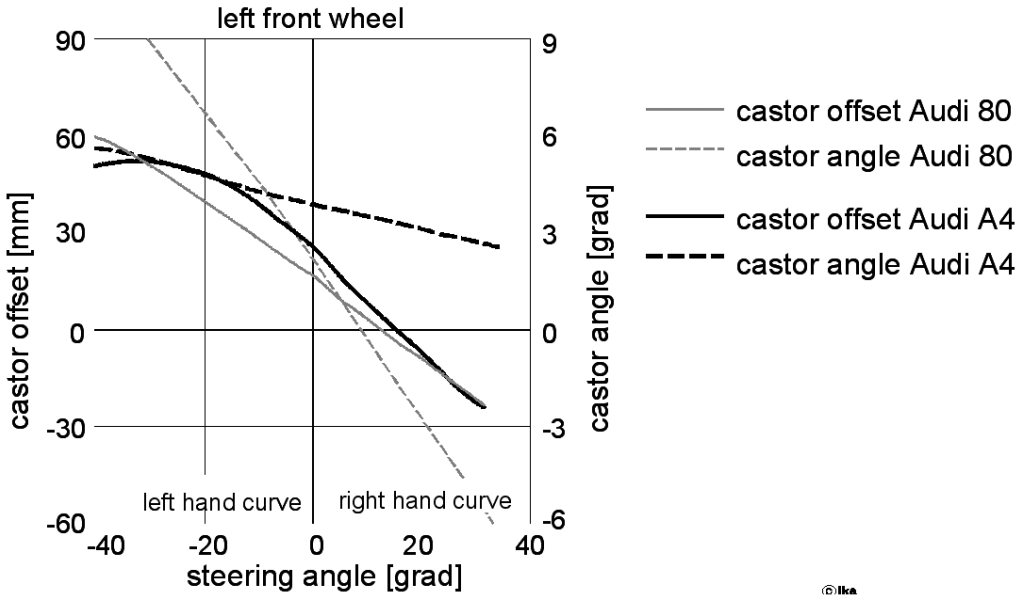

Fig. 2.5-10: Castor angle and castor offset in relation to the steering angle for a four-link wheel suspension and a McPherson axle

In order to avoid a veering-in effect in the limitation stop positions of the steering system, it has to be assured during the configuration of the castor change according to the steering angle, that the sum of inner and outer castor value remains positive, Fig. 2.5-11.

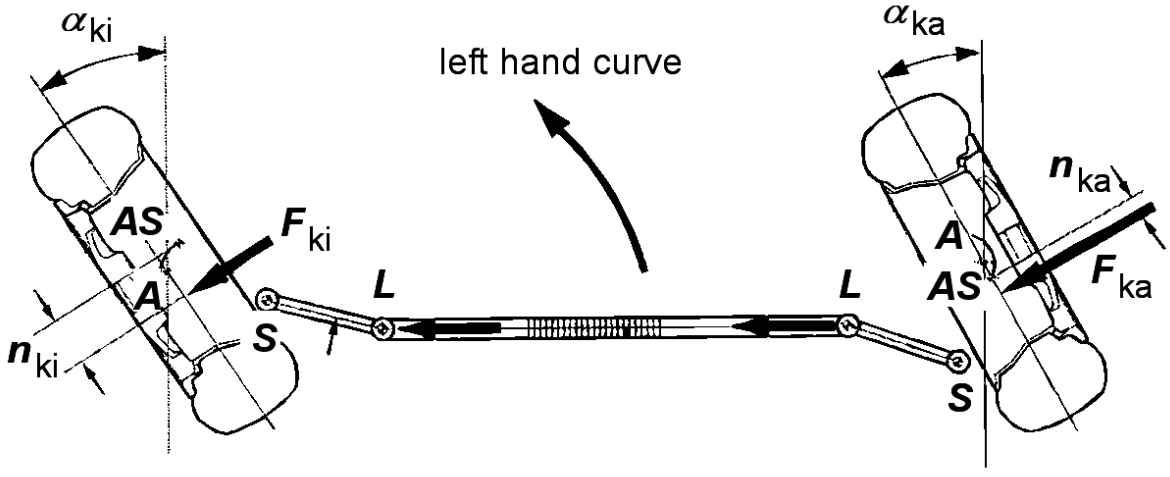

Fig. 2.5- 11: Steering system alignment resulting from the lateral forces

- Spread angle and disturbing force lever arm

Due to the process of construction, it is difficult to arrange the steering axis in such a way that tire radial forces do not cause reaction torques in the steering system. The required space for ball-and-socket joints in the rim disc, is needed for the positioning of the brake system. With suspension and shock-absorber strut axles, such a construction cannot be implemented as a matter of principle.

The rolling-friction forces and, with powered front axles, the driving forces, act on the wheel carrierer at the height of the wheel center line. The resulting reaction torques in the steering system depend on the size of the disturbing force lever arm “a”, Fig. 2.5-12.

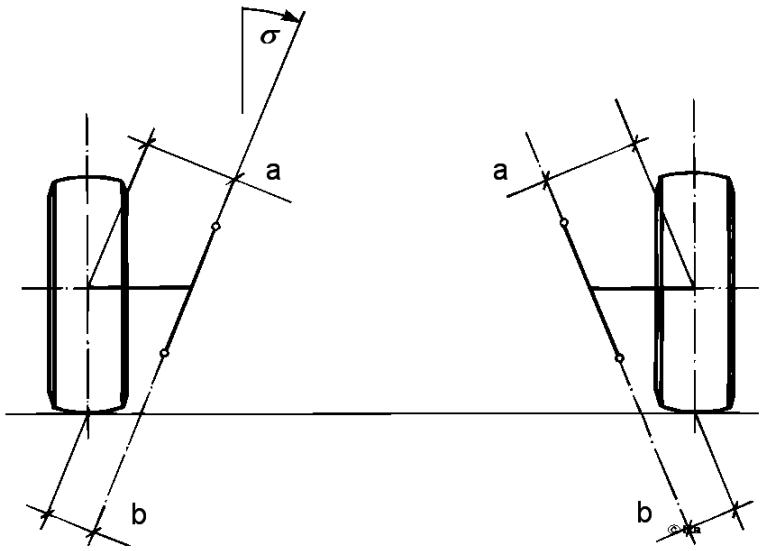

Fig. 2.5-12: Disturbing force lever arms of the longitudinal tire forces at the steering system

During straight-ahead driving (no difference in tire compression, no lateral offset of the tire contact patch) these reaction torques at the right and left wheel are compensated, since the rolling-friction forces differ insignificantly and the driving torques are almost identical due to the differential gear conditions.

Contrary to rolling-friction and traction forces, the braking forces acting on the wheel carrier in the point of wheel contact (external brakes fastened at the wheel carrier) may differ significantly for right and left wheel (μ-split).

In order to reduce the disturbing force lever arm “b” of the braking forces, the steering axle is inclined with the spreading angle value “σ” in the vehicle lateral plane, Fig. 2.5-12. By that, a smaller moment of inertia around the steering axle of the parts of the wheel suspension deflected with steering movements is obtained, and the tendency of the steering system to flutter vibrations is lowered.

The disturbing force lever arm “b” is directly proportional to the steering roll-radius r_L:

$$b = r_L \cdot \cos \sigma \qquad (2.5\text{-}2)$$

The inclined position of the steering axle with the spreading angle σ entails two further effects:

- Variation of the self-steering response: With steering movements, wheel camber modifications occur, which increase the understeer tendency of the vehicle (paragraph 2.4.3.5).

- Weight-caused self-alignment: In combination with the lever arm “a”, the vertical force F_N produces a weight-caused resetting of the steering element at the point of wheel contact, which is essential for the automatic return of the steering element to the neutral position as well as for the avoidance of the veering-in of the steering element during slow travel, since, in this case, there are no lateral forces acting on the tires, Fig. 2.5-13.

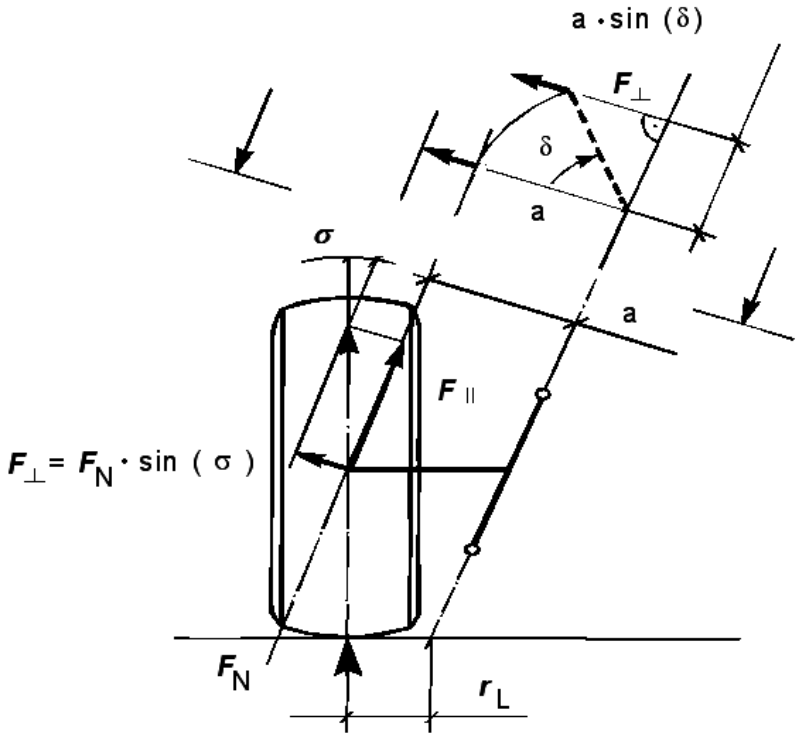

Fig. 2.5-13: Weight-caused self-alignment as a consequence of the spread angle σ

- Kingpin offset

With a large distance between center of tire contact and meeting point of the steering axis and the roadway surface, the wheel would roll approximately along a circular arc around the meeting point during the steering movement. Therefore, the distance is called steering king-pin offset r_L.

As mentioned above, the kingpin offset should be as small as possible in order to reduce reaction torques in the steering system caused by asymmetrical braking forces. In addition, these reaction torques can be used to influence the driving behavior directly.

On the one hand, it is possible to cause the driver to countersteer early by transmitting the steering torque to the steering wheel. On the other hand, there can be caused steering angle variations by the utilization of the elasticity of the wheel suspension, the steering linkage and the steering column which act against the yaw moment caused by the asymmetrical braking force, similar to the elasto-kinematic bump toe-in described in paragraph 2.4.4.4 for the improvement of the braking stability.

This can be obtained by a negative kingpin offset. The difference in braking force while braking on a road with varying friction coefficients for both wheel toes produces a reaction torque in the steering system, which makes the wheels steer to the direction of the less decelerated wheel and, by that, causes a countersteer to the right direction in order to equalize the yaw rotation caused by the asymmetrical braking forces.

The variation of the disturbing force lever arm a and the kingpin offset r_L during the process of steering for the four-link wheel suspension and the McPherson axle (Fig. 2.5-7) is represented in Fig.2.5-14.

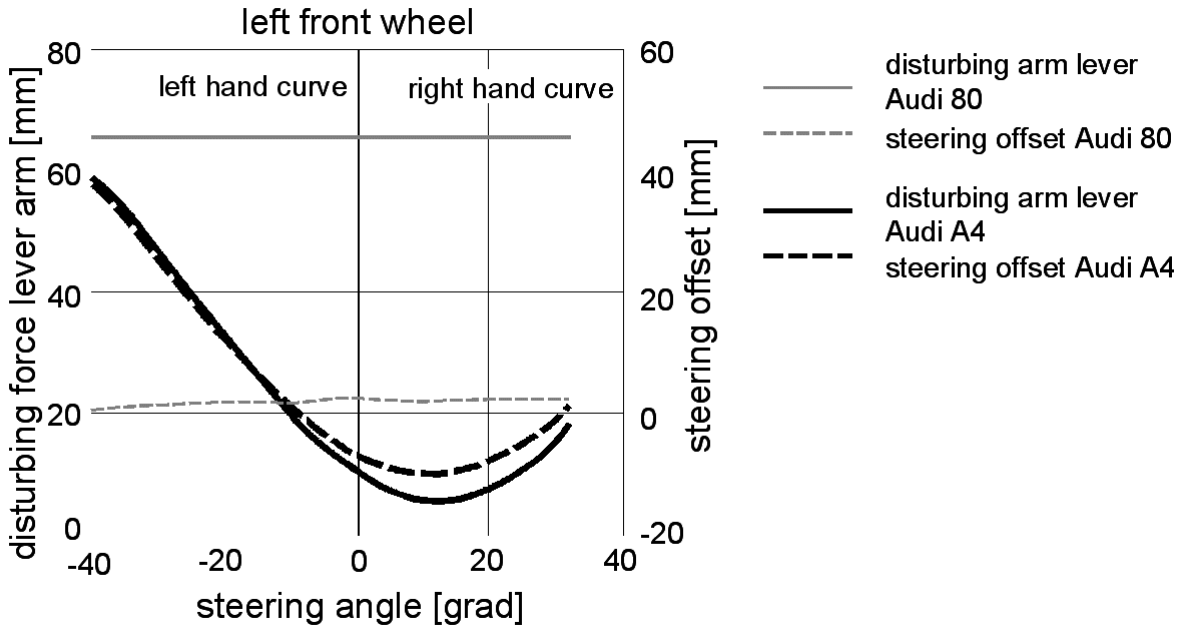

Fig. 2.5-14 : Disturbing force lever arm and kingpin offset in relation to the steering angle for a four-link wheel suspension and a McPherson axle

Disturbing force lever arm and kingpin offset adopt fixed, invariable values in case of the conventional McPherson axle, whereas in case of the four-link wheel suspension, the

constructional values tend to increase at the inside wheel and to decrease at the outside wheel.

- Toe-in / Toe-out

The difference between the distance of the rim flange in front of and behind the wheel center line is called toe-in (in case of a negative sign: toe-out) of an axle, Fig. 2.5-15.

Instead of the difference in length, the total toe-in angle can also be indicated: (2.5-4)

$$\delta_{toe\text{-}in} = arctan\frac{s_1 - s_2}{d}$$

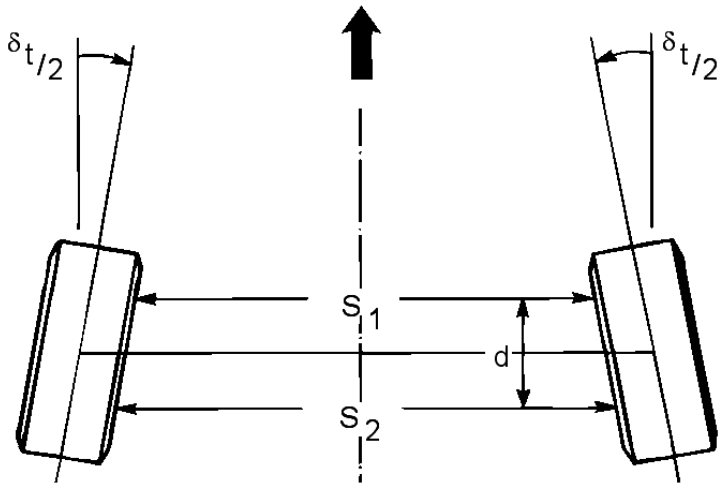

Fig. 2.5-15: Definition of the toe-in

Under the influence of the rolling resistance forces and, in case of powered axles, due to the driving forces, the wheels are pushed into toe-in or toe-out depending on the elasto-kinematics of the wheel suspension. From a toe-in angle, there results an additional running resistance (KFZ I), and the tire abrasion is increased by the continuously appearing tire slip while driving straight ahead..

As a consequence, in the construction position of the vehicle a small toe-in angle is adjusted usually, which is compensated while traveling straight ahead under normal conditions by the toe-in variation caused by elasticities occuring in the wheel suspension and in the steering system.

The influence of the kinematic and elasto-kinematic toe-in variation on the handling characteristics was already described in paragraph 2.4.3.5 and .2.4.4.4.

- Wheel camber angle

In paragraph 2.4.3.5, there was already described, how static camber angles in the construction position and kinematic camber angle variations can be applied to influence the handling characteristics.

The wheel camber variations caused by the inclination of the steering axle during steering movements (wheel castor angle and wheel spread angle) have also to be considered.

A positive wheel camber angle at the front wheels, intended for the decrease of the kingpin offset in earlier vehicle constructions, can not be found any in modern wheel suspensions any more. A small kingpin offset is achieved today by a large rim offset, which permits the positioning of the brake disk close to the wheel center plane and, by that, provides a favorable position for the ball-and-socket joints of the steering swivel mounting.

The variation of the wheel camber related to the steering angle for the two exemplary axles from Fig. 2.5-7 is shown in Fig. 2.5-16.

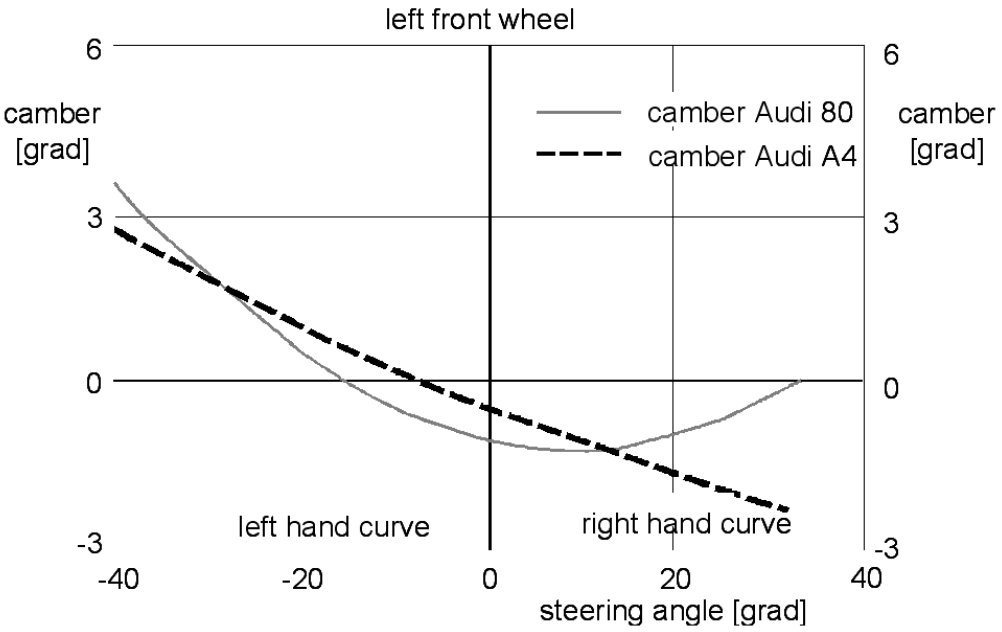

Fig. 2.5-16: Variation of wheel camber while steering for a four-link wheel suspension and a McPherson axle

In order to keep the lateral force potential while cornering, at the inside wheel a positive wheel camber modification occurs and at the outside wheel a negative wheel camber modification occurs as a function of the steering angle.

2.5.3 Steering Kinematics

The allocation of the wheel steering angles to the steering wheel angle and of the wheel steering angles to each other is described by non-linear relations, since this allocation

depends on the instantaneous angle between the components of the steering linkage. By that, these relations include trigonometric functions.

As far as the constructional boundary conditions (space, number of joints, steering gear design) permit this, these connections can be designed specifically by the appropriate arrangement and dimensions of the linkage components, Fig. 2.5-17.

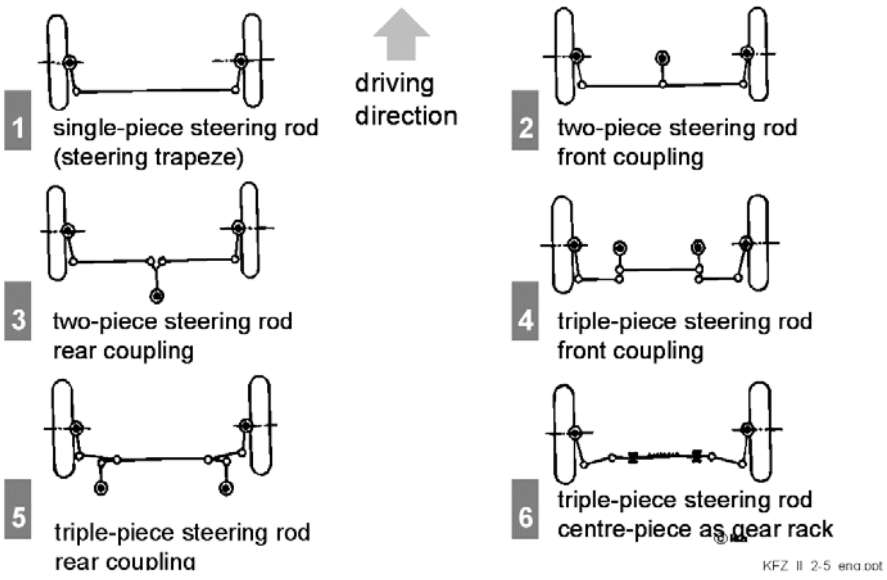

Fig. 2.5-17: Steering linkage configurations /14/

The dimensioning can be made with the consideration of demands on the static (without the influence of the tire lateral force) or the dynamic (with the influence of the tire lateral force) steering performance.

2.5.3.1 Static Layout of the Steering Element

At low speed cornering, the wheels roll without a tire slip angle and accordingly without any lateral forces, if the elongations of all wheel center lines intersect at one point, which is the center of the curve (Rudolf Ackermann, 1816), Fig. 2.5-18.

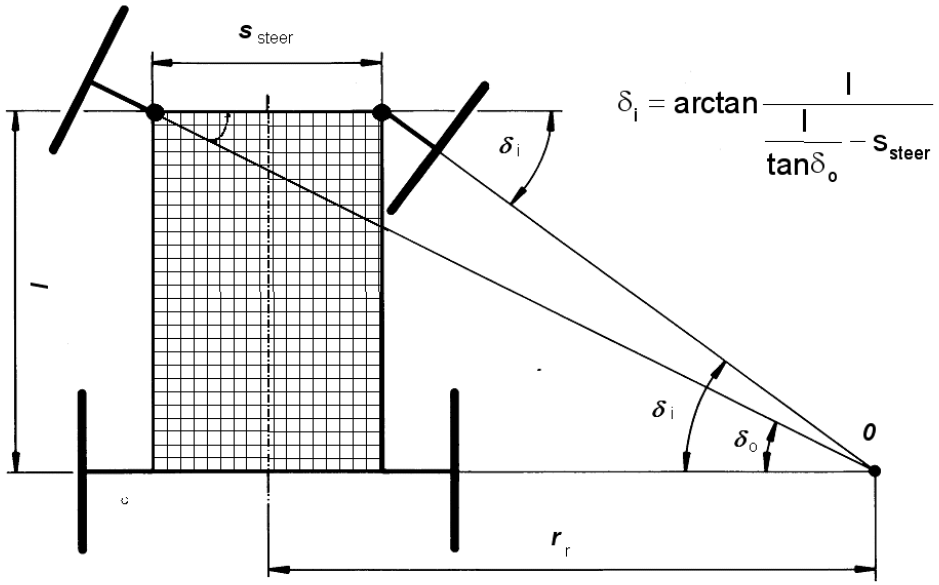

Fig. 2.5-18: Geometrical condition for side slip-free rolling for slow cornering (Ackermann condition)

The geometrical relationships for this rolling of the wheels without forces leads to the following desired functions for the wheel steering angle of inner wheel δ_i as a function of the wheel steering angle at outer wheel

$$\delta_i = \arctan \frac{l}{\frac{l}{\tan\delta_o} - s_{steer}} \qquad (2.5\text{-}5)$$

with:

δ_i, δ_o	wheel steering angle
l	wheel base
s_{steer}	kingpin track width
r_r	course radius of the rear axle

While traveling straight ahead, the wheel planes of the steered wheels are placed parallel to each other in the driving direction. A result of the Ackermann condition is that while cornering, the difference in toe-in angles between outside (δ_o) and inside wheel (δ_i) reaches values in the range of toe-out.

2.5.3.2 Real Layout of Steering Elements

While cornering with higher driving speed, tire slip angles occur at the wheels, which result in the wheel lateral forces which are necessary to support the centrifugal force. The curve center results from the intersection of the normal of the direction of motion of the wheels and their centers of wheel contact under these conditions, Fig. 2.5-19.

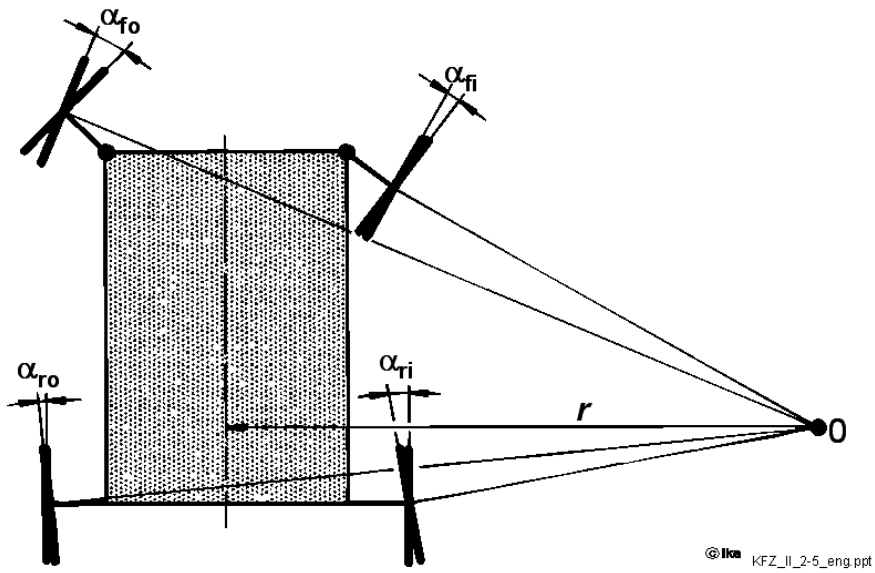

Fig. 2.5-19: Relationship between wheel steering angles, tire slip angles and position of the center of the curve

If the steering kinematics are dimensioned according to the Ackermann condition (Fig. 2.5-18), then the outside tire slip angles are always smaller than the inside tire slip angles.

In order to utilize the same friction coefficient at the outside wheels affected by higher wheel load as at the inside wheels, the tire slip angles should be larger at the outside /12/. A real layout of the steering elements therefore requires to diverge from the Ackermann condition such that the wheels are rather steered parallel than with increasing toe-out /29/. A further advantage of this layout is that it can be implemented easier concerning the kinematics.

In practice, a parallel steering-in of the front wheels (real layout) is targeted up to a steering angle of about 20° and only with larger steering angles, an approximation of the Ackermann condition is implemented, Fig. 2.5-20.

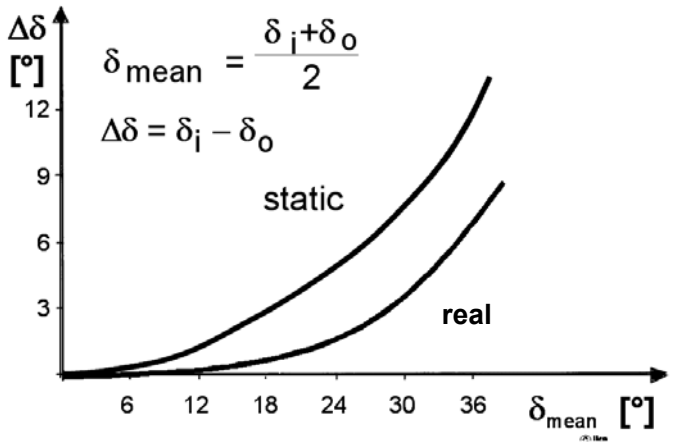

Fig. 2.5-20: Toe-out angle as a function of the mean steering angle for static and real steering element layout

2.5.4 Steering Angle - Steering Torque Diagram

Some important characteristics of a vehicle steering system can be determined by a steering angle – steering torque diagram recorded while driving with a measuring steering wheel.

Fig. 2.5-21 shows the typical characteristic of the steering torque while driving on a sinusoidal course, applied as a function of the steering angle.

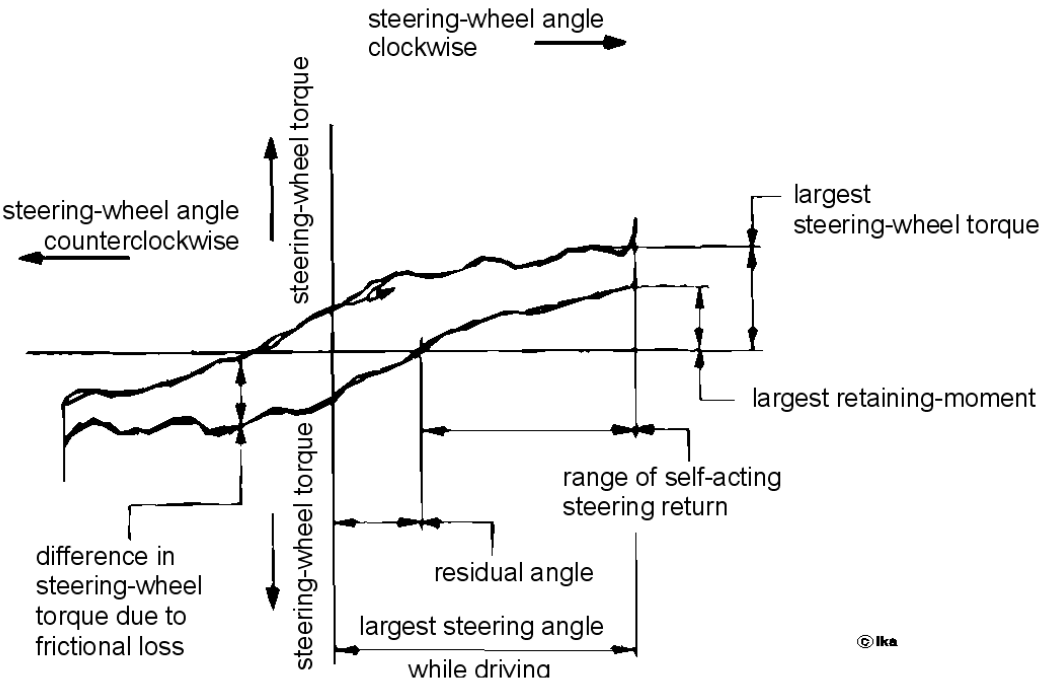

Fig. 2.5-21: Steering angle - steering torque diagram

On the one hand, the diagram gives information about the steering force level, on the other hand, there are results given about the driver's steering feel from the shape of the hysteresis loop, which is an important aspect for the assessment of the vehicle's straight-running properties.

The driver perceives the steering element as precisely working, if the steering moment hysteresis loop is small at the zero point (low friction in the steering system) and the rise of the steering moment from the zero position is clearly noticeable ("center point feeling"). In order to keep the overall steering moment level low at the same time, the further characteristic curve of the steering torque in relation to the steering angle should be degressive /39/.

Particularly for the assessment of the straight-running properties, the steering angle - steering torque diagram can also be recorded at high driving speeds for small steering angle amplitudes /10/.

2.5.5 Steering Elasticity

As a consequence of the elasticity in the impact-absorbing and noise-insulating rubber bushings of the wheel suspension as well as of the component elasticity of the wheel suspension and the steering system, there appears a loss angle between steering wheel rotation and wheel angle, whose value depends on the transmitted steering torque. The torsional elasticity of the steering system reduced to the steering column is called steering elasticity. Due to the steering elasticity, the effective steering transmission ratio perceived by the driver differs especially at the mean position of the steering element from the purely kinematic steering transmission ratio, which depends only on the geometry of the steering gear and the steering linkage /39/.

In Fig. 2.5-22, the steering transmission ratio as a function of the steering wheel angle, influenced by steering elasticity, is shown.

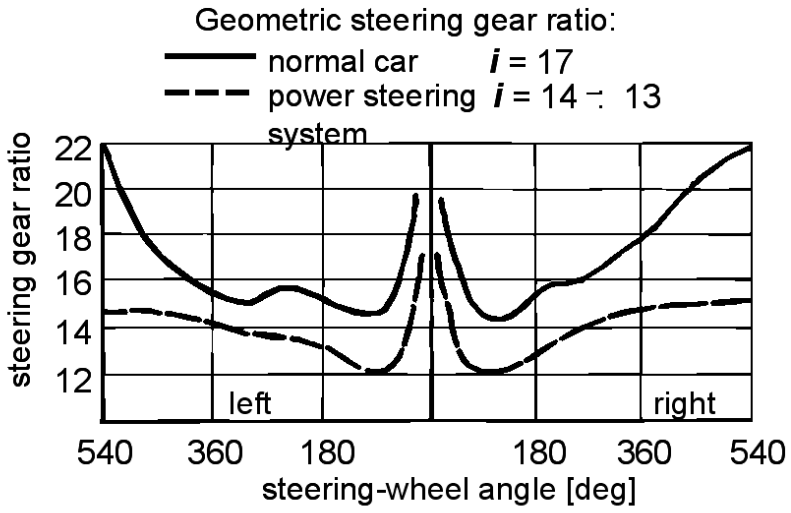

Fig. 2.5-22: Steering transmission ratio influenced by steering torque (measurement on ball rolling plates)

According to Fig. 2.5-22, the geometrical transmission ratio is achieved only for steering wheel angles greater then 30 - 60°. Therefore, with the small steering corrections necessary for straight-ahead driving, a significantly more indirect transmission ratio is effective.

2.5.6 Components of the Steering System

The steering of independently guided front wheels usually consists of the elements specified in Fig. 2.5-23.

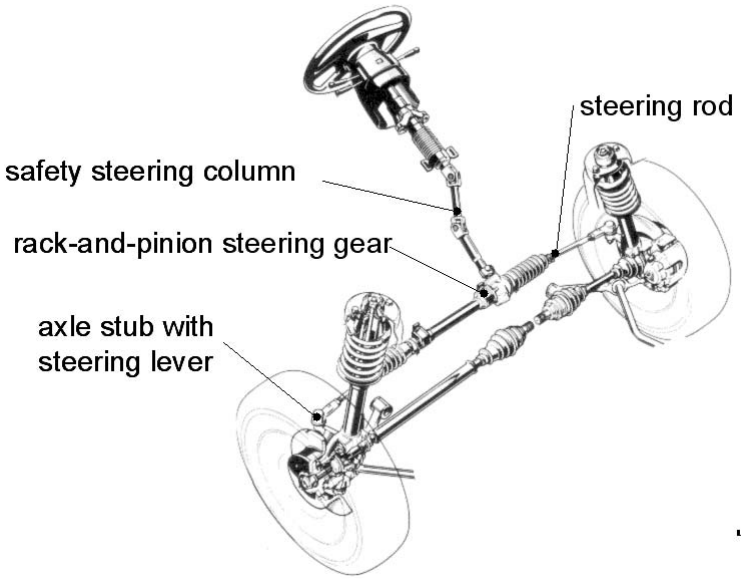

Fig. 2.5-23: Steering system components

In the two preceding paragraphs, it was described that small frictional forces and small elasticity in the steering system positively affects the steering feel in straight-ahead driving. however, it should not be ignored that elasticity reduces the impact susceptibility of the steering system while driving on uneven ground and that a petty self-friction reduces the transfer of vibration excitation of the steering system to the steering wheel within the range of the wheel natural frequency.

For vibration and noise insulation, there is often inserted an elastic joint disc as a connecting element between steering gearbox and steering column. Steering dampers are not as effective in the suppression of high frequency vibration as in the reduction of impact excitations and the damping of those oscillations, which can result from the moment of inertia of the steering system concentrated on the steering axle and from the aligning torque resulting from steering geometry and tire characteristics /29/.

In the following, it is only dealt with the steering gearbox as the only component of the steering system, since numerous of the requirements described in this paragraph so far have to be accomplished just by this steering component.

2.5.6.1 Steering Gearbox without auxiliary Power

The torque necessary for steering movements is reduced to values which can be applied by humans by the steering gearbox. The steering gearbox has to operate without play and with a low coefficient of friction, in order to fulfil the requests for small physical stress of the driver and for sensitivity of the steering system.

For steering gearboxes, there has to be differentiated between rack-and-pinion steering with translatory output and steering gearboxes with rotary output (Fig. 2.5-4).

The tie rods are directly connected to the rack-and-pinion steering by ball-and-socket joints. The fastening is placed either at the front side of the steering rack, Fig. 2.5-24 above, or in the center, Fig. 2.5-24 down, which permits the application of longer tie rods, which results in smaller toe-in variations in the case of spring compression.

Steering racks are characterized by a simple structure and a small space requirement. Unfortunately, the design possibilities of the steering kinetics are limited due to the direct fastening of the tie rods, (paragraph 2.5.3). More degrees of freedom are offered in case of the use of a steering gearbox with rotary output.

Two of the most common steering gearboxes with rotary output are the worm-and-roller steering (Fig. 2.5-25) and the ball-and-nut steering (Fig. 2.5-26).

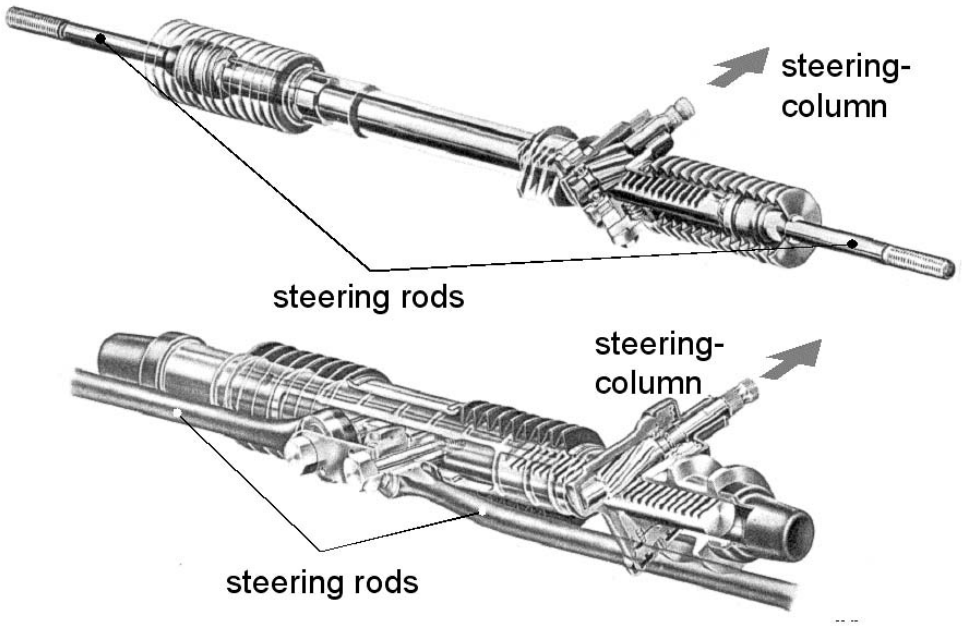

Fig. 2.5-24: Rack-and-pinion steering

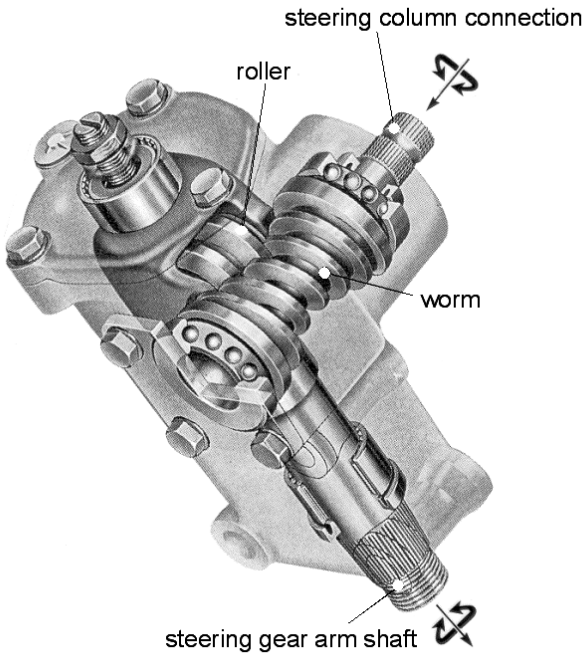

Fig. 2.5-25: Worm-and-roller steering, ZF

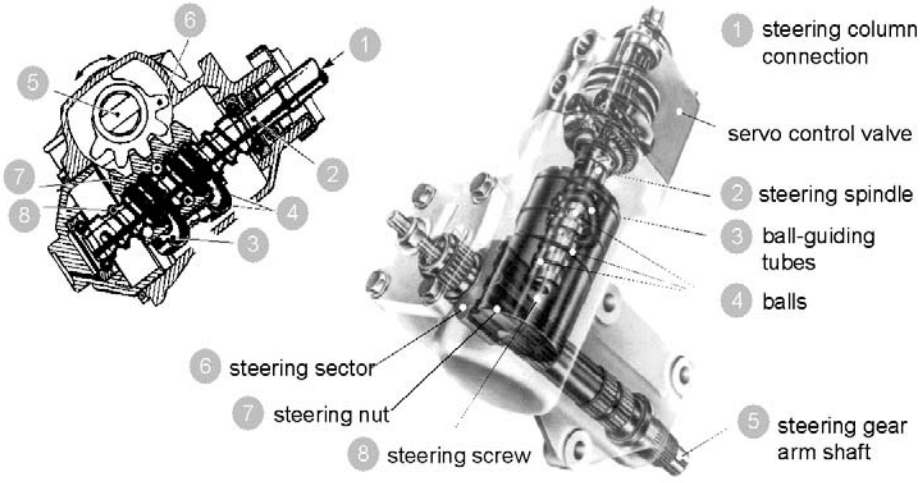

Fig. 2.5-26: Ball-and-nut steering

The worm-and-roller steering represents a worm gear with the teeth of the worm wheel segments realized as tooth roll. By that, they can roll almost friction-free on the worm.

In the steering gearbox with ball circulation, by the turn of the steering screw, an only translatory moved steering-gear nut is displaced, which itself propulses a steering segment, which is placed at the output shaft by a meshing. To decrease friction, the balls rotate in the thread between the steering screw and the steering nut.

2.5.6.2 Power Steering

In order to keep the steering torques in an acceptable range during slow travel, a very indirect steering transmission ratio is necessary for many vehicles, which has an unfavorable influence on the steering behavior at higher driving speeds, since fast steering reactions require large hand movements at the steering wheel in this case.

The application of a power steering enables the configuration of a more direct steering transmission ratio and the reduction of the required steering forces at the same time. The decrease of the physical stress of the driver attainable thereby represents an important contribution for the increase of the active safety. The auxiliary energy necessary for the operation of the power steering, is usually produced hydraulically by a pump driven by an engine-powered v-belt, due to the high energy density. Electric-powered servo steering systems are in the development state at present. The functional scheme of a ball-and-nut power steering system is shown in Fig. 2.5-27.

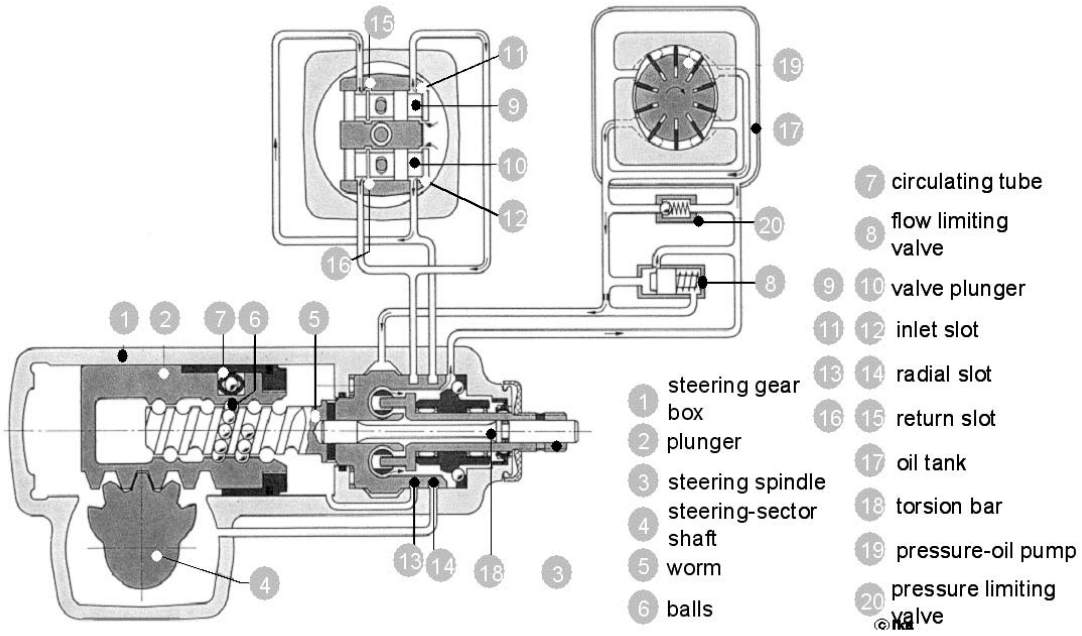

Fig. 2.5-27: Functional scheme of a ball-and-nut power steering, ZF

A torsion bar is inserted between steering column and steering screw, whose twist under the effect of a steering torque leads to the actuation of two control valves. By the throttling of the oil flow conveyed by the pump at the control valves, a differential pressure is induced at the steering nut designed as a working piston, and by that the auxiliary power is produced.

The operating principle is applicable also for rack-and-pinion steering systems. Then, the working piston is fastened on the gear rack acting as piston rod, Fig. 2.5-28.

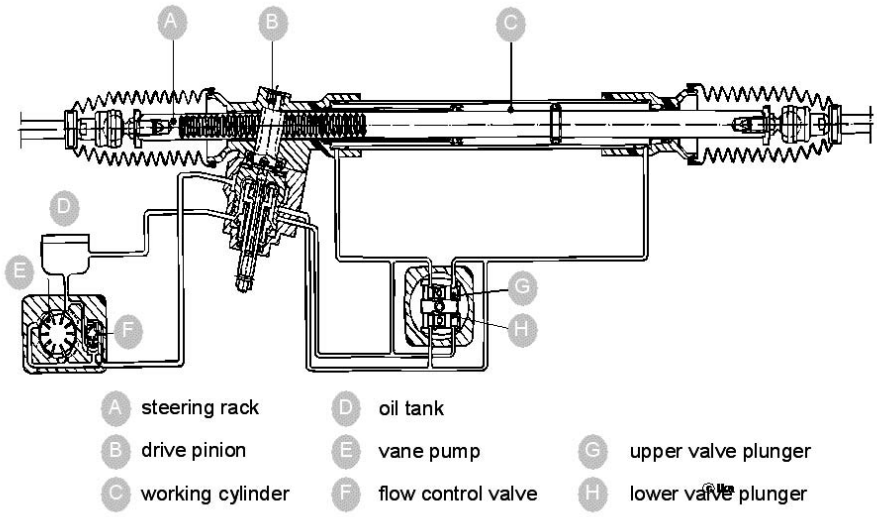

Fig. 2.5-28: Rack-and-pinion power steering, ZF

The magnitude of the auxiliary force should be dimensioned in such a way that a proportionality between steering resistance at the wheels and the hand force at the steering wheel is preserved for the operating range (velocities above 3 m/s), since the driver needs information about the grip between tire and road necessarily. The proportionality factor should be selected in such a way that the road contact is transferred to the driver genuine and well perceptibly, but that for steering only small hand forces are required.

In the majority of the cases, the design of the power steering systems represents a compromise between the demand for a high steering force support while parking and the demand for a clear feedback of the steering torques at high driving speeds.

A power steering with speed-dependent steering force support offers additional degrees of freedom in its design. Here, the proportionality factor of the steering torque-dependent auxiliary force is influenced by an electrically operated solenoid valve in the hydraulic circuit. The control of the solenoid valve is performed by a microprocessor, which receives a signal for the driving speed, Fig. 2.5-29.

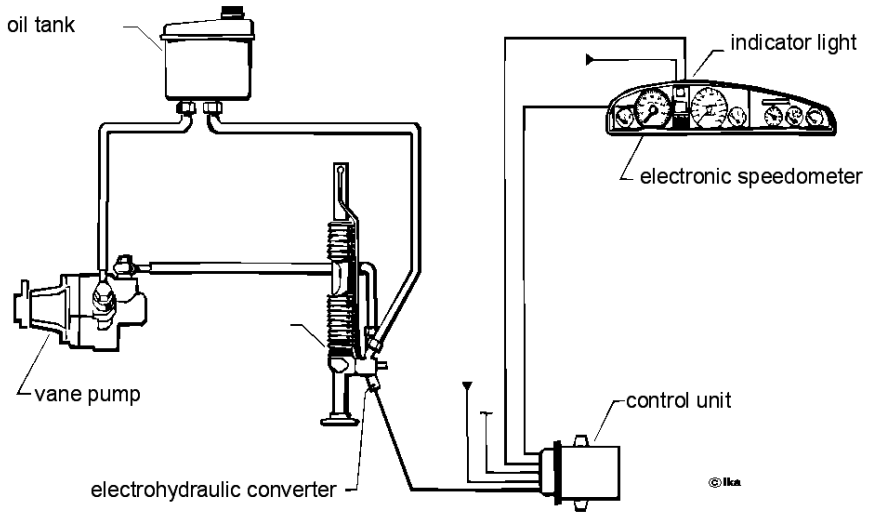

Fig. 2.5-29: Operating principle of the servotronic

In the servotronic, the steering force support decreases with higher driving speed. This dependency enables comfortable parking as well as high speed driving at small steering effort, Fig. 2.5-30.

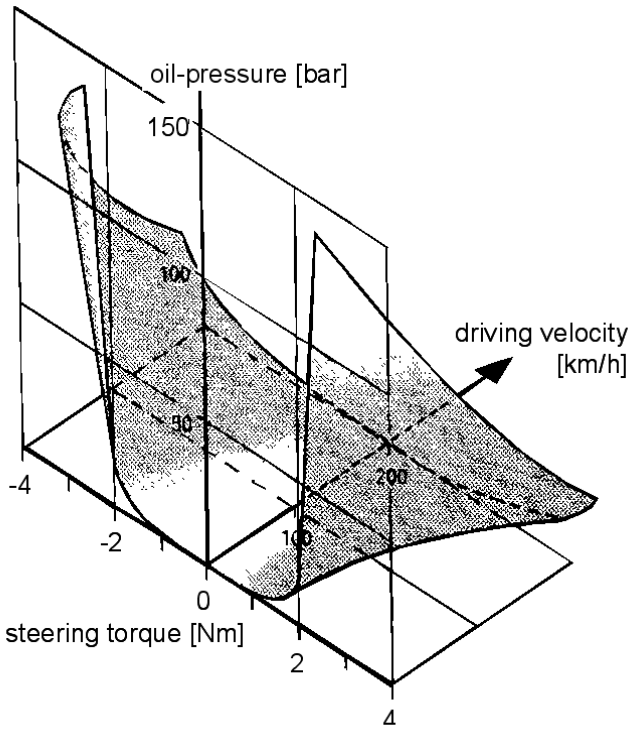

Fig. 2.5-30: Valve characteristic map of the servotronic

The steering torque of the servotronic and of the conventional power steering of the predecessor model depending on the lateral acceleration is represented in Fig. 2.5-31. The servotronic features a reduction of the required of steering force in comparison with the conventional power steering.

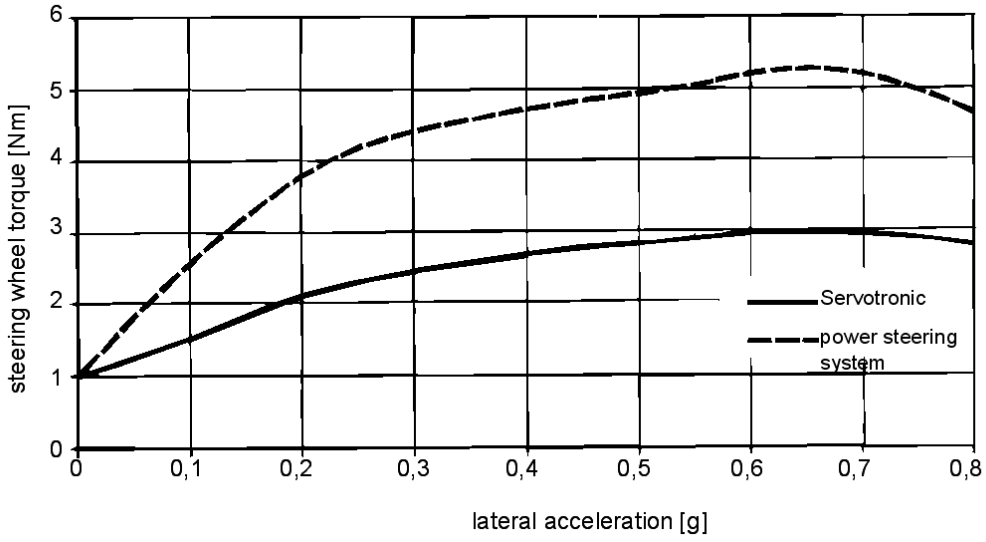

Fig. 2.5-31: Characteristic curve of the steering wheel torque in relation to the lateral acceleration during stationary circular-course driving (r = 100m)

2.6 Wheel Suspensions

2.6.1 Basic Concepts of Wheel Suspension

Automotive wheel and body are linked to each other via the wheel suspension system. The function of the wheel suspension system is to guide the wheel relative to the body in a manner permitting on the one hand largely vertical compression movement and on the other hand transmission of the tire forces, which act in horizontal direction in the footprint (tire-contact) center, and of the tire moments, to the body.

Independent wheel suspension, rigid axle suspension and composite (compound) axles are the principle systems distinguished.

Relative to the body, the relieved wheel carrier of independent wheel suspension possesses the six degrees of freedom of movement of a rigid body in space. By means of 5 links with ball joints at both ends, these degrees of freedom are canceled, except for the degree of freedom of compression. In controllable independent wheel suspension systems, one of the links is a tie rod. A-arms can be formed by the combination of two links each (e.g. double-wishbone suspension), Fig. 2.6-1.

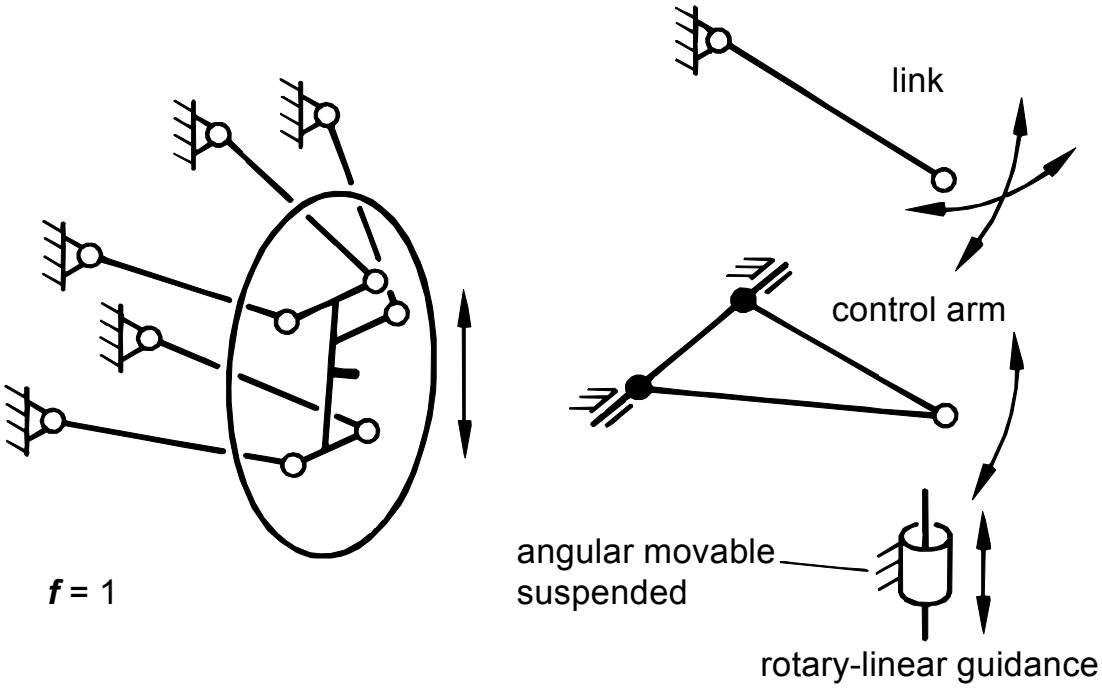

Fig. 2.6-1: Schematic of independent wheel suspension

A link may be replaced by a twisting-sliding guide representing a link of infinite length (suspension strut, damper strut suspension). The rotation axes of the links may coincide (e.g. semi-trailing link wheel suspension).

A rigid axle is characterized by a rigid connection between the two wheel carriers. For differently dimensioned compression travels of the two wheels to be possible, the rigid axle must possess 2 degrees of freedom relative to the body (vertical and rolling motion around a vehicle longitudinal axis). Consequently, four links are required for 4 of the originally 6 degrees of freedom to be canceled, Fig. 2.6-2.

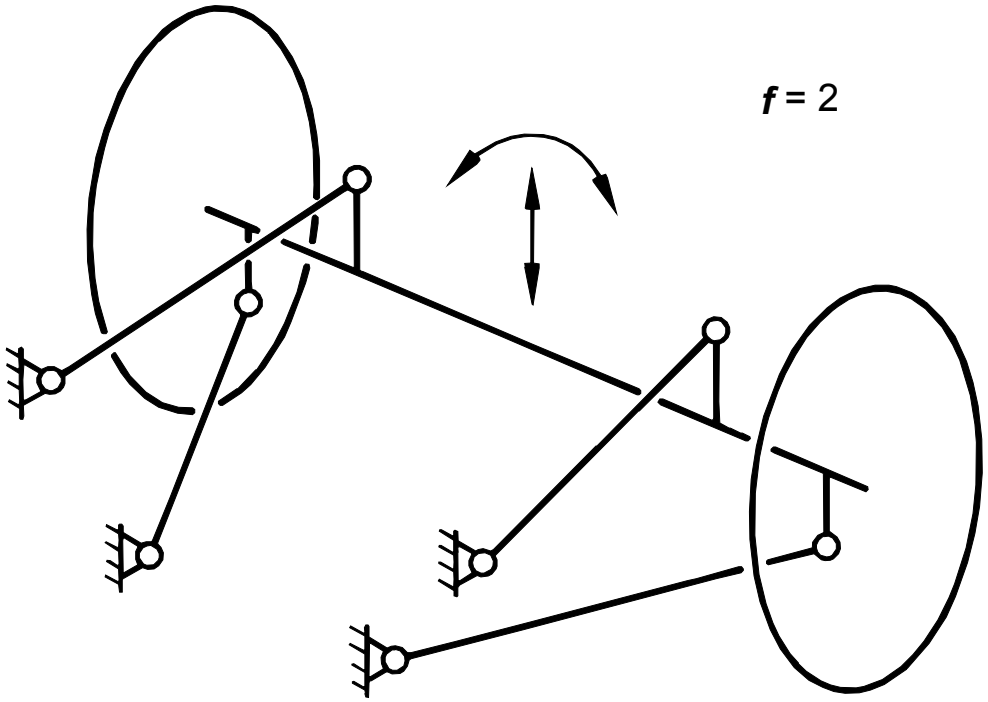

Fig. 2.6-2: Schematic of a rigid axle

Here, too, the links can be arranged in the most diverse way or combined to form control arms. Unlike independent wheel suspensions, rigid axle suspensions are often kinematically overdefined (overrigid)/29/.

Rigid axles guided by leaf springs, for example, possess two degrees of freedom due to the elasticity in the spring attachments.

Axles whose wheel carriers are not rigidly connected to each other but are also not capable of completely independent spring movements are called composite (compound) axles.

The layout as shown in Fig. 2.6-3, with the wheel carriers, which are directly attached to the body, being connected by means of a twisting-sliding guide, is not a general case but one of many possible designs, and it is often used.

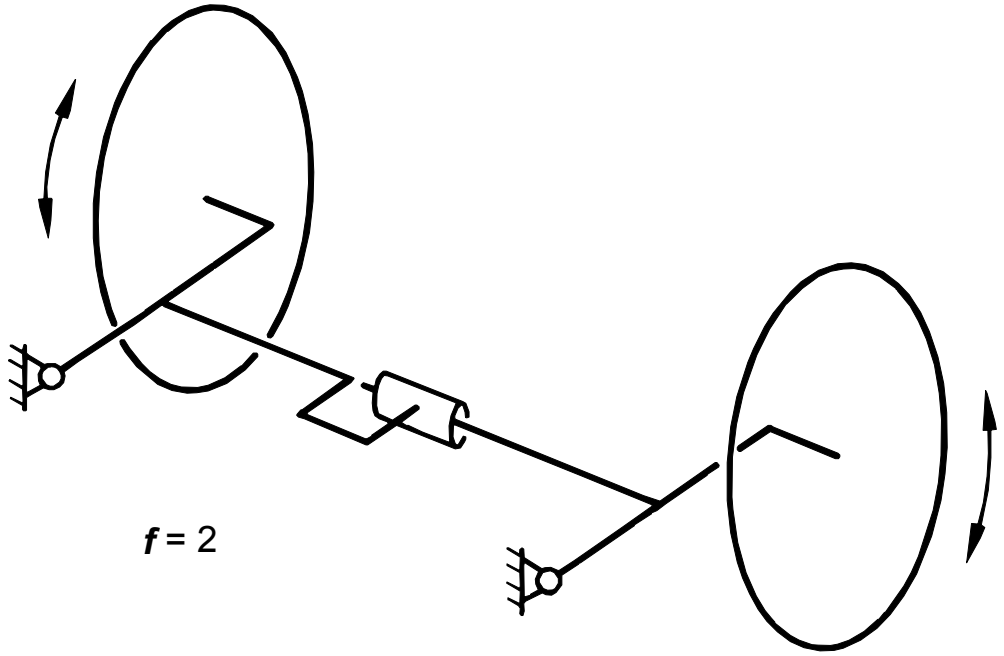

Fig. 2.6-3: Composite (compound) axle, schematic

In the practical application of this version, a torsion section is used instead of the twisting-sliding guide. The degree of freedom of sliding of the twisting-sliding guide thus not available is substituted by the elasticity of rubber mounts in the attachment points (pivot points) on the body.

2.6.2 Kinematics of Wheel Suspensions

The preceding section described how the degrees of freedom of movement of the wheel relative to the body are canceled by the wheel suspension, except for the degree of freedom of compression. Since the struts or links guiding the wheel are of a finite length, the wheel carrier will as a rule perform a three-dimensional movement during compression.

If this movement corresponds to the most general movement of a body in space, then it can at any time be represented as "instantaneous screw motion", i.e. as a movement around an instantaneous axis of rotation in space with advance in axis direction, and we speak of a "three-dimensional wheel suspension ", Fig. 2.6-4.

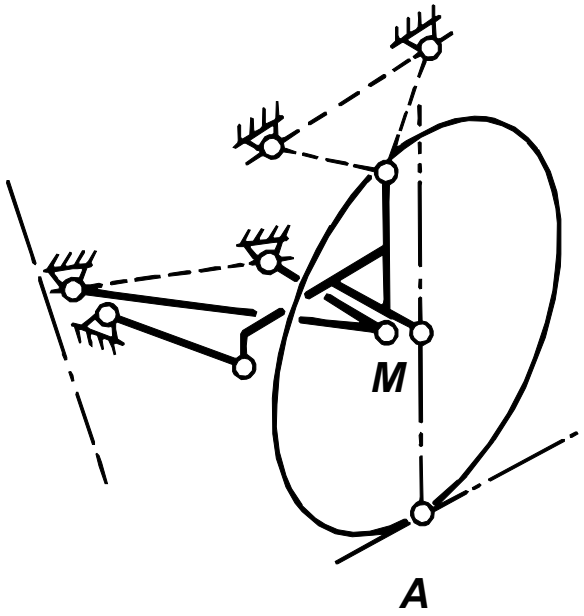

Fig. 2.6-4: "Three-dimensional" wheel suspension

If movement of the wheel carrier can at any point in time be considered as a pure rotation around an instantaneous axis of rotation, whose orientation relative to the body changes but which nevertheless always runs through a body-fixed point, then we are dealing with a "spherical wheel suspension", Fig. 2.6-5.

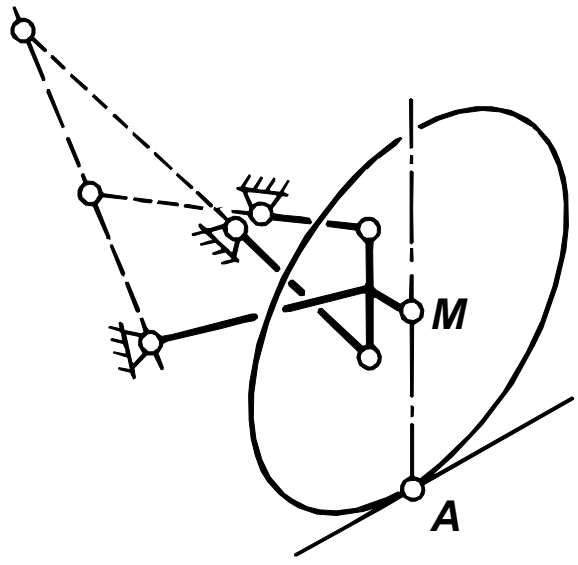

Fig. 2.6-5: "Spherical" wheel suspension

If the wheel carrier at any point in time performs pure rotations around an instantaneous axis of rotation, which changes its position but maintains its orientation relative to the body (parallel displacement), then we are dealing with a "plane wheel suspension", Fig. 2.6-6.

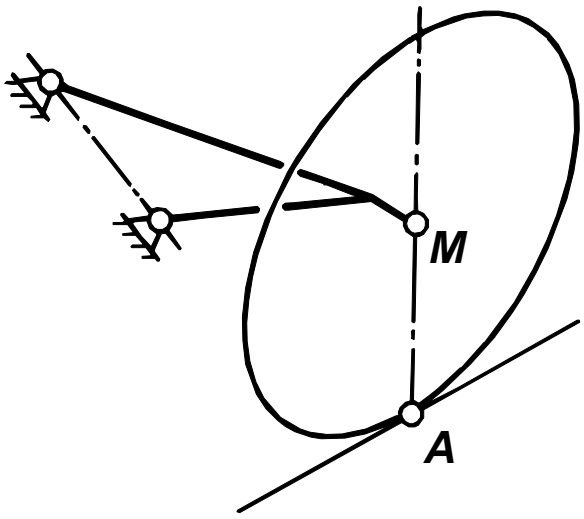

Fig. 2.6-6: "Plane" wheel suspension

As a special case of plane wheel suspension, a body-fixed instantaneous axis of rotation constitutes the kinematically simplest case (e.g. trailing-link suspension).

Suspension movement depends on wheel suspension kinematics and results in wheelbase, track width, camber angle and toe-angle changes of the wheel relative to the body or the roadway. The influence of these kinematic wheel-position changes on vehicle handling was described in Section 2.4.

If the position of the instantaneous axis of rotation for a certain compression position is known, then this characterizes the wheel-position changes for minor suspension movement around this initial situation. All points of the wheel carrier move in the direction of tangents on circular arcs around the instantaneous axis of rotation.

In three-dimensional wheel suspensions, the speed components of the translational movement in the direction of the axis of rotation must also be considered.

Fig. 2.6-7 illustrates the relation between the position of the instantaneous axis of rotation and wheelbase or track changes during suspension movement using the example of a plane semitrailing-arm wheel suspension.

The piercing points (penetration points) of the instantaneous axis of rotation through the planes of projection appear here in the respective views as instantaneous centers of rotation (velocity poles) (L, Q).

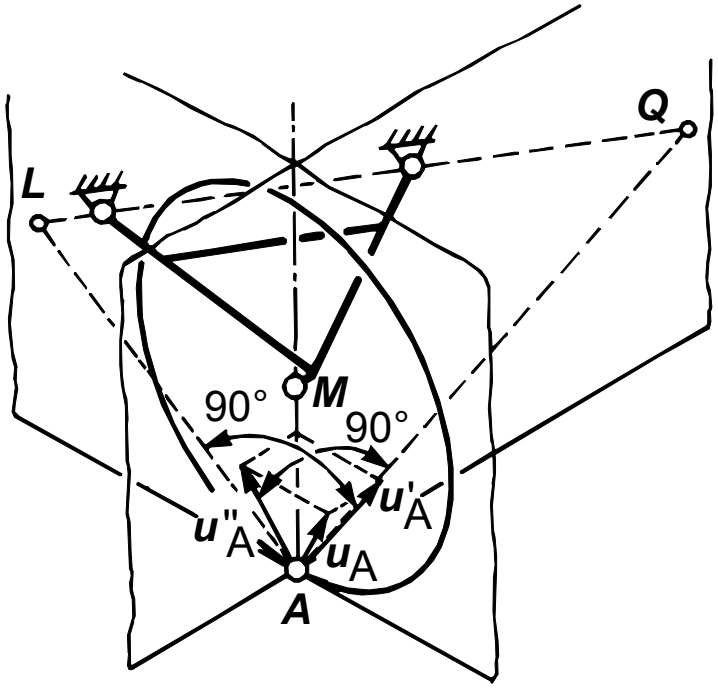

Fig. 2.6-7:Wheelbase and track changes in a plane semitrailing-arm wheel suspension

The position of the instantaneous axis of rotation not only determines wheel-position changes with minor suspension movement but also power transmission between footprint center and body.

In plane and spherical wheel suspensions, forces whose lines of action intersect or run parallel to the instantaneous axis of rotation possess no torque around the axis of rotation and are transmitted to the body without suspension movement. In three-dimensional wheel suspensions, torque results also from forces acting in the direction of the axis of rotation if the instantaneous pitch is not zero.

These relations determine the position of the roll center of an axis and the magnitude of braking-torque and starting-torque compensation (vide infra).

In spherical and plane wheel suspensions, a torque balance of the force components operative around the piercing point (penetration point) of the instantaneous axis of rotation can be established by the respective planes of projection (instantaneous center/velocity pole) separately for longitudinal and transverse views.

In three-dimensional wheel suspensions, these piercing points are not identical with the longitudinal or transverse center, because the advance movement in axle direction must also be considered.

"Equivalent centers/poles" can be determined if the speed components of suspension movement are known in the respective views of two points of the wheel carrier. The

instantaneous center searched then corresponds to the intersecting point of the vertical with the directions of speed in these two points (polar rays/radials), Fig. 2.6-8.

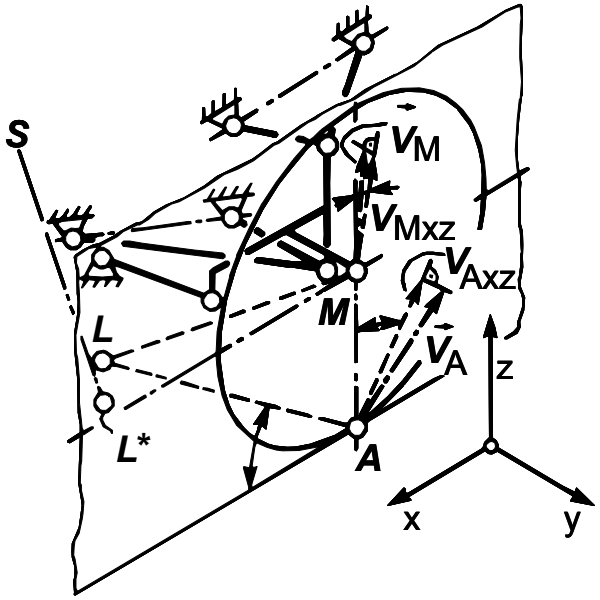

Fig. 2.6-8: "Equivalent center" in longitudinal plane of a three-dimensional wheel suspension

2.6.2.1 Roll Center

Fig. 2.6-9 illustrates by means of a plane double-wishbone suspension (here with parallel axes of rotation in vehicle longitudinal direction) the forces acting additionally in the footprint centers during cornering compared to the static position of rest (for wheel-related body suspension rates, cf. Section 1.3.2.3).

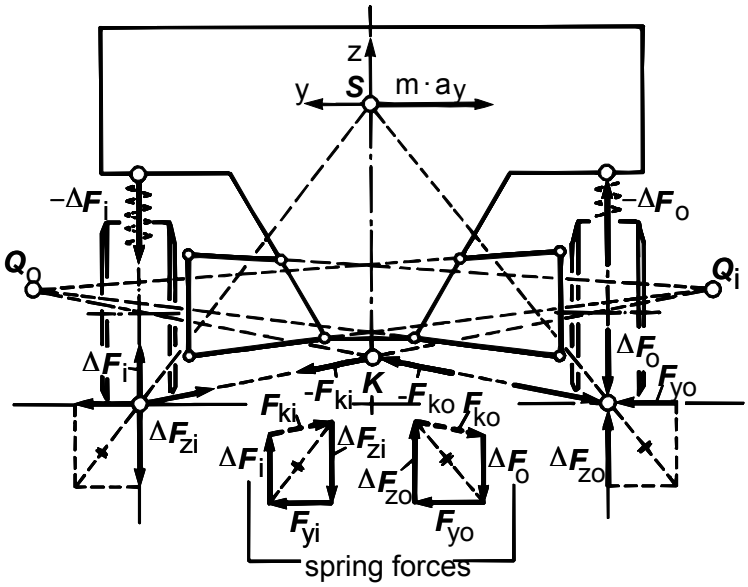

Fig. 2.6-9: Force transmission between footprint centers and body during cornering (plane double-wishbone suspension)

Transverse acceleration and therefore wheel-load differences and roll angle are assumed to be insignificant. Since in steady-state cornering, the torque balances around the instantaneous centers (piercing points of the instantaneous axis of rotation through the plane of projection) reappear, the resultants of the forces acting additionally in the footprint centers during cornering (wheel-related suspension forces presupposed) can only be directed towards the instantaneous axes of rotation (or instantaneous centers).

Minor wheel-load differences presupposed, the lateral tire forces are of the same magnitude, and the resulting lateral force of the axle will attack in the virtual point K on the body while the vertical components of the resultants will cancel each other out in the footprint centers.

Since the lines of action of the resultants in the two footprint centers run through the respective instantaneous centers, these lines of action agree with the polar rays of the speed vectors in the footprint centers, and the virtual point K (since compression travel is to be the same) represents the mutual instantaneous center of the reciprocal suspension movement with the body thought fixed, Fig. 2.6-10.

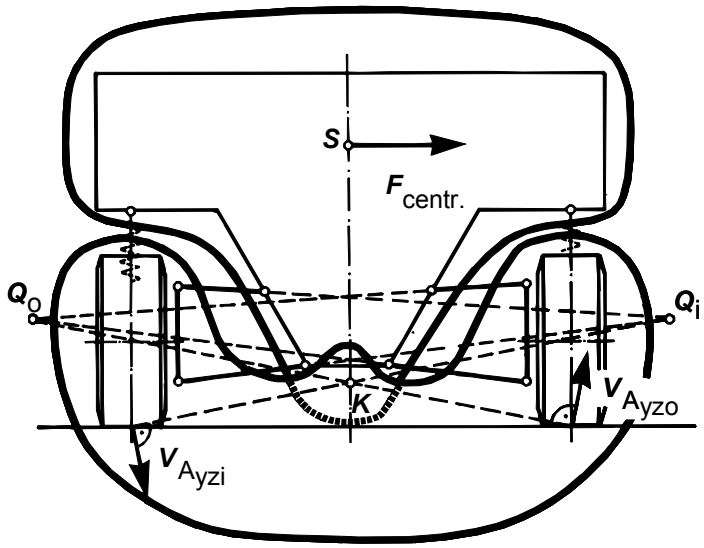

Fig. 2.6-10: Instantaneous center of reciprocal suspension movement

Rolling motion is the kinematic reversal of this reciprocal suspension movement. The point K is therefore also the instantaneous center of the rolling motion of the body relative to the roadway surface. This roll center was already introduced in Section 1.6.1, though simplified as an assumed body-fixed hinge point (fulcrum).

In most real wheel suspensions, the position of the roll center is significantly altered as a result of suspension movement.

Simple determination of this position change during cornering is not possible, because the same magnitude of inside and outside compression travel can only be assumed for very minor transverse acceleration. This is easily comprehended if, for example, a kinematically very simple swing axle is studied, Fig. 2.6-11.

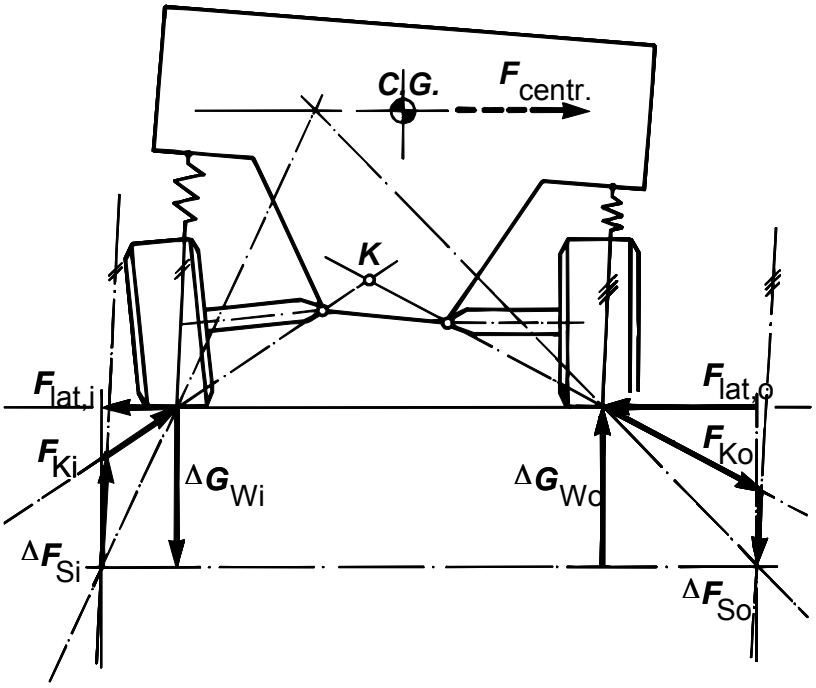

Fig. 2.6-11: Position change of the roll center during cornering (double-jointed swing axle)

In this independent suspension, the instantaneous axis of rotation of the movement of the wheel carrier relative to the body runs at any point in time through the actual fulcrums (→ instantaneous centers) and is thus body-fixed.

In the ideal case, distribution of the tire lateral forces among inside and outside wheels corresponds to the relationship between lateral force, wheel load and slip angle determined by the tire performance maps. On the outside wheel, the torque of the change in wheel load around the associated instantaneous center of the wheel-carrier movement relative to the body (fulcrum) is largely compensated by the torque of the tire lateral force. Therefore, the change in spring force bringing about torque balance is much smaller on the outside wheel than on the inside wheel, where nearly the entire torque of the change in wheel load around the instantaneous center has to be supported by a change in spring force.

As a result of this asymmetry of forces, rebound on the inside wheel during cornering will be much more pronounced than compression on the outside wheel. This effect is referred to as "bump effect" (bottoming-out effect) /29/.

In early vehicles with swing-axle type rear axles and a roll center high above the roadway, this bump effect was feared, because the center of gravity of the vehicle was elevated during cornering and this not only impaired vehicle handling of the high vehicles of those days, but could even result in the loss of rollover resistance.

It can be demonstrated that the bottoming-out tendency is so much the more reduced the lower the roll-center height is and the deeper the drop of the roll center during parallel

compression of the body. In modern wheel suspension systems this is realized by means of a specific kinematic layout.

2.6.2.2 Braking-Torque and starting-Torque Compensation (anti-dive/anti-squat)

During braking and acceleration, axle-load displacement in the vehicle center of gravity results from the force couple composed of longitudinal tire forces and inertia force, Fig. 2.6-12.

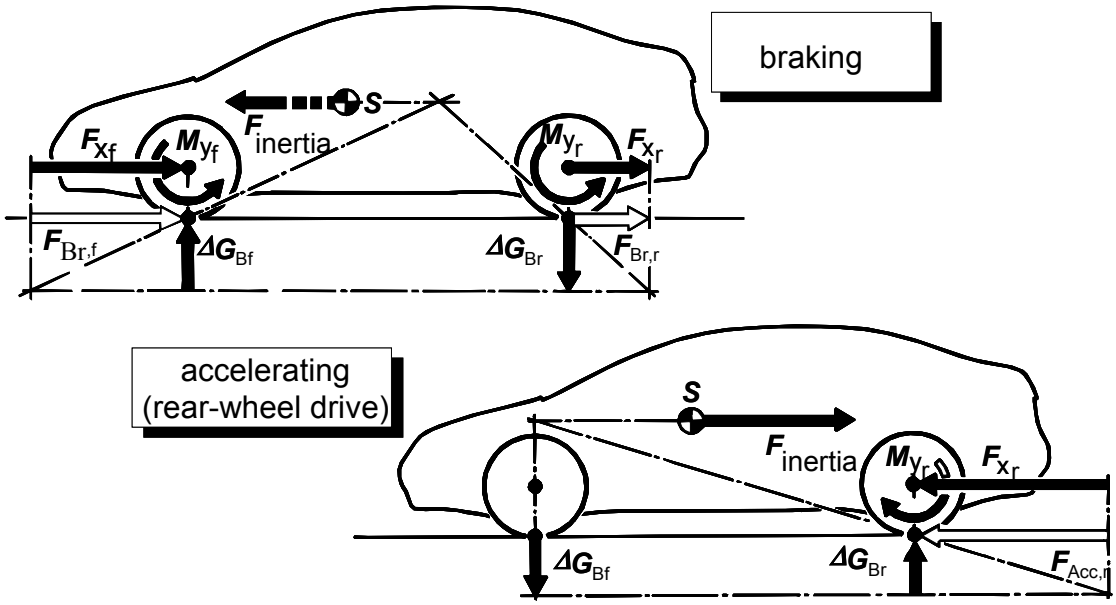

Fig. 2.6-12: Forces acting on the wheel carrier during braking or accelerating

In contrast to the static position of rest, a longitudinal force F_x and a wheel-load difference ΔG_W act on the wheel carrier in the center of rotation of the wheel.

During propulsion, the torque $M_y = F_x \cdot R_{dyn}$ in most wheel suspension systems is supported directly on the body via the drive shafts and therefore has no effect on the reaction forces in the wheel suspension (exception: e.g. rigid axle with integrated differential gear).

During braking with the usual "outboard brakes", however, the torque M_y acts on the wheel carrier, because it supports the brake torque via the brake anchor plate or the brake caliper. The reaction forces in the wheel suspension then correspond to a force F_x acting in the footprint center on the wheel carrier. (Exception: "inboard brakes", where the brake torque is supported via the propeller shaft on brake disks with brake calipers mounted to the differential gear).

The torque of the forces around the longitudinal center of the suspension acting additionally on the wheel carrier during braking or accelerating has to be compensated by the torque of the spring-force changeΔF_F. Fig. 2.6-13 illustrates the relationship for braking (wheel-related body suspension rates).

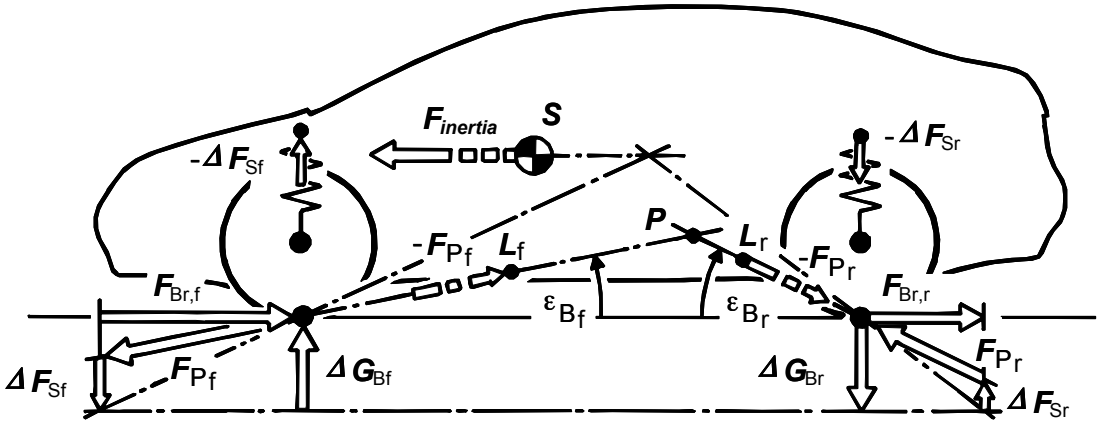

Fig. 2.6-13: Force transmission between footprint centers and the body during braking

Dive-in intensity, i. e. compression of the front axle (brake dive) and rebound of the rear axle, depends on the (instantaneous) position of the longitudinal center. If the position of the longitudinal center agrees with the line of action of the force resulting in the footprint center from the brake force and the wheel-load differences, then there will be no suspension movement during braking, and we speak of "complete braking-torque compensation" on the axle considered. For design reasons, such a layout is very difficult to realize in practice. The quality of partial braking-torque compensation can be described with the help of the braking support angle ε.

The braking support angle ε_{tat}s actually realized by wheel suspension design is constituted by the angle between a straight through footprint center and longitudinal center and the horizontal, cf. Fig. 2.6-13.

The optimum support angle ε_{opt} corresponds to the angle between the line of action of the resultant F_{res} in the footprint center and the horizontal:

front: $$\tan\varepsilon_{opt.f} = \frac{h}{l}\cdot\left(1+\frac{1}{F_{B,f}/F_{B,r}}\right) \qquad (2.6\text{-}1)$$

rear: $$\tan\varepsilon_{opt.r} = \frac{h}{l}\cdot\left(1+\frac{F_{B,f}}{F_{B,r}}\right) \qquad (2.6\text{-}2)$$

F_{Bv}/F_{Bh} brake-power distribution (cf. vehicle I)

h center-of-gravity height

l wheelbase

A torque balance around the instantaneous center for the design attitude of the vehicle provides as a measure of the quality of braking-torque compensation that proportion of the

wheel-load transfer during braking that is supported by the wheel suspension without suspension movement:

$$X \cdot \Delta G_f \cdot l_f = F_{B,f} \cdot h_f \qquad (2.6\text{-}4)$$

l_v horizontal distance

h_v vertical distance, footprint center – longitudinal center

X "braking-torque compensation" (anti-dive)

rather: $X = \frac{F_{B,f}}{\Delta G_f} . \frac{h_f}{l_f}$

$$= \frac{1}{\tan \varepsilon_{opt.}} \cdot \tan \varepsilon_{real} \cdot 100\% \qquad (2.6\text{-}5)$$

Sometimes the so-called dive-in factor T is used to characterize braking-torque compensation (anti-dive):

$$S = 1 - \frac{\tan \varepsilon_{real}}{\tan \varepsilon_{opt}} \qquad (2.6\text{-}6)$$

In a similar way as for braking, the suspension movements during acceleration can be described through indication of the "starting-torque compensation" (anti-squat) X of the powered axle.

Fig. 2.6-14 shows the support angles acting during acceleration for a powered rear axle with independent suspension:

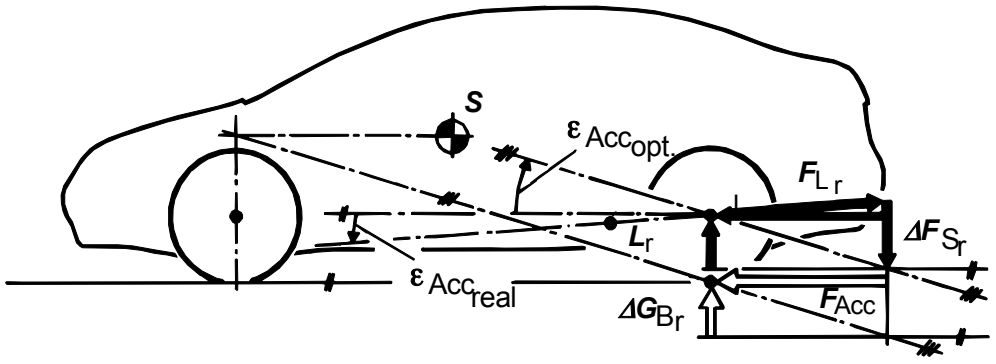

Fig. 2.6-14: Force transmission between footprint center and body during acceleration

2.6.3 Elastokinematics

Road irregularity not only causes vertical but also horizontal shock forces in the footprint center.

For these to be moderated and transmission of vibration and noise to the body to be minimized, rubber mounts are usually used between wheel suspension components and the body instead of rigid joints, Fig. 2.6-15.

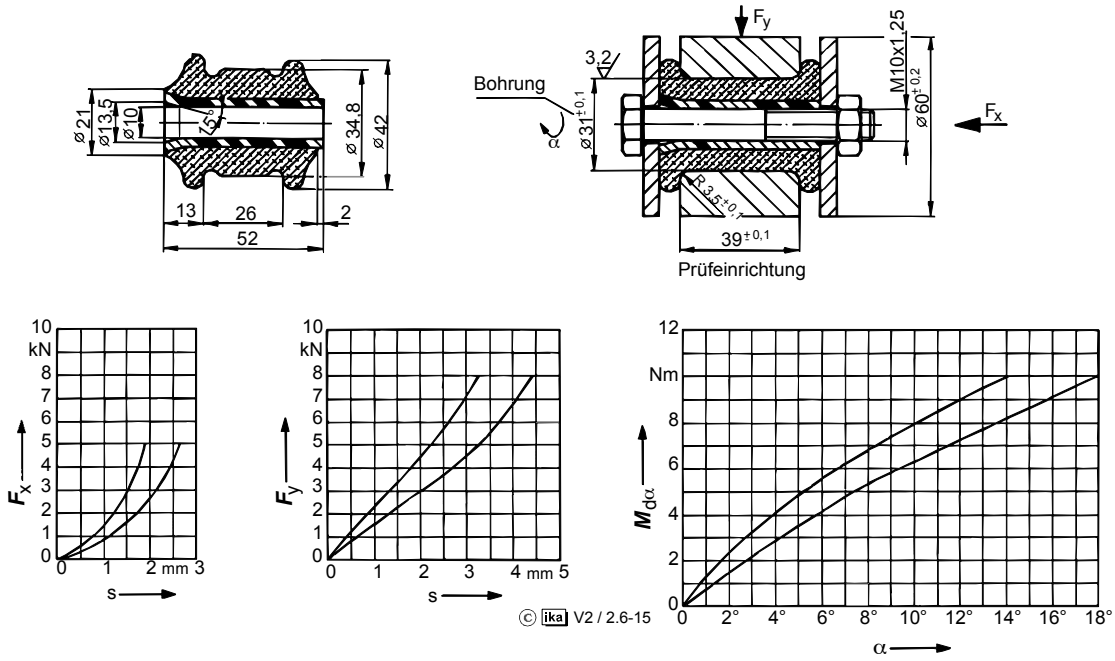

Fig. 2.6-15: Rubber wishbone mount with scorched internal bushing

Due to the plasticity of the rubber, such rubber mounts also offer the advantage that the required angular elasticity can be realized without relative movement of surfaces, which means they are non-wearing, maintenance-free and only subject to material aging.

As a result of the elasticity of the rubber mounts, the effect of the tire forces and tire moments acting on the wheel causes elastic wheel-position changes. Magnitude and direction of these wheel-position changes are determined by the geometry of the layout of the struts or links of a wheel suspension combined with the elasticity of the rubber mounts in the fulcra. Fig. 2.6-16 illustrates these facts, with a wheel carrier guided by five links being used as an example.

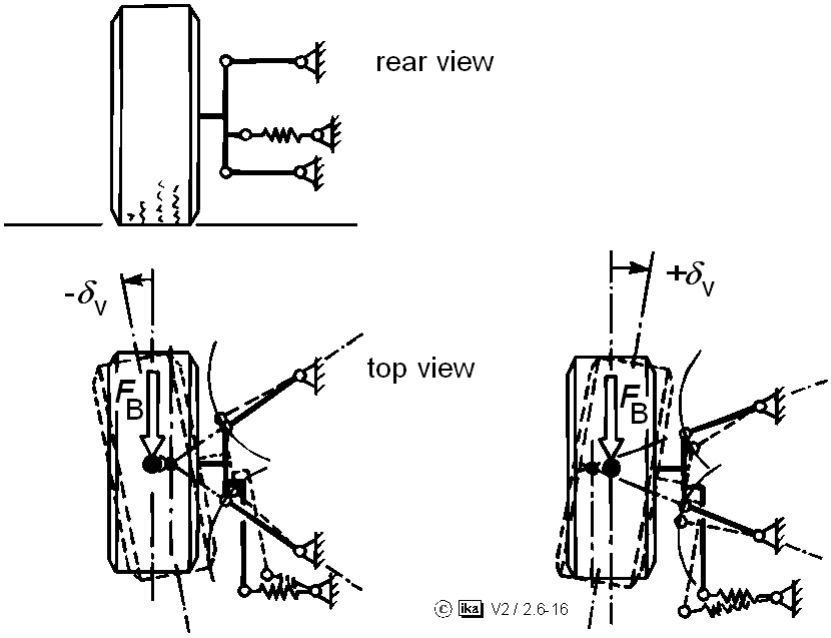

Fig. 2.6-16: Elastokinematics of a five-link wheel carrier with elastic tie rod

Depending on the position of the virtual steering axis, either toe-in or toe-out is caused on the wheel by the radial force due to the elasticity. The great importance of such wheel-position changes for vehicle handling was already described in Sections 2.4.3.5 and 2.4.4.4.

Fig. 2.6-16 gives an idea of the fact that not every wheel suspension design that makes sense from the point of view of kinematics will also allow favorable elastokinematic tuning. High levels of ride comfort require high levels of elasticity of the wheel suspension, above all in vehicle longitudinal direction. To avoid negative influences affecting vehicle handling, the tire forces acting on the wheel in different directions must not cause any undesired steering angles.

Wheel suspensions that to a large extent fulfill the most diverse requirements regarding kinematic and elastokinematic properties usually require a rather complex design featuring a multitude of potential influencing factors. For practical reasons, optimum configuration of the geometry of the layout of struts and links and the tuning of the elasticity of the rubber mounts are carried out with the aid of specific computer programs.

2.6.4 Requirements to be met by Wheel Suspension

The kinematic and elastokinematic properties of wheel suspension systems described in the preceding paragraphs significantly influence vehicle handling (driving safety) and the ride comfort of a vehicle.

In addition to the requirements resulting from these relationships, wheel suspension design has to fulfill economy requirements regarding manufacturing cost and compatibility with the overall vehicle design.

This section summarizes the assessment criteria for wheel suspension designs to be derived from the requirements, Fig. 2.6-17.

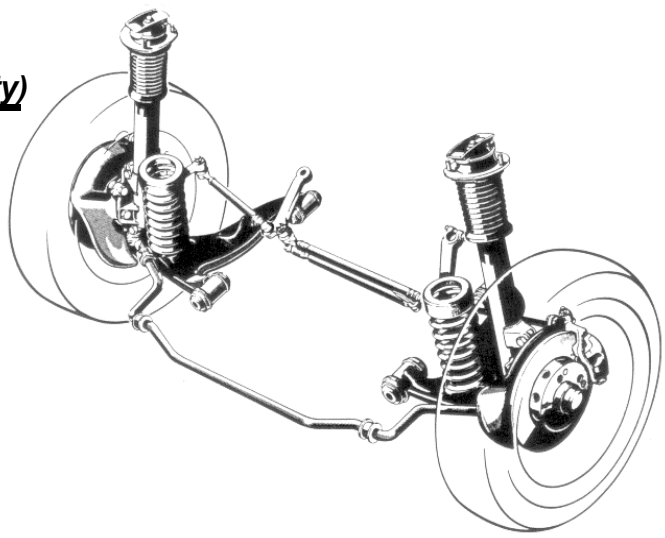

1. ***driving behaviour (driving safety)***
- parameters of wheel position
  - -wheel base
  - -track width
  - -camber
  - -toe-in
  - -roll pole
  - -unsprung mass

2. ***comfort***
- longitudinal springing
- lateral springing
- anti-dive and anti-squat

3. ***economy***
- design effort
- space requirements

Fig. 2.6-17: Assessment criteria for wheel suspensions

2.6.4.1 Handling

a) Wheel lifting curves

Wheel lifting curves describe the position of a wheel relative to the body (superstructure) or the roadway surface subject to the compression position of the wheel (cf. Fig. 2.4-19). Wheel position is characterized by the following parameters:

- tread width
- wheelbase
- camber angle
- toe angle (toe-in)

• Tread width

Tread changes during compression movement of the wheels force lateral movement of the tire contact areas and that way cause fluctuations of the lateral tire forces, which have a negative effect on the straight-running properties of the vehicle. Moreover, tire wear is

increased due to the transverse movement of the tire contact areas. Therefore, kinematic tread changes should be as limited as possible.

• Wheelbase

Wheelbase changes of the magnitude as they occur during compression movement of the wheels do not significantly influence the steering behavior of a vehicle. A wheelbase change in such a way that the wheel passing a bump simultaneously with the compression movement to a certain degree also responds to the horizontal impact force (oblique suspension) has a positive on ride comfort. Major kinematic wheelbase changes, however, cause torsional vibration in the drive train due to the speed fluctuations of the wheels during suspension movement on powered axles, and affect the quality of the signals for ABS control picked up by speed sensors on the wheels /29/.

• Camber angle and toe angle

Kinematic camber-angle variation and kinematic and elastokinematic toe-angle variation considerably affect vehicle handling, cf. Sections 2.4.3.5 and 2.4.4. The requirements to be met by wheel suspension design derived from this fact cannot be summarized in a generalized form, because they vary according to vehicle concept (center-of-gravity location, powered axle) and intended application. Wheel suspension concepts allowing a specific kinematic and elastokinematic design, e.g. multi-link suspensions, are as a rule superior to those whose design permit only limited leeway for layout, e.g. rigid axles.

b) Roll center

The position of the roll center and its position change during cornering are directly related to the kinematic wheel-position changes during suspension movement, cf. Section 2.6.2.1. Wheel lifting curves and lateral-force suspension between footprint centers and the body can therefore not be optimized independently and separately. A compromise is required between the

- dimension of the centrifugal force lever arm Δh, cf. Section 1.6.1,
- intensity of the bump effect, cf. Fig. 2.6-11,
- tread and camber changes during suspension movement, cf. Fig. 2.6-10.

Such a compromise needs to consider even further factors if these kinematic effects in the vehicle transverse plane due to the wheel suspension concept are linked to kinematic effects in the vehicle longitudinal plane and in the roadway plane. These are:

- starting-torque and braking-torque compensation, cf. Fig. 2.6-13, 2.6-14,
- wheelbase and caster changes during suspension movement, cf. Fig. 2.6-7,

- toe-angle changes during suspension movement.

c) Unsprung mass

The term unsprung mass refers to those components of the suspension system that are only suspended via the wheel suspension (wheel springs) and not via the body suspension (body springs), that is wheel, wheel-bearing unit, brake disk, wheel carrier, brake caliper, plus proportionately the masses of links, struts, springs, dampers, tie rods, propeller shafts, etc. The amount of unsprung mass should be as small as possible in view of low dynamic wheel-load fluctuations and a good road grip of the wheels (driving safety).

2.6.4.2 Comfort

a) Longitudinal and transverse suspension (spring action)

Longitudinal and transverse suspension or spring action refers to the elasticity of wheel suspension regarding horizontal impact forces caused by roadway irregularity. Transmission of the impact forces to the body is thus dampened, which has a positive effect on vibration comfort. Wheel-suspension elasticity is achieved by the use of rubber elements in the mounting points on the body. Impact forces in vehicle longitudinal direction can also be absorbed by means of oblique suspension (spring action). Oblique suspension or spring action is characterized by horizontal impact forces directed towards the wheel axis resulting in compression movement of the wheel.

Oblique spring action is based on the same principle as braking-torque compensation. Wheel control kinematics is designed in such a way that the lifting curve of the wheel center in the vehicle transverse plane is rearward inclined relative to the vertical. One component of the body spring force is thus effective in vehicle longitudinal direction, Fig. 2.6-18.

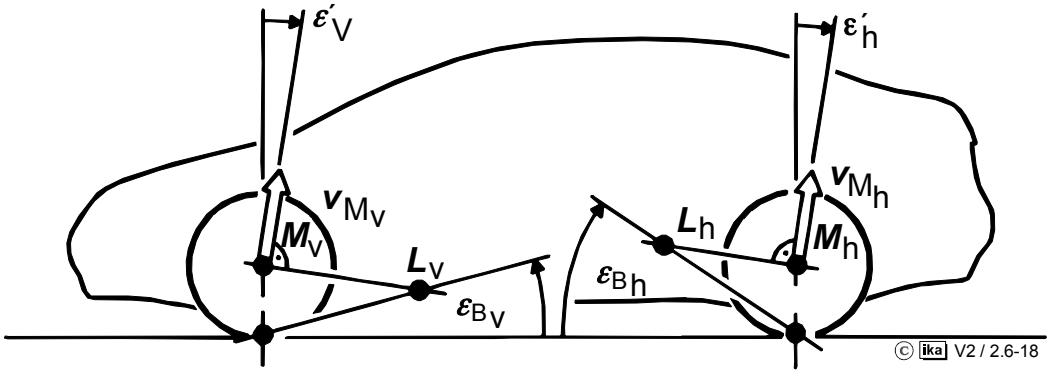

Fig. 2.6-18: Oblique suspension angle and braking support angle

b) Vibration isolation and noise insulation

Especially radial tires with their stiff bracing ply are excited by roadway irregularity to produce relatively high-frequent vibration, which is transmitted to the wheel suspension. To keep such vibration excitation away from the body and to suppress the transmission of structure-borne noise, a relatively high degree of longitudinal elasticity of the wheel suspension is necessary, which can be achieved by means of large-volume rubber mounts in the mounting points (pivot points) of the wheel suspension on the body. To avoid adverse effects on vehicle handling, wheel suspension must be designed in a manner that no unfavorable elastokinematic wheel-position changes are caused, cf. Fig. 2.6-16.

c) Braking-torque and startingting-torque compensation (anti-dive/anti-squat)

Layout of wheel-suspension kinematics in such a way that longitudinal forces in the footprint center possess a component in the direction of the lifting curve of the footprint center during suspension movement makes it possible for the braking-induced compression movement of the front axle / rebound movement of the rear axle to be less intense than it would be the case for purely vertical-force variation (axle-load displacement) in conjunction with wheel-related spring rates.

Such a braking-torque compensation reduces pitching motion of the body (angular movement around the vehicle transversal axis) during braking and thus has a positive effect on suspension comfort. Moreover, bottoming-out during extreme braking deceleration is avoided.

Starting-torque compensation can be realized in a similar way as braking-torque compensation. Since in the case of single-axle drive, longitudinal-force components for influencing compression movement are only available on the powered axle, complete compensation is not possible here, cf. Fig. 2.6-14.

In most wheel-suspension concepts, braking support angle, starting support angle and oblique suspension angle (cf. Fig. 2.6-18) are not independently selectable and closely linked to the wheel lifting curves. Especially with regard to steered wheels, attention must be paid to the fact that design in view of favorable support angles must not result in major caster changes, because they have an adverse effect on the steering quality, cf. Section 2.5.2.

2.6.5 Rigid Axles

Rigid axles are characterized by normally minor construction effort and favorable attachment possibilities on the body. To guarantee freedom of motion of the axle tube, which runs across the underside of the vehicle floor, during compression movement, the spatial requirements of rigid axles with extended suspension travel are relatively high.

The reciprocal interference of the suspension movements of both wheels has a negative effect on the dynamic wheel-load variations. Especially in the case of powered axles with the differential gear integrated in the axle tube, the effect of mass coupling will be operative in addition to that of kinematic coupling.

Guiding of the axle relative to the body in vehicles with leaf springs usually takes place via the spring leafs, Fig. 2.6-19.

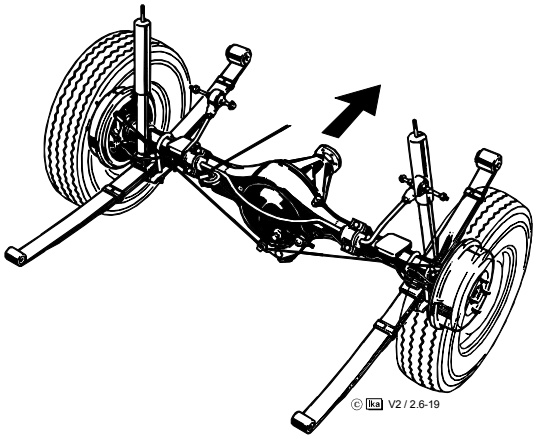

Fig. 2.6-19: Automobile rear axle guided by leaf springs (Ford Capri)

Suspension of link-guided rigid axles is rarely statically defined, Fig. 2.6-20.

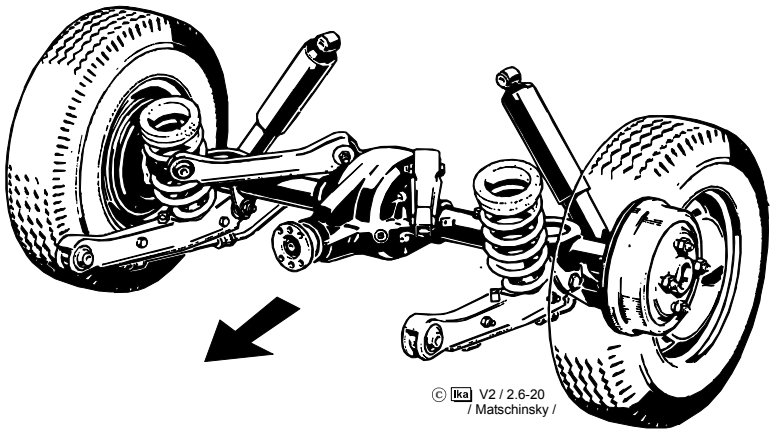

Fig. 2.6-20: Statically defined suspension of an automobile rear axle (Ford Taunus)

Due to easier attachment on the body or less spatial requirement, statically indetermined suspension is chosen as a rule, Fig. 2.6-21.

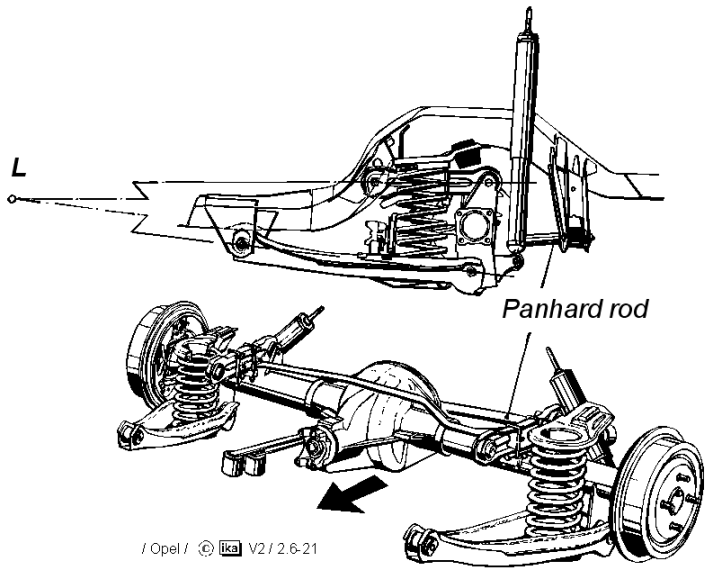

Fig. 2.6-21: Statically indetermined suspension of an automobile rear axle (Opel Rekord)

Transverse control is either effected via a so-called Panhard rod (cf. Fig. 2.6-21), or via a Watt linkage, Fig. 2.6-22.

The Panhard rod should be as long as possible, for transverse offset of the axle during suspension movement to be kept as low as possible, because this would have a negative effect on straight-running properties.

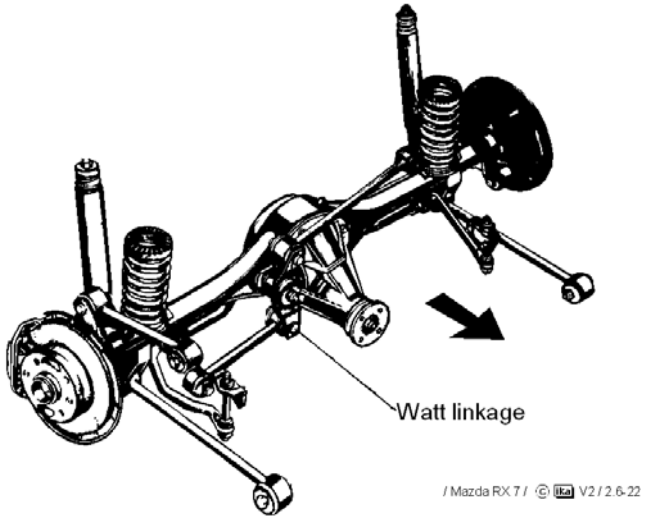

Fig. 2.6-22: Transverse control of a rigid rear axle of an automobile by means of a Watt linkage (Mazda RX 7)

The position of the roll center agrees with the virtual point of power transmission of lateral forces between axle and body. For rigid axles suspended by leaf springs, the roll center is located at the height of the spring-mounting points (pivot points) on the body; for transverse suspension via Panhard rod, at the height of the (horizontal) Panhard rod; for the Watt linkage, at the height of the middle hinge etc.

Depending on the type of longitudinal suspension, braking torque and starting torque compensation can be realized, (cf. Fig. 2.6-21), and toe-angle variations during rolling motion of the body can be influenced, Fig. 2.6-23.

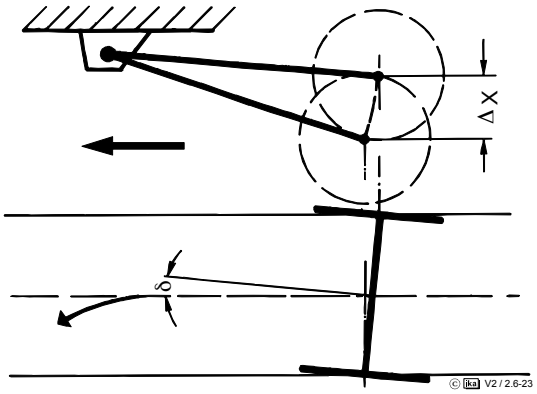

Fig. 2.6-23: Toe-angle variation on a rigid axle with reciprocal suspension movement (roll steer)

With rigid axles, the relative camber angles always correspond to the roll angle, the absolute camber-angle variations are thus always zero (except for deviations due to different tire deflections).

A special type of attachment on the body is represented by the so-called drawbar axle, where one of the mounting points is designed as a ball joint which directly links axle and body, Fig. 2.6-24

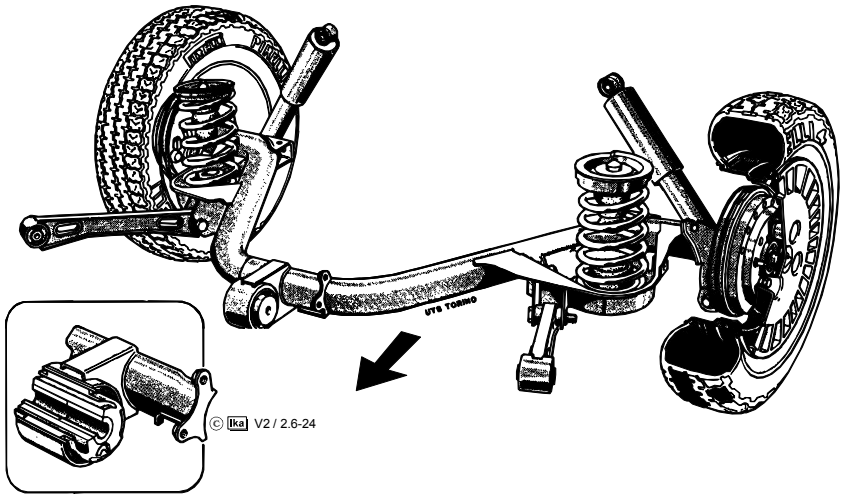

Fig. 2.6-24: Rigid automobile rear axle designed as a drawbar axle (Lancia Y10)

A special concept of a powered rigid axle is represented by the so-called De Dion axle (Albert DeDion, 1899), where the two wheel carriers are linked by a rigid carrier but the differential gear is fixed to the body and linked to the wheels via propeller shafts, Fig. 2.6-25. With this axle design, the wheel-load difference occurring in rigid axles with axle-tube-integrated differential gear in response to the propeller shaft torque is absent and the amount

of unsprung masses is smaller, but these advantages are offset by the disadvantage of considerable design effort.

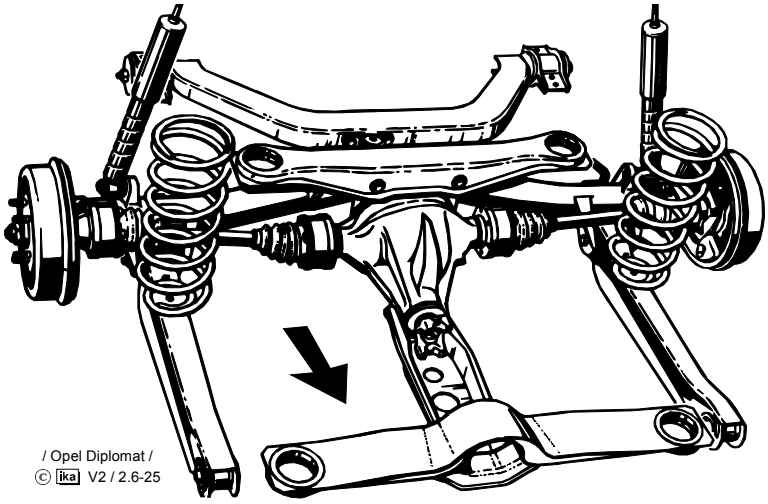

Fig. 2.6-25: De Dion rigid axle (Opel Diplomat)

2.6.6 Semi-rigid Axles

The semi-rigid axles used today in many FWD vehicles as rear axle represent a special version of compound axles, cf. Section 2.6-1.

All semi-rigid axles are characterized by a very simple design and therefore very cost-efficient production. Torsion crank axle (flex arm suspension), twist beam rear axle (semi-independent suspension) and twist beam rear axle (semi-independent suspension) with rearward displaced cross member are differentiated from each other.

The torsion crank axle (flex arm suspension) is the oldest design form, Fig. 2.6-26.

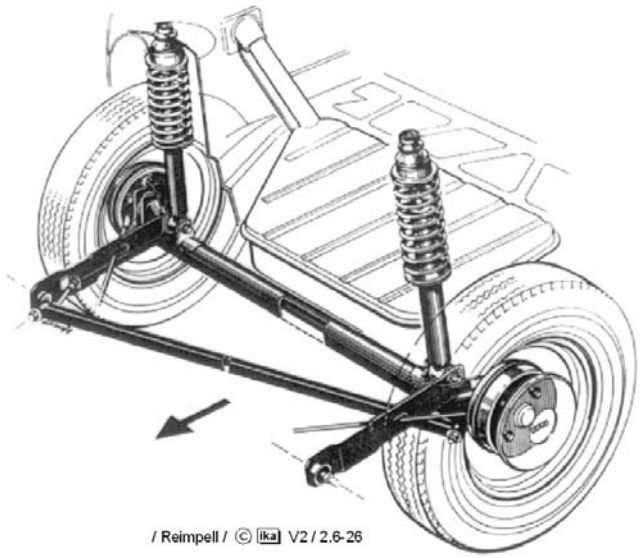

Fig. 2.6-26: Torsion crank axle (Audi 80, 1972)

Similar to a rigid axle, the two wheel carriers are firmly linked to each other by means of a bending-resistant but torsionally weak section.

Longitudinal axle control is effected via longitudinal links welded to the cross member. During reciprocal suspension movement, the cross member is distorted and thus functions as a stabilizer spring.

Transversal axle control is effected by a Panhard rod, which can also run diagonally underneath the vehicle floor if this provides a more favorable mounting point for force application on the body, cf. Fig. 2.6-26.

Body suspension is effected via spring carriers hinged to the axle tube. The kinematic properties of the torsion crank axle largely correspond to those of a rigid axle. The positions of the longitudinal centers are determined by the positions of the mounting points of the longitudinal links on the body. The position of the roll center depends on the location of the Panhard rod.

By contrast, the twist-beam rear axle largely has the kinematic properties of a trailing-link suspension, Fig. 2.6-27.

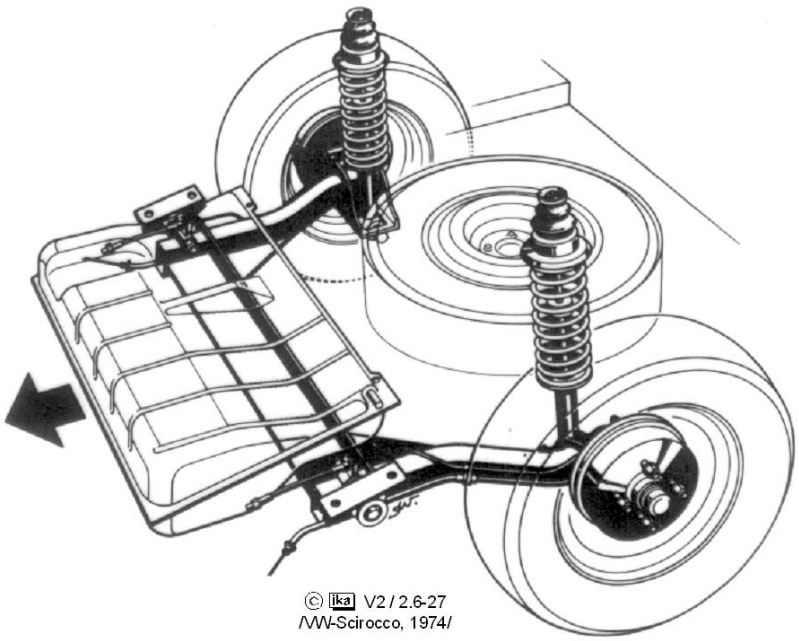

Fig. 2.6-27: Twist-beam rear axle (VW Scirocco, 1974)

This semi-rigid axle consists of two rigid links connected to each other at the height of the mounting points on the body by means of a bending-resistant but torsionally weak cross member welded to the links.

With the twist-beam rear axle, the space required with the torsion crank axle for the co-jouncing axle tube can be used otherwise.

Use of the connecting section (cross member) considerably simplifies mounting of the trailing links on the body compared to trailing-link independent wheel suspension. The use of torsion bar springs, however, is not opportune. Body suspension is effected via spring carriers (spring brackets) hinged to the wheel carrier. During reciprocal suspension movement, the connecting section between the links is distorted and thus acts like a stabilizer spring.

Fig. 2.6-28 shows the twist-beam rear axle of the Audi A4 as another example. A stabilizer in front of the axis of rotation of the axle body is provided for additional reduction of roll angle. Due to its position, the stabilizer simultaneously increases transversal stiffness of wheel control.

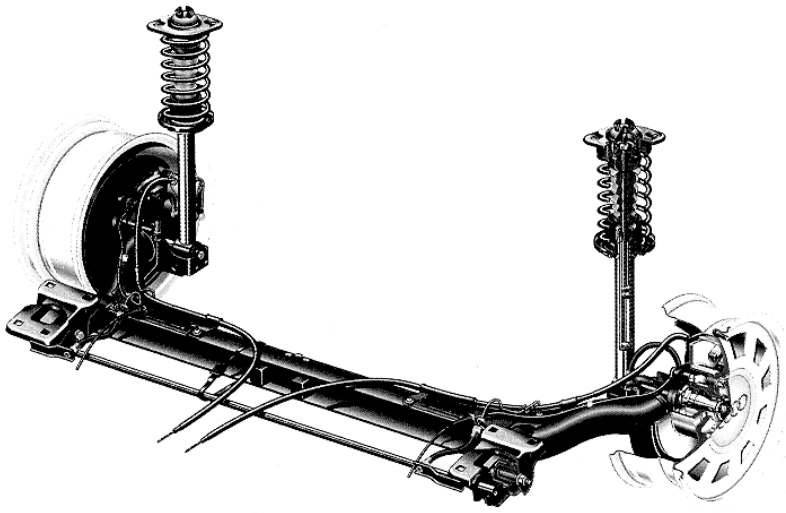

Fig. 2.6-28: Twist-beam rear axle (Audi A4, 1994)

The design of the twist-beam rear axle with rearward-displaced cross member corresponds to that of the twist-beam rear axle, however the connecting section (cross member) of the trailing links is not arranged at the height of the link pivot points on the body but is rearward displaced, Fig. 2.6-29. Twist-beam rear axles are often also referred to as semi-independent or cross-member-type suspension. The twist-beam rear axle is nowadays the standard solution In vehicles such as the Ford Fiesta and the VW Polo.

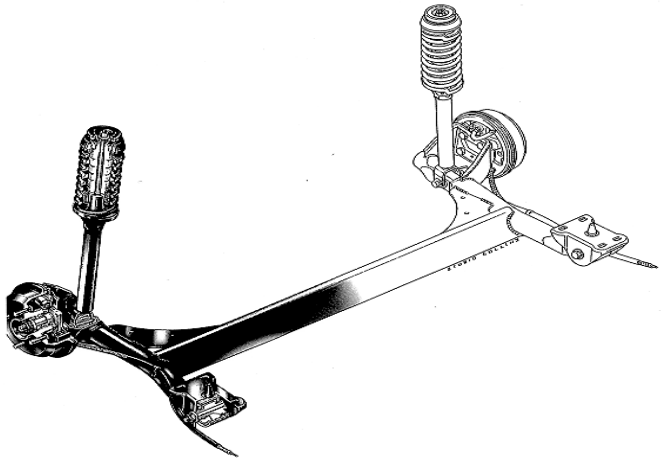

Fig. 2.6-29: Twist-beam rear axle with rearward-displaced cross member (Ford Fiesta,1995)

When this axle type was introduced with the Audi 50, arrangement of the connecting section was probably intended to provide more space for the fuel tank in front of the axle, so that there could be more legroom in front of the rear seat bench.

However, this axle type also proved to have favorable kinematic properties. With parallel springing, the twist-beam rear axle with rearward-displaced cross member behaves like a trailing-link axle; with roll springing, however, it behaves like a semi-trailingarm axle.

The virtual link rotation axes (pivot axes) run through the pivot points of the trailing links on the body and through the shear center of the connecting section distorted by reciprocal suspension. In contrast to the twist-beam rear axle, cornering will therefore be associated with relative camber changes, which will reduce the absolute, positive camber angle of the outside wheel, and the roll center will not be at the level of the roadway surface, Fig. 2.6-30.

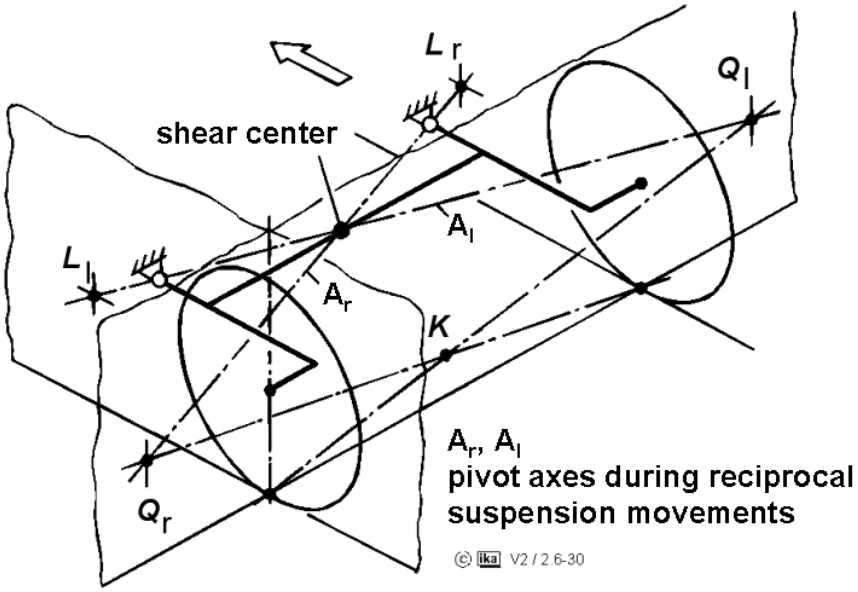

Fig. 2.6-30: Geometry of the twist-beam rear axle with rearward-displaced cross member with roll springing

The twist-beam rear axle with rearward-displaced connecting section is more widely used nowadays than the twist beam rear axle. Lateral forces in the footprint centers produce a force couple in the mounting points of the axle on the body, which consists of a traction force on the outside bearing acting in vehicle longitudinal direction and of a corresponding pressure force on the inside bearing.

With soft rubber mounts for suspension comfort, this results in an elastokinematic toe-angle variation with oversteer effect, which negatively affects the steering behavior of the vehicle during non-stationary (transient) driving maneuvers.

This effect can be suppressed by the use of so-called track-aligning bearings. Their design is such that the effect of an axial lateral force results in radial displacement. During cornering, elastic deformation of the bearings is compensated by the reaction forces in the mounting points (pivot points), Fig. 2.6-31.

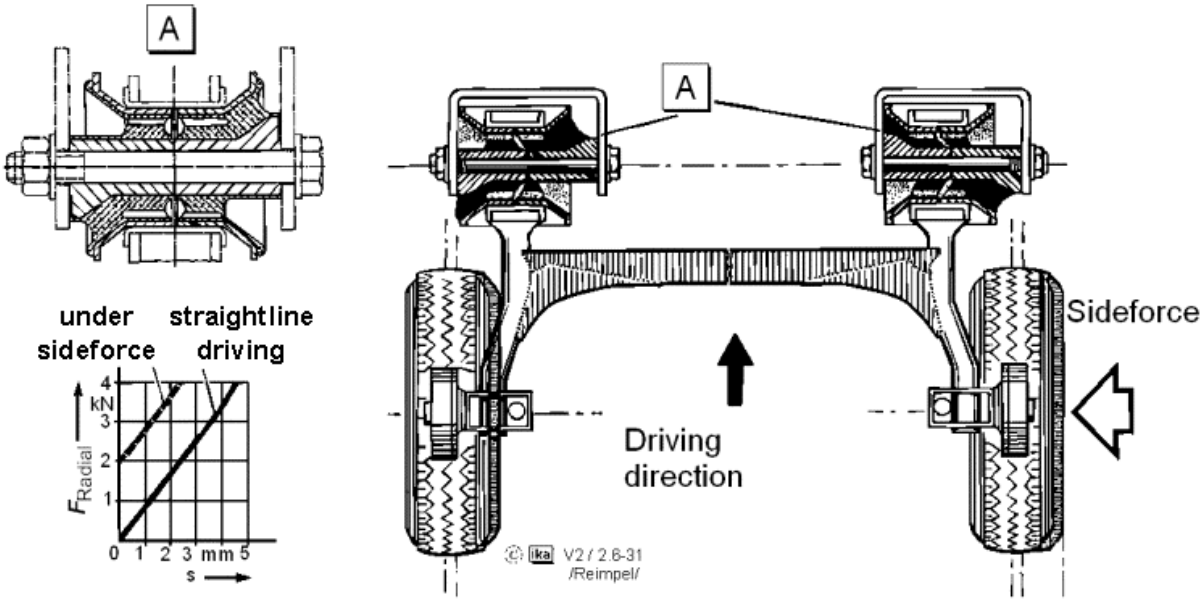

Fig. 2.6-31: Mode of operation of track-aligning bearings on the twist-beam rear axle (with rearward-displaced connecting section) of the VW Passat /33/

2.6.7 Independent Suspension

2.6.7.1 Swing Axles

A swing axle consists of two rigid half axles hinged to the body in the center of the vehicle. Longitudinal force suspension is usually effected via tension struts (trailing links), Fig. 2.6-32.

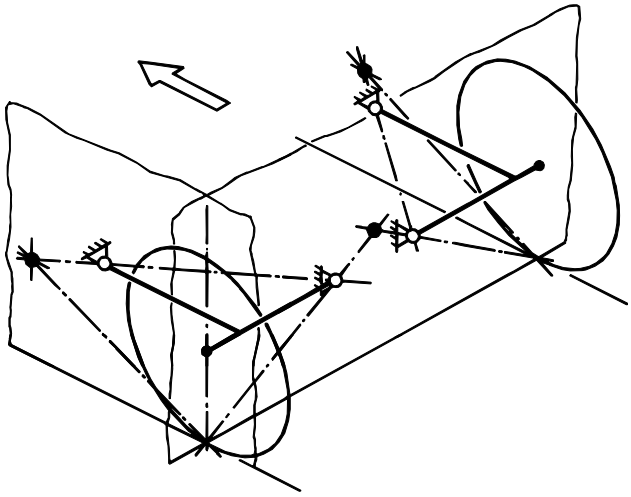

Fig. 2.6-32: Geometry of the double-jointed swing axle

Since the 1930s, the double-jointed swing axle has often been used for powered axles as a moderately complex independent wheel suspension system with a relatively low amount of unsprung masses. Starting-torque or braking-torque compensation can be realized through specific arrangement of the struts. The drive-shaft joints to the right and left of the differential gear served as mounting points on the body, Fig. 2.6-33.

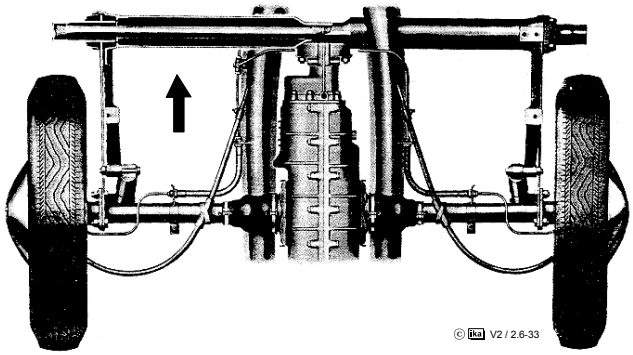

Fig. 2.6-33: Double-jointed swing axle with torsion-bar suspension and longitudinal control via torsionally weak trailing links (VW Beetle) (view from above)

The kinematics of this wheel suspension version is largely determined by this type of control. Suspension movement is associated with significant camber-angle variation and tread changes. The roll center is very high above the roadway, and the axle therefore has a tendency for a distinct bump effect, cf. Fig. 2.6-11.

On account of these drawbacks, this axle design is no longer used today. The single-jointed swing axle (Edmund Rumpler, 1903), with its somewhat more favorable kinematic properties and reduced camber-angle variations and tread changes due to the increased swing-arm radius and its (body-fixed) lower roll center, also no longer meets the requirements to be fulfilled today by a wheel suspension for powered axles, Fig. 2.6-34.

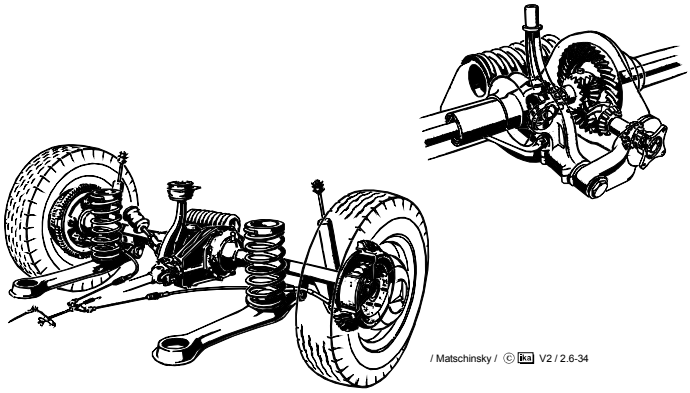

Fig. 2.6-34:Single-jointed swing axle with compensating spring. Lateral-force suspension is effected via the vertical pendulum joint suspension and the strut obliquely hinged to it (MB 220, 1959)

2.6.7.2 Trailing-link Suspension

Trailing-link suspension systems (or trailing-link or crank axles) are characterized by the fact that the wheels are independently guided by links arranged in vehicle longitudinal direction, with the axis of rotation being oriented in vehicle transverse direction, Fig. 2.6-35.

Trailing links (link rotation axis in direction of travel in front of wheel center line/wheel axis) are often used for the control of non-powered rear wheels.

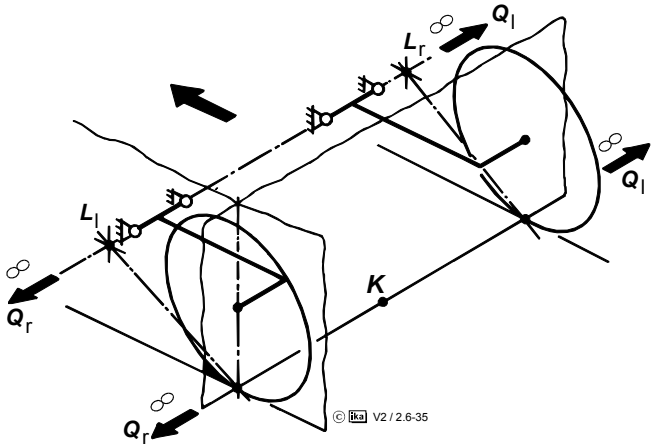

Fig. 2.6-35: Geometry of trailing-link suspension

Pure trailing-link suspension is no longer used on front axles, because angular movement of the link is associated with the steering-knuckle pin changing its tilt (Citroën 2CV), i. e. kinematic caster angle changes occur, which have a negative effect on steering quality.

In conjunction with torsion-bar suspension, trailing-link suspension is characterized by the very little space needed and favorable mounting points on the lower longitudinal members (door sill) that are ideal for force application on the body, Fig. 2.6-36.

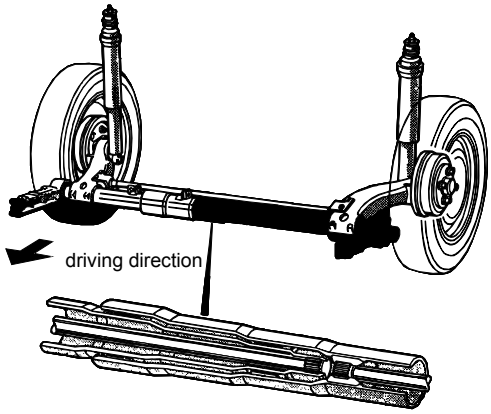

Fig. 2.6-36: Trailing-link rear-wheel suspension with torsion-bar suspension (Renault 9, 11)

The trailing links are subject to bending as well as torsion and must therefore possess a considerable cross section. Due to the orientation of the axes of rotation of the links, neither kinematic bump toe-in and camber-angle variation nor tread changes occur.

On account of the rolling motion of the body, the absolute camber angle of the outside wheel during cornering is always positive. Moreover, due to the elasticity in the link mounts, the tire lateral force causes toe-out on the wheel. Both effects minimize the understeer tendency of a vehicle. This is the reason why trailing-link suspension is preferred for the rear axles of FWD vehicles.

According to the wheel control kinematics, the roll center is on the roadway surface, cf. Fig. 2.6-35.

The longitudinal centers crucial for braking-torque compensation constitute the piercing points of the axes of rotation of the links through the wheel disk plane and are thus body-fixed points.

In FWD automobiles, the brake power on the rear axle is relatively low. Full braking-torque compensation on the rear axle thus requires a wide braking support angle, which in turn requires a major vertical distance between longitudinal center and footprint center or an accordingly minor horizontal distance, cf. Fig. 2.6-13.

The vertical distance in trailing-link suspension is limited by spatial conditions. Determination of link length requires the fact to be considered that progressiveness of wheel-related spring rates increases with decreasing link length.

2.6.7.3 Semitrailing-link Wheel Suspension

Semitrailing-link suspension nowadays very often used as powered rear axle constitutes a further development of the powered swing axle.

As an additional component, semitrailing-link suspension features a wheel-carrier-side drive-shaft joint, so that the axis of rotation of the wheel-carrier movement relative to the body does not have to run through the body-side joint on the differential, Fig. 2.6-37.

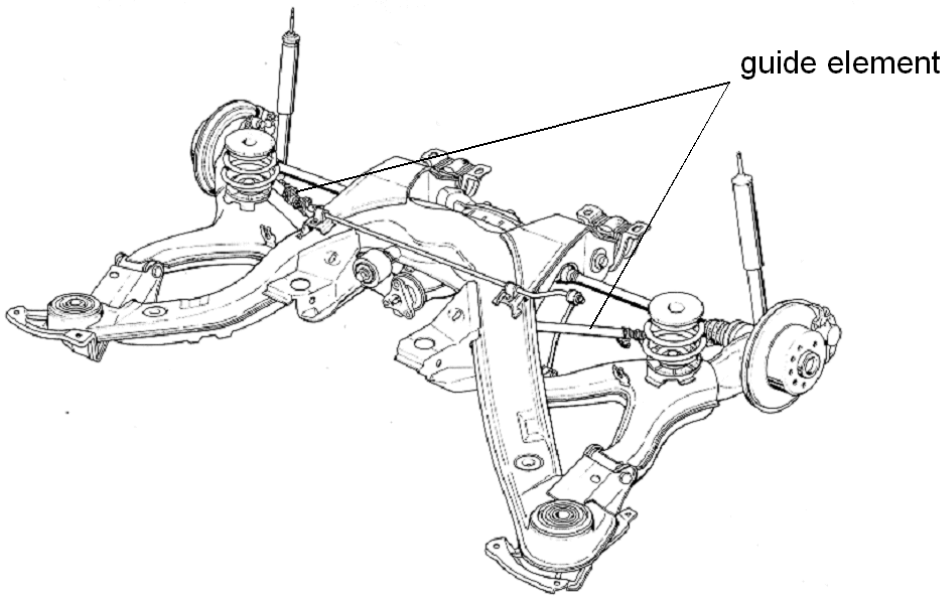

Fig. 2.6-37: Semitrailing-link suspension of a powered rear axle of an automobile (Opel Omega, 1994)

Compared to the swing axle, semitrailing-link suspension offers much more leeway in the specification of the wheel lifting curves or the longitudinal and transverse centers. For favorable kinematic properties to be realized in modern designs, the link rotation axis in the projection on the vehicle transverse plane is inclined by the so-called top/roof angle β; in the projection on the roadway plane, it is inclined by the so-called sweep (angle) α, Fig. 2.6-38.

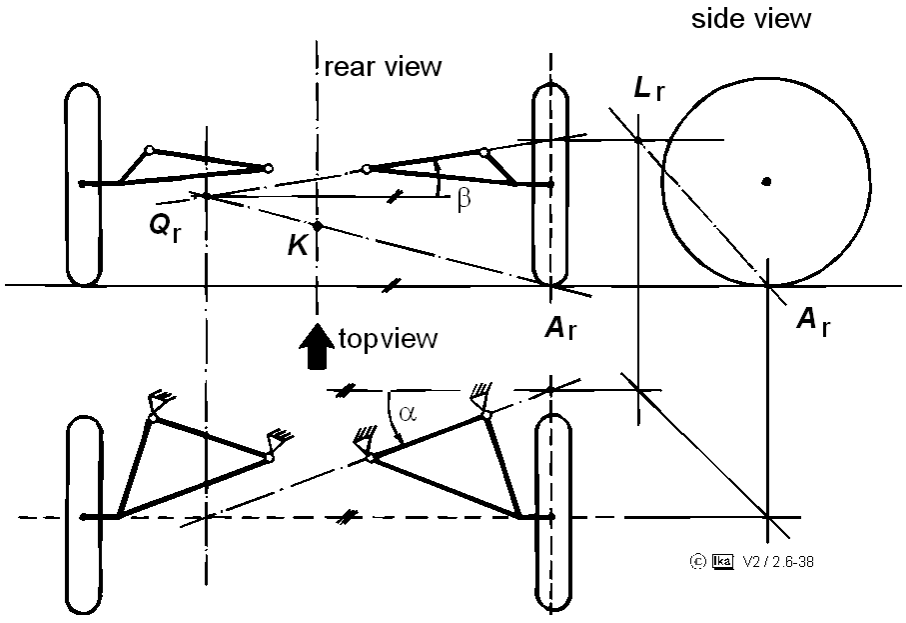

Fig. 2.6-38: Geometry of semitrailing-link suspension

Longitudinal and transverse center positions can be determined by simple graphic means, cf. Fig. 2.6-38. The difference between camber angle γ and top/roof angle β (magnitude: ±3°) decisively influences toe-angle variation during suspension movement /29/. The magnitude of kinematic toe-angle variation and the height of the roll center above the roadway surface are essentially determined by the sweep (angle) α (magnitude: 10 - 25°).

An additional feature of the semitrailing-link suspension of the Opel Omega shown in Fig. 2.6-37 is represented by a control element that is fixed to the chassis subframe and the wheel carrier and supports the wheel forces. This way, load is taken off the A-arm.

Attitude and position of the control element are calculated in a way to make sure that only minor bump toe-in can occur on the wheels during driving. This improves lateral-force stability of the axle.

A semitrailing-link suspension system with additional degrees of freedom of design is represented by the worm-and-nut-steered rear axle used in the 5 and 7 series of BMW until the model years ´96 / ´94.

Each semitrailing link has an additional short link fixed to it, which causes axial displacement of the semitrailing link on its rotation axis during suspension movement, Fig. 2.6-39. Plane semitrailing-link suspension is thus turned into three-dimensional wheel suspension with body-fixed instantaneous axis of rotation, cf. Section 2.6.1.

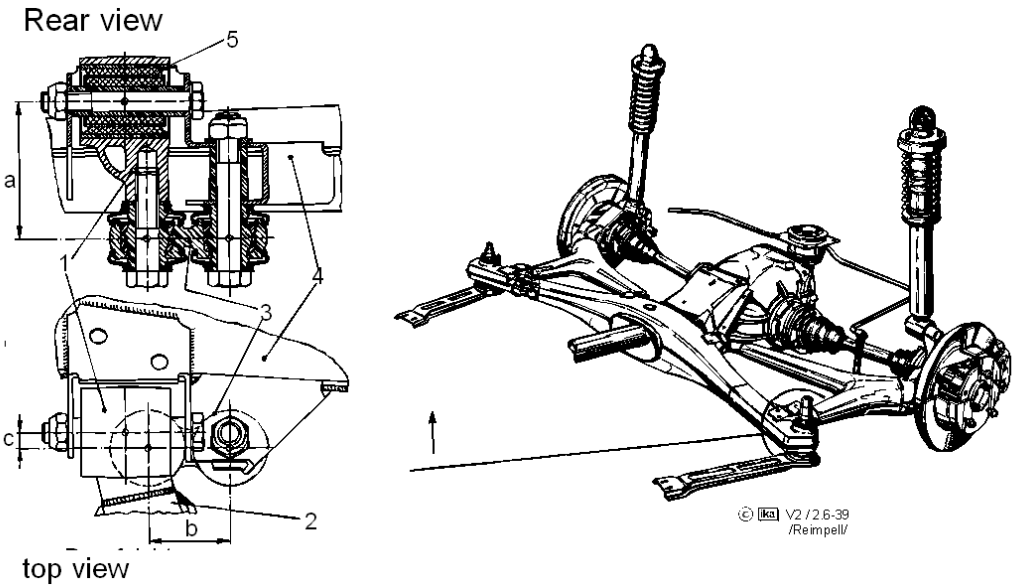

Fig. 2.6-39: “screwing linkage rear axle” (BMW 5, 7 up to MY ´96 / ´94) /33/

In the present example, use of the extra link allowed the sweep angle to be reduced for an increase of braking and starting support angles without abandonment of the change of position of the roll center during cornering, which is favorable regarding avoidance of the bump effect (cf. Fig. 2.6-11).

Fig. 2.6-40 shows the semitrailing-link rear axle of the VW Sharan as an example for a non-powered rear axle.

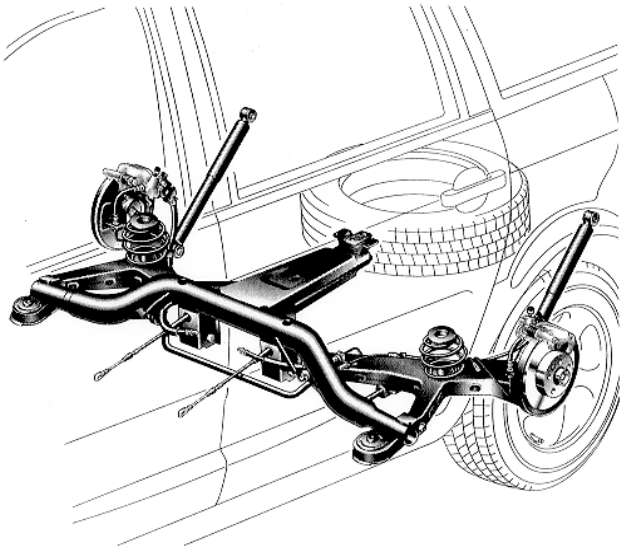

Fig. 2.6-40: Non-powered semitrailing-link rear axle (VW Sharan, 1996)

Miniblock springs permit axle layout under the low load floor without restriction of loading-area width. For packaging reasons, the rear-axle vibration dampers are mounted in a rearward-inclined position.

2.6.7.4 Double-wishbone Suspension

In double-wishbone suspension, the wheel carrier is not hinged directly to the body but forms a kinematic four-link chain together with the body and two A-arms, Fig. 2.6-41.

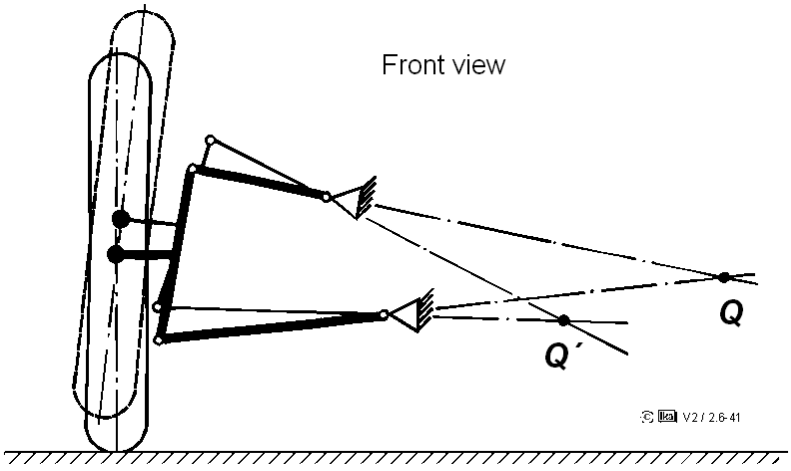

Fig. 2.6-41: Geometry of plane double-wishbone suspension

Depending on the position of the axes of rotation, plane (parallel rotation axes), spherical (intersecting rotation axes) or three-dimensional (skew rotation axes) wheel suspension is obtained (cf. Section 2.6.1).

A wide range of variation of wheel lifting curves, the position of the roll center and the magnitude of starting-torque or braking-torque compensation is thus available, Fig. 2.6-42.

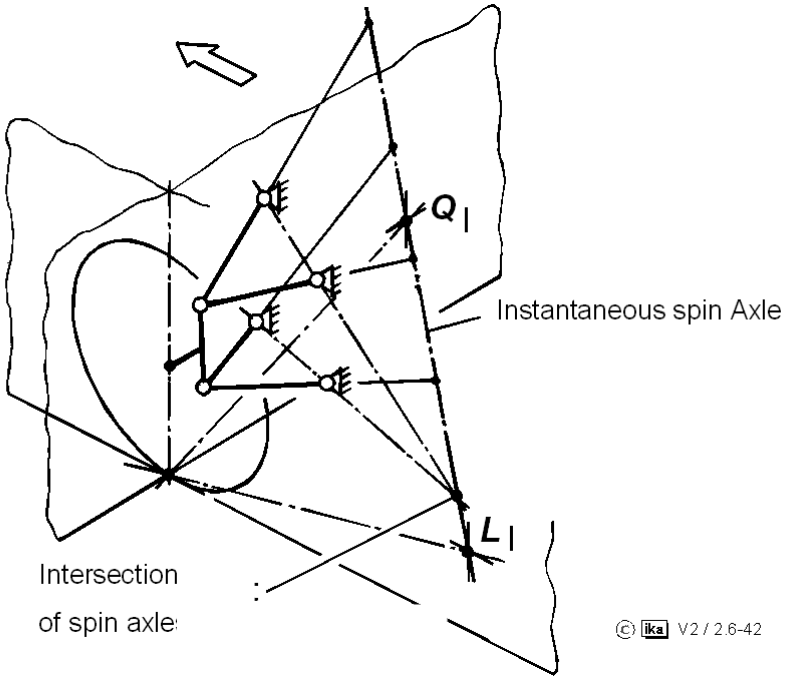

Fig. 2.6-42: Geometry of spherical double-wishbone suspension

In conventional double-wishbone suspension, the relatively strong joint forces in the pivot points (mounting points) on the body are disadvantageous. On the one hand, they result from the small vertical support base for the brake and reaction torque of the tire forces acting on the wheel carrier; on the other hand, they result from the usually high spring ratio (cf. Section 1.3.2.3).

Due to the strong joint forces, wishbones are as a rule not directly mounted to the body structure but to a chassis subframe which links both wheel suspensions and thus relieves the body structure of internal forces.

Chassis subframe and body are mostly linked by means of vibration-isolating and noise-insulating rubber elements.

Modern double-wishbone suspensions often feature an upper wheel carrier ball joint extending far beyond the wheel disk, so that the vertical support base is extended. This does away with the need for a chassis subframe. The link rotation axes are usually three-dimensionally arranged, so that certain kinematic properties can be realized, Fig. 2.6-43.

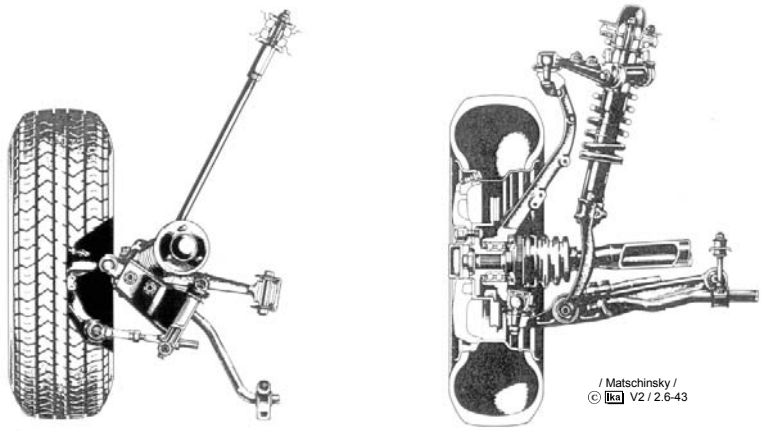

Fig. 2.6-43: Three-dimensional double-wishbone suspension of a powered front axle (Honda Prelude)

Occasionally, double-wishbone suspension is also used on non-powered front axles. Fig. 2.6-44 shows the front axle of the Mercedes-Benz E (1995) as an example.

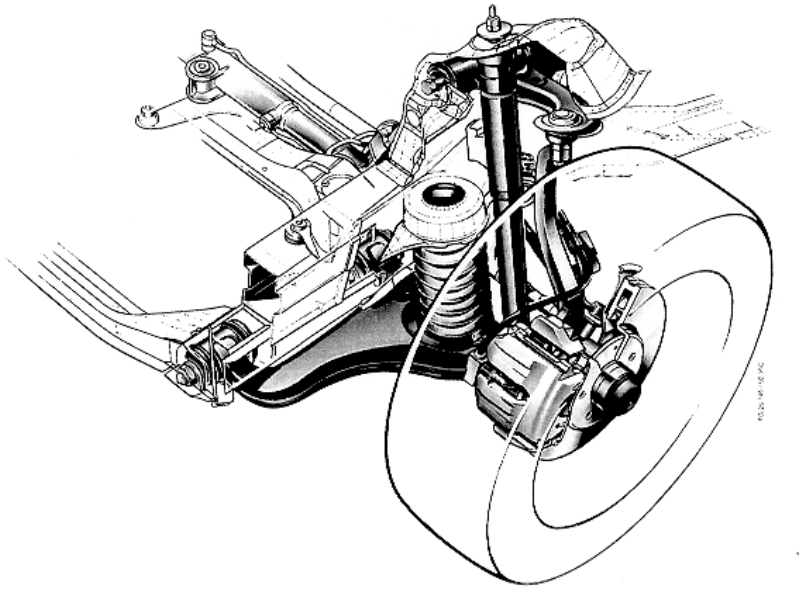

Fig. 2.6-44: Double-wishbone front axle (Mercedes-Benz E, 1995)

In spite of considerable design expenditure, double-wishbone suspensions are also used as rear axles. Their design offers clear advantages especially in very powerful vehicles because of their manifold kinematic and elastokinematic layout possibilities compared to other axle concepts. Fig. 2.6-45 shows the "center-point-controlled" spherical double-wishbone suspension of the BMW Z1.

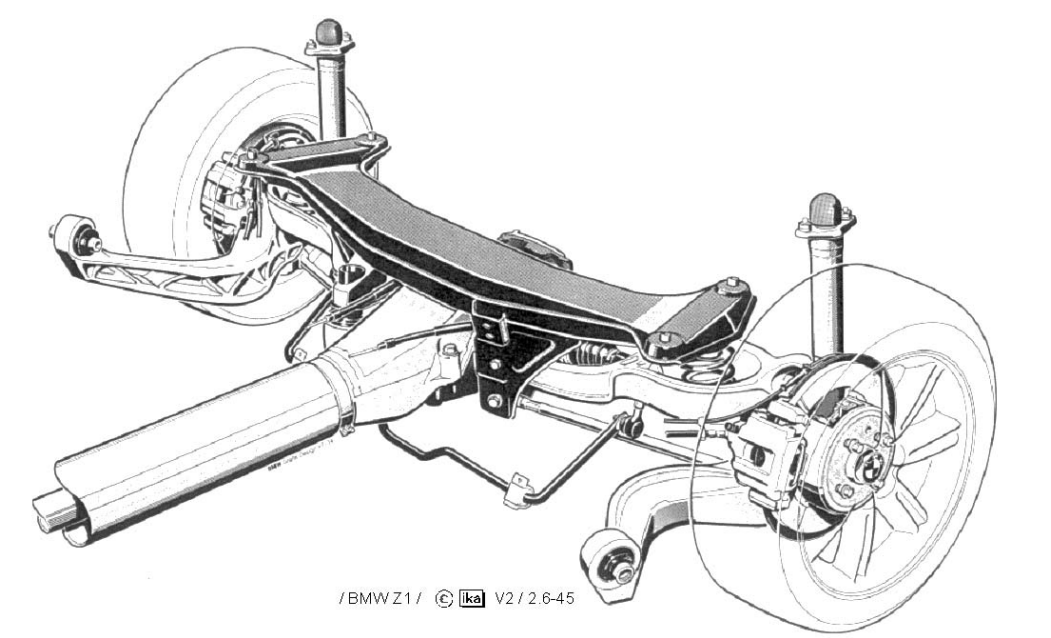

Fig. 2.6-45: "Center-point-controlled" spherical double-wishbone suspension of the powered rear axle of the BMW Z1

The wheel-controlling components of the central-link rear axle are composed of a longitudinal link as a third link in addition to the two transverse links (wishbones) arranged one upon the other. The longitudinal link is elastically mounted to the body. The wishbones are linked via rubber mounts to a rear-axle bracket, which is elastically mounted to the body. The three links thus form a spherical gear.

This design permits clear task sharing of the links (with the longitudinal link mainly responding to longitudinal forces and the wishbones mainly responding to the lateral forces), which facilitates separate tuning of longitudinal and transverse dynamics.

A rear axle with nearly identical kinematics is also found in the BMW 3 Series since MY ´91.

2.6.7.5 Strut Suspension

In the 70s, double-wishbone suspension was largely replaced by spring-strut-type suspension (Fiat, 1926) as a wheel suspension concept for front axles.

The kinematics of strut suspension corresponds to that of a double-wishbone suspension in which the upper wishbone is of infinite length or has been replaced by a sliding guide. In the strut suspensions realized, this sliding guide corresponds to the telescopic shock absorber whose casing is firmly fixed to the wheel carrier and whose shock-absorber rod is also used for wheel control.

Compared to double-wishbone suspension, the advantages of strut suspension include the reduced design expenditure and the reduced requirements in space at the level of the wheel axles, which can be utilized especially in FWD automobiles with transversally installed engine-transmission unit.

With regard to the determination of wheel control kinematics, strut suspension offers less leeway than double-wishbone suspension.

In the strut suspension concept according to the McPherson principle (Earl McPherson, 1945), the lower A-arm is made up of a wishbone and a stabilizer, Fig. 2.6-46.

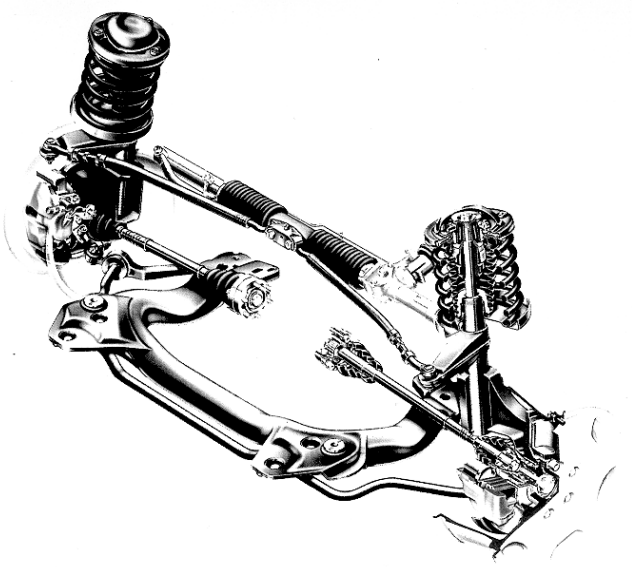

Fig. 2.6-46: McPherson front axle (Audi 100, 1991).

Similar designs with other wishbones are nowadays also referred to as McPherson axles /33/. Fig. 2.6-47 shows the McPherson front axle of the VW Polo (1995). While in the Audi 100 the stabilizer also performs a wheel-controlling function, this function is effected in the VW Polo by a lower A-arm. Similar designs are nowadays found in all compact-size automobiles.

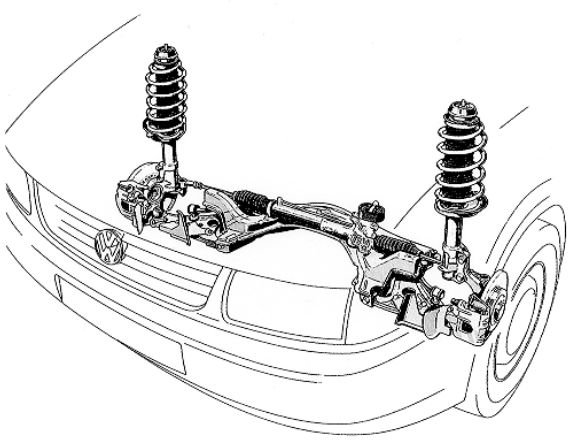

Fig. 2.6-47: Strut suspension (VW Polo, 1995)

Inclination of the damper piston rod in the vehicle transverse plane, for the transverse center to be influenced, is limited on the one hand by the tire inside flank and on the other hand by the steering-axle position being determined by the upper suspension-strut mounting point, cf. Fig. 2.5-12.

Inclination of the damper piston rod in the vehicle longitudinal plane, for the longitudinal center to be influenced, is limited by the fact that on the one hand a certain position of the steering axle (caster angle) is to be realized and on the other the clamping force in the piston rod guide of the damper is to be minimized, with this force resulting from the non-alignment of the line of action of the spring force with the point of intersection of the line of action of the vertical force in the footprint center and the line of action of the axial force of the A-arm, Fig. 2.6-48.

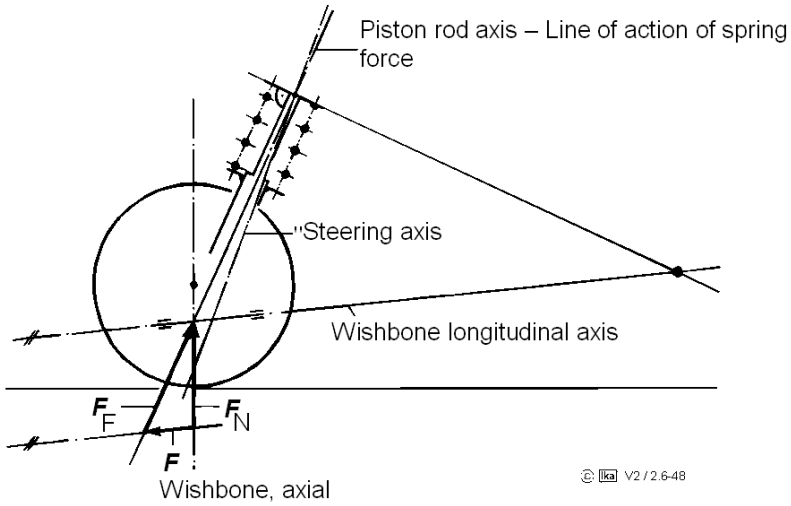

Fig. 2.6-48: Reduction of the clamping force in the piston rod guide of the strut suspension through alignment of the line of action of the spring force, vehicle longitudinal plane

Reduction of the clamping forces in the piston rod guide, which adversely influence spring response, is also contributed to by the inclined position of the body suspension relative to the damper tube in the vehicle transverse plane.

Clamping force is minimized through alignment of the line of action of the spring force with the point of intersection of the line of action of the vertical force in the footprint center and the line of action of the link force, Fig. 2.6-49.

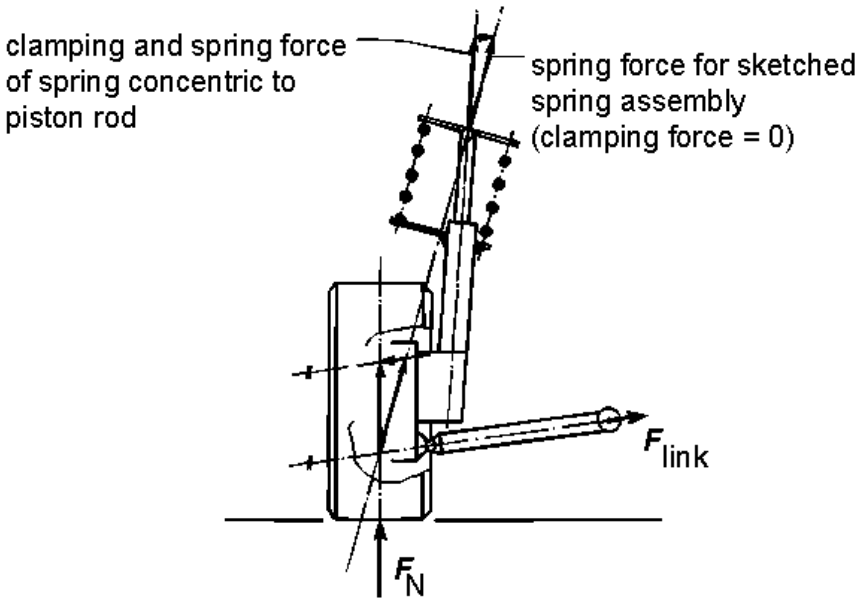

Fig. 2.6-49: Reduction of the clamping force in the piston rod guide of the strut suspension through alignment of the line of action of the spring force, vehicle transverse plane

Arrangement of body suspension above the wheel is necessary for the damper tube to run alongside the wheel as closely as possible and for an acceptable spread angle to be realized. By means of a specific design of the transverse-link mounts in strut suspension, longitudinal elasticity of wheel control favorable for suspension comfort can be achieved without unfavorable elastokinematic toe-angle changes, Fig. 2.6-50.

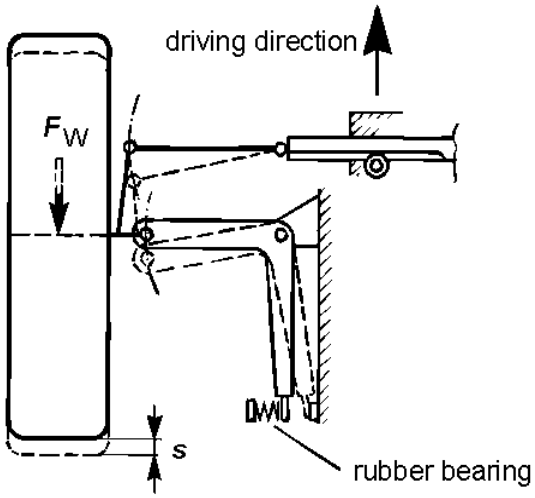

Fig. 2.6-50: Elastokinematically tuned strut-type front axle

The front axles of the current BMW 5 and BMW 7 series can be considered as further developed traditional strut-type suspension, Fig. 2.6-51.

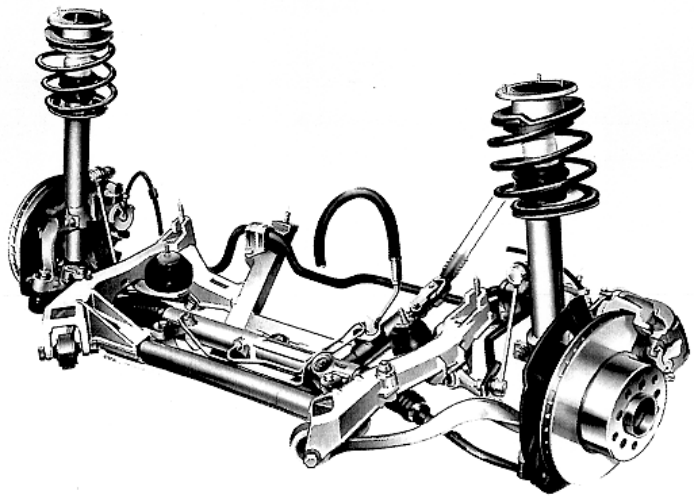

Fig. 2.6-51: Double-jointed strut-type front axle with ideal steering axis (BMW 5, 1996)

Substitution of the lower A-arm by two struts is the common hallmark of these axle concepts. For the steering axis, this results in a virtual piercing point in the lower wishbone plane, which on the one hand causes a minor steering offset, which increases with the steering angle, as well as a disturbing force lever arm, and on the other hand permits a larger brake disk to be installed due to a minor wheel offset, Fig. 2.6-52.

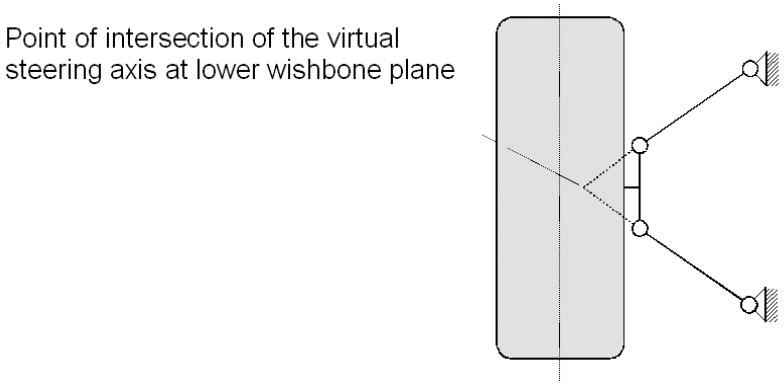

Fig. 2.6-52: Piercing point of the virtual steering axis

The fact that the front-axle bracket is an aluminum weld assembly is another special feature of the axle design shown in Fig. 2.6-52. Compared to the preceding model, the axle is characterized by a weight reduction of 5.4 kg.

Damper strut suspension, where the spring force of the body suspension is transferred to the wheel carrier via the ball joint of the transverse link, is also a further development of strut-type suspension, Fig. 2.6-53.

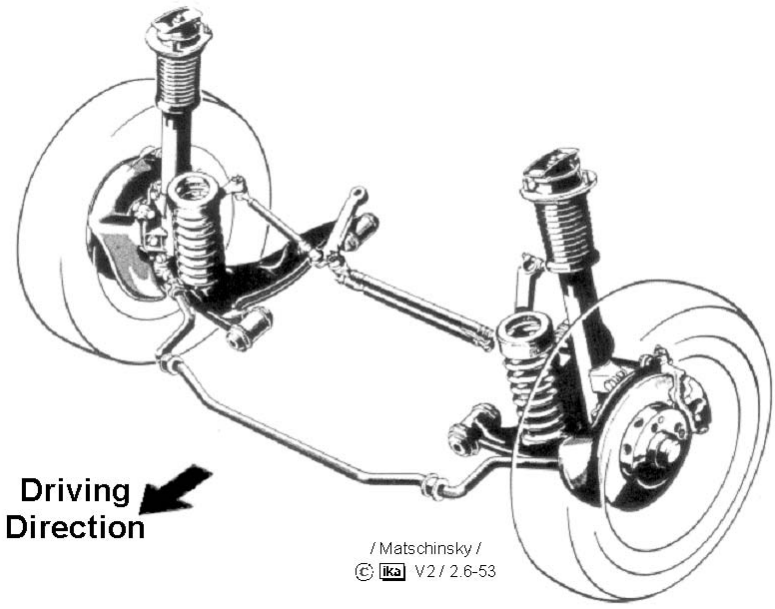

Fig. 2.6-53: Damper strut front axle (MB 190)

In addition to a somewhat reduced overall height, this design offers the advantage that caster angle and longitudinal center can be determined without consideration of the clamping forces in the piston rod guide of the damper caused by the spring force, cf. Fig. 2.6-48.

2.6.7.6 Multilink Wheel Suspensions

Realization of a wheel suspension system that meets high riding-comfort requirements and at the same time offers favorable handling characteristics is possible if kinematic and elastokinematic properties are specifically tuned and matched, cf. Fig. 2.6-16.

The more variable parameters there are, the more aspects can be realized in design. Consequently, a multilink axle offers optimum conditions.

A wheel suspension system whose design follows the basic concept of three-dimensional wheel control, with the wheel carrier being linked to the body via 5 links, is referred to as multilink wheel suspension, cf. Fig. 2.6-1. Design of such a wheel suspension system can be based on the most diverse objectives.

Fig. 2.6-54 shows the four-link front axle of the Audi A4. In this axle type, the wheel is controlled via four rod-shaped links, the tie rod and the suspension strut. Due to the independent control elements, the design principle of the A4 axle possesses a great potential regarding the optimization of comfort and kinematic properties.

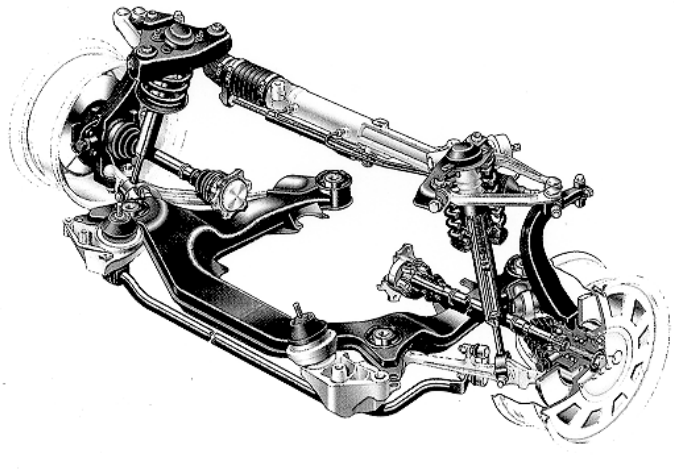

Fig. 2.6-54: Four-link front axle (Audi A4, 1994)

The large support base between upper and lower link plane is the characteristic feature of the design of the four-link front axle of Audi. It is the source of a high camber rate.

The four links are linked to the swiveling bearing via low-friction ball joints. A bearing bracket featuring rubber-bonded metal mounts (silent bearings) carries the two upper links as well as the spring seats and shock-absorber mounts. Spring seats and shock-absorber mounts function separately. Even the supplementary spring (helper spring) is supported via the bearing bracket directly on the body, so that it is possible to tune the shock-absorber mount exclusively to the shock-absorber forces. The shock absorber features an internal stop spring that supports kinematic starting-torque compensation (anti-squat control).

The axle spring is arranged concentrically around the damper. With its fork-shaped end, this spring-and-damper assembly is supported via a rubber-metal bearing by the front lower link, the supporting link. The rearward lower link, the radius link, only supports the link forces and essentially determines elastokinematic longitudinal control of the wheel. Therefore, it features a technically very complex rubber-metal bearing with hydraulic damping for optimum tuning of tire comfort and the vibrational behavior of the axle.

The rack-and-pinion steering with external sensing of the tie rod is rigidly bolted to the body above the transmission and thus very close to the upper link plane. This permits a relatively precise geometric assignment between tie rod and link for precise toe-in kinematics.

The virtual steering axis (cf. Fig. 2.5-8) is an outstanding hallmark of this axle design. With a narrow spread angle, it is located near the wheel center and supports a small disturbing force lever arm for driving power, which is important for FWD automobiles.

While multilink wheel suspension is still the exception on the front axle, multilink wheel suspension on the rear axle is more widely spread. Fig. 2.6-55 shows the five-link rear axle of the Chevrolet Corvette in a rear view from below.

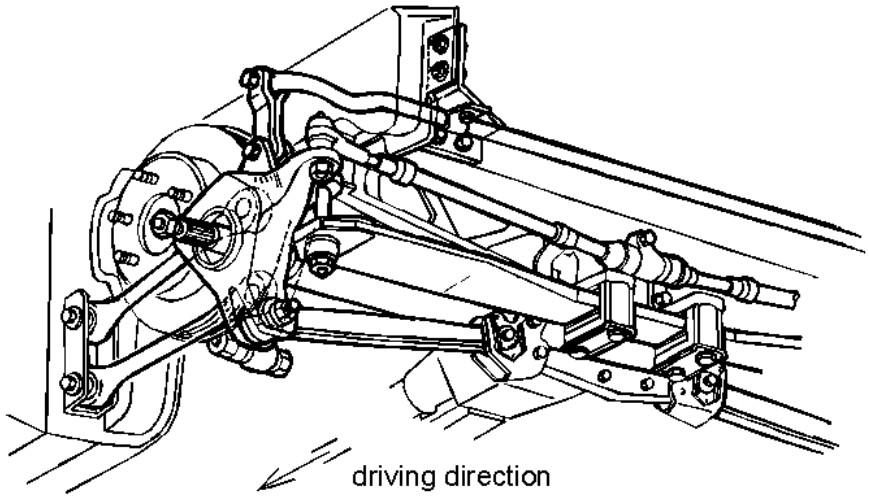

Fig. 2.6-55: Five-link rear axle (Chevrolet Corvette, 1983)

In the "Corvette", longitudinal forces and braking torque are essentially supported via two pull/push rods arranged in vehicle longitudinal direction. Corresponding dimensioning of the components facilitates realization of a lightweight design.

The angular position of the links in relation to each other in the vehicle longitudinal plane decisively determines the position of the longitudinal center, i.e. the magnitude of braking or starting compensation.

Transverse control of the wheel carrier is effected via another pull/push rod arranged in vehicle transverse direction and the axle drive shaft, which is also used as a push/pull rod and features joints both on the body end as well as the wheel carrier end.

The positions of the transverse centers or the roll center are essentially determined by the angular position between the jointed shaft and the transverse strut in the vehicle transverse plane.

A fifth adjustable strut arranged behind the axle performs the same function as the tie rod on a steering axle. A plastic transverse leaf spring, which is decoupled from the wheel control forces by means of a short pull/push rod, is employed for body suspension. For undesired elastokinematic toe-angle changes to be suppressed, the rubber mounts in the fulcrums of this wheel suspension must be relatively stiff. The associated negative effects on riding comfort are accepted in view of the intended purpose of the axle (sports car).

In the multilink rear suspension systems of the Mercedes-Benz model series W 201 and W 124, the wheel carriers are linked to the body via 5 links (or struts) each, Fig. 2.6-56.

Four of the links essentially only support pull/push forces; one link also transmits the spring and damper forces to the wheel carrier. The upper and lower pairs of links each perform the function of an A-arm. The fifth link, which is located roughly at the level of the wheel center line, functions as a tie rod.

In the top view, the intersecting point of the lines of action of the upper pair of links is located on the outside of the wheel center plane; that of the lower pair of links is located on the inside. The position of the "steering axis" determined thereby, cf. Fig. 2.6-16, results, for example, in the longitudinal forces causing elastic bump toe-in to be compensated by kinematic bump toe-in, so that there is zero elastokinematic bump toe-in.

The side view reveals an angular position of the body-end "rotation axes" relative to the "A-arms" formed by the upper and lower pairs of links.

The positions of the transverse centers decisively influenced thereby results in a braking-torque compensation of 60% and a starting-torque compensation of 67%, cf. Section 2.6.2.2. Use of a subframe allows the use of additional rubber elements for vibration isolation and noise insulation between axle (incl. differential) and body. Moreover, this also simplifies vehicle production, since the complete axle can be pre-assembled as a system.

In the kinematic and elastokinematic design of wheel suspension systems, the maximum number of influencing possibilities is only available if exclusively such links are used that cancel only one of the six degrees of freedom of the wheel carrier relative to the body. It is not absolutely necessary for all 5 links to be arranged between wheel carrier and body. If it is accepted that individual links are subject to bending not only by the spring/damper forces, then further possibilities of arrangement will be available.

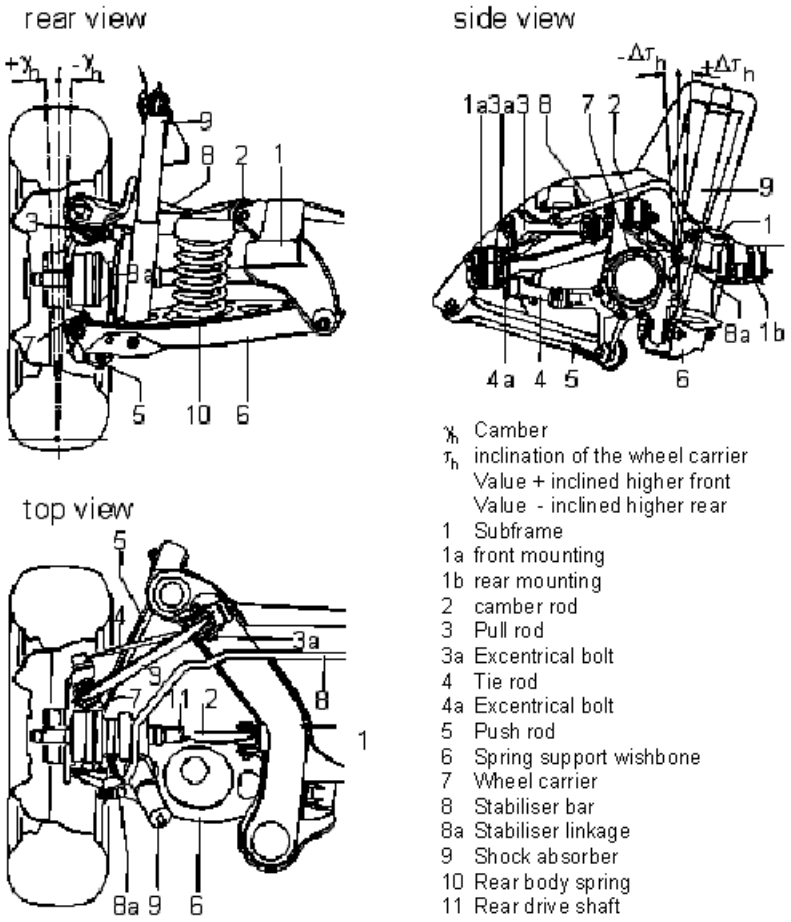

Fig. 2.6-56: Multilink rear suspension MB 190 /33/

The positions of the transverse centers decisively influenced thereby results in a braking-torque compensation of 60% and a starting-torque compensation of 67%, cf. Section 2.6.2.2. Use of a subframe allows the use of additional rubber elements for vibration isolation and noise insulation between axle (incl. differential) and body. Moreover, this also simplifies vehicle production, since the complete axle can be pre-assembled as a system.

In the kinematic and elastokinematic design of wheel suspension systems, the maximum number of influencing possibilities is only available if exclusively such links are used that cancel only one of the six degrees of freedom of the wheel carrier relative to the body. It is not absolutely necessary for all 5 links to be arranged between wheel carrier and body. If it is accepted that individual links are subject to bending not only by the spring/damper forces, then further possibilities of arrangement will be available.

Fig. 2.6-57 shows the multilink rear suspension system of the BMW 5. The rear-axle bracket (aluminum tube welded assembly) is mounted to the body by four large-volume rubber mounts (silent bearings) for optimum noise and tire comfort. Even though this is associated with a relatively soft suspension, optimum tracking has been achieved thanks to an intelligent arrangement of the links. And kinematics as well as elastokinematics are tuned in such a

way as to prevent, for example, adverse steering-angle changes during braking deceleration or acceleration.

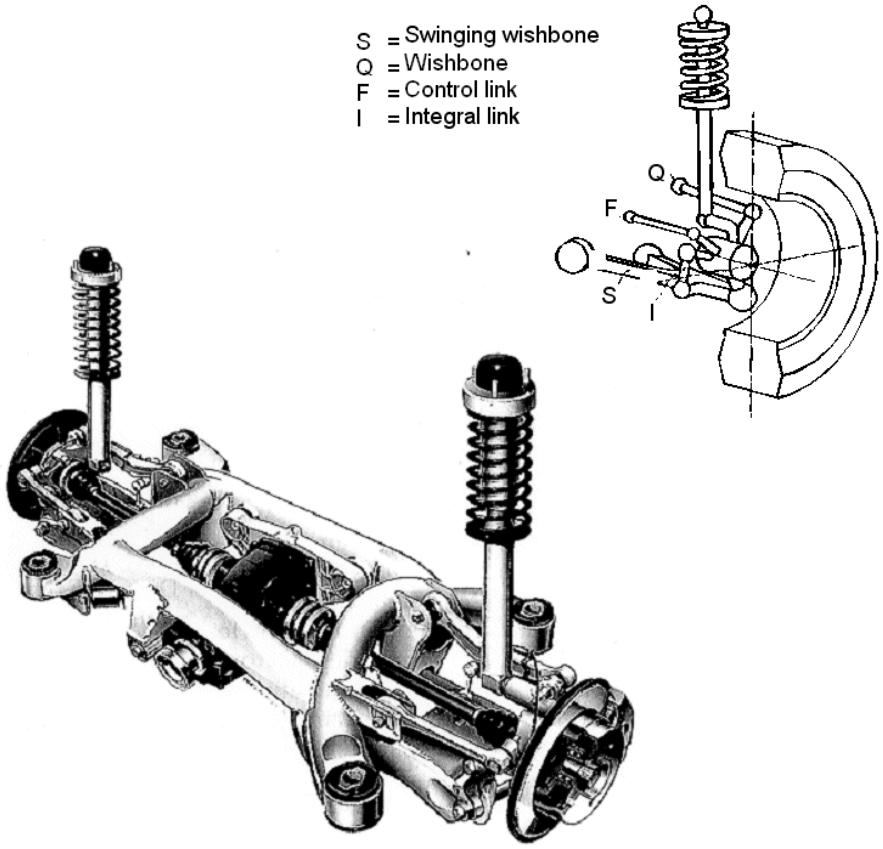

Fig. 2.6-57: Multilink rear suspension (BMW 5, 1996)

Literature

/1/ Adomeit, G. — Umdruck zur Vorlesung Dynamik I und II, Inst. für allg. Mechanik der RWTH Aachen, 1989

/2/ Bantle; M. Braess, H.-H. — Fahrwerksauslegung und Fahrverhalten des Porsche 928, ATZ 1977

/3/ Bergman, W. — The Basic Nature of Vehicle Understeer-Oversteer, SAE-Paper 957 B, 1965

/4/ Berkefeld, V. — Theoretische Untersuchungen zur Vierradlenkung, Stabilität und Manövrierbarkeit

Vortrag auf der HDT-Tagung T-30-930-056-9

Allrad-Lenksysteme bei PKW 11/89

/5/ Bismis, E. — Testverfahren für das instat. Lenkverhalten in: Entwicklungsstand der objektiven Testverfahren

Kolloquiumreihe „Aktive Fahrsicherheit“

Verlag TÜV Rheinland GmbH, Köln 1978

/6/ Bleck, U. Heißing, B. Meyer, G. — Analyse der Lastwechselreaktionen mittels Simu lation und Messung

VDI-Bericht Nr. 699, 1988

/7/ Braun, H. — Untersuchungen über Fahrbahnunebenheiten

Deutsche Kraftfahrforschung und Verkehrstechnik, Heft 186, VDI-Verlag, Düsseldorf

/8/ Burckhardt, M. Der Einfluß der Reifenkennlinien auf Signalgewinnung und Regelverhalten auf Fahrzeuge mit ABS, Automobil-Industrie 3/87 S. 231

/9/ Buschmann
Koessler
Handbuch der Kraftfahrzeugtechnik, Band I u. II, Heyne Verlag München

/10/ Deppermann, K-H. Fahrversuche und Berechnungen zum Geradeauslauf von PKW
VDI-Fortschrittsberichte, Reihe 12, Nr. 133, 1989

/11/ Donges, E.
I. Aspekete der aktiven Sicherheit bei der Führung von PKW, Automobil-Industrie 2/2
II. Aktive Hinterachskinematik - neue Entwicklungsmöglichkeiten der Fahrzeugquerdynamik, VDI-Bericht Nr. 778, 1989
Funktion und Sicherheitskonzept der aktiven Hinterachskinematik von BMW
III. Vortrag auf der HDT-Tagung 30-930-056-9
Allrad-Lenksysteme bei PKW 11/89

/12/ Fiala, E. Kraftkorrigierte Lenkgeometrie unter Berücksichtigung des Schräglaufwinkels, ATZ 61, 1959

/13/ Förster, H.-J.

I. Mercedes-Benz Servolenkungen

ATZ 80 (1978) 3

II. Mercedes-Benz Servolenkungen

Teil 1 ATZ 74 (1972) 2

Teil 2 ATZ 74 (1972) 4

/14/ Forkel, D.

Ein Beitrag zur Auslegung von Fahrzeuglenkungen, Deutsche Kraftfahrtforschung und Verkehrs-technik, Heft 145, 1961

/15/ Gerresheim, M.

Hussmann, A.

Kräfte und Bewegungen in der Aufstandsfläche geradeausrollender Reifen, Teil 1

Automobil-Industrie 3/75

/16/ Gnadler, R.

Naßgriff und Aquaplaningverhalten von PKW-Reifen, Verkehrsunfall und Fahrzeugtechnik

Teil 1 Heft 11/88

Teil 2 Heft 12/88

/17/ Göhring, E.

I. Beitrag zur Entwicklung eines fahrmechanischen Konzepts für Nutzfahrzeuge

Automobil-Industrie 4/80

II. Einfluß des Systems Reifen / Fahrbahn auf das Außengeräusch von Nutzfahrzeugen

VDI-Bericht, Nr. 778, 1989

/18/ Goes, F.
Theoretische und experimentelle Untersuchungen zur Beurteilung der Wirkung von Schwingungsdämpfern im Fahrzeug
Dissertation TH Braunschweig, 1963

/19/ Gough, V.-E.
Seitenkraft und Seitenverschiebung in der Berührungsfläche zwischen Reifen und Fahrbahn
ATZ 19 (1961)

/20/ Hahn, W.-D.
Die Federungs- und Dämpfungseigenschaften von Luftreifen bei vertikaler Wechsellast
Dissertation TU Hannover, 1972

/21/ Hennecker, D.
Jordan, B.
Ocher, U.
Elektronische Dämpfer-Control - eine vollautomatische adaptive Dämpferkraftverstellung für den BMW 635 CSi, ATZ 89 (1987) 9

/22/ Heyer, G.
Trends in der Stoßdämpferentwicklung
Automobil-Industrie Nr. 6 / 88

/23/ Hildebrandt, C.
Der neue VW Santana, ATZ 84 (1982) 2

/24/ Hoffmann R.
Lorenz, K.
Sagan, E.
Der neue BMW 7er
ATZ 89 (1987) 6

/25/ Klinkner, W. Adaptives Dämpfungssystem "ADS" zur fahrbahn- und fahrzustandsabhängigen Steuerung von Dämpfern einer Fahrzeugfederung

VDI-Bericht Nr.778, 1989

/26/ Krempel, G. Experimenteller Beitrag zur Untersuchung am Kraftfahrzeugreifen

Dissertation TH Karlsruhe, 1965

/27/ Laermann, F. J. Seitenführungsverhalten von Kraftfahrzeugen bei schnellen Radlaständerungen

VDI-Fortschrittsberichte, Reihe 12, Nr. 73

/28/ Lohr, F.-W. Opel Omega - Teil 1 ATZ 89 (1987) 1

Teil 2 ATZ 89 (1987) 2

/29/ Matschinsky, W. Die Radführung der Straßenfahrzeuge

Analyse, Synthese, Elasto-Kinematik

Verlag TÜV Rheinland GmbH, Köln 1987

/30/ Mitschke, M. Dynamik der Kraftfahrzeuge, Springer-Verlag

Berlin, Heidelberg, New York, 1975

/31/ Olley, M.
Road Manners of the Modern Car
Proc. Inst. Aut. Engers. 1946/47

/32/ Rake, H.
Umdruck zur Vorlesung Regelungstechnik der RWTH Aachen, 1989

/33/ Reimpell, J.
Fahrwerktechnik: Reifen und Räder
Vogel-Buchverlag, Würzburg 1986

/34/ Richter, B.
Die Vierradlenkung des iRVW4
Vortrag auf der HDT-Tagung T-30-930-056-9
Allrad-Lenksysteme bei PKW 11/89

/35/ Rönitz, R.
Braess, H.-H.
Zomotor, A.
Verfahren und Kriterien zur Bewertung des Fahrverhaltens von PKW
Teil 1 Automobil-Industrie 1/77
Teil 2 Automobil-Industrie 3/77

/36/ Rompe, K.
Donges, E.
Variationsbereiche der Fahreigenschaften heutiger PKW
Automobil-Industrie 2/83

/37/ Rompe, K.
Heißing, B.
Objektive Testverfahren für die Fahreigenschaften von Kraftfahrzeugen
Verlag TÜV Rheinland GmbH, Köln 1984

/38/ Stall, E.
Verfahren zur Vermessung und Simulation von Straßenunebenheiten
Doktorvortrag, TH Aachen 1984

/39/ Waldmann, D.
Untersuchungen zum Lenkverhalten von Kraftfahrzeugen. Deutsche Kraftfahrforschung und Straßenverkehrstechnik, Heft 218, 1971

/40/ Wallentowitz, H.
Hydraulik in Lenksystemen für 2 und 4 Räder
Vortrag auf der HDT-Tagung T-30-302-056-9
Hydraulik und Pneumatik im Kraftfahrzeug 3/89

/41/ Weber, R.
Beitrag zum Übertragungsverhalten zwischen Schlupf und Reifenführungskräften
Automobil-Industrie 4/81

/42/ Weber, R.
Persch, H.-G.
Seitenkraft-Frequenzgänge von Luftreifen
ATZ 77 (1975) 2

/43/ Willumeit, H.-P.
Seitenkraftverlust des schräglaufenden Reifens unter dynamisch veränderlichen Radlasten und konstantem Schräglaufwinkel
Automobil-Industrie 4/70

/44/ Wolff, H.
Untersuchung und Optimierung des Federungsverhaltens von Rettungswagen unter besonderer Berücksichtigung von Reibungseinflüssen
Dissertation TH Aachen, 1975

45/ Zamov, J. Beitrag zur Identifikation unbekannter Parameter für fahrdynamische Simulationsmodelle
VDI-Berichte Reihe 12, Nr. 217

/46/ Zomotor, A. I. Fahrwerktechnik, Fahrverhalten
Vogel-Buchverlag 1987

II. „Meßverfahren bei der Auslegung des Fahrverhaltens“ aus: Entwicklungsstand der objektiven Testverfahren für das Fahrverhalten
Verlag TÜV Rheinland GmbH, Köln 1977

.ict

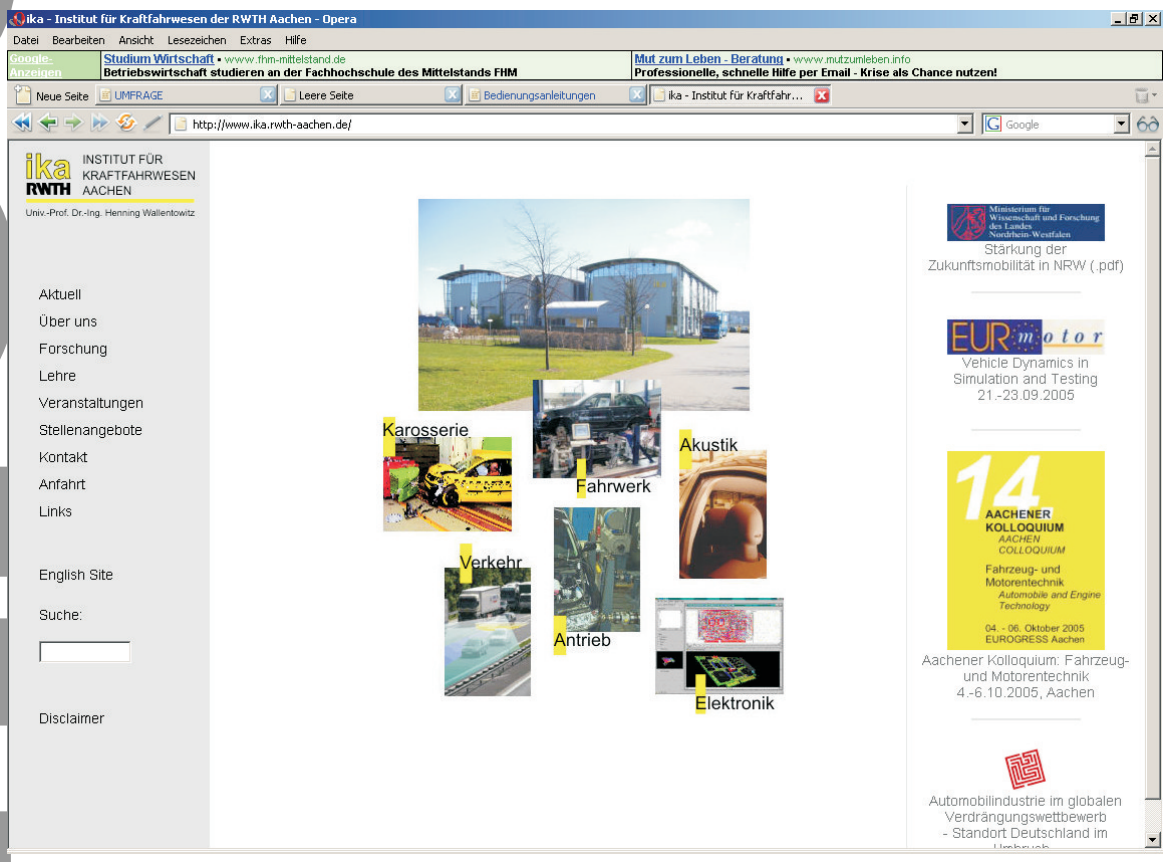

www.ika.rwth-aachen.de

www.fka.de